

ULRR

Development of a novel process for the removal of selected organic compounds from wastewaters.

Item Type	Thesis
Authors	Smart, David
Download date	2026-06-06 16:17:23
Item License	https://creativecommons.org/licenses/by-nc-sa/1.0/
Link to Item	https://hdl.handle.net/10344/1992



UNIVERSITY of LIMERICK

O L L S C O I L L U I M N I G H

**Development of a Novel Process for the Removal of
Selected Organic Compounds from Wastewaters**

Thesis presented for the award of
Doctor of Philosophy (Ph.D.)

by

David Smart, B.Sc.

University of Limerick

Under the supervision of Dr. T. Curtin & Dr. T. O'Dwyer

Submitted to the College of Science and Engineering,
University of Limerick

November 2011



Declaration

The work presented in this thesis is the original work of the author, under the supervision of Dr. Teresa Curtin and Dr. Tom O'Dwyer and due reference has been made, when necessary to the work of others. No part of this thesis has been previously submitted to this or any other University.

David Smart

Abstract

Organic wastewater pollution arising from industry is a growing concern. Industries are increasingly faced with more restrictive environmental regulation with regards to pollutant emissions and an increased interest in reducing water consumption. Existing wastewater treatment can be limited by cost and efficiency.

In this research, a treatment methodology for the treatment of organic wastewater was devised based on a two step aqueous adsorption and catalytic oxidation process. An organic pollutant selected from the EPER database was successfully adsorbed onto a transition metal modified zeolite. The saturated zeolite was then removed from the aqueous phase and then underwent temperature programmed oxidation. In this step the adsorbed pollutant was successfully oxidized into the relatively benign terminal products of carbon dioxide and water. Additionally the desorption of organic chemicals and the production of carbon monoxide were successfully minimized. As a result the modified zeolite was essentially regenerated at the same time as the pollutant was destroyed.

Phenol was selected as the model pollutant due to its aqueous solubility and its environmental toxicity. It is released into waste water streams throughout Europe in large volumes and is particularly prevalent in adsorption research.

The zeolite chosen was zeolite Beta (BEA), a large pore commercial zeolite with an ordered three dimensional structure. A range of silica to alumina ratios for zeolite beta were used including 25:1, 75:1, 150:1 and 300:1. The zeolites were modified with copper by a cation exchange method, and a range of zeolites was created with varying copper loading. It was found that cation exchange under normal conditions was largely dependent on the alumina content of the zeolite, however all samples could be 'over exchanged' by raising the pH to 7. This could result in almost 100% of the copper in solution being exchanged on the zeolite surface. The copper zeolites were found to be stable in solution under a pH range of 5-11, any pH lower than 5 resulted in significant leaching. The modified zeolites were examined by Temperature Programmed Reduction (TPR) which revealed that the nature of the copper species on the surface varied with

available cation sites (silica to alumina ratio), copper loading and pH treatment. Platinum exchanged zeolites were also synthesised as well as bimetallic copper and platinum exchanged zeolites.

The adsorption of phenol from the aqueous phase was examined using eight different zeolites H- β -25, H- β -75, H- β -150, H- β -300, 1.3Cu/ β -25, 2.1Cu/ β -25(p), 0.7Cu/ β -150 and 2Cu/ β -150(p). The adsorption largely followed pseudo second order kinetics and mostly occurred within the first 10 minutes of contact. It was also found to be mostly independent of pH. The adsorption capacity was found to increase as temperature decreased. The thermodynamic parameters reflected this and suggested a spontaneous and exothermic adsorption process. The increase of silica to alumina ratio was found to significantly increase the adsorption of phenol, from 17 mg g⁻¹ (H- β -25) to 36 mg g⁻¹ (H- β -150). It was also found that copper loading increased adsorption: 45 mg g⁻¹ (2.1Cu/ β -25(p)) and 66 mg g⁻¹ (2Cu/ β -150(p)).

Temperature programmed oxidation was carried out on a wide range of phenol saturated copper, platinum and bimetallic zeolites with various loadings. The desorption/oxidation products were analysed through a mass selective detector. The results indicated that the copper modified zeolites reduced the temperature of oxidation considerably from the native zeolite. In addition to this, no desorbed phenol or fragments thereof were detected after modification. Carbon monoxide was also reduced to approximately 5% of the carbon dioxide mass. A comparison of CO₂ peak area and the adsorption studies revealed that up to 95% of adsorbed phenol was oxidised. It was found that increasing the copper loading not only increased the intensity of the CO₂ peak but also noticeably reduced the temperature of oxidation. For example, a peak maximum at 455°C was observed for 0.9Cu/ β -25 and this was reduced to 378°C for 4.6Cu/ β -25(p). The platinum and bimetallic platinum and copper zeolites all exhibited a two step oxidation taking place first at approximately 250°C and then at approximately 400°C. Platinum loading was found to have little effect on oxidation temperature within the range studied. However, increasing the copper loading in the bimetallic zeolites reduced the temperature proportionately.

The over exchanged copper zeolite 2.1Cu/ β -25(p) was examined over six repeat adsorption and oxidation cycles. The adsorption and oxidation was found to be

consistent throughout, however atomic absorption spectroscopic analysis on the reused adsorbent/catalyst found that a substantial amount of leaching occurred leading to a loss of up to 74% of the exchanged copper over five cycles before the leaching ceased. It was discovered that the leaching was largely a result of the high temperature of oxidation. Reducing the oxidation temperature to 500°C reduced copper loss significantly. It was also found that by altering the pH of the adsorption solution to 7, that copper loss could be almost completely eliminated in batch adsorption studies.

Acknowledgments

I would like to acknowledge the help, supervision and guidance of both my supervisors, Dr. Teresa Curtin and Dr. Tom O' Dwyer.

I would also like to thank Bridget, David, Gordon, Serguei and Wynette and all the CES and MSSSI technicians and staff, for all their help throughout my time in UL.

A special word of thanks to my fellow postgrads, in particular Carrol, Darragh, David, Deirdre, Martin, Simon, Treasa and Wiebke.

This research could not have been completed without the generous funding and support from the Environmental Protection Agency under the ERTDI Programme Doctoral Scholarship Scheme (2006-PhD-ET-13).



Dedication

This thesis is dedicated to my mother Gabrielle and to Suzanne. Thank you for all your support and patience.

Table of Contents

1	Introduction.....	1
1.1	EPER Database	1
1.2	Phenol.....	4
1.2.1	Uses and Applications.....	5
1.2.2	Environmental Hazard	5
1.2.3	Toxicity	7
1.2.4	Human Health Effects	9
1.3	Industrial Wastewater Treatment.....	10
1.3.1	Treatment of Organic pollutants	11
1.4	Phenol Treatment in Wastewater	12
1.4.1	Phenol Recovery	12
1.4.2	Phenol Destruction	17
1.5	Proposed System.....	21
1.6	Adsorption.....	22
1.6.1	Adsorbent Materials	23
1.6.2	Zeolite Beta	35
1.7	Oxidation.....	36
1.7.1	Catalysts	37
1.8	Summary of Aims	39
1.9	References.....	40
2	Adsorption of Phenol onto Unmodified Beta Zeolite.....	50
2.1	Introduction.....	50
2.1.1	Adsorption Isotherms	52
2.1.2	Thermodynamics of Adsorption	58
2.1.3	pH.....	62
2.1.4	Kinetics Models	63
2.1.5	Silica to Alumina Ratio.....	65
2.1.6	Surface area analysis	66
2.2	Experimental	68
2.2.1	Materials.....	68
2.2.2	Adsorption Studies	68
2.2.2.1	Kinetics Studies	69
2.2.2.2	pH Studies	69
2.2.2.3	Adsorption Isotherms	70
2.2.3	Adsorbent Characterisation.....	70
2.3	Results and Discussion	71
2.3.1	Kinetic Studies	73
2.3.2	The Influence of pH.....	76
2.3.3	Adsorption Studies	78
2.3.4	Thermodynamic Parameters	85
2.3.5	Silica to Alumina Ratio.....	87
2.4	Conclusion	94
2.5	References.....	97

3	Preparation and Characterisation of the Modified Zeolite	103
3.1	Introduction.....	103
3.1.1	Catalyst Deposition	105
3.1.2	Characterisation Techniques	107
3.1.2.1	Atomic Absorption Spectroscopy	107
3.1.2.2	Temperature Programmed Reduction	108
3.1.2.3	X-Ray diffraction.....	108
3.2	Experimental	110
3.2.1	Catalyst Preparation	110
3.2.2	Catalyst Characterisation	111
3.2.2.1	Atomic absorption spectroscopy	111
3.2.2.2	Temperature Programmed Reduction	112
3.2.2.3	X-Ray Diffraction.....	114
3.3	Results and Discussion	114
3.3.1	Catalyst Preparation	114
3.3.2	Temperature Programmed Reduction	122
3.3.3	X-Ray Diffraction	132
3.4	Conclusions.....	133
3.5	References.....	135
4	Adsorption of Phenol onto Modified Beta Zeolite	140
4.1	Introduction.....	140
4.1.1	Characterization Techniques.....	142
4.2	Experimental	143
4.2.1	Adsorbent Preparation.....	143
4.2.2	Adsorption Studies	143
4.2.3	Surface Characteristics.....	144
4.2.4	Aqueous Stability Studies	144
4.3	Results and Discussion	145
4.3.1	Adsorption Studies	147
4.3.2	Thermodynamic Parameters	155
4.3.3	Aqueous Stability	156
4.4	Conclusion	159
4.5	References.....	162
5	Catalytic Oxidation of Adsorbed Phenol	166
5.1	Introduction.....	166
5.1.1	Thermo Gravimetric Analysis.....	168
5.2	Experimental	168
5.2.1	Catalyst Preparation	168
5.2.2	Temperature Programmed Oxidation Studies.....	169
5.2.3	Thermo Gravimetric Analysis.....	172
5.3	Results and Discussion	173
5.3.1	Temperature Programmed Oxidation.....	173
5.3.1.1	Copper Zeolites	176
5.3.1.2	Platinum Zeolites.....	184
5.3.1.3	Bimetallic Zeolites.....	190
5.3.1.4	Effect of Silica to Alumina Ratio	195
5.3.2	Thermo Gravimetric Analysis.....	197
5.3.3	Mass Balance	201
5.4	Conclusion	202
5.5	References.....	204

6	Regeneration and Reuse of the Catalytic Adsorbent.....	208
6.1	Introduction.....	208
6.1.1	Catalyst Deactivation	208
6.1.2	Catalyst Regeneration	211
6.2	Experimental	213
6.2.1	Catalyst Preparation	213
6.2.2	Atomic Absorption Spectroscopy	213
6.2.3	Temperature Programmed Oxidation Studies.....	214
6.2.4	Thermo Gravimetric Analysis.....	214
6.3	Results and Discussion	215
6.3.1	Temperature Programmed Oxidation.....	216
6.3.2	Effect of oxidation temperature	219
6.3.3	Effect of adsorption pH.....	222
6.4	Conclusion	223
6.5	References.....	225
7	Conclusion.....	228

Chapter 1

Introduction

1 Introduction

1.1 EPER Database

In response to Article 15(3) of the European Council Directive 96/61/EC, the European Pollutant Emission Register (EPER) was established. As stated in a commission decision on 17th July 2000, Member States are required “to inventory and supply data on principal emissions and responsible sources” and that “the commission will publish the results of the inventory every three years and shall establish the formats and particulars for the transmission of information provided by the Member States” (Official Journal of the European Communities 2000).

The EPER covers 50 pollutants or groups thereof, all of which are deemed hazardous to the environment and/or human health. Many of these are listed within Annex X of the Water Framework Directive, Annex I of Directive 67/548/EEC and Regulation 793/93 (*"The European Pollutant Emissions Register - Pollutants"* 2006). Threshold limits are set out in annex A1 of the EPER decision. If these thresholds are exceeded by any facility in any Member State for any of the 50 pollutants covered, then emission data must be included in the report. Annex A3 of the decision contains a list of activities, thus only pollutant emissions produced in these activities are counted towards EPER thresholds (Official Journal of the European Communities 2000). There have been two reporting years for the EPER, in 2001 (for 15 member states) and 2004 (for 25 member states) (*"The European Pollutant Emissions Register - What is EPER?"* 2006). The 2007 report was handed over to the European Pollutant Release and Transfer Register (E-PRTR) and published in 2009. The E-PRTR was set up in accordance with European regulation (EC) No 166/2006 which was in turn brought around as a result of the Aarhus Convention in 1998. It takes into account 91 pollutants, 65 activities, and whereas the EPER deals with emissions to air and water only; the E-PRTR includes emissions to land and offsite waste transfer. Additionally, while the EPER reports mainly on emissions on the facility level; the E-PRTR reports on diffuse emissions where the information is available. The scope is also extended to the 27 EU member

states as well as Iceland, Liechtenstein and Norway. It covers some 24,000 industrial facilities (*"The European Pollutant Release and Transfer Register"* 2010).

The EPER database is hosted on a website by the European Environmental Agency and contains a great deal of information displayed in a number of ways. Information can be viewed by facility, which means searches can be performed on specific regions, cities, towns and villages so that EU citizens can gain information on specific local releases for each pollutant, either measured, calculated or estimated. It can also be viewed by pollutant and by activity.

There are some imperfections with the EPER, firstly its focus on medium to large industrial sites means that the fraction of air pollution recorded is often notably less than actual emissions, for example carbon dioxide emissions recorded by the EPER are estimated to be 42% of the total carbon dioxide emissions and methane is estimated to be only 15% of total methane emissions. European member states are their own organisationally unique nations and as a result methods for monitoring the 50 pollutants featured on the database can differ from place to place. Due to the growth of the EU to 25 member states in 2004 and the addition of many facilities in the second report, a trend between the two years cannot accurately be made. Though the EPER report does include information on individual facilities, comparisons do not indicate their environmental performance. This is because a facility with exceptional environmental performance may still create more emissions than one with comparatively poor performance (*"The European Pollutant Emissions Register - Questions to EPER"* 2006).

Table 1.1 Examples of some of the organic chemical groups featured on the EPER database

Groups	Examples
BETX	Benzene Ethylbenzene Toluene Xylene
Phenols	Phenol Chlorophenols Nitrophenols
Brominated diphenylether (PBDE)	Penta-BDE Octo-BDE Deca-BDE
Polycyclic Aromatic Hydrocarbons (PAH)	Benzo(a)pyrene Benzo(ghi)perylene Benzo(k)fluoranthene Fluoranthene Indeno(1,2,3-cd)pyrene Benzo(b)fluoranthene
Dioxins and Furans	2,3,7,8-tetrachloro-dibenzo-p-dioxin

Organic wastewater pollution as a result of industry is a growing concern. Industries are increasingly faced with more restrictive environmental regulation with regards to pollutant emissions and an increased interest in reducing water consumption. Organic wastewater pollution is a genuine threat to the quality of surface and potable water and to the viability of aquatic ecosystems.

The purpose of this study was to examine one organic chemical covered by the EPER, examples of which are shown in Table 1.1 and develop a treatment method for use in wastewater streams. Phenol was selected on factors such as its environmental hazard, large industrial release, low volatility and high water solubility.

1.2 Phenol

The model pollutant selected for this research is phenol. It is the simplest member of the chemical group known as phenols, all of which contain an aromatic ring bonded to a hydroxyl group. It is also known by the synonyms Carboic acid, Monohydroxybenzene and Phenylalcohol. It is a colourless or light pink crystalline solid. Its molecular formula is C_6H_5OH , it has a boiling point of $181.8^\circ C$, a melting point of $40.9^\circ C$, a relative density of 1.132 g cm^{-3} at $25^\circ C$ and a molecular weight of 94.11 g mol^{-1} . Phenol is water soluble, up to 84 g dm^{-3} at $20^\circ C$ (European Chemicals Bureau 2006). Phenol is approximately 10^7 times more acidic than alcohols of a similar size. Its acidic character is enhanced by the stability of the conjugate base's (known as the phenoxide or phenolate ion) resonance structure (as in Figure 1.1) and the polar effect of the benzene ring on the negative charge.

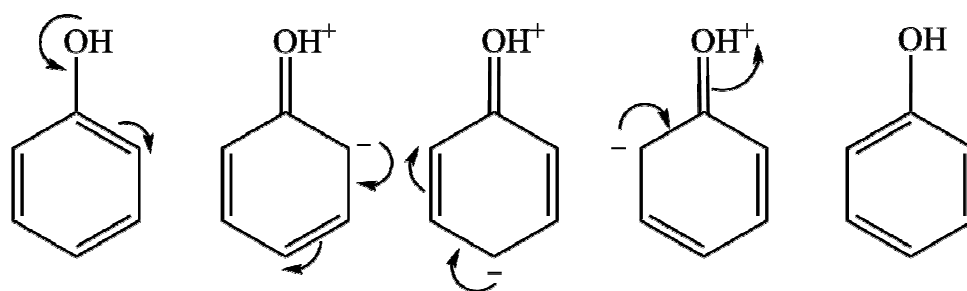


Figure 1.1: Resonance structure of the phenoxide ion.

Because of these factors, less energy is required to form phenoxide from phenol than alkoxides from alcohols. Phenol is thus a weak acid and has a pK_a of 9.95. This means that in Figure 1.2, the equilibrium in water lies towards the left (Marc-Loudon 1995).

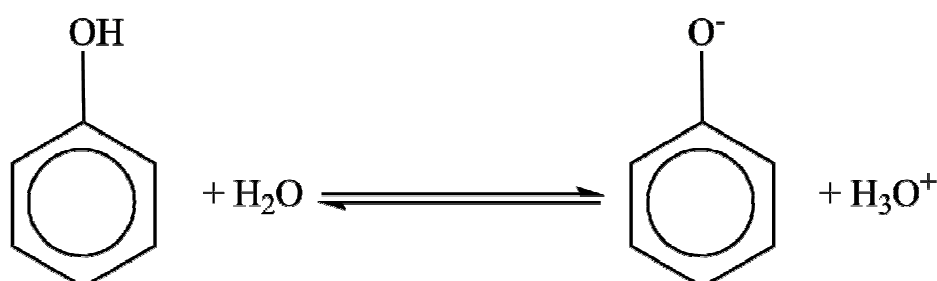


Figure 1.2: Equilibrium of phenol in aqueous solution.

Phenol is combustible and as a liquid it attacks coatings, rubber and some plastics (Busca et al. 2008).

1.2.1 Uses and Applications

The German chemist Runge first isolated phenol from coal tar in 1834 (Busca et al. 2008). Phenol is mainly produced artificially. 98.5% of the world's phenol production is via the Hock method from the three step cumene synthesis and oxidation processes and to a lesser extent via direct oxidation of benzene and by coal or tar processing, and previously by the oxidation of toluene (Schmidt 2005; Busca et al. 2008). As of 2008 phenol production amounted to approximately 8.7 million tons per year (Pilato 2010). Its primary use is as a chemical intermediate in organic synthesis. Major products of this include bisphenol A, phenol resins, alkylphenols, caprolactam, salicylic acid, nitrophenols, aniline, adipic acid, diphenyl ethers and halogen phenols. In particular Bisphenol A accounts for 44% of phenol consumption world wide as of 2007 while phenol-formaldehyde resins accounted for 27%. It is also used to a lesser extent in pharmaceuticals, cosmetics, biocides (slimicide), adhesives and impregnation agents (European Chemicals Bureau 2006). As of 2007 Western Europe represents the largest consumers of phenol, followed by the United States of America. Demand for phenol is increasing especially in developing nations where there is a growing demand for phenolic resins and Bisphenol A (Greiner and Funada 2008).

1.2.2 Environmental Hazard

The primary sources of phenol emissions include automobile exhaust (either by direct release or the photochemical degradation of benzene), animal metabolism and other forms of incomplete combustion including bonfires. Other diffuse sources include domestic wastewaters, agricultural run-off and chemical spills. In industry, phenol emissions can occur in facilities where it is used for organic synthesis and also in low temperature carbonisation plants such as coke ovens and metallurgical processes, fossil fuel refineries, pulp manufacture and leachate from landfills (European Chemicals Bureau 2006; *"The European Pollutant Emissions Register - Pollutants"* 2006). Industrial wastewater can contain phenol concentrations of between 200-2000 mg dm⁻³ (Altunlu and Yapar 2007).

The majority of the atmospheric releases are thought to be from diffuse sources not monitored by the EPER database but under the remit of the new E-PRTR. The actual quantities released into the air may be approximately 97,000 tonnes per annum, but phenol has a short photodegradation half-life of approximately 42 minutes so the larger part does not dwell in any environmental compartment. A further 2,000 tonnes per annum in Europe is thought to be released as a result of human metabolism in the form of sewage (European Chemicals Bureau 2006).

Phenol's half life in surface water lies between 2 and 72 days as a result of biodegradation depending on the time of year (Vázquez et al. 2007). Phenol has a low vapour pressure (20 Pa at 20°C) and relatively high water solubility (84 g dm⁻³ at 20°C) and as a result of this most industrial phenol pollution occurs in the aqueous compartment. Table 1.2 highlights the distribution of environmental phenol and its prominence in the hydrosphere (European Chemicals Bureau 2006).

Table 1.2 Percentage distribution of phenol in the environment (European Chemicals Bureau 2006)

Compartment	Percentage
Air	0.8
Water	98.8
Soil	0.2
Sediment	0.2

Figures 1.3 and 1.4 show the total emission of phenols to water for 378 medium to large facilities above threshold levels in the EPER's 2004 reporting year (European Chemicals Bureau 2006). The principal phenol sources present in both direct and offsite emissions are the metal industry, mineral oil and gas refineries and basic organic chemical production. Coke ovens are overall the second largest contributor, with the majority of their phenol emissions transferred to offsite wastewater treatment.

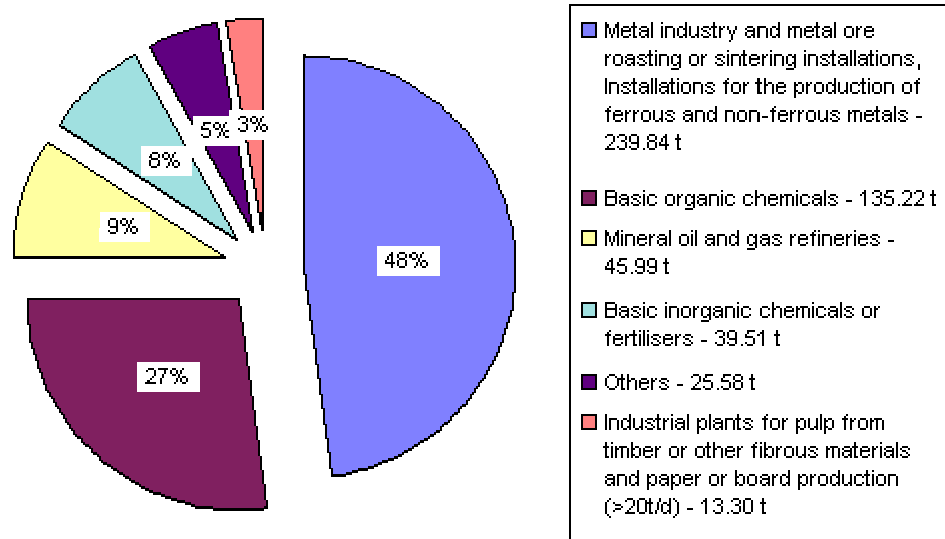


Figure 1.3: Phenol emissions direct to wastewater in 2004 from medium to large facilities in 25 EU member states (*"The European Pollutant Emissions Register - Pollutants" 2006*).

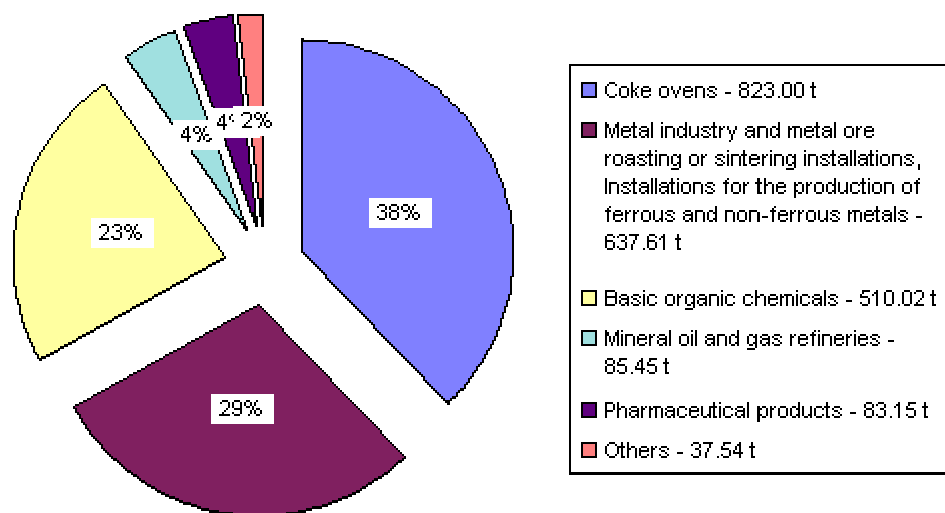


Figure 1.4: Phenol emissions transferred to offsite wastewater treatment in 2004 from medium to large facilities in 25 EU member states (*"The European Pollutant Emissions Register - Pollutants" 2006*).

1.2.3 Toxicity

Extensive toxicity studies have been carried out on a range of aquatic organisms on three trophic levels. Aquatic vertebrates are shown to be sensitive to phenol exposure. The salmonid *Oncorhynchus mykiss* is shown to be particularly sensitive to acute and chronic conditions. A number of sample tests for phenol toxicity on aquatic vertebrates are shown in Table 1.3 representing typical upper and lower limits. In contrast to

Oncorhynchus mykiss, *Jordanella floridae* is relatively more resistant to acute phenol toxicity. Over a longer time span, low phenol concentrations have been observed to affect the fertilised eggs of aquatic invertebrates. This is apparent even in very small concentrations with respect to *Oncorhynchus mykiss*, observed over periods of 4-8 days. The fertilised egg is also affected under acute conditions in the case of *Brachydanio Rerio*.

Table 1.3 Acute and chronic phenol toxicity exposure tests on aquatic vertebrates (European Chemicals Bureau 2006). LC₅₀ = Lethal Concentration, 50%, EC₁₀ = Effective Concentration 10%.

Species	Values	Concentration (mg dm ⁻³)	Exposure Time	Notes
<i>Jordanella floridae</i> - Flag Fish	LC ₅₀	67.5	96 hrs	Acute
<i>Oncorhynchus mykiss</i> – Rainbow Trout	LC ₅₀ EC ₁₀	5.02 0.002 – 0.065	96 hrs 4-8 days	Acute Chronic – Fertilised Eggs
<i>Brachydanio Rerio</i> - Zebra Fish	EC ₅₀	7.9	36 hrs	Acute - Fertilised Eggs
<i>Pimephales promelas</i> – Fathead Minnow	EC ₁₀	0.282	4-8 days	Chronic – Fertilised Eggs

Aquatic invertebrates are similarly affected by low, short term phenol concentrations. In various studies *Daphnia magna* is shown to have a typically low tolerance. Some sample studies for various aquatic invertebrates are shown in Table 1.4. Other invertebrates have wider ranging EC values: mussels 59-1,000 mg dm⁻³, snails 51-580 mg dm⁻³, worms 32-1,080 mg dm⁻³ and insects 7-1,800 mg dm⁻³ (European Chemicals Bureau 2006).

Table 1.4 Acute and chronic phenol toxicity exposure tests on aquatic invertebrates (European Chemicals Bureau 2006). NOEC = No Observable Effect Concentration.

Species	Values	Concentration (mg dm ⁻³)	Exposure Time	Notes
	EC ₅₀	12-21	24 hrs	Acute
<i>Daphnia magna</i>	EC ₅₀	4.2-12	48 hrs	Acute
	LC ₅₀ /NOEC	4/0.5	11 days	Chronic
<i>Palaemonetes Pugio</i>	LC ₅₀	5.8	96 hrs	Acute
<i>Asellus aquaticus</i>	LC ₅₀	180	96 hrs	Acute
<i>Ceriodaphnia dubia</i>	LC ₅₀ /NOEC	9/0.84	8 days	Chronic

Aquatic algae are also vulnerable to phenol in the aqueous phase with acute EC₅₀ values ranging from 7.5 to 370 mg dm⁻³. Microorganisms are somewhat more resistant but problems can occur if larger concentrations enter into organic wastewater treatment where concentrations in excess of 100 mg dm⁻³ can inhibit respiration and in excess of 450 mg dm⁻³ can result in growth inhibition in activated sludge (European Chemicals Bureau 2006).

Phenol has a low potential for bioaccumulation but through acute and chronic exposures within the length of its aquatic half life and the possible range of concentration in industrial wastewater it can negatively affect aquatic life throughout the trophic levels.

1.2.4 Human Health Effects

Phenol and its chlorinated products have an unpleasant taste and odour. This taste and odour is unpleasant in drinking water at low concentrations: 150 µg dm⁻³ for phenols and between 0.2 and 2 µg dm⁻³ for chlorophenols. The negative effects of phenol on humans increases beyond the aesthetic as concentrations rise. The toxic effects of acute phenol exposure in large concentration are dramatic. Phenol is lethal through ingestion (approx 140-290 mg kg⁻¹ of body weight), corrosive and absorbs through the skin and mucus membranes on contact. Adsorption through the skin can also be lethal and effects

are system wide resulting in nervous system and multiple organ failure. Death can occur from 30 minutes to several hours.

Chronic effects include nervous system, hepatic, renal, haematopoietic and immune system effects. Nervous system difficulties observed in animals can include tremor, convulsions, loss of co-ordination, paralysis, reduced motor and spontaneous activity. Chronic exposure to the skin can eventually cause epidermal hyperkeratosis and ulceration. However at low concentrations it can cause skin irritation. Phenol is not believed to be carcinogenic; however in the presence of chlorine it can form potentially carcinogenic compounds. (Eksperiandova et al. 1999; US EPA 2002; European Chemicals Bureau 2006).

The limits of exposure are often difficult to quantify, however in the US the Occupational Safety and Health Administration (OSHA) and the American Conference of Governmental Industrial Hygienists (ACGIH) have assigned a TLV (threshold limit value) of 5 mg dm^{-3} for dermal contact for a time weighted average of an 8 hour working day and a 40 hour working week (*Occupational Safety and Health Administration* 1996). EU law no. 152/2006 sets a limit of $0.5 \text{ } \mu\text{g dm}^{-3}$ in potable water, 0.5 mg dm^{-3} for surface water and 1 mg dm^{-3} for sewage. As of 2000 the “German Framework Administrative Guideline for Minimum Requirements on the Discharge of Wastewater into Water Bodies” stated a phenol index of $\leq 0.15 \text{ mg dm}^{-3}$, in 2002 the Danish EPA set a phenol emission value of 0.02 mg dm^{-3} , in the UK there exists a non statutory environmental quality standard for surface water at $30 \text{ } \mu\text{g dm}^{-3}$, in India the Ministry of Environment and Forests put a maximum phenol concentration in industrial water at 1 mg dm^{-3} , and the World Health Organisation put the maximum potable water concentration at 0.001 mg dm^{-3} (European Chemicals Bureau 2006; Kamble et al. 2008).

1.3 Industrial Wastewater Treatment

Modern industrial processes will often produce wastewater; this waste is frequently toxic, environmentally persistent and if left untreated could cause serious human health and environmental effects. Introducing toxic wastewater to natural surface and ground

water can significantly reduce its quality and deny its use to industry and consumers alike.

In conventional wastewater treatment facilities, wastewater is treated in three basic and subsequent stages:

- Primary Treatment - This focuses on the physical removal of large insoluble solids such as grit, grease and larger objects. This often consists of screening (often called preliminary treatment) followed by sedimentation and/or grinding.
- Secondary Treatment – Involves the removal of soluble organic matter by biological degradation. This can take place in aerobic or anaerobic conditions followed by settling tanks and/or filtration for transfer to tertiary treatment.
- Tertiary Treatment – Where the removal of dissolved and suspended waste is not sufficient in primary and secondary treatment, tertiary treatment is often used. This often involves more specific and advanced biological and physicochemical processes (Ren 2004; Sonune and Ghate 2004).

The end product of wastewater treatment is to generate water of sufficient quality to reintroduce into the environment or for re-use in industrial activities.

1.3.1 Treatment of Organic pollutants

In the past the focus of treatment was the removal of pollutants in the form of collective characteristics such as suspended solids, chemical oxygen demand (COD), biological oxygen demand and harmful microorganisms. However the content of industrial wastewater varies greatly and the individual characteristics of different pollutants have to be accounted for. Many toxic molecular organic pollutants are either functionally resistant to biodegradation (such as polycyclic aromatic hydrocarbons) or they are very slowly biodegraded. The result of this is that the pollutant either ends up in solid biological sludge waste with its toxic qualities intact, or it is released into the environment. Additionally these compounds may be toxic to the organisms used in

biological treatment. A well designed plant may only remove some 65% of COD after secondary treatment. This is why specific tertiary treatments and pretreatments are required for removing molecular organic chemicals (Pera-Titus et al. 2004; Sonune and Ghate 2004; Qu et al. 2006).

1.4 Phenol Treatment in Wastewater

Phenol concentrations in industrial wastewater can vary from the very low (c. 0.1 mg dm⁻³) to dangerously high (c. 7,000 mg dm⁻³). Table 1.5 shows the phenol concentration ranges in a variety of wastewater streams (González-Muñoz et al. 2003).

Table 1.5 Concentration of phenols in wastewater streams in a range of industrial activities (González-Muñoz et al. 2003).

Industrial Process	Phenol Concentration range (mg dm ⁻³)
Refineries	6-500
Coking Operations	28-3900
Coal Processing	9-6800
Petrochemical Manufacture	2.8-1220
Other Processes	0.1-1600

Typically the maximum permissible concentration (MPC) of phenol entering the environment is 0.1 mg dm⁻³ in non chlorinated waters and between 0.001-0.002 mg dm⁻³ in chlorinated waters (to reduce the chance of creating more harmful chlorophenols) (Eksperiandova et al. 1999). As with other organic precursors, at high concentrations it is often worthwhile to recover the compound, however as concentrations decrease this becomes less cost effective and destruction is necessary.

1.4.1 Phenol Recovery

Phenol treatment in wastewater is achievable through a number of available technologies. The optimal system necessary depends on many factors. When

considering treatment methods, often the concentration is significant enough for recovery. This can be achieved using methods such as azeotropic distillation, solvent extraction and/or steam stripping (Busca et al. 2008). These methods often incorporate an integrated system involving a liquid-liquid extraction stage, a distillation column and a recycling stage. The extraction column utilizes an extracting agent. The extracting agent has increased solubility for phenol and separates the bulk of the pollutant to create a phenol rich phase, and a water rich phase. The extracting agent is removed from the top and is cleaned in the distillation stage, the phenol rich phase is ready for re-use and the water rich phase goes to the final recycling stage. The water rich phase can be within the acceptable range of phenol contamination but it contains some trace elements of the extracting agent. The purpose of the recycling stage is to remove these elements, for example through steam stripping ("QVF Engineering GmbH" 2005; Pinto et al. 2005; Busca et al. 2008). Figure 1.5 illustrates an integrated azeotropic distillation process for the removal of phenols.

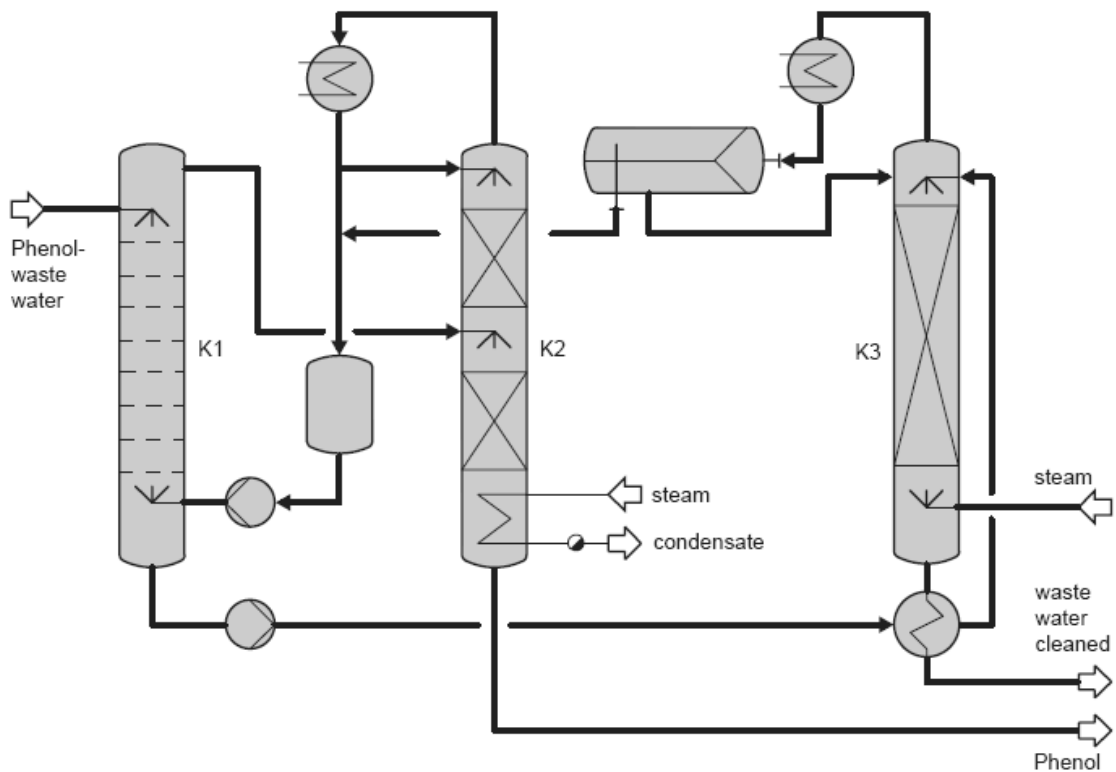


Figure 1.5 Schematic of a 3 step integrated process including an extraction column (K1), a distillation column (K2) and a stripping column (K3) ("QVF Engineering GmbH" 2005).

These processes usually operate between 2 and 12% phenol content and can use environmentally benign solvents for extraction such as methylisobutylketone (MIBK)

which can be used in concentrations up to $30,000 \text{ mg dm}^{-3}$ ("QVF Engineering GmbH" 2005; Pinto et al. 2005). Despite this these methods require multiple cycles to be effective and are costly to operate (Pinto et al. 2005; Busca et al. 2008).

Membrane separation is a form of physical treatment involving a porous membrane, usually made out of a polymeric material which can reject or accept molecules or particles based on shape, size and other properties. There are several different categories of membrane primarily differentiated on pore size:

- Microfiltration – Macropores greater than 50 nm in diameter.
- Ultrafiltration – Mesopores between 2-50 nm.
- Nanofiltration – Micropores smaller than 2 nm.
- Reverse Osmosis (RO) – Microporous under pressures in excess of osmotic pressure.

For small molecular organic compounds, a small pore size is required in order to reject them. Because of this reverse osmosis and nanofiltration are the most suitable. However as pore sizes decrease, shape and size no longer primarily decide the performance of the membrane as there is a greater dependency on other physical and chemical properties of the membrane material and its interactions with the pollutant and its solvent (Judd and Jefferson 2003).

Membrane separation has some advantages in that the system operates continuously; there is no phase change and no need for chemical reactants. RO specifically is efficient at removing a range of organic molecules, especially when combined with composite membranes (Karakulski et al. 2001; Goncharuk et al. 2002). However, both nanofiltration and RO can exhibit low retention for organic monomers of low molecular weight such as phenols (Williams et al. 1999). Additionally, the high and constant pressures required for RO as well as the chance of membrane fouling can drive up the treatment cost. Despite this however, there has been advancement in the form of Ultra-low pressure reverse osmosis membranes which can reduce the pressure required significantly using negatively charged surface characteristics (Ozaki and Li 2001).

A non destructive technique for removing phenol is membrane pervaporation. Unlike other membrane treatments this relatively new process involves the use of a non-porous

hydrophobic membrane with a vacuum or sweep gas applied to the other side. This results in the selective diffusion of the organic component through the membrane which is subsequently desorbed in vapour form on the opposite side. The selectivity of the membrane is based on its chemical potential relative to the target pollutant. This can be maintained by adjusting the vacuum, partial pressure and other parameters. A typical pervaporation system would include the membrane suspended in a module, a feed pre-treatment and delivery system and a permeate recovery system (Peng et al. 2003).

Pervaporation has been reported as a promising method for the removal of phenol from water using polyether-polyamide block copolymer (PEBA), supported polyurethane and cellulose membranes (Busca et al. 2008). Pervaporation is relatively low cost and high performance compared to other forms of membrane separation, providing that the process parameters are closely monitored. However a balance between permeation flux and selectivity needs to be maintained (Peng et al. 2003).

For the purpose of phenol removal (such as in waste streams from the cumene process) pervaporation on its own may not yield sufficient phenol removal, however this can be remedied with a combined system involving a pervaporation step followed by an adsorption step. The first step removes the larger concentrations of phenol to be recovered and the adsorption step takes care of trace phenol still present in the waste stream (Kujawski et al. 2004). A possible hybrid system for the treatment of phenol containing wastewater streams is illustrated in Figure 1.6.

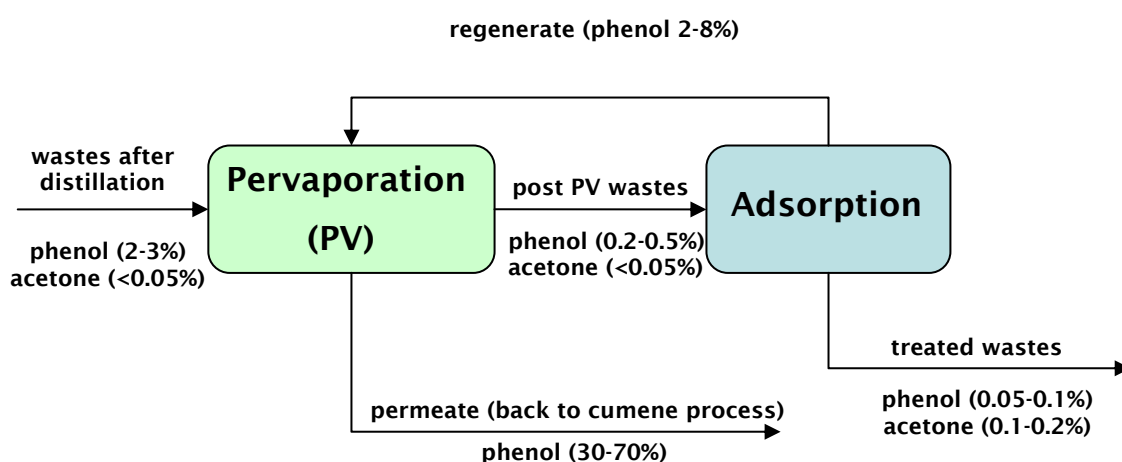


Figure 1.6 Process diagram of a possible hybrid pervaporation-adsorption process for the treatment of phenolic wastewaters resulting from the cumene process (Kujawski et al. 2004).

Adsorption is a common form of wastewater treatment. The process is explained in detail in section 1.6. Typically adsorption systems involve a fixed bed which is removed after adsorption and either regenerated or disposed of depending on the situation. The dominant adsorbent is activated carbon. This micro-mesoporous adsorbent with a large surface area can be made from a wide range of materials and is easily modified e.g. through oxygen gasification. Activated carbon has a large adsorption capacity for phenols, for example Fierro et al. investigated activated carbon prepared from Kraft lignin with sodium hydroxide, potassium hydroxide or phosphoric acid. The resulting adsorption capacity was between 212.77 mg g^{-1} and 238.10 mg g^{-1} depending on the treatment and was reached within 2 hours (Fierro et al. 2008). Where regeneration is used however activated carbon incurs some problems. Phenols often adsorb onto carbons irreversibly through chemisorption covalent bonding, this makes thermal regeneration treatment at high temperatures (c. 800°C) ineffective at removing any phenol that has irreversibly adsorbed.

Polymeric materials such as PS-DVB resins have adsorption capacities for phenol of between 80 and 100 mg g^{-1} (Otero et al. 2005) but have an advantage over activated carbons in that the bonding forces of adsorption are usually weaker with regards to phenols and more reversible. Regeneration is generally achieved through solvent washing and is non-destructive, which allows phenol to be recovered for reuse (Busca et al. 2008).

A summary of the non-destructive treatments discussed in this section is shown in Table 1.6.

Table 1.6 Summary of non-destructive treatments showing examples.

<i>Process</i>	<i>Variations</i>	<i>Details</i>
Liquid-liquid extraction	Azeotropic Distillation Solvent Extraction Steam Stripping	May use environmentally benign solvents. Operate at high concentrations. Requires multiple cycles. Relatively expensive.
Membrane Separation	Membrane- Pervaporation Reverse Osmosis Composite Membranes	Can exhibit low retention for small organics in many cases. Risk of fouling. Pervaporation is low cost, will usually only remove the bulk of phenol.
Adsorption	Activated Carbon Polymeric Resins Zeolites	Usually inexpensive. Efficient at low concentrations. Some adsorbents prone to fouling or damage during regeneration. Regeneration often excludes recovery, can be expensive.

1.4.2 Phenol Destruction

Often phenol concentrations may be too low to recover or simply incinerate or too high and toxic to treat biologically. In these situations or for economic reasons, destruction of the pollutant may be the preferred option.

Wet Air Oxidation (WAO) is a well established destructive liquid phase waste treatment method. It operates without flame in a pressurised (7-2.3 MPa) enclosed container heated to between 200 and 350°C by a start-up boiler and maintained by the internal reaction heat and over certain concentrations can become a net energy producer. These conditions increase the diffusion and solubility of oxygen and the pollutants. It operates through a liquid phase reaction between the organic material and compressed air oxidant injected into the container (Eckenfelder 1989; Matatov-Meytal and Sheintuch 1998). The result is the conversion of phenol into less harmful, simpler organic compounds.

Complete mineralization is impossible as these lower molecular weight compounds prove resistant to oxidation. Due to this WAO is best suited as a form of pre-treatment.

Incomplete oxidation can lead to dangerous pollutants such as dioxins through pyrolysis and isomerisation in complex waste streams and the high pressures and large volumes of water involved can greatly increase running costs. Costs are also much greater when the concentration of the substrate is too low to sustain the reaction temperature.

Although it accentuates the running costs further, Supercritical Water Oxidation (SCWO) (which operates at pressures of 27.6 MPa and temperatures of around 500°C) can increase destruction efficiency, reducing Total Organic Carbon (TOC) to approximately 3.5 mg dm⁻³ in solution (Atwater et al. 1997; Matatov-Meytal and Sheintuch 1998; Busca et al. 2008).

The introduction of metal catalysts into wet air oxidation can augment WAO treatments by reducing operating pressures and temperatures. Homogeneous catalysts in solution such as in the LOPROX Bayer process using Fe cations, can operate effectively below 200°C. Homogeneous catalysts require a second step to separate the catalyst from solution. Because of this it is often more practical to avoid this by using a solid heterogeneous catalyst. For phenol the most active solid catalysts are noble metals such as Pt or Ru or transition metal cations such as Cu, Co, Mn and Fe. These are often supported on metal oxides or zeolites. In heterogeneous catalytic wet air oxidation, removals of >90-95% of phenol can be achieved with relatively mild temperatures and pressures (100 – 200°C, 0.3-3.5 MPa) in 1 to 3 hours residence time (Matatov-Meytal and Sheintuch 1998; Maduna Valkaj et al. 2007; Busca et al. 2008).

Despite the benefits of catalytic wet air oxidation (CWAO), the exposure to the aqueous phase and the conditions of the oxidation process can cause inherent difficulties with catalyst leaching. This can cause secondary pollution of the wastewater and a gradual decrease in catalytic activity.

Other types of liquid phase catalytic oxidation include oxidation with ozone and wet peroxide oxidation (WPO). Both of these operate by forming hydroxyl radicals under certain conditions in the presence of water.

Ozone catalysis is very effective with regards to phenol destruction, Gimeno et al. showed that near complete oxidation of 200 mg dm^{-3} could be achieved in 2 hours at 20°C with no buffer (Gimeno et al. 2005). However, this process was inefficient at removing other Chemical Oxygen Demand (COD)/TOC sources simultaneously. This can be enhanced further with homogeneous or heterogeneous catalysis however this increases the risk of forming secondary contaminants with ozone and polluting wastewater with leached catalyst (Busca et al. 2008).

Oxidation using hydrogen peroxide on its own often yields low reactivity and incomplete oxidation. A more effective form of treatment than WPO is the Fenton process. This uses hydrogen peroxide in conjunction with iron (II) salts (Fentons reagent) to effectively generate larger quantities of hydroxyl radicals. However the reaction operates in a relatively narrow band of low pHs and requires excesses of hydrogen peroxide. It also requires separation of the homogeneous iron salts after reaction.

The application of supported iron on zeolites such as ZSM-5 and mesoporous silicates such as MCM-41 can improve phenol destruction in the presence of hydrogen peroxide to c.100% and simplify the catalyst separation process. However the heterogeneous Fenton process still suffers from the same restraints of pH and repeated cycles cause damage to the porous supports, iron agglomeration and catalyst leaching (Busca et al. 2008).

More recent innovations include Advanced Electrochemical Oxidation (AEO) which takes place in an electrochemical cell with a metal oxide coated anode. This facilitates the production of radicals in the presence of oxygen (Yavuz and Savas Koparal 2005). Another emerging AEO method is electron beam acceleration which uses ionizing radiation from a source such as cobalt-60, on water to form short lived radicals as a product of radiolysis (Chmielewski and Haji-Saeid 2004; Martin et al. 2005). Photocatalysis is also a focus of recent research and uses ultraviolet and in some cases visible light in conjunction with a chemical semiconductor to create oxidizing agents through photolytic and subsequent redox reactions (Amat et al. 2007; Hirakawa et al. 2007). AEO can often have characteristically high degradation efficiency but in most

cases require large amounts of energy, are subject to fouling, dependent on reactants and or liquid phase semiconductors. The costs relative to other forms of treatment can be excessive, especially if complete oxidation is required. As a result AEOs are often used to partially degrade organic compounds as a pre treatment to organic treatment (Wu and Zhou 2001; Zhou et al. 2002; Sampa et al. 2004; Zhou et al. 2004)

A summary of the destructive treatments discussed in this section is listed in Table 1.7.

Table 1.7 Summary of destructive treatments showing examples.

<i>Process</i>	<i>Details</i>
Wet Air Oxidation	Operates under high temperature and pressure. Complete oxidation generally not possible.
Supercritical Wet Air Oxidation	Increased oxidation efficiency, accompanied with increased operating costs
Catalytic Wet Air Oxidation	Reduced temperatures and pressures. Chance of catalyst fouling or leaching
Wet Peroxide Oxidation Ozone Catalysis	Improved production of radicals. Involve feed chemicals which can become secondary contaminants.
Fenton/Photo Fenton Process	More effective than WPO alone. Requires very low pHs. If Fenton reagent is not supported it requires separation.
Advanced Electrochemical Oxidation	High capital costs and in some cases large running costs for complete degradation. Chance of electrode fouling in the case of an electrochemical cell.

1.5 Proposed System

The system proposed in this work involves the combination of adsorption and catalytic oxidation treatment methods into a two step system that will remove and destroy the organic pollutant (phenol).

The two steps are as follows:

1. The removal and pre-concentration of the pollutant species from an aqueous solution (wastewater) by adsorption onto a selective solid adsorbent.
2. The oxidation of the adsorbed pollutant into terminal products (carbon dioxide and water) and simultaneous regeneration of the adsorbent by catalytic dry air oxidation.

Figure 1.7 is a simple schematic diagram illustrating this process.

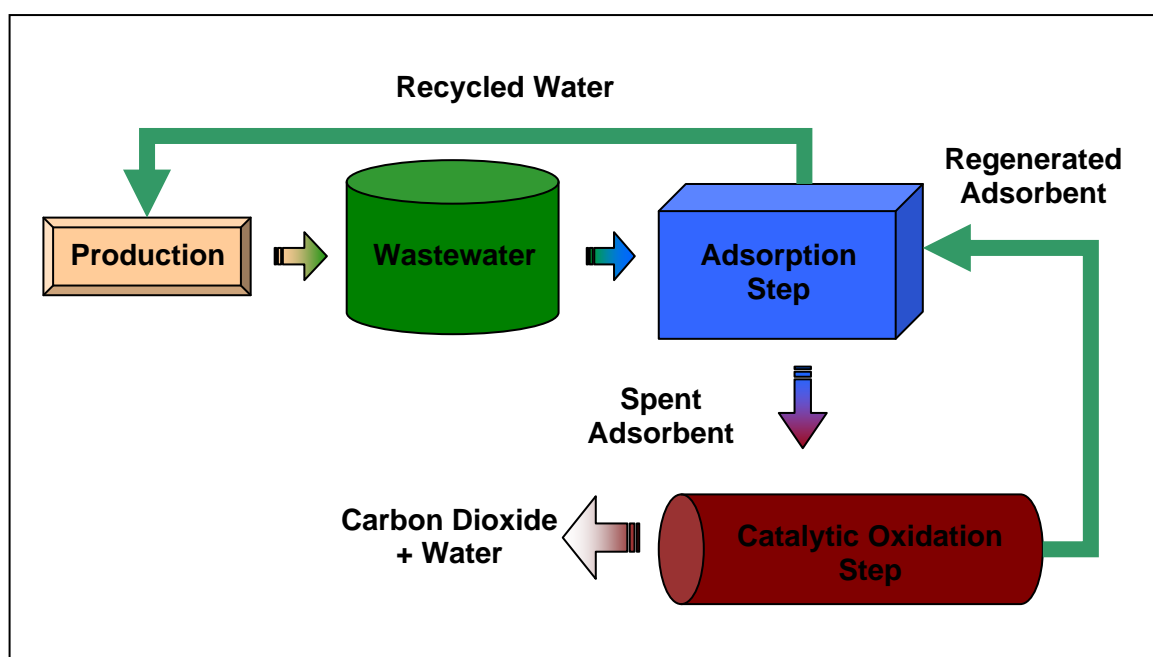


Figure 1.7: Schematic representation of the proposed adsorption/catalytic process

The adsorbent will be prepared so as to facilitate the catalytic adsorption step. The wastewater will enter the adsorption process where the offending organic pollutant will be removed from solution using a zeolite adsorbent. The clean water can then be recycled. The spent zeolite with the pollutant adsorbed onto its surface will be removed.

This second step will oxidize the adsorbed species and the regenerated adsorbent can then be re-used in the adsorption step.

Some possible advantages of a system of this type are:

- Regeneration occurs simultaneously with the catalytic oxidation step, so there is no requirement for a separate adsorbent regeneration step.
- The adsorbent pre-concentrates the pollutant onto a solid, as opposed to treating a large volume of dilute aqueous phase as in WAO.
- Secondary pollutants are less common in catalytic dry oxidation relative to WAO and it is less costly for low concentrations.
- Low adsorption temperatures and pressures mean there is reduced leaching of supported metal catalysts (Wu et al. 2004; Zhao et al. 2004).

In order for this system to work effectively it is necessary for an appropriate zeolite and catalyst to be selected for implementation within the system.

1.6 Adsorption

Sorption is the process in which chemicals become associated with a solid phase. It covers two distinct activities:

- Absorption – Which takes place in a 3 dimensional solid matrix
- Adsorption - Which takes place on a 2 dimensional solid surface

This phase changing process can dramatically affect the way a sorbed chemical can interact with its environment. An adsorbed chemical attached to a solid surface will have different properties when compared to an identical chemical in solution, surrounded by water molecules and ions (Schwarzenbach et al. 1993). It is this quality, particularly with regards to adsorption, which is utilised for wastewater treatment. With the introduction of a solid known as an 'Adsorbent', pollutants will adsorb onto its surface and thus are removed from the liquid or gaseous phases.

Within adsorption there are two major sub divisions. These are; physical adsorption (physisorption) which involves weak van der Waals/Intermolecular interactions with the adsorbent surface, and chemical adsorption (chemisorption) which relates to stronger covalent bonds onto active sites on the adsorbent surface (Atkins 2000).

The level of which a pollutant adsorbs onto the surface of the material depends on its surface properties. These include its surface chemistry relative to that of the target pollutant, heterogeneity and specifically surface area with relation to pore size (Bembnowska et al. 2003). There are three forms of separation active in adsorbents: kinetic which has the fewest applications for waste treatment and is based on difference of diffusion rates for different chemicals through the adsorbent, steric which refers to the sieving qualities of porous adsorbents and how the size of a molecule relates to the size of apertures in an adsorbents crystalline structure, and equilibrium which relates to chemical qualities of the adsorbate such as polarity and dipole moment relative to that of the adsorbent (Yang 2003; Parida et al. 2006).

1.6.1 Adsorbent Materials

The suitability of a material for use as an adsorbent in wastewater treatment is dependent on a number of criteria:

- High affinity and capacity for target compounds
- Regenerability
- Economical and environmentally viable disposal or regeneration
- Tolerance for a wide range of waste parameters (Karcher et al. 2001)

Adsorbents can be derived from a number of sources; both organic and inorganic. However, commercial applications are generally dominated by four primary materials: Activated carbon, zeolites, silica gel and activated alumina (Yang 2003). In recent research a number of novel adsorbents have arisen for the treatment of organics. Amongst these are a group of adsorbents called polymeric resins which will be discussed below. Additionally, new low cost adsorbents derived from industrial/municipal waste products or by products (coal, fly ash, sewage or sludge), modified clays, red muds, and biosorbents have also shown promising results for the adsorption of phenols (Lin and Juang 2009).

Activated Carbon

Activated carbon is by far the most commonly used adsorbent. It has been applied to many different commercial applications. It is used in the purification of a wide variety of gas and liquid phase waste streams and is effective in removing a range of chemicals including many organic pollutants. Its main virtue relative to other adsorbents is its high

micropore and mesopore volumes. This can give it superior adsorption characteristics relative to silica gel, conventional zeolites and others.

Research into existing and novel commercial activated carbons is ongoing. The most common variant is granular activated carbon (GAC). Sulymon and Ahmed investigated the adsorption of phenol and 4-chlorophenol onto GAC under competitive adsorption conditions with furfural. Their research showed a favourable adsorption capacity and the Langmuir isotherm (see Chapter 2) as a representative mathematical model for the adsorption of phenols onto activated carbon (Sulaymon and Ahmed 2008). Kim, Yamato et al. compared commercial activated carbon to carbon cryogel microspheres for the adsorption of phenol and reactive dyes. While they showed good performance for the dyes, the carbon cryogel compared unfavourably in terms of phenol adsorption (Kim et al. 2006). Liao et al. investigated the adsorption of phenolics onto carbon nanotubes (CNTs) undergoing different treatments, finding favourable adsorption on 'pristine multi-walled carbon nano-tubes' as opposed to the acid treated variant (Liao et al. 2008). László examined the adsorption of phenol onto Microporous poly(ethyleneterephthalate) (PET) based activated carbons. Their surface composition was altered using chemical and thermal treatments. Amongst the findings were that increased pH, increased the adsorption capacity and the strength of the interaction of phenol onto the adsorbent surface, with diminishing returns found at pH 11 (László 2005). Table 1.8 summarises some of the recent research into commercial activated carbons.

Table 1.8 Comparison of commercial activated carbons for the adsorption of phenol

<i>Adsorbent</i>	<i>Isotherm Model</i>	<i>pH</i>	<i>Adsorption Capacity</i> (<i>mg g⁻¹</i>)	<i>Reference</i>
GAC	Langmuir	5.7	374.4	(Sulaymon and Ahmed 2008)
CCM200 (carbon cryogel)	Langmuir	-	140	(Kim et al. 2006)
CNTs	Langmuir	-	15.9	(Liao et al. 2008)
APET	Langmuir	5	262	(László 2005)

Activated carbon can be made from a wide range of carbonaceous materials and the properties of the activated carbon differ depending on the material used (Yang 2003). The use of natural sources or waste products for activated carbon precursors can help to reduce the costs (both economic and environmental) of the waste treatment process. Table 1.9 summarizes a number of the synthetic activated carbons in recent literature.

Table 1.9 Comparison of synthetic activated carbons for the adsorption of phenol

<i>Adsorbent</i>	<i>Isotherm Model</i>	<i>pH</i>	<i>Adsorption Capacity</i> (<i>mg g⁻¹</i>)	<i>Reference</i>
ITT Carbon (paper mill sludge)	Freundlich	-	$K_F = 0.44,$ $1/n = 0.87$	(Khalili et al. 2002)
PAC (coffee grounds)	Langmuir	-	3.22	(Namane et al. 2005)
AC (from kraft black liquor)	Langmuir	6	227	(Gonzalez-Serrano et al. 2004)
AC (from corncob)	-	-	177.6	(El-Hendawy et al. 2001)
CS850A (from coconut shell)	-	-	205.8	(Mohd Din et al. 2009)

A major failing of activated carbon systems is their poor resistance to continued regeneration. After the adsorption process, spent adsorbent material must either be cleaned through regeneration or disposed of, depending on which is more economically or environmentally viable. Conventional regeneration methods are either thermal in the presence of steam, carbon dioxide or an inert atmosphere, or chemical such as those involving solvents or a rapid pH swing. These methods are generally time and energy consuming as well as damaging to the adsorbent which reduces its adsorption capacity (Ania et al. 2007). In thermal regeneration this damage could amount to 5-15% of activated carbon along with a decrease in BET surface area and pore distribution (Ania et al. 2005; Okawa et al. 2007). Thermal regeneration can represent up to 80% of the operating cost of activated carbon systems (Valsaraj et al. 1998). In solvent regeneration residual solvent on the adsorbent can reduce adsorption capacity (Okawa et al. 2007). An additional issue is the generation of carbon fines, caused by the brittle nature of activated carbon adsorbents (Lin and Juang 2009).

Silica Gel

Silica gels are a group of amorphous, polar, mesoporous adsorbents (>20Å pore size). They are most commonly used as a desiccant as the Si-OH groups are highly hydrophilic and can adsorb up to 40% of its weight in water. It is synthesised by two primary processes:

1. Aggregation of particles of colloidal silica
2. The sol-gel process

The sol-gel process can produce a diverse range of materials with high surface areas. It involves reactions between water and silicon alkoxides such as methyltrimethoxysilane (MTMS) and trimethylethoxysilane (TMES) (Yang 2003; Štandeker et al. 2007). Aerogels are a type of nanostructured material that can be made via the sol-gel process with certain precursors. They have specific surface areas approaching $1000 \text{ m}^2 \text{ g}^{-1}$, high porosity, good transport to inner layers and controllable hydrophobicity. In order to become more valuable as an adsorbent for toxic organics, the hydrophobic character of the aerogel can be changed by replacing the hydrophilic Si-OH groups with hydrophobic Si-R groups (where $\text{R}=\text{CH}_3$). Aerogels modified in this manner can make

outstanding adsorbents for toxic organics (including toluene, benzene, ethylbenzene, chloroform, 1,2-dichloroethane, xylene and chlorobenzene) with adsorption capacity between 15 and 400 times that of conventional granular activated carbon (Štandeker et al. 2007). Adsorption is further increased by phenomena such as the possible swelling of aerogel granules during adsorption causing the volume to increase. Aerogels are highly reusable, after inert gas regeneration at 100°C in excess of 20 cycles (Štandeker et al. 2007). However, the initial precursor agents need to be used in large quantities and along with the supercritical fluid drying method; can make aerogels quite costly (Bhagat et al. 2007).

Roostaei and Handan Tezel performed a comparative study on the adsorption of phenol on a number of adsorbents including silica gel and found no significant adsorption of phenol (Roostaei and Handen Tezel 2004).

Metal Oxides

Metal oxides such as alumina, zirconia and ferric oxy-hydroxides represent a cheap alternative adsorbent to granular activated carbon and silica gels. Alumina is commonly used for the removal of anionic surfactants from wastewaters. When the alumina is rendered unusable, this surfactant coated exhausted alumina can be used to remove organics from the aqueous phase through a process called adsolubilization (Lin and Juang 2009). When activated in this way they can possess good surface areas, tuneable surface properties and good mechanical strength. However their viability for use in organic wastewater treatment is severely hampered by their hydrophilic interactions. Research into hemimicelles surfactant modified metal oxides shows that the affinity for organic compounds can be increased; however the adsorption capacity is somewhat lower than other commercial adsorbents such as granular activated carbon (Matatov-Meytal and Sheintuch 1998; Valsaraj et al. 1998; Adak et al. 2006).

Adak et. al examined surfactant modified alumina for its ability to remove phenol. 90% removal was achieved under pH optimized conditions and the desorption of phenol was possible using acetone or rectified spirit (Adak et al. 2006). The adsorption characteristics are shown in Table 1.10.

Metal oxides are often used as candidates for combined adsorption and oxidation treatment processes due to their ability to be modified with transition and noble metal catalysts (Garetto et al. 2007).

Table 1.10 Adsorption characteristics of phenol onto sodium dodecyl sulphate modified alumina

<i>Adsorbent</i>	<i>Isotherm Model</i>	<i>pH</i>	<i>Adsorption Capacity (mg g⁻¹)</i>	<i>Reference</i>
SDS-alumina	Langmuir	6.7	6.6	(Adak et al. 2006)

Polymeric Resins

Non-ionic polymer resins are a large family of sorbents proficient in the removal of organic compounds in water. Since 1987, around 75% of polymeric resins were used for this purpose and since 1982, styrene/DVB polymers were shown to have 5 to 10 times the adsorption capacity for some organics relative to conventional activated carbon. Structurally polymer resins are clusters of microgel particles between 0.01 and 15 µm in size. These particles agglomerate into small microspheres. Pore size is usually mesoporous and microporous. The micropore levels depend on cross linking which is determined by the amount of divinylbenzene (DVB) in the polymeric resin (Yang 2003). Polymeric resins have a number of advantages in that they are predominantly microporous, have good intraparticle mass transport, good physical and chemical stability and surface functionality (Lee et al. 2005). Polymeric resins adsorb without functional groups, so adsorption is typically in the form of weak van der Waals interactions (Ku and Lee 2000). They are however simple to regenerate chemically using acids, bases and organic solvents or alternatively with steam or hot gases (Lee et al. 2005).

The most widely used polymeric resin is Amberlite XAD-4 (polystyrene-divinylbenzene and although proven as a good adsorbent for phenol, is extremely hydrophobic and experiences reduced adsorption capacity for ionic organic molecules as a result. The addition of polar functional groups such as esters in the case of XAD-7, can create a tailored hydrophilic alternative (Zeng et al. 2009).

Part of the recent research into polymeric resins has gone into the development of polar post cross linked polymeric adsorbents to increase the surface area and the viability for polar adsorbates. Zeng et al., for example, compared the commercial polymer resins XAD-4 and AB-8, to a hydrophobic macroporous copolymer precursor (PDM-1) and its post crosslinked counterpart (PDM-2) for their phenol adsorption capacity (Zeng et al. 2009). Similarly, Huang compared XAD-4 to the hypercrosslinked adsorbent HJ-1 (Huang 2009). In both cases the crosslinked adsorbent was found to have superior adsorption capacity for phenol compared to the conventional adsorbents. Ersöz et al. examined the adsorption of phenols onto a molecularly imprinted polymer. Methacrylamidoantipyrine (MAAP) was imprinted with nitrophenol to increase its selective adsorption capacity for phenols (Ersöz et al. 2004). Amberlite XAD-16 was examined under various adsorption conditions by Aburri, amongst the results were a repeatable method of regeneration, which over a small number of cycles was found to lead to no loss of adsorption capacity (Aburri 2003). Pan et al. studied the removal of phenols from industrial waste streams onto fixed beds using the macroreticular resin NDA-100.

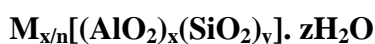
A summary of recent research into phenol adsorption onto polymeric adsorbents is shown in Table 1.11.

Table 1.11 Comparison of various polymeric resins for the adsorption of phenol.

<i>Adsorbent</i>	<i>Isotherm Model</i>	<i>Adsorption Capacity (mg g⁻¹)</i>	<i>Reference</i>
XAD-4	Freundlich	$K_F = 2.293$ $n = 1.870$	(Zeng et al. 2009)
AB-8	Freundlich	$K_F = 0.859$ $n = 1.629$	
PDM-1	Freundlich	$K_F = 1.682$ $n = 1.824$	
PDM-2	Freundlich	$K_F = 5.632$ $n = 2.226$	
HJ-1	Langmuir	167.8	(Huang 2009)
MAAP	K_d	6.2	(Ersöz et al. 2004)
XAD-16	Langmuir	141	(Abburi 2003)
NDA-100	Langmuir	207.7	(Pan et al. 2005)

Zeolites

Zeolites are crystalline aluminosilicates containing alkali metals. Their composition can be expressed by the following formula:



Where x and y are integers, M is the extra-structural cation with valence n and z is the number of water molecules per unit cell.

Zeolites were discovered in 1756 with the first naturally occurring zeolite ‘stilbite’. Since then at least 40 different natural varieties have been discovered and approximately 150 have been artificially synthesised. Their high specific surface, rigid three

dimensional structure and cation exchange capacity makes them effective adsorbents (Bowman 2003; Yang 2003). The zeolite framework structure is composed of vertex-linked aluminium and silicon tetrahedra which form channels and cavities. Each of the aluminium tetrahedra has one negative charge; this facilitates the incorporation of compensating (charge balancing) cations and water molecules. Zeolites are formed from a silicon and aluminium source which is 'aged' with a templating agent and then heated. This templating agent is an anion or cation of a specific shape which determines the shape of the tetrahedral framework. The pore size of the zeolite structure depends largely on the templating agent used during synthesis; for example to obtain micropores (<1.2 nm) an organic base such as TEA (tetraethyl ammonium) is used, whereas liquid crystal templates are used to obtain mesopores (>1.2 nm) (Dann 2000).

Zeolites are often categorised by the number of tetrahedra that constitute the rings of the pore or channel. An 8, 10 or 12 membered ring corresponds to the terms small, medium and large. Any more than 12 members and the zeolite is classed as 'super large pore'. Due to the size of the relevant molecules, medium and large pore zeolites are predominantly used for adsorption and catalysis applications (Weitkamp 2000).

Figure 1.8 shows a 2 dimensional wireframe cross section of a medium pore zeolite. Each joint represents a silica or alumina tetrahedron, with the connecting lines representing the oxygen links between each tetrahedron. Each pore in this example contains 10 such tetrahedra, identifying it as medium pore.

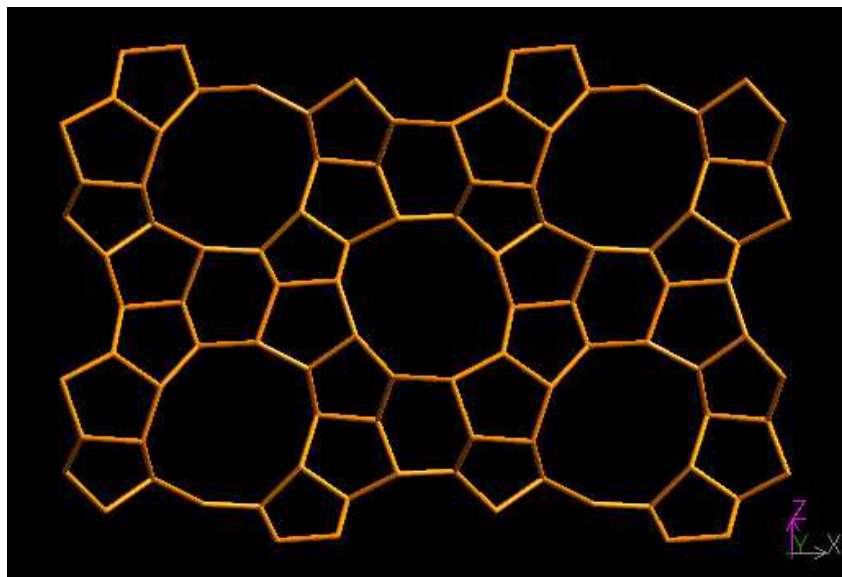


Figure 1.8 Diagram showing the basic 2 dimensional structure of a medium pore zeolite (MFI), with 10 membered rings ("Database of zeolite structures" 2008).

By far, the largest application for both natural and artificial zeolites is as ion exchangers, often for removing toxic or radioactive heavy metals from solution. In this the compensating cation (e.g. alkali metal ions) in the zeolite structure readily exchanges with the heavy metal ions (Dann 2000; Okolo et al. 2000). Catalysis and adsorption make up a smaller proportion of zeolite use. H-zeolites are the acidic derivative of zeolites. These are usually created by ion exchange with ammonium salts followed by thermal treatment at 500°C to remove the ammonia and create an H-zeolite. This product is catalytically active due to acid sites on the zeolite structure and is used in a number of industrial processes (Dann 2000). This acid-catalytic activity is most associated with the Brønsted sites on the zeolite, it is doubtful as to whether Lewis acid sites have any substantial role in zeolite acid catalysis (Weitkamp 2000). Brønsted sites occur in zeolites at the negative charge in the lattice created where the trivalent cation (usually Al^{3+}) isomorphically replaces Si^{4+} creating a negative charge and an associated charge balancing proton (Corma 2003).

Large surface areas, low cost, ease of regeneration and small pores make zeolites good selective adsorbents for organic chemicals and water. Adsorption from aqueous solution depends not only on the pore structure of the zeolite but also on the competition between the organic adsorbate and water for the adsorption site. Increasing framework silica causes the zeolite to exhibit a more hydrophobic effect; this can affect the adsorption of molecules based on their affiliation with water (Shu et al. 1997c).

To date there has been research into the adsorption of phenol onto a number of zeolitic adsorbents. One of the earlier examples was a comparative adsorption study performed by Kawai and Tsutsumi. The zeolites Na-ZSM-5 and Na-Y were examined for the adsorption of surfactants with phenol as a comparison, with a range of silica to alumina ratios. Phenol was found to adsorb on hydrophobic Na-Y with a Type V isotherm (see chapter 2). The hydrophobic-hydrophilic character of the zeolites was at this point already recognised as having an important role in their use as adsorbents (Kawai and Tsutsumi 1995). Recognising that a pre requisite to the adsorption of organic molecules from aqueous solution was their hydrophobicity, Shu et al. compared three adsorbents for the adsorption of phenols: silicalite, zeolite beta and pillared clay modified with a non-ionic surfactant. Silicalite has a zeolitic structure reminiscent of ZSM-5, but typically has much higher silica to alumina ratios, making it significantly more hydrophobic. Due to this effect, silicalite was observed to be the best adsorbent of the three for molecular phenol but excluded larger molecules due to its comparatively small pore size (Shu et al. 1997b). Okolo et al. looked into the adsorption of phenol 2-chlorophenol and 3-chlorophenol onto three adsorbents in an agitated batch system. The zeolites Na-Y and Ni/Na-Y were compared with activated carbon. In this case, activated carbon was found to exhibit superior adsorption with all 3 adsorbates as well as taking less time to achieve equilibrium (2-4 hours) relative to the zeolites. The presence of Na^+ or Ni^{2+} as the charge balancing cation was found to have little effect on adsorption except in the case of chlorophenol uptake, where the monovalent cation achieved improved adsorption capacity. Increased pH was found to aid adsorption in all situations (Okolo et al. 2000). In the research performed by Roostaei and Tezel, two other commercial high silica zeolite structures: HiSiv 1000 (Y-Faujssite type structure) and HiSiv 3000 (ZSM-5 type structure) were compared to silica gel, activated carbon and two kinds of activated alumina. It was found that the HiSiv zeolites, which were originally designed for high humidity air vents, had much better adsorption capacities than silica gel and activated alumina, as well as no significant drop in capacity after 14 regeneration cycles. However, the adsorption capacity of activated carbon was found to be several times larger (Roostaei and Handen Tezel 2004).

Khalid et al. examined a range of different conventional zeolites for the adsorption of phenol and again compared them with an activated carbon. Three large pore zeolites

where used (HFAU, HBEA and HMOR) and one medium pore zeolite (MFI). A broad range of silica to alumina ratios were chosen, the highest of which was a completely siliceous BEA zeolite ($\text{Si/Al} = \infty$), this was found to be the best performing adsorbent for phenol and was easily regenerated in the presence of air at 400°C at a rate of 2°C a minute (Khalid et al. 2004). Ghiaci et al. prepared ‘organo-zeolites’ by modifying the natural zeolite clinoptilolite and the synthetic zeolite ZSM-5(MFI) with the quaternary amines hexadecyltrimethylammonium (HDTMA) and cetylpyridium bromide (CPB). Also included in this research was the synthetic mesoporous silicate MCM-41. It was found that the removal of phenol by MCM-41 exceeded ZSM-5 and Clinoptilolite (Ghiaci et al. 2004). The research undertaken by Yousef et al. using Jordanian natural zeolite, highlighted two distinct types of interaction between phenol and the zeolite surface. The first was a pH independent interaction between the aromatic ring of the phenol molecule and the hydrophobic sites of the zeolite. The second is pH dependent and represents the complexation of the phenolate ion with the metal cations on the hydrophilic sites on the zeolite surface (Yousef and El-Esweed 2009). Table 1.12 summarises the performance of a number of the zeolites and zeolitic silicates mentioned for the adsorption of phenol from aqueous solutions.

Table 1.12 Comparison of various zeolites and silicates for the adsorption of phenol.

<i>Adsorbent</i>	<i>Isotherm Model</i>	<i>Adsorption Capacity (mg g^{-1})</i>	<i>Reference</i>
Na-Y	Langmuir	75.2	(Okolo et al. 2000)
HiSiv-1000 (Y-Structure)	Langmuir- Freundlich	319	(Roostaei and Handen Tezel 2004)
BEA(∞)	Langmuir	160	(Khalid et al. 2004)
HDTMA- Clinoptilolite	Langmuir	11.4	(Ghiaci et al. 2004; Lin and Juang 2009)
ZSM-5-31 (HDTMA-Zeolite)	Langmuir	7.4	
MCM-41	Langmuir	59.4	
Jordanian Tuff	Zeolitic Langmuir	41.078	(Yousef and El-Esweed 2009)

1.6.2 Zeolite Beta

The proposed zeolitic adsorbent for use in this project is Zeolite Beta. Zeolite Beta was first synthesised by Wadlinger et al. in 1967, but a natural counterpart was also discovered in 1990 (Wadlinger et al. 1967; Szostak 1998). It is designated a high silica zeolite with a silica to alumina ratio ranging from 5:1 to over 500:1 (Bregolato et al. 2007).

Zeolite Beta is composed of the disordered intergrowth of three related structures known as polymorph A (tetragonal), polymorph B (monoclinic) and polymorph C (monoclinic). Polymorph A is chiral and consists of two conversely rotated enantiomorphs while B and C are achiral. These polymorphs are permeated by a three dimensional network of 12 membered channels. Two perpendicular straight channels intersect to form a tortuous sinusoidal channel (shown in Figure 1.10). The dimensions of the identical linear channels are 0.73 x 0.6 nm for polymorph A and 0.73 x 0.68 nm for polymorph B. The tortuous channel system formed by the intersections of the two linear channels has approximate dimensions of 0.56 x 0.56 nm for polymorph A and 0.55 x 0.55 nm for polymorph B. A summary of the zeolite dimensions is displayed in Table 1.13. As polymorphs A and B intergrow the adjacent layers shift to form helical 12 ring straight channels (Smirniotis and Ruckenstein 1993; Tang et al. 2008). Zeolite beta is classed as a large pore zeolite due to the 12 membered rings that constitute its channels. The twelve membered rings are visible in Figure 1.9.

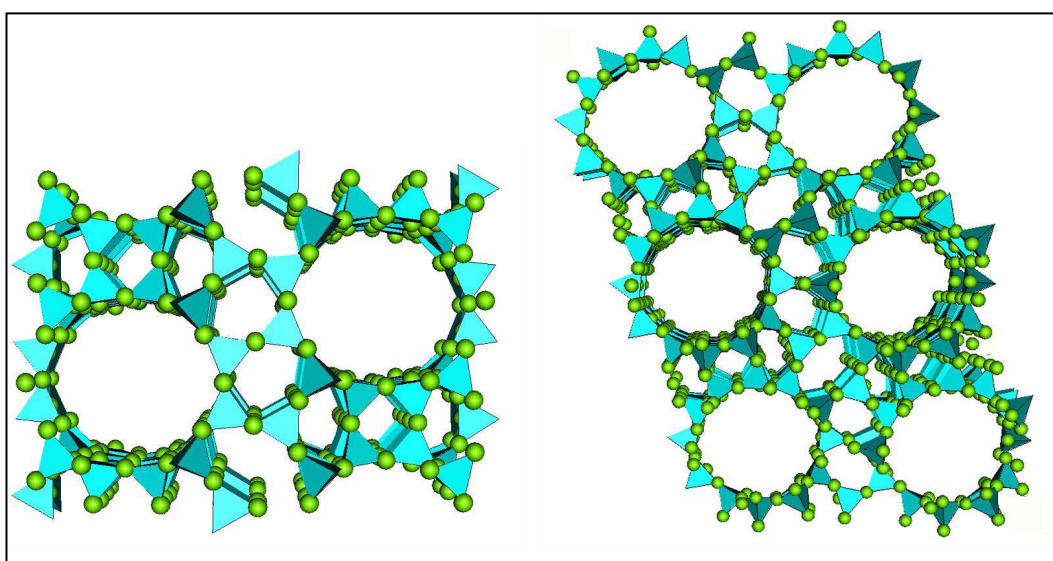


Figure 1.9: Diagram of Polymorphs A and B in zeolite beta

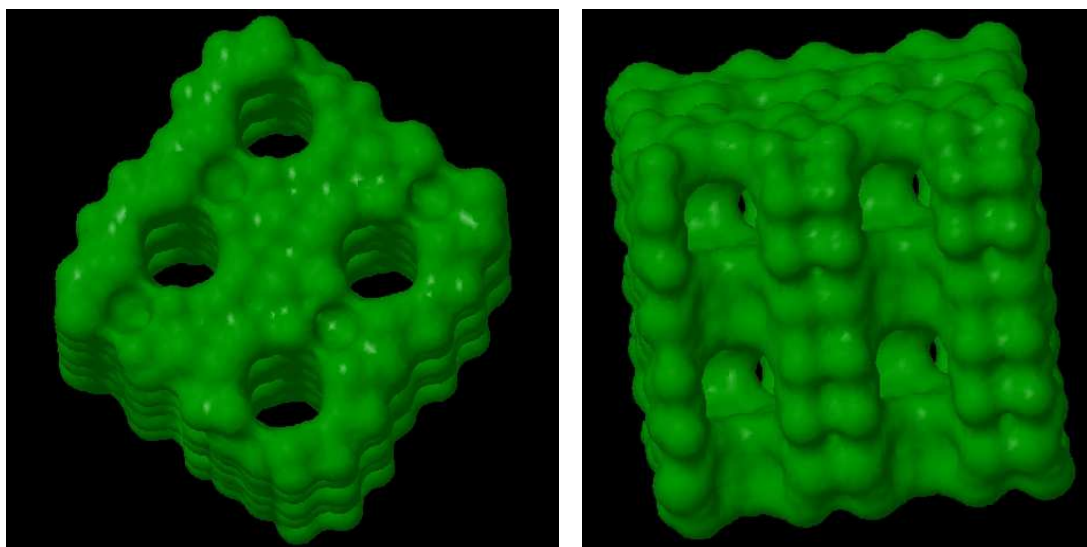


Figure 1.10 3D diagrams of beta zeolite structure showing framework wrap around ionic radii. Diagram on the left shows straight channels, diagram on the right is rotated to show perpendicular tortuous channels ("Database of zeolite structures" 2008).

Table 1.13 : Common pore dimension and surface area statistics for Zeolite Beta (Smirniotis and Ruckenstein 1993; Ali et al. 2002; Bregolato et al. 2007; Ding et al. 2007)

<i>Polymorph</i>	<i>Pore Diameter: Straight channels (nm)</i>	<i>Pore Diameter: Tortuous channels (nm)</i>	<i>BET Surface area (m² g⁻¹)</i>	<i>Micropore volume (cc g⁻¹)</i>	<i>Total Pore volume (cc g⁻¹)</i>
Polymorph A	0.73 x 0.6	0.56 x 0.56	400 - 570	0.06 - 0.13	0.44 - 0.93
Polymorph B	0.73 x 0.68	0.55 x 0.55			

Zeolite beta is commonly used as an acid catalyst in a number of organic synthesis processes including: hydroisomerization, hydrocracking, aromatic alkylation and disproportionation (Ding et al. 2007).

1.7 Oxidation

The segregation of the aqueous adsorption step from the oxidation step allows the oxidation of the adsorbed organic to take place in the presence of air without the high pressures typically required in wet air oxidation. The complete gas phase oxidation of adsorbed phenol may be possible with the catalytic potential of the zeolite alone, however the introduction of a catalytic component into the zeolite can further decrease

the activation energy and allow the oxidation to take place at lower and more economical temperatures and residence times.

1.7.1 Catalysts

The ability of zeolites as well as other solids, to be modified by metals and metal oxides can greatly increase their performance as catalysts. In wet air oxidation the presence of the metal based catalytic component either propagates the formation of free radicals from the reactant (homolytic oxidation) or an ionic environment (heterolytic oxidation). In the case of phenols these oxidation mechanisms result in a ring opening reaction (Matatov-Meytal and Sheintuch 1998).

In oxidation systems the support, in this case the zeolite serves three important roles in the catalytic system.

- It increases the surface of the metal or metal oxide by providing a matrix that enables their dispersion as very small particles.
- It inhibits the sintering of the active catalyst material and improves its hydrophobicity and its thermal, hydrolytic and chemical stability.
- The support stability is critical, as it will govern the useful lifetime of a catalyst.

Reports on the dry air oxidation of phenols are relatively few however other systems have been extensively examined.

Supported metal oxides such as CuO, CoO, Cr₂O₃, NiO, MnO₂, Fe₂O₃, YO₂, Cd₂O₃, ZnO, TiO₂ and Bi₂O₃ have all been examined for their catalytic wet oxidation of phenol, with CuO proving to be the most effective. However, they are somewhat less effective than solid metal catalysts which can yield improved reaction rates and lower reactor temperatures in wet air oxidation (Matatov-Meytal and Sheintuch 1998). These can include: transition metals such as rhodium, copper and nickel, noble metals such as platinum and palladium.

The use of zeolite supported metals for the catalytic decomposition and selective reduction of nitrous oxide has been extensively verified. These include copper, palladium, nickel and platinum loaded zeolites such as ZSM-5 (MFI), Beta, Y (Torre-

Abreu et al. 1997b; Huuhtanen et al. 2005), mordenite and KL (Ho et al. 1998). Copper is especially valued due to the reduced formation of N_2O (de Oliveira et al. 2009). Supported bimetallic catalysts have also been observed for NO_x SCR in the presence of organics. Copper is a common constituent, combined with other metals such as Mn, Ni, Pd, Co, Cr. These bimetallic catalysts exhibit reduced light off temperature and increased selectivity (Öhman et al. 2002).

Copper modified solids in particular are shown to yield good performance in dry and wet air oxidation, in the former reducing the formation of side products such as CO and NO_x , and exhibiting less leaching in the latter (Centi et al. 2000). For example in the presence of peroxide, copper modified ZSM-5 was shown to be effective for the wet oxidation of phenols (Maduna Valkaj et al. 2007)

Noble metals have been studied extensively, and can show greater activity at lower temperatures when compared to metal oxides, although they are generally more expensive. Of the noble metals, platinum shows the highest activity in relation to the catalytic wet air oxidation of phenol (Neyestanaki et al. 1994; Matatov-Meytal and Sheintuch 1998). In studies involving high silica zeolites, copper and platinum catalysts in dry oxidation where shown to yield good catalytic combustion efficiency for the complete oxidation of propane and for platinum alone; ethane, propane and butane. (Neyestanaki et al. 1994; Garetto et al. 2007). Catalytic activity for platinum supported on zeolites is also superior to metal oxide supports (Garetto et al. 2007).

1.8 Summary of Aims

The aim of this work is to develop a stable, solid and regenerable material for the adsorption and subsequent oxidation of phenol. With zeolite beta acting as the adsorbent and support, it will be modified with catalyst metals in order to improve its oxidative effect. Ideally the finished solid will be resistant to leaching in solution, maintain a good adsorption capacity and completely oxidise the pollutant under reasonable temperature conditions. The studies covered in this thesis will cover the following areas:

- The adsorption of phenol onto zeolite beta and relevant isotherm models under a number of conditions to examine the effects of:
 - Temperature
 - pH
 - Kinetics
 - Silica to alumina ratio
- The modification of zeolite beta with copper and platinum, including an analysis of:
 - Preparation techniques
 - Copper loading on the zeolite
 - Aqueous stability
 - Adsorption capacity and isotherms of the modified zeolite
- The characterisation of the modified zeolite, including:
 - BET surface area analysis
 - Temperature Programmed Reduction
 - X-Ray Diffraction
- The catalytic oxidation of phenol on the modified zeolite, including:
 - Temperature Programmed Oxidation
 - The effect of repeat adsorption and oxidation steps.

1.9 References

- Abburi, K. (2003). *Adsorption of phenol and p-chlorophenol from their single stage and bisolute aqueous solutions on Amberlite-16 resin*. Journal of Hazardous Materials **B105**: 143-156.
- Adak, A., A. Pal and M. Bandyopadhyay (2006). *Removal of phenol from water environment by surfactant-modified alumina through adsolubilization*. Colloids and Surfaces A: Physicochemical and Engineering Aspects **277**: 63-68.
- Ali, M. A., T. Tatsumi and T. Masuda (2002). *Development of heavy oil hydrocracking catalysts using amorphous silica-alumina and zeolites as catalyst supports*. Applied Catalysis A: General **233**: 77-90.
- Altunlu, M. and S. Yapar (2007). *Effect of OH/Al^{3+} and $\text{Al}^{3+}/\text{clay}$ ratios on the adsorption properties of Al-pillard bentonites*. Colloids and Surfaces A: Physicochemical Engineering Aspects **306**: 88-94.
- Amat, A. M., A. Arques, M. A. Miranda, S. Seguí and R. F. Vercher (2007). *Degradation of rosolic acid by advanced oxidation processes: ozonation vs. solar photocatalysis*. Desalination **212**: 114-122.
- Ania, C. O., J. B. Parra, J. A. Menéndez and J. J. Pis (2007). *Microwave-assisted regeneration of activated carbons loaded with pharmaceuticals*. Water Research **41**(15): 3299-3306.
- Ania, C. O., J. B. Parra, C. Pevida, A. Arenillas, F. Rubiera and J. J. Pis (2005). *Pyrolysis of activated carbons exhausted with organic compounds*. Journal of Analytical and Applied Pyrolysis **74**: 518-524.
- Atkins, P. W. (2000). *Physical Chemistry*. Oxford, Oxford University Press.
- Atwater, J. E., J. R. Akse, J. A. McKinnis and J. O. Thompson (1997). *Low temperature aqueous phase catalytic oxidation of phenol*. Chemosphere **34**(1): 203-212.
- Bembnowska, A., R. Pelech and E. Milchert (2003). *Adsorption from aqueous solutions of chlorinated organic compounds onto activated carbons*. Journal of Colloid and Interface Science **265**: 276-282.
- Bhagat, S. D., Y. Kim, M. Moon, Y. Ahn and J. Yeo (2007). *A cost-effective and fast synthesis of nanoporous SiO_2 aerogel powders using water-glass via ambient pressure drying route*. Solid State Sciences **9**: 628-635.
- Bowman, R. S. (2003). *Application of surfactant-modified zeolites to environmental remediation*. Microporous and Mesoporous Materials **61**: 43-56.

- Bregolato, M., V. Bolis, C. Busco, P. Upliendo, S. Bordiga, F. Cavani, N. Ballarini, L. Maselli, S. Passeri, I. Rossetti and L. Forni (2007). *Methylation of phenol over high-silica beta zeolite: Effect of zeolite acidity and crystal size on catalyst behaviour*. *Journal of Catalysis* **245**: 285-300.
- Busca, G., S. Berardinelli, C. Resini and L. Arrighi (2008). *Review: Technologies for the removal of phenol from fluid streams: A short review of recent developments*. *Journal of Hazardous Materials* **160**: 265-288.
- Centi, G., M. Gotti, S. Perathoner and F. Pinna (2000). *Rinse water purification using solid regenerable catalytic adsorbents*. *Catalysis Today* **55**: 51-60.
- Chmielewski, A. G. and M. Haji-Saeid (2004). *Radiation technologies: past, present and future*. *Radiation Physics and Chemistry* **71**: 16-20.
- Official Journal of the European Communities(2000) "*Commission Decision of 17 July 2000 on the implementation of a European pollutant emission register (EPER) according to Article 15 of Council Directive 96/61/EC concerning integrated pollution prevention and control (IPPC)*", The Commission of the European Communities: 36-43.
- Corma, A. (2003). *State of the art and future challenges of zeolites as catalysts*. *Journal of Catalysis* **216**: 298-312.
- Dann, S. E. (2000). *Reactions and Characterization of Solids*. Cambridge, The Royal Society of Chemistry.
- "Database of zeolite structures."(2008).International Zeolite Association - Structure Commission, from <http://www.iza-structure.org/>.
- de Oliveira, M. L. M., C. M. Silva, R. Moreno-Tost, T. L. Farias, A. Jiménez-López and E. Rodríguez-Casellón (2009). *A study of copper exchanged mordenite natural and ZSM-5 zeolites as SCR-NO_x catalysts for diesel road vehicles: Simulation by neural networks approach*. *Applied Catalysis B: Environmental* **88**: 420-429.
- Ding, L., Y. Zheng, Y. Hong and Z. Ring (2007). *Effect of particle size on the hydrothermal stability of zeolite beta*. *Microporous and Mesoporous Materials* **101**: 432-439.
- Eckenfelder, W. W. (1989). *Industrial Water Pollution Control*, McGraw-Hill, Inc.
- Eksperiandova, L. P., I. I. Fokina, A. B. Blank, T. I. Ivkova and B. P. Soukhomlinov (1999). *Determination of small quantities of phenol in water*. *Analytica Chimica Acta* **396**: 317-320.

- El-Hendawy, A. N. A., S. E. Samra and B. S. Girgis (2001). *Adsorption characteristics of activated carbons obtained from corncobs*. Colloids and Surfaces A: Physicochemical Engineering **180**: 209-221.
- Ersöz, A., A. Denizli, I. Sener, A. Atilir, S. Deiltemiz and R. Say (2004). *Removal of phenolic compounds with nitrophenol-imprinted polymer based on π - π and hydrogen-bonding interactions*. Separation and Purification Technology **38**: 173-179.
- "The European Pollutant Emissions Register - Pollutants" (2006) European Environment Agency
- "The European Pollutant Emissions Register - Questions to EPER" (2006) European Environment Agency
- "The European Pollutant Emissions Register - What is EPER?" (2006) European Environment Agency
- "The European Pollutant Release and Transfer Register" (2010) European Environment Agency
- European Risk Assessment Report: Phenol, 1st Priority List (2006). European Chemicals Bureau, Institute for Health and Consumer Protection. **64**.
- Fierro, V., V. Torné-Fernandez, D. Montané and A. Celzard (2008). *Adsorption of phenol onto activated carbons having different textural and surface properties*. Microporous and Mesoporous Materials **111**: 276-284.
- Garetto, T. F., E. Rincón and C. R. Apesteguía (2007). *The origin of the enhanced activity of Pt/zeolites for combustion of C₂-C₄ alkanes*. Applied Catalysis B: Environmental **73**: 65-72.
- Ghiaci, M., A. Abbaspur, R. Kia and F. Seyedejn-Azad (2004). *Equilibrium isotherm studies for the sorption of benzene, toluene, and phenol onto organo-zeolites and as-synthesized MCM-41*. Separation and Purification Technology **40**: 217-229.
- Gimeno, O., M. Carbajo, F. J. Beltran and F. Rivas (2005). *Phenol and substituted phenols AOPs remediation*. Journal of Hazardous Materials **B119**: 99-108.
- Goncharuk, V. V., D. D. Kucheruk, V. M. Kochkodan and V. P. Badekha (2002). *Removal of organic substances from aqueous solutions by reagent enhanced reverse osmosis*. Desalination **143**: 45-51.
- González-Muñoz, M. J., S. Luque, J. R. Álvarez and J. Coca (2003). *Recovery of phenol from aqueous solutions using hollow fibre contactors*. Journal of Membrane Science **213**: 181-193.

- Gonzalez-Serrano, E., T. Cordero, J. Rodriguez-Mirasola, L. Cotoruelo and J. J. Rodriguez (2004). *Removal of water pollutants with activated carbons prepared from H_3PO_4 activation of lignin from kraft black liquors*. *Water Research* **38**: 3043-3050.
- Greiner, E. and C. Funada (2008). *Chemical Economic Handbook: Phenol*, SRI Consulting.
- Hirakawa, T., T. Daimon, M. Kitazawa, N. Ohguri, C. Koga, N. Negishi, S. Matsuzawa and Y. Nosaka (2007). *An approach to estimating photocatalytic activity of TiO_2 suspension by monitoring dissolved oxygen and superoxide ion on decomposing organic compounds*. *Journal of Photochemistry and Photobiology A: Chemistry* **190**: 58-68.
- Ho, L., C. Hwang, J. Lee, I. Wang and C. Yeh (1998). *Reduction of platinum dispersed on dealuminated beta zeolite*. *Journal of Molecular Catalysis A: Chemical* **136**: 293-299.
- Huang, J. (2009). *Treatment of phenol and p-cresol in aqueous solution by adsorption using carbonylated hypercrosslinked polymeric adsorbent*. *Journal of Hazardous Materials* **168**(2-3): 1028-1034.
- Huuhtanen, M., K. Rahkamaa-Tolonen, T. Maunula and R. L. Keiski (2005). *Pt-loaded zeolites for reducing exhaust gas emissions at low temperatures and in lean conditions*. *Catalysis Today* **100**: 321-325.
- Jordan, W., H. van Barneveld, O. Gerlich, M. Kliene-Boymann and J. Ullrich (2002). *Ullmann's Encyclopedia of Industrial Chemistry*, Wiley-VCH Verlag.
- Judd, S. and B. Jefferson (2003). *Membranes for Industrial Wastewater Recovery and Re-Use*. Oxford, Elsevier Ltd.
- Kamble, S. P., P. A. Mangrulkar, A. K. Bansawal and S. S. Rayalu (2008). *Adsorption of phenol and o-chlorophenol on surface altered fly ash based molecular sieves*. *Chemical Engineering Journal* **138**(1-3): 73-83.
- Karakulski, K., M. Gryta and A. W. Morawski (2001). *Pilot plant studies on the removal of trihalomethanes by composite reverse osmosis membranes*. *Desalination* **140**: 227-234.
- Karcher, S., A. Kornmüller and M. Jekel (2001). *Screening of commercial sorbents for the removal of reactive dyes*. *Dyes and Pigment* **51**: 111-125.
- Kawai, T. and K. Tsutsumi (1995). *Adsorption characteristics of surfactants and phenol on modified zeolites from their aqueous solutions*. *Colloid Polymer Science* **273**: 787-792.

- Khalid, M., G. Joly, A. Renaud and P. Magnoux (2004). *Removal of Phenol from Water by Adsorption Using Zeolites*. *Industrial Engineering and Chemistry Research* **43**: 5275-5280.
- Khalili, N. R., J. D. Vyas, W. Weangkaew, S. J. Westfall, S. J. Parulekar and R. Sherwood (2002). *Synthesis and characterization of activated carbon and bioactive adsorbent produced from paper mill sludge*. *Separation and Purification Technology* **26**: 295-304.
- Kim, S., T. Yamamoto, A. Endo, T. Ohmori and M. Nakaiwa (2006). *Adsorption of phenol and reactive dyes from aqueous solution on carbon cryogel microspheres with controlled porous structure*. *Microporous and Mesoporous Materials* **96**(1-3): 191-196.
- Ku, Y. and K. Lee (2000). *Removal of phenols from aqueous solution by XAD-4 resin*. *Journal of Hazardous Materials* **80**(1-3): 59-68.
- Kujawski, W., A. Warszawski, W. Ratajczak, T. Porebski, W. Capala and I. Ostrowska (2004). *Removal of phenol from wastewater by different separation techniques*. *Desalination* **163**: 287-296.
- László, K. (2005). *Adsorption from aqueous phenol and aniline solutions on activated carbons with different surface chemistry*. *Colloids and Surfaces A: Physiochemical and Engineering Aspects* **265**(1-2): 32-39.
- Lee, J., H. Jung, D. Kwak and P. Chung (2005). *Adsorption of dichloromethane from water onto a hydrophobic polymer resin XAD-1600*. *Water Research* **39**: 617-629.
- Liao, Q., J. Sun and L. Gao (2008). *The adsorption of resorcinol from water using multi-walled carbon nano tubes*. *Colloids and Surfaces A: Physiochemical and Engineering Aspects* **312**(2-3): 160-165.
- Lin, S. and R. Juang (2009). *Adsorption of phenol and its derivatives from water using synthetic resins and low-cost adsorbents: A review*. *Journal of Environmental Management* **90**: 1336-1349.
- Maduna Valkaj, K., A. Katovic and S. Zrncevic (2007). *Investigation of the catalytic wet peroxide oxidation of phenol over different types of Cu/ZSM-5 catalyst*. *Journal of Hazardous Materials* **144**: 663-667.
- Marc-Loudon, G. (1995). *Organic Chemistry*, Benjamin/Cummings.
- Martin, D. I., I. Margaritescu, E. Cirstea, I. Togoe, D. Ighigeanu, M. R. Nemptanu, C. Oproiu and N. Iacob (2005). *Application of accelerated electron beam and microwave irradiation to biological waste treatment*. *Vacuum* **77**: 501-506.

- Matatov-Meytal, Y. I. and M. Sheintuch (1998). *Catalytic Abatement of Water Pollutants*. Industrial Engineering and Chemistry Research **37**: 309-326.
- Mohd Din, A. T., B. H. Hameed and A. L. Ahmad (2009). *Batch adsorption of phenol onto physiochemical-activated coconut shell*. Journal of Hazardous Materials **161**: 1522-1529.
- Namane, A., A. Mekarzia, K. Benrachedi, N. Belhaneche-Bensemra and A. Hellal (2005). *Determination of the adsorption capacity of activated carbon made from coffee grounds by chemical activation with $ZnCl_2$ and H_3PO_4* . Journal of Hazardous Materials **B119**: 189-184.
- Neyestanaki, A. K., N. Kumar and L. Lindfors (1994). *Catalytic combustion of propane over Pt and Cu modified ZSM-5 zeolite catalysts*. Fuel **74**(5): 690-696.
- *Occupational Safety and Health Guideline for Phenol*. (1996). US Department of Labour, Occupational Safety & Health Administration.
- Öhman, L. O., B. Ganemi, E. Björnbom, K. Rahkamaa, R. L. Keiski and J. Paul (2002). *Catalyst preparation through ion-exchange of zeolite Cu-, Ni-, Pd-, CuNi- and CuPd-ZSM-5* Materials Chemistry and Physics **73**: 263-267.
- Okawa, K., K. Suzuki, T. Takeshita and K. Nakano (2007). *Regeneration of granular activated carbon with adsorbed trichloroethylene using wet peroxide oxidation*. Water Research **41**: 1045-1051.
- Okolo, B., C. Park and M. A. Keane (2000). *Interaction of phenol and chlorophenols with activated carbon and synthetic zeolites in aqueous media*. Journal of Colloid and Interface Science **226**: 308-317.
- Otero, M., M. Zabkova and A. E. Rodrigues (2005). *Comparitive study of the adsorption of phenol and salicylic acid from aqueous solution onto nonionic polymeric resins*. Separation and Purification Technology **45**: 86-95.
- Ozaki, H. and H. Li (2001). *Rejection of organic compounds by ultra-low pressure reverse osmosis membrane*. Water Research **36**(1): 123-130.
- Pan, B. C., F. W. Menga, X. Q. Chen, B. J. Pan, X. T. Li, W. M. Zhang, X. Zhang, J. L. Chena, Q. X. Zhang and Y. Sun (2005). *Application of an effective method in predicting breakthrough curves of fixed-bed adsorption onto resin adsorbent*. Journal of Hazardous Materials **B124**: 74-80.
- Parida, S. K., S. Dash, S. Patel and B. K. Mishra (2006). *Adsorption of organic molecules on silica surface*. Advances in Colloid and Interface Science **121**: 77-110.
- Peng, M., L. M. Vane and S. X. Liu (2003). *Recent advances in VOCs removal from water by pervaporation*. Journal of Hazardous Materials **B98**: 69-90.

- Pera-Titus, M., V. García-Molina, M. A. Baños, J. Giménez and S. Esplugas (2004). *Degradation of chlorophenols by means of advanced oxidation processes: a general review*. Applied Catalysis B: Environmental **47**: 219-256.
- Pinto, R. T. P., L. Lintomen, L. F. L. Luz Jr. and M. R. Wolf-Maciel (2005). *Strategies for recovering phenol from wastewater: thermodynamic evaluation and environmental concerns*. Fluid Phase Equilibria **228-229**: 447-457.
- Qu, X., J. Zheng and Y. Zhang (2006). *Catalytic ozonation of phenolic wastewater with activated carbon fibre in a fluid bed reactor*. Journal of Colloid and Interface Science **309**: 429-434.
- "Recovery of high Boiling Point Solvents from Waste Water (phenol)." (2005). QVF Engineering GmbH, from http://www.qvf.com/de/Company_5/documents/P145_e.pdf.
- Ren, S. (2004). *Assessing wastewater toxicity to activated sludge: recent research and developments*. Environmental International **30**: 1151-1164.
- Roostaei, N. and F. Handen Tezel (2004). *Removal of phenol from aqueous solutions by adsorption*. Journal of Environmental Management **70**(2): 157-164.
- Sampa, M. H. O., P. R. Rela, A. L. Casas, M. N. Mori and C. L. Duarte (2004). *Treatment of industrial effluents using electron beam accelerator and adsorption with activated carbon: a comparative study*. Radiation Physics and Chemistry **71**: 457-460.
- Schmidt, R. J. (2005). *Industrial catalytic processes - phenol production*. Applied Catalysis A: General **280**: 89-103.
- Schwarzenbach, R. P., P. M. Gschwend and D. M. Imboden (1993). *Environmental Organic Chemistry*. New York, John Wiley & Sons, Inc.
- Shu, H. T., D. Li, A. A. Scala and Y. H. Ma (1997). *Adsorption of small organic pollutants from aqueous streams by aluminosilicate-based microporous materials*. Separation and Purification Technology **11**(1): 27-36.
- Smirniotis, P. G. and E. Ruckenstein (1993). *Comparison between zeolite β and $Y-Al_2O_3$ supported Pt*. Journal of Catalysis **140**: 562-542.
- Sonune, A. and R. Ghate (2004). *Developments in wastewater treatment methods*. Desalination **167**: 55-63.
- Štandeker, S., Z. Novak and Ž. Knez (2007). *Adsorption of toxic organic compounds from water with hydrophobic silica aerogels*. Journal of Colloid and Interface Science **310**: 362-268.

- Sulaymon, A. H. and K. W. Ahmed (2008). *Competitive adsorption of furfural and phenolic compounds onto activated carbon in fixed bed column*. Environmental Science and Technology **42**: 392-397.
- Szostak, R. (1998). *Molecular Sieves*. London, Blackie Academic and Professional.
- Tang, L., L. Shi, C. Bonneau, J. Sun, H. Yue, A. Ojuva, B. Lee, M. Kritikos, R. G. Bell, Z. Bacsik, J. Mink and X. Zou (2008). *A zeolite family with chiral and achiral structures built from the same building layer*. Nature Materials **7**: 381-385.
- Torre-Abreu, C., M. F. Ribeiro, C. Henriques and F. R. Ribeiro (1997). *Selective catalytic reduction of NO with propene over CuMFI zeolites: dependence on Si/Al ratio and copper loading*. Applied Catalysis B: Environmental **11**: 383-401.
- *Toxicological Review of Phenol EPA/635/R-02/006*. (2002). US Environmental Protection Agency.
- Valsaraj, K. T., P. M. Jain, R. R. Kommalapati and J. S. Smith (1998). *Reusable adsorbents for dilute solution separation. I. Adsorption of phenanthrene on surfactant-modified alumina*. Separation and Purification Technology **13**: 137-145.
- Vázquez, G., J. González-Álvarez, A. I. García, M. S. Freire and G. Antorrena (2007). *Adsorption of phenol on formaldehyde-pretreated Pinus pinaster bark: Equilibrium and Kinetics*. Bioresource Technology **98**: 1535-1540.
- New York(1967) "US Patent No. 3308069". M. O. Corporation. USA.
- Weitkamp, J. (2000). *Zeolites and catalysis*. Solid state Ionics **131**: 175-188.
- Williams, M. E., J. A. Hestekin, C. N. Smothers and D. Bhattacharyya (1999). *Separation of Organic Pollutants by Reverse Osmosis and Nanofiltration Membranes: Mathematical Models and Experimental Verification*. Industrial Engineering and Chemistry Research **38**(10): 3683-3695.
- Wu, R., J. Qu, H. He and Y. Yu (2004). *Removal of azo-dye Acid Red B (ARB) by adsorption and catalytic combustion using magnetic CuFe₂O₄ powder*. Applied Catalysis B: Environmental **48**: 49-56.
- Wu, Z. and M. Zhou (2001). *Partial degradation of phenol by advanced electrochemical oxidation process*. Environmental Science and Technology **35**: 2698-2703.
- Yang, T. R. (2003). *Adsorbents: Fundamentals and Applications*. New Jersey, John Wiley & Sons, Inc.

- Yavuz, Y. and A. Savas Koparal (2005). *Electrochemical oxidation of phenol in a parallel plate reactor using ruthenium mixed metal oxide electrode*. Journal of Hazardous Materials **B136**: 296-302.
- Yousef, R. I. and B. El-Esweed (2009). *The effect of pH on the adsorption of phenol and chlorophenols onto natural zeolite*. Colloids and Surfaces A: Physiochemical and Engineering Aspects **334**: 92-99.
- Zeng, X., Y. Fan, G. Wu, C. Wang and R. Shi (2009). *Enhanced adsorption of phenol from water by novel polar post-crosslinked polymeric adsorbent*. Journal of Hazardous Materials **169**(1-3): 1022-1028.
- Zhao, J., Z. Liu and D. Sun (2004). *TPO-TPD Study of an activated carbon-supported copper catalyst-sorbent used for catalytic dry oxidation of phenol*. Journal of Catalysis **227**: 297-303.
- Zhou, M., Z. Wu, X. Ma, Y. Cong, Q. Ye and D. Wang (2004). *A novel fluidized electrochemical reactor for organic pollutant abatement*. Separation and Purification Technology **34**: 81-88.
- Zhou, M., Z. Wu and D. Wang (2002). *Electrocatalytic degradation of phenol in acidic and saline wastewater*. Journal of Environmental Science and Health **A37**(7): 1263-1275.

Chapter 2

Adsorption of Phenol onto Unmodified Zeolite Beta

2 Adsorption of Phenol onto Unmodified Beta Zeolite

2.1 Introduction

Molecules can attach to the surface of adsorbents through two methods:

- Physisorption – The molecule attaches through Van der Waals forces with no electron transfer. These interactions have a long range but are comparably weak which means the adsorption is easily reversed. Physisorption is not dependent on specific sites on the surface of the solid but more so the magnitude of the surface area. The enthalpy change is low; in the range of 10-20 kJ mol⁻¹ and it is always exothermic. This also means that there is little bond breaking upon adsorption onto the solid and the molecule remains mostly in the same state. The energy released is usually comparable to the enthalpy of condensation. Physisorption occurs relatively fast and unlike chemisorption it can form multiple layers on the surface of the solid.
- Chemisorption – The molecule is attached to the solid by chemical bonds; usually covalent/electrostatic forces and electron transfer. These bonds are shorter but are much stronger than Van der Waals forces and because of this, less reversible. Chemical adsorption is dependent on the number of active sites on the adsorption surface and is limited to a single monolayer. Enthalpy change is much greater, approximately 80-200 kJ mol⁻¹ and with a few exceptions is exothermic. The rate of chemisorption is temperature dependent. Unsatisfied valences on the surface atoms of a solid can tear chemisorbed molecules apart and is one way in which solid surfaces can catalyse reactions (Hagen 1999; Atkins 2000).

The main method of discriminating between these two processes is through a study of the enthalpy change accompanying adsorption. Usually if the enthalpy change is more than (or less negative than) -25 kJ mol⁻¹ it indicates physisorption

is taking place, and if it is less than (more negative than) -40 kJ mol^{-1} it points towards chemisorption (Atkins 2000). The variation of potential energy as an adsorbate molecule approaches the surface of the adsorbent is illustrated in Figure 2.1. As the molecule approaches the adsorbent surface there is a corresponding drop in potential energy as it becomes physisorbed. As the bonds to the surface are formed and then fully stretched, there is a corresponding rise in energy. When the adsorbate to surface bonds contract to their normal size and full strength in the chemisorbed state; there is a sharp decrease in potential energy. As the molecule approaches the surface there is a further increase in potential energy as the bonds adjust. The relative enthalpies of physisorption (ΔH (P)) and chemisorption (ΔH (C)) are illustrated. Physisorption has a much smaller negative enthalpy and occurs further from the surface relative to chemisorption. E_c is the activation energy required for chemisorption (Atkins 2000).

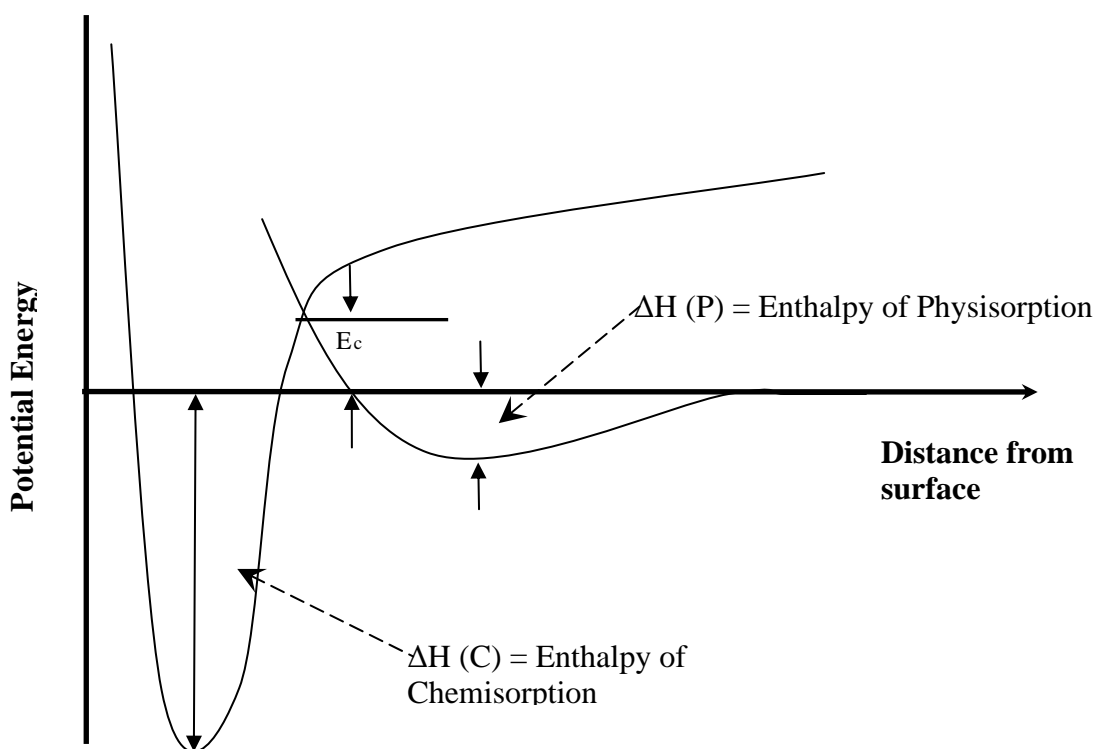


Figure 2.1 Potential Energy Profiles for Adsorption Processes (Atkins 2000).

2.1.1 Adsorption Isotherms

The free adsorbate and the adsorbed fraction are in dynamic equilibrium with each other, the coverage of the surface of the adsorbent depends on the pressure of the overlying gas or the concentration of solution in the liquid phase. So the concentration of adsorbate adsorbed, graphed against the concentration of the adsorbate in solution at a constant temperature constitutes an adsorption isotherm (Atkins 2000). At the thermodynamic equilibrium between adsorbate solution and adsorbent there is no further net adsorption, this usually depends on conditions such as pH, viscosity and temperature. A number of different equilibrium models have been devised to predict the relationship of between adsorbate and adsorbent (Proctor and Toro-Vasquez 1996).

Distribution Coefficient

The simplest form of equilibrium model is the single parameter distribution coefficient (K_d). It is a simple ratio of the quantity of adsorbate adsorbed per gram of adsorbent to the quantity of adsorbate remaining in solution at equilibrium. K_d can be expressed as in Equation 2.1 where C_0 is the initial concentration of adsorbate and C_e is the concentration of the adsorbate at equilibrium.

$$K_d = \frac{C_0 - C_e}{C_e} \quad \text{Equation 2.1}$$

If the equilibrium concentration subtracted from the initial concentration can be said to be representative of the concentration of adsorbate adsorbed onto the surface of the adsorbent, then the equation can be expressed linearly as in Equation 2.2 where Q_e is the concentration adsorbed at equilibrium.

$$Q_e = K_d C_e \quad \text{Equation 2.2}$$

A graph of Q_e on the y axis and C_e on the x axis will generate a straight line with slope K_d .

Brunauer et al. originally classified 5 different isotherm shapes shown in Figure 2.2 and a number of different isotherm models have been derived and applied to adsorption processes (Brunauer et al. 1940).

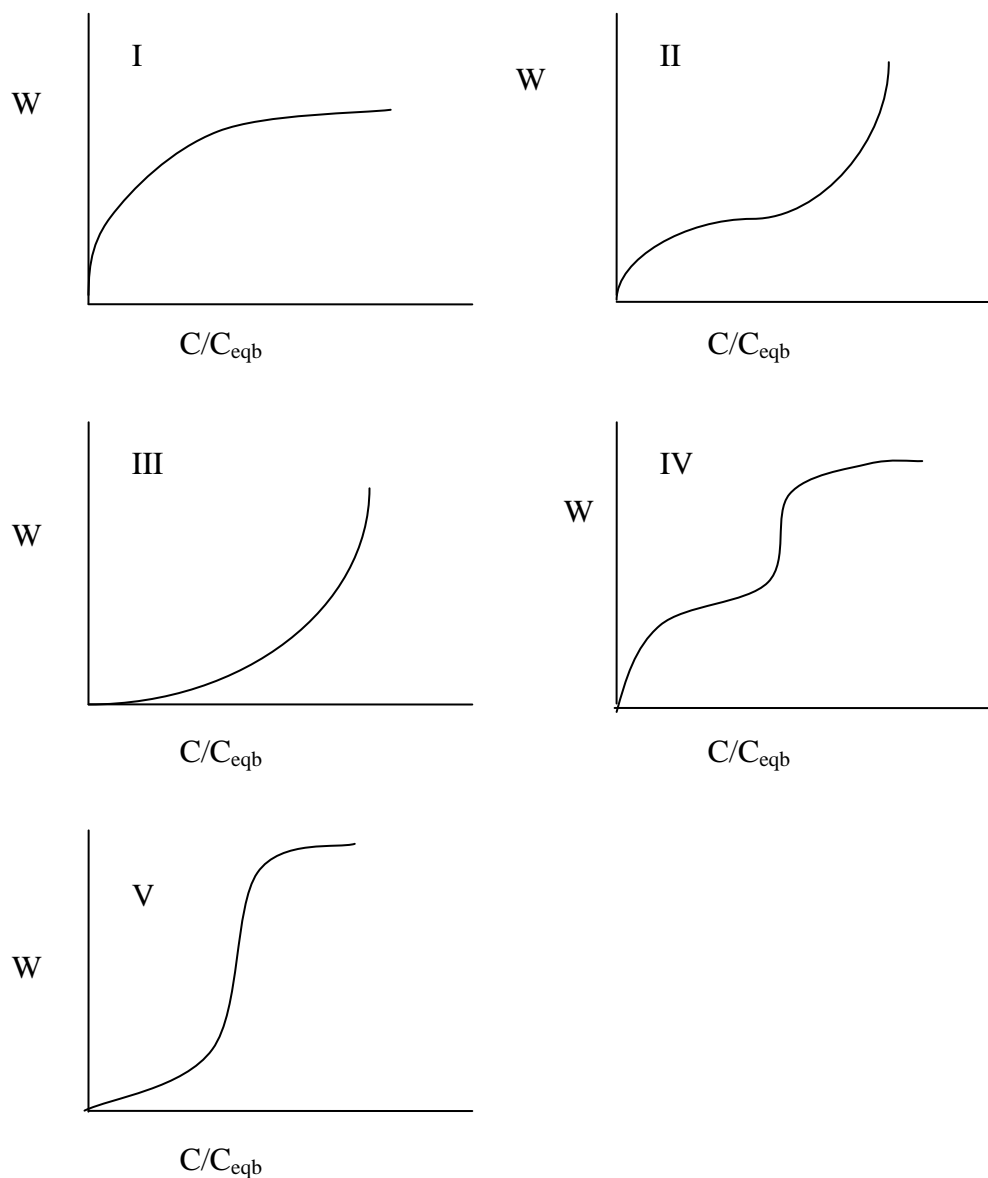


Figure 2.2 The Brunauer classification of isotherms. W is the weight adsorbed, C/C_{eqb} is the relative concentration of the adsorbate at equilibrium.

Type I profiles may occur from either physisorption or chemisorption processes. A plateau is reached where the physically adsorbed species does not significantly exceed the pore diameter of the microporous solid and the micropores become

saturated. In the case of chemical adsorption, the adsorbate has completely occupied all the surface sites.

Type II and III isotherms are usually observed in macroporous adsorbent. They show a progression from monolayer to multilayer adsorption as the adsorbate concentration increases. At the completion of the first monolayer, an inflection point occurs in the type II isotherm. As the concentration increases successive layers will form until saturation where the number of layers becomes infinite. The convex shape of the type III isotherm is due to weak adsorption forces between the adsorbate and adsorbent. Uptake is relatively weak until the first layer is formed and adsorption increases through a stronger interaction between the adsorbate in solution and the already adsorbed layer.

Type IV isotherms occur where two or more surface layers are formed. Usually this results from an increased uptake at higher concentrations as the pores are filled. Similar to type II, the inflection point occurs when the first layer is completed. Type IV isotherms often occur where the adsorbent pore radius ranges between 15-1000 Å.

Type V isotherm combines the small adsorbate-adsorbent interaction potentials of the type III isotherm with the pore size range characteristic of type IV. The inflection point generally occurs at much higher concentrations so that the isotherm reaches a plateau in the multi-layer region. This type of isotherm is attributable to adsorption in coarse mesopores and macropores (Barrer 1978).

Langmuir Isotherm

The most common isotherm expression is the Langmuir isotherm. Derived by Langmuir in 1915, it fits the type I isotherm shape proposed by Brunauer. It was originally developed to describe the adsorption of gas molecules onto metal surfaces but has seen many other successful applications. The Langmuir equation is defined in Equation 2.3 and can be expressed in its linear form as in Equation 2.4.

$$Q_e = \frac{K_L C_e}{1 + A_L C_e} \quad \text{Equation 2.3}$$

$$\frac{C_e}{Q_e} = \frac{1}{K_L} + \frac{A_L}{K_L} C_e \quad \text{Equation 2.4}$$

Where C_e is the aqueous phase sorbate concentration, Q_e is the solid phase adsorbate concentration, and K_L and A_L are the Langmuir isotherm constants. A plot of C_e/Q_e versus C_e gives a straight line graph.

The Langmuir isotherm predicts that adsorption takes place at specific homogeneous sites and that only a monolayer of adsorption takes place on the adsorbent surface. This model assumes that there is one-to-one binding between the adsorbent and adsorbate, which infers that there is a finite quantity of adsorbate that can be adsorbed, meaning that there will be a saturation point at which no further adsorption occurs (Brunauer et al. 1940; Kanô et al. 2000; Wong et al. 2004).

BET Isotherm

Another major isotherm model is the BET (Brunauer Emmett and Teller) isotherm defined in 1938. It incorporates the Type I (Langmuir) and type II isotherm shapes and assumes that multiple layers of adsorption can take place successively over a flat homogeneous adsorbent, each layer attaching itself to preceding layers of adsorbate. It also implies however that the molecules adsorbed do not interact laterally, multiple layers cannot adsorb in between already adsorbed layers and that adsorption capacity increases continuously with increasing concentration (Brunauer et al. 1938a; Brunauer et al. 1940; Cerofolini and Meda 1998).

Freundlich Isotherm

The Freundlich model was described by Freundlich in 1924 as an alternative adsorption model. Unlike the Langmuir isotherm which is theoretical, the Freundlich is experimentally derived (Kanô et al. 2000). It again deals with the possibility of multilayer adsorption but takes into account a heterogeneous

“amorphous” solid using the heterogeneity factor $1/n$ (where n is greater than or equal to 1). The Freundlich isotherm can be expressed empirically as in Equation 2.5. It can be expressed linearly using the natural logarithmic form of the empirical Freundlich equation, as in Equation 2.6.

$$Q_e = K_F C_e^{(1/n)} \quad \text{Equation 2.5}$$

Where K_F is the Freundlich constant and $(1/n)$ is the heterogeneity factor.

$$\ln Q_e = \ln K_F + \frac{1}{n} \ln C_e \quad \text{Equation 2.6}$$

A plot of $\ln Q_e$ on the y axis and $\ln C_e$ on the x axis will give a straight line with the slope $(1/n)$ and the intercept K_F .

The Freundlich isotherm predicts reversible adsorption and like the BET isotherm; predicts continual increase with increasing equilibrium concentration. It is more favourably used over small concentration ranges (Proctor and Toro-Vasquez 1996; Wong et al. 2004). The Freundlich equation has been shown to be mainly useful in the middle of the adsorption isotherm, it has also shown a stronger fit relative to the Langmuir isotherm with regards to the adsorption of organic molecules onto activated carbon from aqueous solution (Kanô et al. 2000).

Generalised Langmuir-Freundlich Isotherm

The generalised Langmuir-Freundlich isotherm is also sometimes applied. It takes into account that some adsorption systems correspond best to the Langmuir and Freundlich at different concentration ranges. It accommodates a heterogeneous solid as in the Freundlich model but with a finite saturation point as in Langmuir (Cheung et al. 2000; Yang 2003). With three isotherm parameters it is no longer possible to derive using linear regression. The empirical formula is shown in Equation 2.7.

$$Q_e = \frac{K_L (C_e)^{(1/n)}}{1 + A_L (C_e)^{(1/n)}} \quad \text{Equation 2.7}$$

Toth Isotherm

The Toth isotherm was first suggested by Toth in 1971 for the adsorption of vapours on solids, but it has been adapted for use in solution based adsorption systems (Toth 1971). In some situations the Freundlich isotherm may not provide a good fit at the high and low ends of the concentration scale, in such situations the Toth isotherm is popular as it satisfies both end limits (Terzyk et al. 2003). The empirical formula for the Toth Isotherm is shown in Equation 2.8.

$$Q_e = \frac{Q_0 b C_e}{[1 + (b C_e)^{nt}]^{(1/nt)}} \quad \text{Equation 2.8}$$

Where Q_0 is the maximum adsorption density, b is the adsorption affinity and nt is the Toth exponent.

Polanyi Isotherm

The Polanyi theory was developed in 1914 to describe gas adsorption onto activated carbon (Polanyi 1914). It was successively developed by Dubinin, Manes et al. into a theory of the volume of micropores and a model for aqueous adsorption onto activated carbon, respectively (Dubinin 1960; Manes and Hofer 1969). Because of this it is often referred to as the Polanyi-Dubinin-Manes (PDM) model. The Polanyi model has found wide application in the adsorption of organics onto a range of adsorbents including: activated carbon, zeolites, soils, organoclays and polymeric resins (Xu et al. 2007). The Polanyi model is expressed in Equation 2.9.

$$Q_e = Q_0 10^{-A[\log(S_w / C_e)]^B} \quad \text{Equation 2.9}$$

Where S_w is the aqueous solubility of the adsorbent material, A and B are the Polanyi isotherm parameters.

Linear Partitioning

In some cases involving the adsorption of organic adsorbates onto hydrophobic adsorbents such as organoclays, partitioning occurs between the hydrophobic bulk of the adsorbent and the solution. This may occur at a point after the adsorption sites on the surface of the solid are saturated. The effect is for a proportionate increase in apparent adsorption capacity after a certain concentration threshold. Non-linear adsorption isotherm models can be adapted to take this into account by adding a linear element to the equation; this is referred to as a dual-mode isotherm expression. For example the Langmuir isotherm with linear partitioning is shown in Equation 2.10.

$$Q_e = \frac{K_L C_e}{1 + A_L C_e} + K_d C_e \quad \text{Equation 2.10}$$

2.1.2 Thermodynamics of Adsorption

The Gibbs function (free energy) of an adsorbate (A) in solution at any concentration (C) can be expressed as:

$$G_L = G_L^\circ + nRT \ln C_A \quad \text{Equation 2.11}$$

Or alternatively the Gibbs function can be given in molar terms as:

$$\mu_L = \mu_L^\circ + RT \ln \frac{C_A}{C_A^\circ} \quad \text{Equation 2.12}$$

Where:

μ_L = the chemical potential of the liquid phase

μ_L° = the standard chemical potential of the liquid phase

C_A° = the concentration of adsorbate in solution under standard conditions

During adsorption, it is necessary to consider the surface layer which consists of the adsorbent and adsorbate as being in a single phase and having the general properties of a solution. The condition for equilibrium between the adsorbed layer and the bulk solution phase can be described as follows in Equation 2.13.

$$\mu_A = \mu_L \quad \text{Equation 2.13}$$

Where:

μ_A = the chemical potential of the adsorbed layer

When Equation 2.13 is incorporated into Equation 2.12, a relationship between the Gibbs free energy of the adsorbed layer and the adsorbate in solution can be found.

$$\mu_A = \mu_A^o + RT \ln \frac{C_A}{C_A^o} \quad \text{Equation 2.14}$$

The enthalpy change resulting from the adsorption process can be established through the Gibbs-Helmholtz relationship, which shows the temperature dependence of the chemical potential of the adsorbed layer.

$$\left(\frac{\partial(\mu_A/T)}{\partial T} \right) = \frac{-H_A}{T^2} \quad \text{Equation 2.14}$$

Where

H_A = the enthalpy of the adsorbed layer

Substitution of Equation 2.15 into Equation 2.14 gives the following:

$$\frac{-H_A}{T^2} = \frac{-H_L^o}{T^2} + R \left(\frac{\partial \ln C_A}{\partial T} \right)_w \quad \text{Equation 2.15}$$

Where:

H_L^o = the standard enthalpy of the solution phase at a constant adsorbed weight (W)

When rearranged, Equation 2.15 can give an expression that relates the enthalpy change resulting from the adsorption process to the adsorbed adsorbate concentration with varying temperature.

$$\left(\frac{\partial \ln C_A}{\partial T} \right)_w = \frac{H_L^o - H_A}{RT^2} \quad \text{Equation 2.16}$$

If we assume that the standard enthalpy of the bulk solution is independent of composition then H_L^o is equal to H_L and therefore Equation 2.16 can be rewritten as:

$$\left(\frac{\partial \ln C_A}{\partial T} \right)_w = \frac{\Delta H_{ads}}{RT^2} \quad \text{Equation 2.17}$$

Where:

ΔH_{ads} = the enthalpy change resulting from adsorption

Assuming that the adsorbent in the adsorbed phase and that the heat capacity of the bulk of the solution phase are negligible, then the enthalpy change of adsorption ΔH_{ads} is independent of temperature and as a result Equation 2.17 can be integrated to generate the following equation:

$$\ln C_A = \text{constant} - \left(\frac{\Delta H_{ads}}{RT} \right) \quad \text{Equation 2.18}$$

From Equation 2.18 it is possible to plot $\ln C_A$ versus $1/T$ in order to derive a straight line, the slope of which corresponds to the enthalpy divided by R .

The Gibbs free energy of adsorption can be derived from using the isotherms equilibrium constant K , where R is the gas constant and T is the temperature of adsorption.

$$\Delta G_{ads} = -RT \ln K \quad \text{Equation 2.19}$$

ΔG relates to the change in surface energy resulting from adsorption or is required for the adsorption process to occur. If ΔG is less than zero its value is proportional to the amount of energy obtained and the reaction is spontaneous, however if ΔG is greater than zero then its value is proportional to energy required and it is non-spontaneous.

The entropy change of adsorption is a measure of disorder or randomness on the adsorption surface before and after adsorption. A negative entropy change represents an increase in surface order and a decrease in the freedom of an adsorbed species. A positive entropy change represents an increase in order. It also can relate to the effects of temperature and the stability of the adsorbed species on the solid surface (Schwarzenbach et al. 1993; Kim et al. 2007b).

Entropy change for adsorption can be derived using the Gibbs free energy equation for a constant temperature (Ramachandran et al. 2005).

$$\Delta S_{ads} = \frac{\Delta H_{ads} - \Delta G_{ads}}{T} \quad \text{Equation 2.20}$$

Each of these thermodynamic properties is interdependent so there are finite number of basic configurations that can occur relative to each other as outlined in Table 2.1.

Table 2.1 Potential configuration of thermodynamic properties

ΔG	ΔH	ΔS
(-)	(-)	(+)
(-)	(-)	(-)
(-)	(+)	(+)
(+)	(+)	(-)

2.1.3 pH

As with temperature, the pH of solution can greatly affect the performance of an adsorption system. Changes in the pH can alter the ions in solution, the ionic state of the adsorbate and the surface properties of the adsorbent. As highlighted in section 1.1.1 the pK_a of phenol is 9.95. The Henderson–Hasselbalch equation shown in Equation 2.21 in conjunction with the pK_a allows the relationship between pH and the ionic equilibrium of a chemical to be determined. In the case of phenol, in all pH values below pH 9.95 ($pK_a > pH$) the ratio of phenol to its ionic form (the phenolate anion) will be in favour of its unionized state. In pHs greater than 9.95 ($pK_a < pH$) the opposite will be true. The ionic state may affect the manner in which phenol interacts with the zeolite surface, depending on the type of bonding interaction. In Kamble et al., the formation of phenolate ions at high pHs was cited as a possible cause for reduced adsorption onto fly ash based zeolites (Kamble et al. 2008). Phenolate anions are known to be more soluble in water and should be more difficult to remove from solution due to the stronger

bonds with water that must be broken. Conversely the unionized phenol molecule will adsorb poorly onto polar surface sites due to the adsorption competition with water (Busca et al. 2008).

$$pH = pK_a + \log \left[\frac{Base}{Acid} \right] \quad \text{Equation 2.21}$$

Low pHs may also increase the amount of positively charged sites on the adsorbent surface which may increase the chances of adsorption through electrostatic interaction from an acidic organic chemical. Conversely higher pHs decrease the amount of protonated sites. If this trend is not present it can indicate the activity of other adsorption pathways such as covalent chemisorption or physisorption. High and low pHs can cause the formation of OH^- and H^+ ions in solution which can also compete for sites with the adsorbate. (Namasivayam and Kavitha 2002; Tsai et al. 2006; Kamble et al. 2008).

2.1.4 Kinetics Models

The speed of adsorption is dependent on how well the adsorbent can dissipate the energy of the incoming adsorbate particles. If the energy is not quickly dissipated then the particle will eventually return to solution, so the probability of a colliding particle adsorbing is proportional to the rate at which the adsorbent surface is covered (Atkins 2000). On a practical scale, adsorption rate can also be affected by experimental parameters such as: adsorbent/adsorbate concentration, temperature of solution, pore structure/infrastructure, surface properties and particle size. The importance of determining the rate of adsorption for wastewater treatment is so that the residence time needed to reach adsorption equilibrium can be derived. A short residence time can allow for greater volumes to pass through a smaller system.

Kinetics models are useful tools for determining kinetics parameters for adsorption studies and for the determination of adsorption mechanisms. The first rate order equation to be dedicated specifically to liquid/solid systems and one of the most widely used is the pseudo first order Lagergren equation, developed in

1898. It is generally expressed in its linear form as in Equation 2.22. (k_1) is the pseudo first order rate constant and (q_e) and (q_t) are the quantities adsorbed per unit weight of adsorbent at equilibrium and time (t) respectively.

$$\frac{dq_t}{dt} = k_1(q_e - q_t) \quad \text{Equation 2.22}$$

However this differs from the true first order equation in that ' $k_1(q_e - q_t)$ ' does not represent the number of available sites. After integration and by applying boundary conditions for $t = 0$ and $q = 0$, Equation 2.22 becomes Equation 2.23 (Ho and McKay 1999).

$$\log(q_e - q_t) = \log q_e - \left(\frac{k_1 t}{2.303} \right) \quad \text{Equation 2.23}$$

$\log q_e$ is an adjustable parameter and doesn't represent the intercept in a plot of $\log(q_e - q_t)$ vs. t as it would be in a true first order process. The Lagergren pseudo first order equation does not fit well for the whole range of contact time so it is necessary to either experimentally extrapolate data to $t = \infty$ or treat Q_e (the adsorption capacity at equilibrium) as an adjustable parameter to be determined by trial and error (Ho and McKay 1998).

The pseudo second order model can often provide a better representation for the entire reaction, where as the Lagergren may only fit for the initial reaction step. It also has the advantage of not requiring the assignation of an effective sorption parameter; the values of k and h can be determined without knowing any parameter beforehand.

Where the sorption capacity is assumed to be proportional to the number of active sites, the pseudo second order rate equation can be written as in Equation 2.24.

$$\left(\frac{dq_t}{dt}\right) = k(q_e - q_t)^2 \quad \text{Equation 2.24}$$

Integrating, rearranging and applying the boundary conditions $t = 0$ to $t = t$ and $q_t = 0$ to $q_t = q_t$ gives Equation 2.25.

$$\frac{t}{q_t} = \frac{1}{h} + \frac{1}{q_e}t \quad \text{Equation 2.25}$$

This can then be solved for the initial sorption rate h in Equation 2.26.

$$h = k_2 q_e^2 \quad \text{Equation 2.26}$$

(Ho and McKay 1999; Zou et al. 2006)

2.1.5 Silica to Alumina Ratio

Altering the ratio of silica to alumina in the zeolite structure can affect the adsorption and catalytic performance of zeolites (Armaroli et al. 2006). This is usually achieved by removing framework aluminium using acid treatment (Shu et al. 1997a). The Si/Al ratio is never less than 1 but there is no upper limit and it is possible to form pure silica zeolite structures. The alumina rich zeolite structures have a much higher affinity for water than the hydrophobic zeolite structures of high Si/Al ratios. This means that water soluble organic molecules can be competing with water molecules for hydrogen bonding onto surface groups on low silica zeolites (Roostaei and Handen Tezel 2004; Terzyk 2004). In lower ratios however there are more cations in the structure to balance the difference between the Si^{4+} and Al^{3+} ions. This balance increases the heterogeneity of the zeolite surface which may attract more polar molecules such as phenol (Roostaei and Handen Tezel 2004). Reducing the number of aluminium sites will also reduce the number of exchangeable ions on the zeolite surface.

2.1.6 Surface area analysis

The Brunauer, Emmet and Teller equation (B.E.T.) was developed in order to determine the surface area of a solid (Brunauer et al. 1938b). The solid is characterised by the weak physical adsorption of gases onto the solid surface. This is achieved through an isotherm representing the equilibrium of gas adsorbed on the solid at a fixed temperature and as a function of pressure. The volume of gas adsorbed is plotted against P/P_o (P is the pressure, P_o is the saturation pressure at the measurement temperature). At low pressures (P/P_o is less than 0.1) monolayer formation follows the Langmuir isotherm. However it is difficult to determine the point where there is exactly monolayer coverage as multilayer physisorption starts before monolayer coverage is complete. To address this the B.E.T. equation (Equation 2.27) extends the Langmuir isotherm to multilayer adsorption

$$\frac{P}{V(P_o - P)} = \frac{1}{V_m C} + \frac{(C - 1)P}{C V_m P_o} \quad \text{Equation 2.27}$$

$V =$ The volume, reduced to standard conditions (STP), of gas adsorbed per unit mass of adsorbent at a given pressure, P and constant temperature

$P_o =$ The saturation pressure at the measurement temperature

$V_m =$ The volume of gas adsorbed at STP per unit mass of adsorbent, when the surface is covered by a unimolecular layer of adsorbate

$C =$ The equilibrium constant

From Equation 2.27, a plot of $P/V(P_o - P)$ versus P/P_o should yield a straight line in the form $y = M.x + I$. The slope ' M ' of the straight line along with the intercept ' I ' gives two equations from which V_m can be obtained.

$$M = \frac{(C - 1)}{V_m C} \quad \text{Equation 2.28}$$

$$I = \frac{1}{V_m C} \quad \text{Equation 2.29}$$

$$V_m = \frac{1}{M + I} \quad \text{Equation 2.30}$$

From these the surface area is then calculated using:

$$S_{BET} = \frac{V_m A_m N_A}{V_{mol}} \quad \text{Equation 2.31}$$

Where: N_A = Avogadro's number (6.023×10^{23})

V_{mol} = Molar volume of adsorbate gas at STP (22.4 l mol^{-1})

A_m = Cross sectional area of adsorbed gas

(A_m for $N_2 = 0.162 \text{ nm}^2$)

Thus when nitrogen is the adsorbate gas, Equation 2.31 reduces to:

$$S_{BET} = 4.353 V_m \quad \text{Equation 2.32}$$

The B.E.T. equation (Equation 2.27) is applicable within a relative pressure range of $0.05 < P/P_o < 0.3$. At higher relative pressures, the B.E.T. equation is usually inaccurate due to the effects of capillary condensation in the smallest micropores (Baiker, 1985).

In this chapter the commercial adsorbent Zeolite Beta, will be examined for its ability to adsorb the model pollutant phenol from water. Its adsorption

characteristics and optimal adsorption conditions shall be ascertained through the examination of the effects of solution pH, thermodynamics, kinetics and the effect of altering framework silica to alumina ratio. The work in this chapter will also attempt to determine a suitable adsorption model for phenol adsorption onto Zeolite Beta.

2.2 Experimental

2.2.1 Materials

Powdered Zeolite Beta was supplied by Zeolyst International. A number of variants with different $\text{SiO}_2:\text{Al}_2\text{O}_3$ ratios were used: H- β -25, H- β -75, H- β -150 and H- β -300. Phenol crystals $\geq 99.5\%$ were supplied by Fluka. Variable phenol concentrations were made using stock solutions of 1g of phenol crystals made up to 1 liter with distilled water (1000 mg dm^{-3}).

2.2.2 Adsorption Studies

Batch adsorption studies were carried out using a fixed zeolite weight and variable phenol concentrations. 200 mg of zeolite powder was added to 50 ml centrifuge flasks followed by 20 ml of phenol solution. The centrifuge flasks were attached to an Analogue Orbital shaker for the required contact period (1 hour). The centrifuge flasks were then centrifuged in a Hettich Rotofix 32 centrifuge at 6000 rpm for 20 min to separate the zeolite from solution. Subsequently 10 ml of the supernatant was removed. The phenol concentration in this solution was determined using a Shimadzu UV-160IPC UV-Visible spectrophotometer at 270 nm against a standard range of solutions with known phenol concentrations. Figure 2.3 shows a typical calibration graph for phenol at 270 nm. Controls using phenol alone were used to ensure reproducibility. Distilled water was used as the solvent.

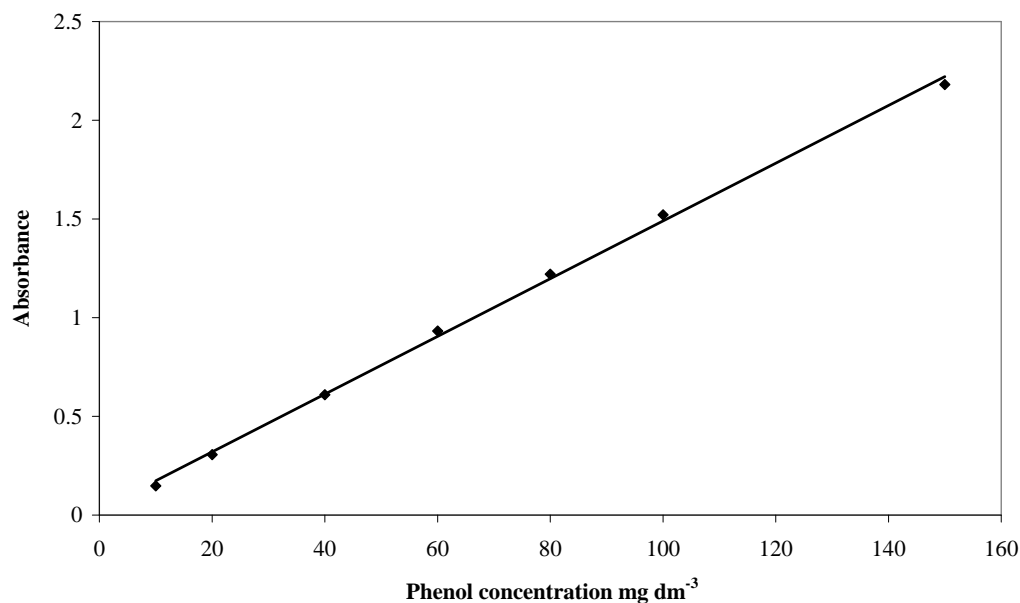


Figure 2.3 UV-Vis spectrophotometer calibration graph for phenol at 270 nm. R^2 value 0.999.

2.2.2.1 Kinetics Studies

For the kinetics study phenol adsorption was examined on Zeolite Beta with a $\text{SiO}_2:\text{Al}_2\text{O}_3$ ratio of 25:1 over a period of 180 minutes. Measurements were taken at 0, 10, 30, 60, 120 and 180 minutes. Three different phenol concentrations were used: 50, 100 and 200 mg dm^{-3}

2.2.2.2 pH Studies

Phenol adsorption on H- β -25 was examined over a pH range between 2 and 12 in a 100 mg dm^{-3} phenol solution with a contact time of 1 hour. The pH of the solution was lowered and raised using concentrated HCl (ACS 37%) and NH_4 (ACS 30%) respectively. The pH was measured using a Thermo Orion model 420A+ pH meter.

2.2.2.3 Adsorption Isotherms

The effects of changing temperature and the thermodynamic parameters were studied using H- β -25 at 4 different solution temperatures: 283 K, 294 K, 313 K and 333 K. The temperature was kept constant throughout the residence time using hotplates for higher temperatures and ice slush baths for lower temperatures. The IsoFit Isotherm Fitting software was used to fit experimental data to a range of isotherm models. IsoFit determines isotherm parameters from given experimental data sets. It does this by minimizing the weighted sum of squared errors between experimental data and the computed isotherm values (Oyanedel-Craver et al. 2007). It uses a hybrid “heuristic-plus-regression” search algorithm and calculates a wide range of diagnostic and statistical measures. It supports more isotherms than many of its contemporaries, including dual-mode isotherms and in comparative tests with MS-Solver it achieved comparable or superior fits to a variety of isotherms (Shawn Matott and Radibeau 2008).

2.2.3 Adsorbent Characterisation

The samples were characterized by nitrogen gas adsorption/desorption isotherms using a Quantachrome Autosorb AS-1 gas sorption system in order to determine surface area and pore volume. Samples were pretreated under vacuum at 300°C for 18 hours before analysis. The apparent surface areas of the zeolites were measured using the Brunauer-Emmett-Teller (BET) (Brunauer et al. 1940) method, the mesopore volume by the Barret-Joyner-Halenda (BJH) (Barrett et al. 1951) method, and the micropore volume by the Dubinin-Radushkevich (DR) (Dubinin et al. 1947) method.

2.3 Results and Discussion

Generally, adsorption is dependent on the interaction between three components: The adsorbent, adsorbate and solvent. This relationship is loosely illustrated in Figure 2.4.

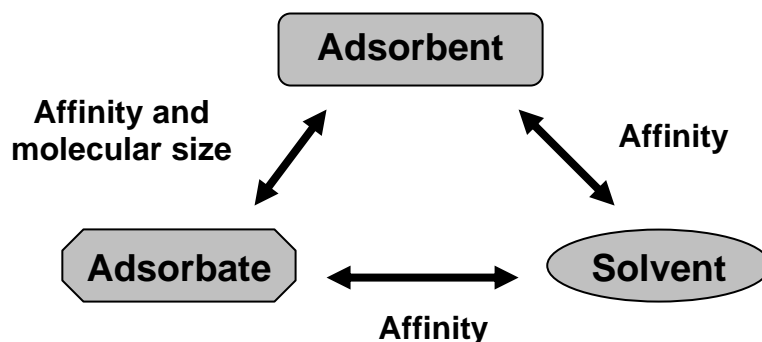


Figure 2.4 Diagram depicting the relationship between the three components in an adsorption system (Furuya et al. 1997)

The term ‘affinity’ differs depending on the components in question. Between the adsorbent and the solvent (in this case water) the most important relationship is the hydrophobic/hydrophilic nature of the adsorbent; a hydrophobic adsorbent would repulse water, possibly in favour of the adsorbate. Between the adsorbate and water the same affinity is present, defined by the adsorbates solubility; an adsorbate with low solubility would be ‘pushed’ towards an adsorbent. The relationship between the adsorbate and adsorbent is more complex, not only does it depend on the chemical affinity between the adsorbate molecule and the surface of the adsorbent, but the shape of the adsorbent and the relative shape and size of the molecule can decide whether it will be admissible into the adsorbent structure (Furuya et al. 1997).

Five types of interaction have been described in the literature with regards to phenol adsorption onto the surface of zeolitic adsorbents:

- Hydrophobic interaction
- Surface charge
- Hydrogen bonding
- Encapsulation in the zeolite pores
- Metal ion complexation

Although the benzene ring and the O-H bond largely counter act each other, phenol is relatively polar when compared to many other organic pollutants including other phenols. This presents a particular problem with regards to phenol adsorption as it has a comparatively high aqueous solubility. As a result a particularly hydrophobic adsorbent may be required to affect significant phenol adsorption.

Negatively charged surface groups may repulse disassociated phenol, this could possibly result in reduced phenol adsorption at high pHs ($\text{pH} \geq \text{pK}_a$). However in some cases this has been shown not to be a limiting step in the adsorption process (Yousef and El-Esweed 2009).

Hydrogen bonding can occur between the non-disassociated phenol molecule and negatively charged surface groups on the zeolite surface. The hydrogen atoms in the aromatic ring or the hydroxyl group are attracted to oxygen atoms in silanol and aluminol surface groups. (Su et al. 2000; Yousef and El-Esweed 2009).

Bonding can also occur between the π electron cloud of the benzene ring and the extra framework cations on the zeolite surface. Complexation can also occur due to charge transfer between the phenolate anion and the empty d-orbitals of surface metals, however Okolo et al. suggested that interaction was primarily with the aromatic ring (Okolo et al. 2000; Su et al. 2000; Yousef and El-Esweed 2009).

As discussed in Chapter 1 the channels of the adsorbent zeolite beta, have typical dimensions of 0.73 x 0.60 nm for the straight channels and 0.56 x 0.56 nm for the torturous channels. The adsorbate phenol is seen as a ridged planer molecule; however its molecular dimensions vary in the literature. The molecular dimensions of phenol as defined by the WINMOPAC program are 0.80 x 0.67 x 0.15 nm, however this did not take into account Van der Waals radii which could increase the radius by up to 0.12 nm for hydrogen or 0.14 nm for oxygen (Furuya et al. 1997; Tanthapanichakoon et al. 2005). Bertoncini et al. took average dimensions of 0.838 nm x 0.37 nm, while Shu et al. found a minimum cross

sectional distance of 0.43 nm (Shu et al. 1997b; Bertoncini and Odetti 2000). For the most part estimates of phenol molecular diameter would appear to allow for the accommodation of phenol into the microporous channels of zeolite beta.

2.3.1 Kinetic Studies

The purpose of this study was to determine the contact time needed for the reaction to reach equilibrium, the effect of phenol concentration on the rate of uptake and related parameters. It is necessary to know the time dependent factor the rate of adsorption in order to design an adsorption system. To this end, the selection of an appropriate kinetic model is useful for deriving the adsorption rate. The relationship between contact time and adsorption of phenol is represented at several different initial concentrations in Figure 2.5.

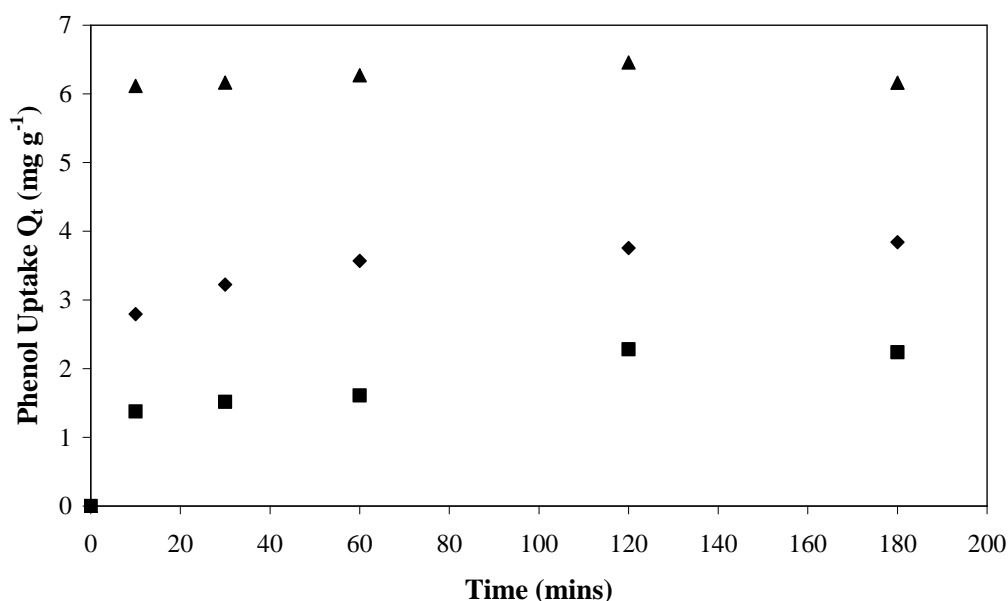


Figure 2.5 Amount of phenol adsorbed at 24 °C onto H- β -25 relative to time using three different initial phenol concentrations: ■ 50 mg dm^{-3} , ♦ 100 mg dm^{-3} and ▲ 200 mg dm^{-3} .

Initial adsorption appears to be fast, resolving to equilibrium within 1 hour, mostly taking place within the first 10 minutes regardless of initial phenol concentration. This rapid adsorption may indicate that adsorption mainly occurs on the external surface. Meteš et al. observed a similar scenario were rapid

adsorption within the first 30 minutes followed by minor fluctuations (Meteš et al. 2004). This rapid adsorption is significant as it indicates that a relatively short residence time is required for the adsorption stage of the proposed integrated system.

Second order rate equations can be difficult to achieve experimentally, however in sorption systems one reactant (in this case the adsorbent) is constant. This permits the use of the pseudo first order approximation. Lagergren's pseudo first order kinetic expression can be applied to the kinetics data in order to assess the dependency of the sorption process on phenol concentration.

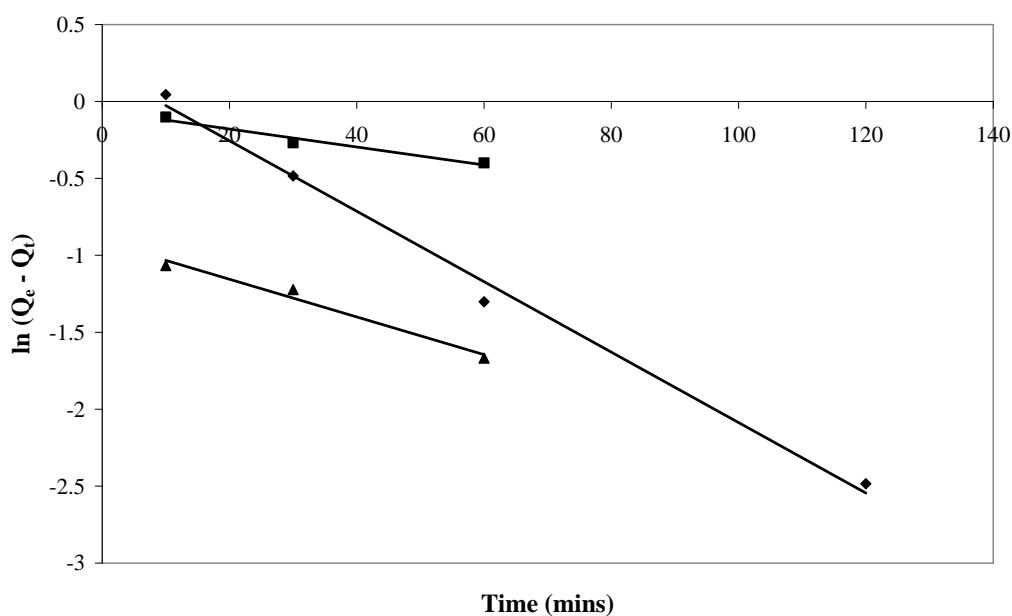


Figure 2.6 Pseudo first order sorption kinetics of phenol on H-β-25 at 24°C. Three different initial phenol concentrations were used: ■ 50 mg dm⁻³, ● 100 mg dm⁻³ and ▲ 200 mg dm⁻³.

Figure 2.6 shows the pseudo first order kinetic plot with varying phenol concentration. The relevant constants are listed in Table 2.2. Although the correlation coefficient is relatively high, the change in the rate constant is inconsistent with the change in concentration.

Table 2.2 Pseudo first order constants for phenol adsorption onto H- β -25

Initial phenol concentration (mg dm^{-3})	Correlation coefficient R^2	Equilibrium phenol uptake Q_e (mg g^{-1})	Rate constant k (min^{-1})
50	0.966	2.281	0.0058
100	0.993	3.840	0.0229
200	0.976	6.459	0.0123

In order to establish a better model for the comparison, the pseudo second order reaction model developed by Ho et al. was also applied (Ho et al. 2000). The pseudo second order plot is shown in Figure 2.7 and the associated constants are summarised in Table 2.3.

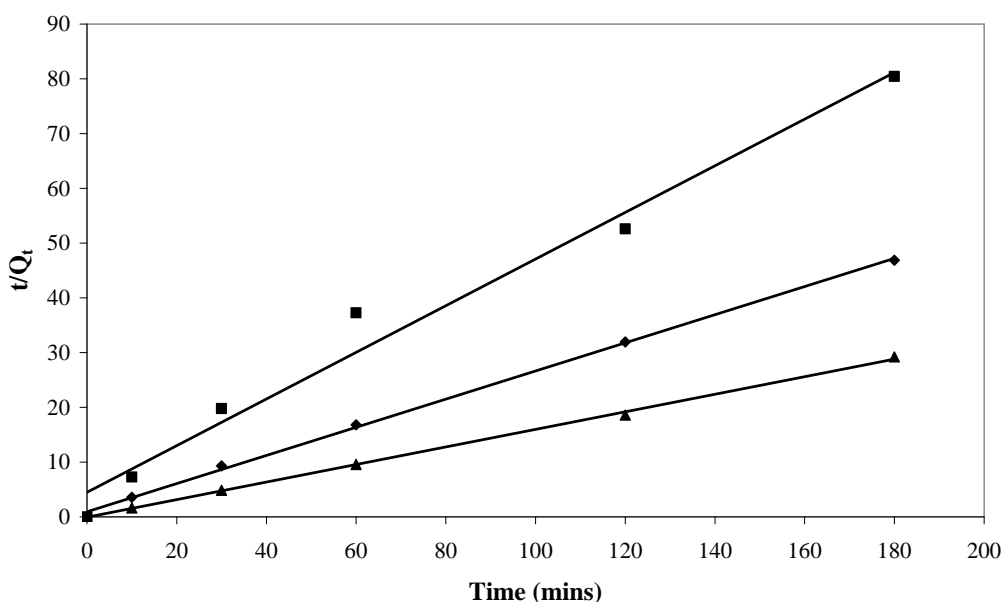


Figure 2.7 Pseudo second order sorption kinetics of phenol on H- β -25 at 24°C. Three different initial phenol concentrations were used: ■ 50 mg dm^{-3} , ♦ 100 mg dm^{-3} and ▲ 200 mg dm^{-3} .

Table 2.3 Pseudo second order kinetic constants for phenol adsorption on H- β -25.

Initial phenol concentration (mg dm^{-3})	Correlation coefficient R^2	Equilibrium phenol uptake Q_e (mg g^{-1})	Rate constant k_2 [$\text{g}/(\text{mg}/\text{min})$]	Initial sorption rate h [$\text{mg}/(\text{mg min})$]
50	0.980	2.347	0.0403	0.222
100	0.999	3.889	0.0701	1.0599
200	0.999	6.234	0.5417	21.0526

The correlation coefficients from the pseudo second order plot are noticeably higher than the pseudo first order equivalents. There is also a clear trend with the change in the rate constant and initial sorption rate relative to concentration. The rate constant and initial sorption rate increase with increasing concentration. This would imply that more phenol is adsorbed at higher concentrations, and also that maximum saturation is reached earlier.

The probability of a reaction fitting the pseudo second order model over the pseudo first order is concentration dependent. At high reactant concentrations the reaction is often only dependent on one reactant and the pseudo first order model reflects this. At lower concentrations the reaction tends to obey the pseudo second order equation (Azizian 2004).

2.3.2 The Influence of pH

A study on the relationship between pH and phenol adsorption was performed over a pH range of 2-12. The effect of variable pH on adsorption capacity was studied in tandem with the variation of pH in solution over time.

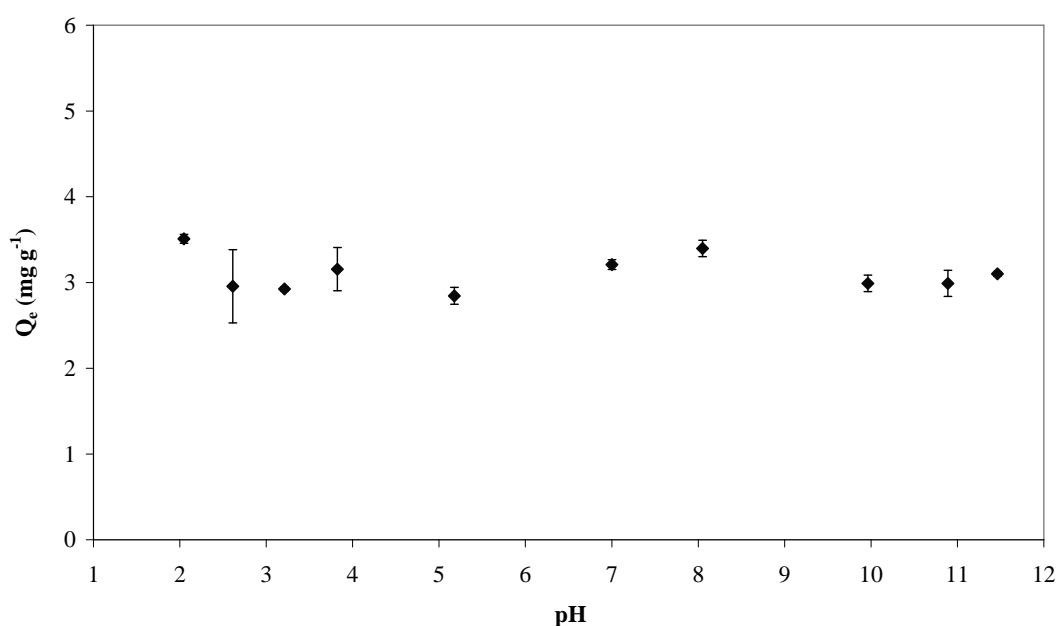


Figure 2.8 Phenol adsorption at equilibrium with variable pH from a 100 mg dm⁻³ phenol solution. Temperature 294 K. Contact time 1 hour. H- β -25.

In Figure 2.8 there is no distinct correlation between adsorption of phenol at equilibrium and initial solution pH. As mentioned in section 2.1.3, data points after pH 9.95 should be in a solution where the majority of phenol has disassociated into phenolate; however there is no apparent effect on adsorption. It was also observed that the pH of solution did not change throughout the contact period.

Yousef et al. noted that at higher pH values the surface of the zeolite may become negatively charged which may repulse the negatively charged phenolate ion and reduce adsorption. Additionally hydrogen bonding between the hydroxyl group on the phenol molecule and the silanol or aluminol surface groups on the zeolite should decrease at higher pHs due to the deprotonation of these groups (pK_a 5 and 10 respectively). Conversely the complexation of phenolate ions with the metal ions on the zeolite surface will increase with the increase of pH (Yousef and El-Esweed 2009). One possible reason why these factors do not seem to elicit a trend in this research is that it is the π electrons on the benzene ring as opposed to the hydroxyl group that interacts with the zeolite surface. This interaction is independent of pH. This assumption is supported by the research of Okolo et al., which found such interactions to be more common in the case of synthetic zeolite (Okolo et al. 2000).

2.3.3 Adsorption Studies

An initial adsorption isotherm study was performed on H- β -25 against a variable phenol concentration (Figure 2.9).

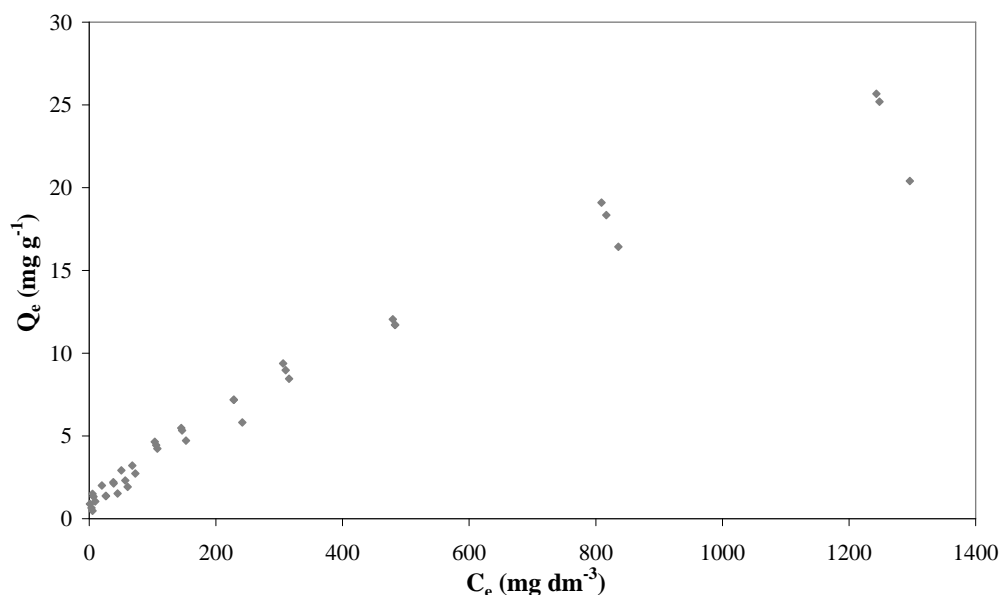


Figure 2.9 Adsorption isotherm for phenol on H- β -25. Phenol adsorbed per mass of zeolite vs. equilibrium concentration. Phenol concentration range 10 to 1500 mg dm^{-3} . All concentrations repeated in triplicate. Temperature 294 K.

The adsorption curve does not appear to approach a definitive limiting value and adsorption capacity increases throughout the concentration range. There is a possibility that the highest recorded Q_e at 25.7 mg g^{-1} (at 1500 mg dm^{-3}) could be exceeded with increasing phenol concentration. From this graph it is not clearly discernable as to which Brunauer classification fits best, however, there does appear to be some levelling off which would indicate that the isotherm is approaching a Type I relationship. From the graph it is apparent that the amount of error between samples increases at higher concentrations. This could be due to the isotherm approaching equilibrium with the presence of weaker adsorption interactions causing variation.

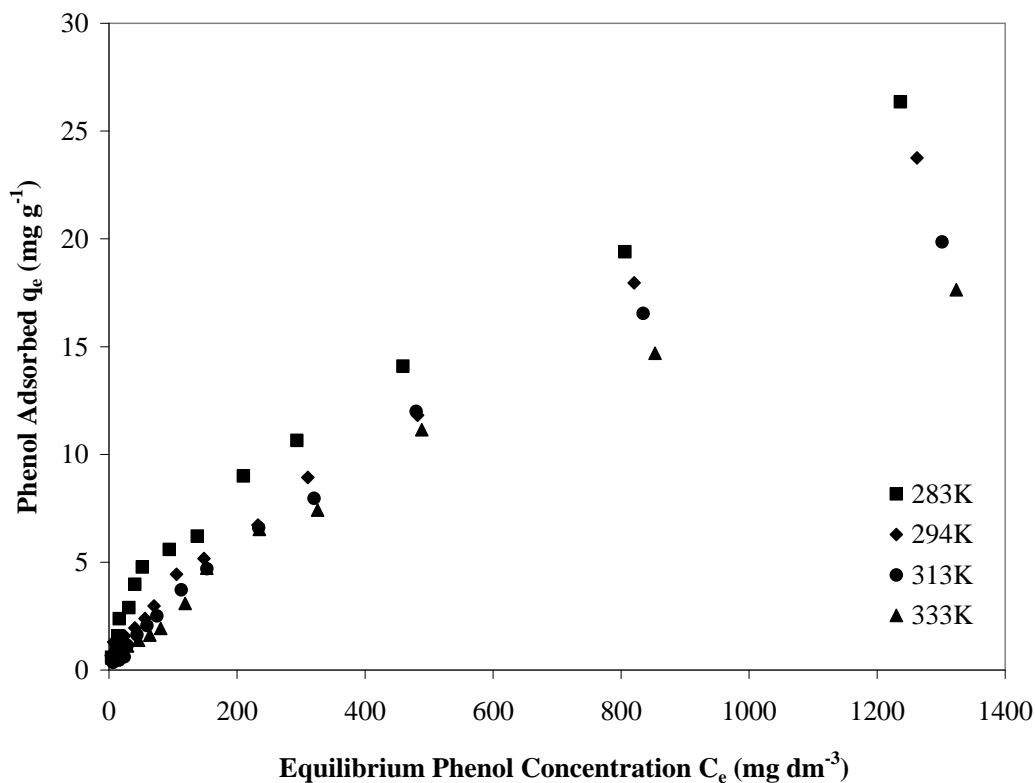


Figure 2.10 Phenol adsorption isotherms at four adsorption temperatures on H- β -25. ■ 283 K, ♦ 294 K, ● 313 K and ▲ 333 K. Phenol concentration range 10 – 1500 mg dm⁻³.

The temperature study in Figure 2.10 shows a negative relationship between phenol adsorption and increasing temperature, with the isotherm at 283 K yielding the highest level of phenol adsorption at 26.4 mg g⁻¹ with a starting solution of 1500 mg dm⁻³. This would suggest that the adsorption process is exothermic. The adsorption curve appears similar to the Type I Brunauer classification and no clear saturation point was observed within the concentration range.

In order to determine the most appropriate isotherm model to fit to the experimental data, it is necessary to have some method of the ‘goodness of fit’. The conventional method involves the comparison of the coefficient of determination (R^2) for the isotherm model plot, which when multiplied by 100 represents the percentage of variance from the mean. In its normal form the closer R^2 is to unity, the better the fit. The ISOFIT program provides two ‘standard’ measurements for goodness of fit, they are the correlation between

measured and fitted observations (R_y) from which we can derive the coefficient of determination and the root-mean-square-error (RMSE) (Kinniburgh 1986; Oyanedel-Craver et al. 2007; Shawn Matott and Radibeau 2008). RMSE is acquired through Equation 2.33 where (WSSE) is the weighted sum of square error, (m) is the number of observations and (p) is the number of parameters in the isotherm model. WSSE is an objective function acquired by the ISOFIT program. The closer RMSE is to zero, the better the fit.

$$RMSE = \sqrt{\frac{WSSE}{(m - p)}} \quad \text{Equation 2.33}$$

Table 2.4 shows the coefficient of determination and root-mean-square-error data generated by ISOFIT for one set of adsorption data at 294K. The coefficient of determination is highest on four isotherms, the Freundlich, Freundlich with linear partitioning, generalised Langmuir-Freundlich and Toth. These isotherm models also show lower RMSE values, the lowest value coming from the Freundlich model. The Polanyi and Polanyi with partitioning can be excluded due to relatively high RMSE values, despite their high coefficients of determination. Overall the BET isotherm model showed the poorest correlation, this is to be expected as it is rarely implemented for aqueous adsorption systems of this kind.

Table 2.4 Table summarising goodness-of-fit measurements for ten isotherm models for the adsorption of phenol onto H- β -25 at 294 K. Phenol concentration range 10 – 1500 mg dm⁻³.

<i>Isotherm model</i>	R_y^2	RMSE
Linear	0.983	1.69
Langmuir	0.996	0.64
Langmuir w/ Linear partitioning	0.983	0.95
Freundlich	0.998	0.32
Freundlich w/ Linear Partitioning	0.998	0.33
Generalised Langmuir-Freundlich	0.998	0.39
Toth	0.998	0.42
Polanyi	0.997	6.87
Polanyi w/ Linear Partitioning	0.997	7.20
BET	0.828	4.84

Figure 2.11 includes plots of a number of studied isotherm models relative to the experimentally measured adsorption data. The majority of the isotherm models fit closely with the observed data. Graphically only the Langmuir and Linear model deviate visibly from the observed data.

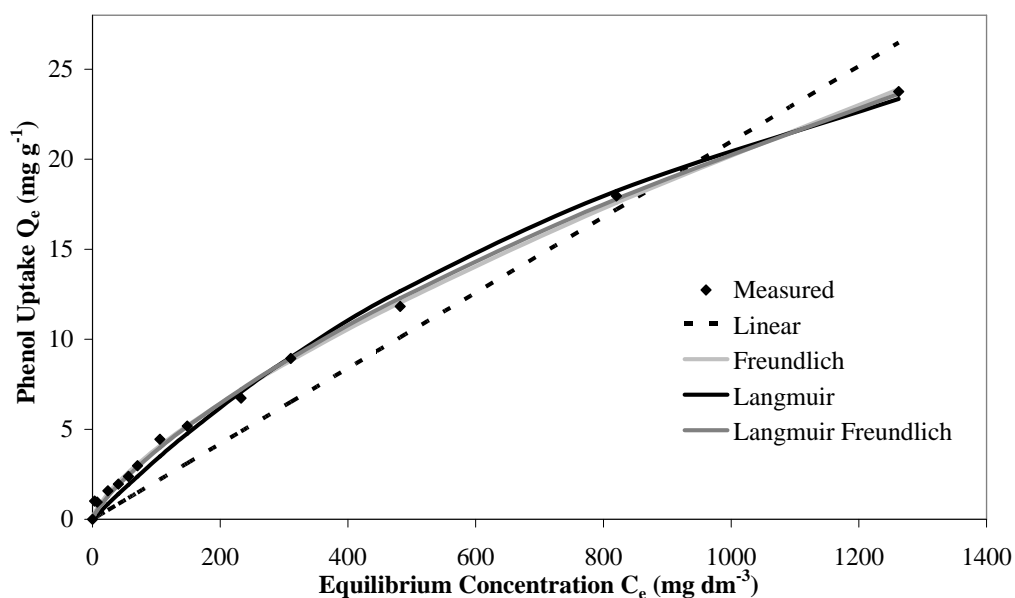


Figure 2.11 Plots of adsorption isotherms comparing observed data to simulated data from a range of isotherm models. H-BEA (SiO₂/Al₂O₃ = 25:1) at 294K . Phenol concentration range 10 – 1500 mg dm⁻³.

Amongst the best fitting isotherms was the Freundlich model, the parameters of which are shown in Table 2.5. The Freundlich model is commonly applied to heterogeneous systems. It predicts a continual increase in phenol uptake with increasing equilibrium concentration. It also predicts reversible adsorption on an amorphous adsorbent with heterogeneous adsorption sites (Wong et al. 2004). In this case the coefficient of determination shows a good quality of fit for the two lower temperatures but decreases significantly at 333 K. The Freundlich constant (K_F) is an indication of the adsorption capacity. Kanô related the Freundlich constant also to the binding capacity and to the adsorbate affinity (Kanô et al. 2000). In this case there is no consistent correlation between K_F and temperature, except for the much larger value for 284K, indicating a notable increase of adsorption affinity at low temperature. The heterogeneity of the adsorption is characterised by the heterogeneity factor ($1/n$). The value of n can also be related to the number of binding sites wasted by the binding of the adsorbate, so it can be relative to the size of the adsorbate molecule (Kanô et al. 2000; Allen et al. 2004). This is emphasised by the observed values for $(1/n_f)$ which remain roughly the same for the entire range of temperatures, this is to be expected due to the constant size of the adsorbate and unchanged surface heterogeneity. In this case, the constants for the Freundlich isotherm with linear partitioning were almost identical to those of the standard Freundlich isotherm.

Table 2.5 Freundlich constants for the adsorption of phenol onto H- β -25 at 3 different temperatures.

<i>Temperature (K)</i>	$K_F (dm^3 g^{-1})$	$1/n_f$	R^2
283	0.353	0.603	0.997
294	0.148	0.712	0.998
333	0.156	0.666	0.979

The Langmuir parameters are shown in Table 2.6. It usually predicts adsorption onto a homogeneous surface, where the sorption of each molecule has the same activation energy, with little interaction between these adsorbate molecules and as a result no multilayer adsorption (Allen et al. 2004). It assumes that when adsorption takes place that there will be no further adsorption, thus adsorption isotherms that fit the Langmuir model often show a plateau where all the

adsorption sites are occupied and a maximum adsorption is obtained. The Langmuir constants (K_L) and (A_L) are representative of adsorption capacity and the affinity or energy of adsorption, respectively (Yousef and El-Esweed 2009). K_L appears to be temperature dependent showing a decrease in capacity relative to increasing temperature. A_L on the other hand shows little correlation with temperature. By dividing K_L by A_L we can derive the maximum adsorption capacity Q_0 . In this case there is no specific correlation between Q_0 and temperature, however the value of Q_0 seem realistic relative to the maximum adsorption capacities shown in the isotherms in Figure 2.10. In contrast to the Freundlich model, the correlation coefficient for the Langmuir model decreases at the lowest temperature. This could be because the higher temperature appears to be closer to a plateau within the concentration range. The fit for the Langmuir and Freundlich isotherms are both similarly good, this is not uncommon with adsorption systems involving phenol and could mean that there is a combination of monolayer and heterolayer formation on the surface of the adsorbent at different concentrations (Mohd Din et al. 2009). Commonly, the Freundlich and Langmuir models are in agreement under moderate concentration ranges and only differentiate at higher concentrations where either the isotherm approaches a plateau as in Langmuir or the isotherm approaches a linear relationship between equilibrium concentration and adsorbed concentration as in Freundlich (Allen et al. 2004).

Table 2.6 Langmuir constants for the adsorption of phenol onto zeolite H- β -25 at 3 different temperatures.

<i>Temperature (K)</i>	$K_L (dm^3 g^{-1})$	$A_L (dm^3 mg^{-1})$	$Q_0 (mg g^{-1})$	R^2
283	0.0547	0.00139	39.3	0.984
294	0.0356	0.000731	48.7	0.996
333	0.0331	0.0011	30.2	0.991

The Langmuir-Freundlich isotherm was amongst the best fitting 3-parameter isotherms. Its parameters are shown in Table 2.7. It includes some constants from the Langmuir model and the Freundlich model, notably the heterogeneity factor ($1/n$). When the value of n approaches unity the isotherm reduces to Langmuir.

The typical Langmuir-Freundlich isotherm is similar to the Freundlich at lower temperatures in that when it is plotted logarithmically it will form a straight line, but at high concentrations it will approach an adsorbed maximum similar to the Langmuir isotherm (Kinniburgh 1986). The observed values for $1/n$ are similar to those derived from the Freundlich model, the constant b (related to A_L in the Langmuir isotherm) is only comparable at 333 K and decreases significantly as temperature is decreased. Unlike the Langmuir isotherm the predicted maximum adsorption (Q_0) is considerably larger and increases with decreasing temperature.

Table 2.7 Generalised Langmuir-Freundlich constants for the adsorption of phenol onto zeolite H- β -25 at 3 different temperatures.

<i>Temperature (K)</i>	<i>Q_0 (mg g⁻¹)</i>	<i>b (dm³ mg⁻¹)</i>	<i>$1/n$</i>	R^2
283	543	0.00000629	0.618	0.996
294	125	0.000126	0.790	0.998
333	108	0.00103	0.733	0.982

In contrast to the Langmuir-Freundlich model, the Toth isotherm was developed to take into account a linear relationship at low concentrations, an adsorption maximum at high concentrations and a smooth curve at intermediate concentration when plotted logarithmically. The Toth isotherm model also includes a heterogeneity factor (n_t), which is in this case noticeably higher than the equivalent values in the Freundlich or Langmuir-Freundlich models (Kinniburgh 1986; Terzyk et al. 2003). The constants (b^*Q_0) and (b) are related to the Langmuir constants (K_L) and (A_L), respectively. The value for (b^*Q_0) increases with decreasing temperature as does the predicted maximum adsorption (Q_0). However the predicted maximum adsorption is much higher than those predicted by the other examined isotherm models. The high Q_0 values for 284 and 294 K are unprecedented in similar adsorption systems and could not be reconciled with the measured adsorption data.

Table 2.8 Toth constants for the adsorption of phenol onto zeolite H- β -25 at 3 different temperatures.

Temperature (K)	$b*Q_0$ ($dm^3 g^{-1}$)	b ($dm^3 mg^{-1}$)	n_t	Q_0 ($mg g^{-1}$)	R^2
283	1.34	0.000144	0.139	9328	0.998
294	0.0926	0.0000711	0.265	1303	0.998
333	0.0476	0.000684	0.537	70	0.987

All the adsorption isotherms studied with the exception of the Langmuir isotherm show slightly decreased correlation coefficients at 334K. This could be because the lower adsorption capacity at higher temperatures causes it to reach an adsorbed maximum earlier and thus resemble the Langmuir isotherm more closely.

2.3.4 Thermodynamic Parameters

As mentioned in section 1.1.2, by making a plot of the natural log of the equilibrium concentration ($\ln Q_e/C_e$) versus $1/T$ for a range of temperatures, it is possible to derive the enthalpy change (ΔH) from the slope for each initial concentration. By adapting Equation 2.19 for use with Freundlich isotherm constants we can determine Gibbs free energy change (ΔG) (Zhang et al. 2009). The modified equation is shown below:

$$\Delta G = -nRT \quad \text{Equation 2.34}$$

Where (n) is the heterogeneity factor from the Freundlich model.

The values for the three thermodynamics parameters are displayed in Table 2.9.

Table 2.9 Thermodynamic parameters for phenol adsorption onto zeolite H- β -25 at three different temperatures.

Temperature (K)	ΔG ($kJ mo dm^{-3}$)	ΔH ($kJ mol^{-1}$)	ΔS ($J mol^{-1} K^{-1}$)
283	-1.42		-21.5
294	-1.74	-7.51	-19.6
333	-1.85		-17.0

The enthalpy change is negative which implies that the adsorption process is exothermic; this trend is confirmed in the isotherm data as a negative relationship with increasing temperature. The value for ΔH displayed in Table 2.9 was an average of the ΔH values obtained from each concentration. However an analysis of these values reveals two distinct groups of concentration where the enthalpy change remains roughly the same, these groups are shown in Table 2.10.

Table 2.10 Enthalpy change values over different concentration ranges.

<i>Initial concentration range (mg dm⁻³)</i>	<i>Average ΔH (kJ mol⁻¹)</i>
10 - 150	-11.17
200-1500	-4.46

Between the initial concentrations of 10-150 mg dm⁻³ a significant enthalpy change close to the enthalpy of physisorption was found, whereas between 200-1500 mg dm⁻³ a less negative enthalpy was found as the isotherm approaches equilibrium. The likely cause of this distinct change in enthalpy is that at lower concentrations the phenol adsorbs on high energy sites on the zeolite, resulting in a more negative enthalpy change. When the high energy sites become saturated, the phenol adsorbs onto lower energy sites or possibly onto other adsorbed phenol molecules. This results in a less negative enthalpy change (Zhang et al. 2009).

The negative Gibbs free energy change (ΔG) indicates a spontaneous and feasible adsorption process.

The negative entropy change (ΔS) implies a significantly less chaotic distribution of the adsorbate on the solid surface relative to solution (Saltali et al. 2007). The entropy appears to be temperature dependent; with increasing disorder as temperature increases. Entropy is dependent on the degree of freedom of a molecule, as a molecule becomes confined in the zeolite structure its freedom is reduced and a corresponding reduction in entropy is observed. Larger molecules with molecular diameters approaching that of the pore diameter are likely to lose

more entropy than a smaller molecule or alternatively a larger pore diameter (Myers 2004). The significantly negative entropy may imply that the phenol molecule is being confined in the zeolite structure.

2.3.5 Silica to Alumina Ratio

To examine the effects of silica to alumina ratio a range of different zeolites were tested under the same conditions. The resulting adsorption isotherms are shown in Figure 2.12.

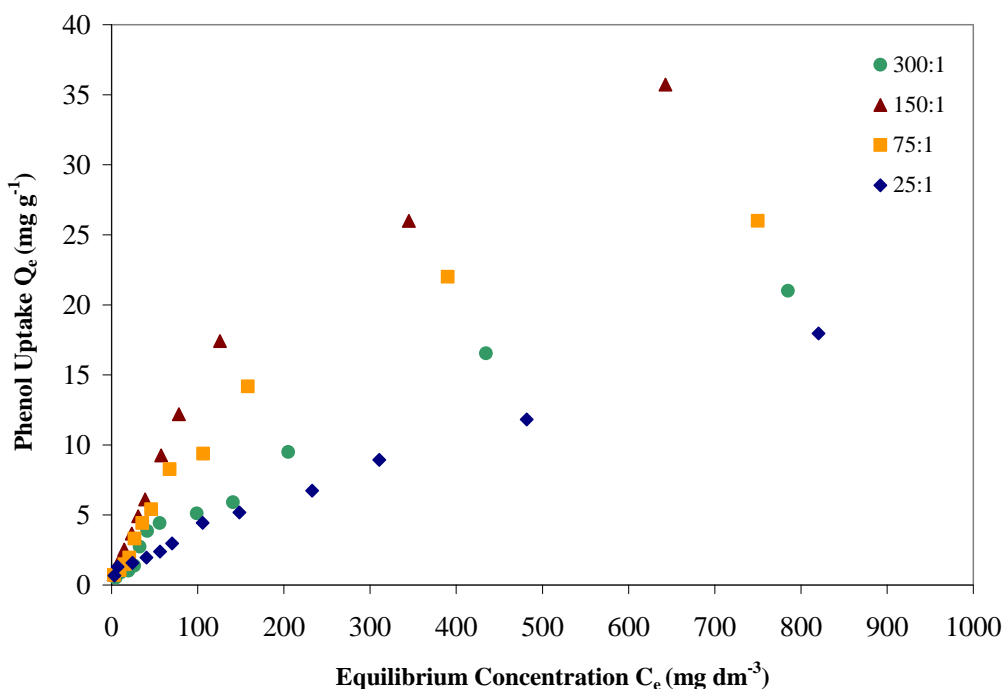


Figure 2.12 Phenol adsorption isotherms for four different zeolites with varying silica to alumina ratio @ 294K. Initial concentration range 10-1000 mg dm⁻³. ♦ H-β-25, ■ H-β-75, ▲ H-β-150 and ● H-β-300.

The isotherm data shows a distinctly positive relationship between phenol uptake and increasing silica to alumina ratio. The exception to this is the H-β-300 zeolite which is closer to the H-β-25. This could mean that there is an optimal silica to alumina ratio, somewhere between 75:1 and 300:1 and any increase in excess of this begins to counteract the adsorption benefits of increasing silica to alumina ratio. Optimum phenol uptake occurred at a silica to alumina ratio of 150:1.

The isotherm curves for the 75:1 and 150:1 zeolites appear similar to the Type I Brunauer isotherm classification, with a change in the relationship between equilibrium concentration and adsorbed concentration between 100 and 200 mg dm⁻³ initial concentration.

The ISOFIT program was used to apply isotherm models to each of these zeolites.

Table 2.11 shows the goodness of fit parameters for an appropriate range of isotherm models for the four silica to alumina ratios.

Table 2.11 Table summarising goodness-of-fit measures for a range of isotherm models for the adsorption of phenol onto H- β -25), H- β -75, H- β -150, H- β -300 @ 294K .

<i>Isotherm Model</i>	<i>SiO₂/Al₂O₃</i>	<i>R²</i>	RMSE
Linear	25	0.983	1.64
	75	0.876	3.99
	150	0.685	11.7
	300	0.944	2.31
Langmuir	25	0.996	0.64
	75	0.996	0.55
	150	0.988	1.87
	300	0.987	0.79
Freundlich	25	0.998	0.32
	75	0.971	1.51
	150	0.919	4.99
	300	0.988	0.76
Generalized Langmuir- Freundlich	25	0.998	0.38
	75	0.996	0.58
	150	0.988	1.94
	300	0.99	0.70
Toth	25	0.998	0.4146
	75	0.996	0.5768
	150	0.988	1.9397
	300	0.990	0.6967

From

Table 2.11 a number of observations can be drawn. The two poorest performing zeolites (25:1 and 300:1) exhibit certain similarities in isotherm correlation. They are both the more linear isotherms and correspond relatively well with the Freundlich isotherm with high correlation coefficients and low RMSE. The Freundlich model tends to suggest the prevalence of weak, reversible physisorption and multilayer adsorption. This may be more common on the poorer adsorbing zeolites, which may continue to adsorb on multiple layers, however it may be that a distinct adsorption maximum is difficult to distinguish at relatively low adsorption uptakes.

For the silica to alumina ratios of 75:1 and 150:1 there is a shift of correlation from the Freundlich to the Langmuir model. This is illustrated in Figure 2.13 where a close fit for the Langmuir model on H-BEA 150:1 can be seen. This correlates with a distinct Type I Brunauer classification isotherm and a visible maximum adsorption c. 42 mg g⁻¹. As the observed data approaches the Langmuir model, the simulated Langmuir-Freundlich data becomes identical to that of the Langmuir. Because of this, the two are indistinguishable in Figure 2.13.

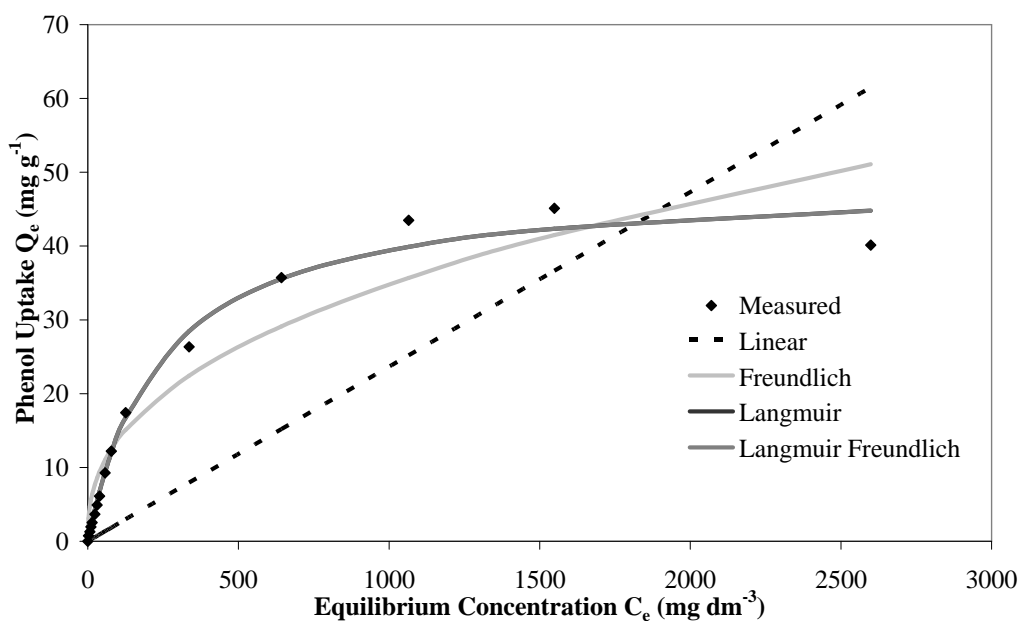


Figure 2.13 Plots of adsorption isotherms comparing observed data to simulated data from a range of isotherm models. H-BEA (SiO₂/Al₂O₃ = 150:1) @ 294K . Phenol concentration range 10 – 3000 mg dm⁻³.

The general purpose Langmuir-Freundlich and Toth isotherm models show the broadest application with a consistently good fit for all silica to alumina ratios.

Table 2.12 Langmuir constants for the adsorption of phenol onto zeolite beta for 4 different silica to alumina ratios.

SiO_2/Al_2O_3	$K_L (dm^3 g^{-1})$	$A_L (dm^3 mg^{-1})$	$Q_0 (mg g^{-1})$	R^2
25	0.0356	0.000731	48.7	0.996
75	0.139	0.00385	36.1	0.996
150	0.202	0.00412	50.3	0.988
300	0.0729	0.00210	34.7	0.987

The Langmuir isotherm constants shown in Table 2.12 show a distinct correlation between the values for K_L and A_L and the observed trend in Figure 2.12.

Table 2.13 Freundlich constants for the adsorption of phenol onto zeolite beta for 4 different silica to alumina ratios.

SiO_2/Al_2O_3	$K_F (dm^3 g^{-1})$	$1/n_f$	R^2
25	0.148	0.712	0.998
75	0.661	0.570	0.971
150	2.169	0.402	0.919
300	0.315	0.641	0.988

The Freundlich isotherm constants are shown in Table 2.13. Adsorption capacity (K_F) increases with the established trend, however the heterogeneity factor ($1/n$) decreases. This may correspond to the increasing homogeneity on the surface of the zeolite as silica becomes more prevalent (with the exception of 300:1).

Table 2.14 Generalized Langmuir-Freundlich constants for the adsorption of phenol onto zeolite beta for 4 different silica to alumina ratios.

SiO_2/Al_2O_3	$Q_0 (mg g^{-1})$	$b (dm^3 mg^{-1})$	$1/n$	R^2
25	125	0.000126	0.790	0.998
75	36.1	0.00361	0.999	0.996
150	49.0	0.00413	0.999	0.988
300	58.9	0.000667	0.796	0.990

Table 2.15 Toth constants for the adsorption of phenol onto zeolite beta for 4 different silica to alumina ratios.

SiO_2/Al_2O_3	$b*Q_0 (dm^3 mg^{-1})$	$b (dm^3 mg^{-1})$	n_t	$Q_0 (mg g^{-1})$	R^2
25	0.0926	0.0000711	0.265	1303	0.998
75	0.139	0.00386	0.990	36.1	0.996
150	0.203	0.00416	0.999	48.9	0.988
300	0.142	0.00108	0.408	131	0.990

The Langmuir-Freundlich and Toth constants are shown in Table 2.14 and Table 2.15. Notably in the case of 75:1 and 150:1 the heterogeneity factor in both isotherm models is very close to unity, under these conditions the Langmuir-Freundlich and Toth models are said to reduce to the Langmuir model (Kinniburgh 1986). This correlates with the affinity that these two isotherms have with the Langmuir model. The values for Q_0 (the adsorption maximum) in the Toth and Langmuir-Freundlich for these two isotherms, also show similar values to those acquired through the Langmuir model.

The best performing adsorbents: H-BEA (SiO_2/Al_2O_3 75:1) and H-BEA (SiO_2/Al_2O_3 150:1) show a distinct correlation to the Langmuir isotherm model. This is characterised by a sharp increase in adsorption of phenol relative to adsorption capacity followed by a plateau as the adsorption capacity is reached and additional phenol uptake is severely reduced. The Langmuir model predicts an irreversible, monolayer adsorption onto the adsorbent surface with a maximum adsorption. The poorer performing adsorbents H-BEA (SiO_2/Al_2O_3 25:1) and H-BEA (SiO_2/Al_2O_3 300:1) showed a transitory relationship between

the Langmuir and Freundlich, with no observed maximum adsorption and instead a relatively mild decline in adsorption uptake at higher concentrations. The Freundlich isotherm predicts continual increase in adsorption uptake with relatively weak, reversible and multilayer adsorption. By virtue of their versatility the general purpose Toth and Langmuir-Freundlich models show good correlation with all sets of isotherm data. The root mean square error and correlation coefficient values for the two models are almost identical for all four isotherm data sets.

The positive effects of increasing silica to alumina ratio in zeolites for the adsorption of phenol has been established in research (Shu et al. 1997b; Khalid et al. 2004; Damjanović et al. 2010). The effect by most accounts is cumulative, with completely siliceous adsorbents achieving maximum adsorption in a number of cases. As mentioned in section 2.1.5 a decrease in the ratio of framework alumina produces a more hydrophobic adsorbent. Phenol is noted for its relatively high aqueous solubility relative to other organic chemicals. This makes its competition with water for adsorption sites a crucial determinant in an adsorbents ability to adsorb phenol. Su et al. studied the adsorption of benzene onto large pore zeolites, it was found that an increase in silica to alumina ratio led to a shift from hydrogen bonding and metal complexation to condensation of the benzene on the zeolite surface (Su et al. 2000). This is a function of decreasing extra framework cations; however phenol is more polar than benzene, therefore a hydrophilic zeolite may inhibit the utilisation of these adsorption sites at lower silica to alumina ratios.

Another important consideration is the surface acidity of the zeolite. As the amount of framework alumina decreases, the amount of Brønsted and Lewis acid sites decrease. This has the effect of making it more basic and more attractive to acidic molecules (Pai et al. 2007). Phenol is a weak acid, and because of this should have a greater affinity to a less acidic adsorbent.

The surface area and pore volumes for each of the four zeolites were determined in order to identify any structural change between different $\text{SiO}_2:\text{Al}_2\text{O}_3$ ratios. The results are displayed in Table 2.16.

Table 2.16 Surface characteristics of zeolite Beta at different SiO₂:Al₂O₃ ratios.

Sample	Surface	Mesopore	Micropore
	Area (m ² g ⁻¹)	Volume (cc g ⁻¹)	Volume (cc g ⁻¹)
H-β-25	529	0.772	0.298
H-β-75	514	0.885	0.291
H-β-150	541	0.964	0.305
H-β-300	630	0.289	0.365

The mesopore volume is shown to increase with increasing silica. The exception appears to be H-β-300 which has a significantly lower mesopore volume, less than half that of the other zeolites. Of all the zeolites tested, the 300:1 has the highest surface area and micropore volume however its phenol adsorption capacity is the second lowest. This would suggest that the lower mesopore volume is a significant limiting factor and that the 300:1 zeolite is structurally different from the other three examples. It is likely that the mesopores provide improved adsorbate transport into the zeolite structure.

The nitrogen adsorption/desorption isotherms for the 25:1, 75:1 and 150:1 zeolites all show a mixed type I + IV isotherm which corresponds with combined mesopore and micropore adsorption (Schneider 1995). The isotherm for 300:1 is less well defined, with an earlier and narrow hysteresis loop. Analysis of mesopore distribution by the BJH method shows mesopores almost exclusively in the 20-30 Å pore radius range. All other isotherms show a broad pore distribution between 20 and 275 Å.

The 300:1 ratio zeolite did outperform the much more mesoporous 25:1 zeolite (as seen in Figure 2.12), this would suggest that the zeolites hydrophobicity is the dominant factor and can make up somewhat for the loss in adsorption capacity due to a significantly lower mesopore volume.

As outlined in Shu et al. the adsorption of molecular organic waste benefits from a hydrophobic zeolite. In activated carbon this can be achieved by adding organic functional groups, however in siliceous adsorbents such as zeolites, a hydrophobic nature is obtained by increasing the ratio of silica to alumina.

Phenol however is perceived as somewhat more difficult to adsorb due to its relatively high solubility in water (Shu et al. 1997a). The results show that there is a positive trend with increasing silica to alumina ratio in the case of phenol adsorption; this trend is likely to be the result of the increasing hydrophobic effect caused by successively more siliceous zeolites. The disadvantage of this increased adsorption effect however is that increasing the $\text{SiO}_2:\text{Al}_2\text{O}_3$ ratio reduces the amount of aluminium sites for cation exchange. Exchanged cations can alter the properties of the zeolite in a number of ways, with regards to adsorption the ionic radii of the cation can effect entry into the zeolite pores. For the purpose of the proposed system, a catalytically active metal must be exchanged to improve the redox properties in the catalytic oxidation step. Because of this a balance must be found between the increase of adsorption capacity with increasing $\text{SiO}_2:\text{Al}_2\text{O}_3$ and available cations.

2.4 Conclusion

Adsorption of phenol at room temperature onto H- β -25 was successfully performed with an observed maximum adsorption at 25.6 mg g^{-1} at an initial phenol concentration of 1500 mg g^{-1} . The adsorption of phenol onto zeolite beta was found to conform strongly to the pseudo second order rate equation. Adsorption is relatively fast, with the bulk of uptake occurring within the first 10 minutes. No distinct correlation was found between phenol adsorption and changing pH. Solution temperature was found to have a noticeable effect on phenol adsorption, with a distinct exothermic trend for the entire range. Adsorption was found to be highest at 10°C with an observed maximum of 26.8 mg g^{-1} . Examination of the enthalpy change confirmed that the adsorption process was exothermic and indicated the presence of energetically heterogenic adsorption sites, but primarily in the form of physisorption. The Gibbs free energy was shown to be negative, which suggests a feasible and spontaneous adsorption process. The entropy change was significantly negative suggesting a significant reduction in surface disorder and the possibility of adsorbate confinement within the zeolite structure.

Analysis of the adsorption of phenol on a number of beta zeolites with differing silica to alumina ratios revealed a significant increase in adsorption with increasing silica to alumina ratio. This would suggest that the hydrophobicity of the adsorbent is a significant limiting step with regard to phenol adsorption. The 300:1 zeolite broke this trend however, the decline in adsorption performance is suspected to be due to a significant change in pore structure relative to the other adsorbents. The result being a significant decrease in mesopore volume. This would imply that adsorption does take place within the zeolite pore structure.

Out of the ten different adsorption isotherm models applied, the multipurpose Generalized Langmuir-Freundlich and Toth isotherms were found to be the most widely applicable, exhibiting good correlation data with all observed adsorption isotherms. The isotherm data also suggests that the best performing zeolites H- β -75 and H- β -150 approached a good fit with the Langmuir isotherm while the poorer performing zeolites H- β -25 and H- β -300 exhibited transitional correlation between the Freundlich and Langmuir. In the latter case this is synonymous with low level adsorbate coverage where the Langmuir and Freundlich isotherms differ very little. It is possible to assume that at much higher equilibrium concentrations, the two zeolites will exhibit an adsorption maximum and conform to the Langmuir isotherm. The Langmuir constants suggest a maximum adsorption of 48.6 mg g⁻¹ and 34.7 mg g⁻¹ for 25:1 and 300:1 respectively. The highest observed maximum was 47.2 mg g⁻¹ at an initial concentration of 1500 mg dm⁻³ for 150:1.

The correlation with the Langmuir model suggests that the adsorption is mostly at homogeneous sites with a single layer of adsorption on the zeolite surface, where as Freundlich correlation generally suggests multilayer adsorption onto heterogeneous adsorption sites. Examination of the heterogeneity factors in the Freundlich model show a relative decrease in heterogeneity as silica to alumina ratio increases.

The adsorption process is more likely to be a combination of the two, and this is represented by the more complex systems represented in the 3 parameter general purpose isotherms.

2.5 References

- Ahmaruzzaman, M. (2008). *Adsorption of phenolic compounds on low-cost adsorbents: A Review*. *Advances in Colloid and Interface Science* **143**: 48-67.
- Allen, S. J., G. McKay and J. F. Porter (2004). *Adsorption models for basic dye adsorption by peat in single and binary component systems*. *Journal of Colloid and Interface Science* **280**: 322-333.
- Armaroli, T., L. J. Simon, M. Digne, T. Montanari, M. Bevilacqua, V. Valtchev, J. Patarin and G. Busca (2006). *Effects of crystal size and Si/Al ratio on the surface properties of H-ZSM-5 zeolites*. *Applied Catalysis A: General* **306**: 78-84.
- Atkins, P. W. (2000). *Physical Chemistry*. Oxford, Oxford University Press.
- Azizian, S. (2004). *Kinetic models of sorption: a theoretical analysis*. *Journal of Colloid and Interface Science* **276**(1): 47-52.
- Barrer, R. M. (1978). *Zeolites and Clay Materials*. London, Academic Press.
- Barrett, E. P., L. G. Joyner and P. P. Halenda (1951). *The determination of pore volume and area distributions in porous substances. I. Computations from nitrogen isotherms*. *Journal of the American Chemical Society* **73**: 373-380.
- Bertoncini, C. and H. Odetti (2000). *Computer simulation of phenol physisorption on graphite*. *Langmuir* **16**(19): 7457-7463.
- Brunauer, S., L. S. Deming, W. E. Deming and E. Teller (1940). *On a theory of the van der Waals adsorption of gases*. *Journal of the American Chemical Society* **62**: 1723-1732.
- Brunauer, S., P. H. Emmett and E. Teller (1938a). *Adsorption of gases in multimolecular layers*. *Journal of the American Chemical Society* **60**: 309-319.
- Busca, G., S. Berardinelli, C. Resini and L. Arrighi (2008). *Review: Technologies for the removal of phenol from fluid streams: A short review of recent developments*. *Journal of Hazardous Materials* **160**: 265-288.

- Caro, J., D. Albrecht and M. Noack (2009). *Why is it so extremely difficult to prepare shape-selective Al-rich zeolite membranes like LTA and FAU for gas separation?* Separation and Purification Technology **66**(1): 143-147.
- Cerofolini, G. F. and L. Meda (1998). *A theory of multilayer adsorption on rough surfaces in terms of clustering and melting BET piles.* Surface Science **416**: 403-422.
- Cheung, C., J. F. Porter and G. McKay (2000). *Sorption kinetics for the removal of copper and zinc from effluents using bone char.* Separation and Purification Technology **19**: 55-64.
- Damjanović, L., V. Rakić, V. Rac, D. Stošić and A. Auroux (2010). *The investigation of phenol removal from aqueous solutions by zeolites as solid adsorbents.* Journal of Hazardous Materials.
- Dubinin, M. M. (1960). *The potential theory of adsorption of gases and vapors for adsorbents with energetically nonuniform surfaces.* Chemical Reviews **60**(2): 235-241.
- Dubinin, M. M., E. D. Zaverina and L. Radushkevich (1947). *Adsorption cycle modelling.* Doklady Akademii Nauk SSSR **21**: 1351.
- Furuya, E. G., H. G. Chang, Y. Miura and K. E. Noll (1997). *A fundamental analysis of the isotherm for the adsorption of phenolic compounds on activated carbon.* Separation and Purification Technology **11**: 69-78.
- Hagen, J. (1999). *Industrial Catalysis: A Practical Approach.* Weinheim, Wiley-VCH.
- Ho, Y. S. and G. McKay (1998). *The sorption of lead(II) ions on peat.* Water Research **33**(2): 578-584.
- Ho, Y. S. and G. McKay (1999). *Pseudo-second order model for sorption processes.* Process Biochemistry **34**: 451-465.
- Ho, Y. S., G. McKay, D. A. J. Wase and C. F. Forster (2000). *Study of the sorption of divalent metal ions onto peat.* Adsorption Science and Technology **18**: 639-650.
- Kamble, S. P., P. A. Mangrulkar, A. K. Bansiwala and S. S. Rayalu (2008). *Adsorption of phenol and o-chlorophenol on surface altered fly ash based molecular sieves.* Chemical Engineering Journal **138**(1-3): 73-83.

- Kanô, F., I. Abe, H. Kamaya and I. Ueda (2000). *Fractal model for adsorption on activated carbon surfaces: Langmuir and Freundlich adsorption*. *Surface Science* **467**: 131-138.
- Khalid, M., G. Joly, A. Renaud and P. Magnoux (2004). *Removal of phenol from water by adsorption using zeolites*. *Industrial Engineering and Chemistry Research* **43**: 5275-5280.
- Kim, T., Y. Son and Y. Lim (2007). *Thermodynamic analysis of 1,4-diaminoanthraquinone adsorption on polyethylene terephthalate in alkaline media*. *Dyes and Pigments* **72**: 246-250.
- Kinniburgh, D. G. (1986). *General purpose adsorption isotherms*. *Environmental Science and Technology* **20**: 895-904.
- Kuzniatsova, T., Y. Kim, K. Shqau, P. K. Dutta and H. Verweij (2007). *Zeta potential measurements of zeolite Y: Application in homogeneous deposition of particel coatings*. *Microporous and Mesoporous Materials* **103**(1-3): 102-107.
- Manes, M. and L. J. E. Hofer (1969). *Application of Polanyi adsorption potential theory to adsorption from solution on activated carbon*. *Journal of Physical Chemistry* **73**(3): 584-590.
- Meteš, A., D. Kovačević, D. Vujević and S. Papić (2004). *The role of zeolites in wastewater treatment of printing inks*. *Water Research* **28**: 3373-3381.
- Mohd Din, A. T., B. H. Hameed and A. L. Ahmad (2009). *Batch adsorption of phenol onto physiochemical-activated coconut shell*. *Journal of Hazardous Materials* **161**: 1522-1529.
- Myers, A. L. (2004). *Characterization of nanopores by standard enthalpy and entropy of adsorption of probe molecules*. *Colloids and Surfaces A: Physiochemical and Engineering Aspects* **241**: 9-14.
- Namasivayam, C. and D. Kavitha (2002). *Removal of Congo Red from water by adsorption onto activated carbon prepared from coir pith, an agricultural solid waste*. *Dyes and Pigment* **54**: 47-58.
- Okolo, B., C. Park and M. A. Keane (2000). *Interaction of phenol and chlorophenols with activated carbon and synthetic zeolites in aqueous media*. *Journal of Colloid and Interface Science* **226**: 308-317.
- Oyanedel-Craver, V. A., M. Fuller and J. A. Smith (2007). *Simultaneous sorption of benzene and heavy metals onto two organoclays*. *Journal of Colloid and Interface Science* **309**(2): 485-492.

- Pai, S., U. Gupta and S. Chilukuri (2007). *Butylation of toluene: Influence of zeolite structure and acidity on 4-tert-butyltoluene selectivity*. Journal of Molecular Catalysis A: Chemical **265**(1-2): 109-116.
- Polanyi, M. (1914). Verhandlungen Deutsche Physikalische Gesellschaft **16**: 1012.
- Proctor, A. and J. F. Toro-Vasquez (1996). *The Freundlich isotherm in studying adsorption in oil processing*. Journal of American Oil Chemists' Society **73**(12): 1627-1633.
- Ramachandran, C. E., B. A. Williams, J. A. van Bokhoven and J. T. Miller (2005). *Observation of a compensation relation for n-hexane adsorption in zeolites with different structures: implications for catalytic activity*. Journal of Catalysis **233**: 100-108.
- Roostaei, N. and F. Handen Tezel (2004). *Removal of phenol from aqueous solutions by adsorption*. Journal of Environmental Management **70**(2): 157-164.
- Saltali, K., A. Sari and M. Aydin (2007). *Removal of ammonium ion from aqueous solution by Turkish (Yildizeli) zeolite for environmental quality*. Journal of Hazardous Materials **141**(1): 258-263.
- Schneider, P. (1995). *Review: Adsorption isotherms of microporous-mesoporous solids revisited*. Applied Catalysis A: General **129**: 157-165.
- Schwarzenbach, R. P., P. M. Gschwend and D. M. Imboden (1993). *Environmental Organic Chemistry*. New York, John Wiley & Sons, Inc.
- Shawn Matott, L. and A. Radibeau, J (2008). *ISOFIT- A program for fitting sorption isotherms to experimental data*. Environmental Modelling and Software **23**: 670-676.
- Shu, H., D. Li, A. A. Scala and Y. H. Ma (1997). *Adsorption of small organic pollutants from aqueous streams by aluminosilicate-based microporous materials*. Separation and Purification Technology **11**: 27-36.
- Su, B. L., V. Norberg and C. Hansenne (2000). *Toward a better understanding on the adsorption behavior of aromatics in 12 R window zeolites*. Adsorption **6**: 61-71.
- Tanthapanichakoon, W., P. Ariyadejwanich, P. Japthong, K. Nakagawa, S. R. Mukai and H. Tamon (2005). *Adsorption-desorption characteristics of phenol and reactive dyes from aqueous solution on mesoporous activated carbon prepared from waste tires*. Water Research **39**: 1347-1353.

- Terzyk, A. P. (2004). *Molecular properties and intermolecular forces - factors balancing the effect of carbon surface chemistry in adsorption of organics from dilute aqueous solutions*. Journal of Colloid and Interface Science **275**: 9-29.
- Terzyk, A. P., J. Chatłas, P. A. Gauden, G. Rychlicki and P. Kowalczyk (2003). *Developing the solution analogue of the Toth adsorption isotherm equation*. Journal of Colloid and Interface Science **266**: 473-476.
- Toth, J. (1971). *State equations of the solid-gas interface layer*. Acta Chimica Academiae Scientiarum Hungaricae **69**: 311-317.
- Tsai, W., H. Hsu, T. Su, K. Lin and C. Lin (2006). *Adsorption characteristics of bisphenol-A in aqueous solutions onto hydrophobic zeolite*. Journal of Colloid and Interface Science **299**: 513-519.
- Wong, Y. C., Y. S. Szeto, W. H. Cheung and G. McKay (2004). *Adsorption of acid dyes on chitosan-equilibrium isotherm analyses*. Process Biochemistry **39**: 693-702.
- Xu, Z., W. Zhang, B. Pan, C. Hong, L. Lv, Q. Zhang, B. Pan and Q. Zhang (2007). *Application of the Polanyi potential theory to phthalates adsorption from aqueous solution with hyper-cross-linked polymer resins*. Journal of Colloid and Interface Science **319**(2): 392-397.
- Yang, T. R. (2003). *Adsorbents: Fundamentals and Applications*. New Jersey, John Wiley & Sons, Inc.
- Yousef, R. I. and B. El-Esweed (2009). *The effect of pH on the adsorption of phenol and chlorophenols onto natural zeolite*. Colloids and Surfaces A: Physicochemical and Engineering Aspects **334**: 92-99.
- Zhang, W., Q. Du, B. Pan, L. Lv, C. Hong, Z. Jiang and D. Kong (2009). *Adsorption equilibrium and heat of phenol onto aminated polymeric resins from aqueous solution*. Colloids and Surfaces A: Physicochemical and Engineering Aspects **346**: 34-38.
- Zou, W., R. Han, Z. Chen, Z. Jinghua and J. Shi (2006). *Kinetic study of adsorption of Cu (II) and Pb (II) from aqueous solutions using manganese oxide coated zeolite in batch mode*. Colloids and Surfaces **279**: 238-246.

Chapter 3

Preparation and Characterisation of the Modified Zeolite

3 Preparation and Characterisation of the Modified Zeolite

3.1 Introduction

Zeolites play an important role in a wide range of economically significant chemical reactions. In the petroleum industry alone it is estimated that the cost of refining has been reduced by some \$10 billion US due to the availability of zeolitic catalysts. Their first catalytic usage in industry was in 1962 with the large scale catalytic cracking of heavy petroleum distillate following the development of synthetic faujasites (also known as zeolite X and Y). These early synthetic zeolites had a distinct advantage over the amorphous aluminosilicates used previously in that they had a defined chemical composition and an ordered porous structure (Weitkamp 2000). This porous structure lends a shape selective quality to zeolites, which is not present in amorphous catalysts. Most industrial methods utilize the acidic (and in some cases basic) sites, intrinsic to the zeolite, to catalyze reactions; however another advantage of zeolitic catalysts is the ability to apply metals through direct synthesis or ion exchange to add redox functionality. The redox properties and acid sites can co-exist and work cooperatively (Mravec et al. 2005).

Metallo-zeolites as catalysts have been examined for the treatment of organic compounds in waste water streams primarily in the case of aqueous phase catalytic wet air oxidation (Pirkanniemi and Sillanpää 2002). Conversely the work presented here examines the catalytic oxidation of the water pollutant phenol in the gaseous phase. Metal modified zeolites have been studied extensively in the field of gas phase environmental catalysis in the last two decades. Much of the research has focused on HC-SCR-NO_x, a process of reducing NO_x containing flue gases in the presence of an oxidizing organic chemical such as propane in excess oxygen. Examples include ZSM-5 (MFI), mordenite (MOR), ferrierite (FER) and Beta (BEA) zeolite structures modified with various metallic species including Cu, Co, Ga, In, Fe, Pd, Ce, Pt, Ag, Ni and

Rh (Traa et al. 1999; Wichtelová et al. 2003). A large amount of this research has been dedicated specifically to Cu/ZSM-5 which exhibits exceptional redox activity. However, it is unsuited for conventional HC-SCR applications such as catalytic converters for engine exhaust due to fouling from diesel fuels and low exhaust temperatures. Cu/ZSM-5 has a maximum NO_x reduction/ HC oxidation at approximately 300 °C, however NO_x can start to desorb at approximately 120 °C. By contrast Pt catalysts have been examined using ZSM-5, MCM-41, mordenite and ferrierite. These catalysts exhibited a maximum NO reduction in the presence of propene at 200-250 °C, significantly lower than many metallic zeolites (Traa et al. 1999) and also shows stability in the presence of water vapour (Huuhtanen et al. 2005). Scirè et al. (2003) compared a series of Pt catalysts for the oxidation of chlorobenzene in the gas phase. It was found that the Pt modified zeolites exhibited superior reaction rates than the more conventional alumina supported Pt, and in turn BEA exhibited better performance than MFI type zeolites (Scirè et al. 2003). Similarly, Neyestanaki et al. (1994) examined the gas phase oxidation of propane on Pt and Cu modified ZSM-5. It was shown that Pt/ZSM-5 exhibited a light off temperature 30°C lower than Cu/ZSM-5 (Neyestanaki et al. 1994).

The disadvantage of mono-metallic catalysts is the narrow temperature range. Although platinum catalysts have a lower light off temperature than copper equivalents, they also often exhibit a narrower active temperature range. This can be somewhat augmented by creating bi-metallic catalysts. For example Pt/Cu ZSM-5 was examined by Mohd Saaid et al. (2002) for the reduction of NO_x. Amongst the findings was an increased temperature range of 250-520°C (Mohd Saaid et al. 2002).

For the purposes of this work, the catalyst metals Cu and Pt were chosen to increase the capacity of the zeolite to oxidize phenol.

3.1.1 Catalyst Deposition

The two most commonly used methods of depositing metal catalysts to zeolites are as follows:

1. Introduction of metal catalysts into the zeolite during synthesis (hydrothermal synthesis)
2. Cation exchange

The former involves the addition of the relevant metal catalyst salts into solution along with the silica and alumina source with the appropriate template.

Ion exchange is performed post synthesis, taking advantage of the usually trivalent metal ions in the zeolite structure. Most commonly these are Al^{3+} but can also include Ga^{3+} , Fe^{3+} and other metals (Wichtelová et al. 2003). The charge imbalance is corrected by the incorporation of a charge balancing cation. In practice the ion-exchange method involves the addition of a metal salt to a zeolite in solution. The introduced metal displaces one or more existing cations and is bonded to the zeolite primarily through electrostatic interactions.

Hydrothermal synthesis procedures are generally preferred for aqueous phase catalytic techniques such as catalytic wet peroxide oxidation due to the increased stability and activity under these conditions (Maduna Valkaj et al. 2007). However, in the case of gas phase catalysis, ion exchanged mono and bimetallic catalysts have been shown to have superior activity and broader temperature ranges when compared to directly synthesised counterparts (Neyestanaki et al. 1994; Mohd Saaid et al. 2002). Procedurally, ion exchange is simpler and more convenient, it can be performed on a commercial or pre prepared zeolite and the procedure can be repeated to add an additional metal or increase the loading. For these reasons an ion exchange procedure was chosen for this study.

Figure 3.1 shows the basic process of cation exchange on an acid zeolite with copper ions. The charge balancing or ‘counter ions’ in this case are H^+ , and these

are displaced by the Cu^{2+} ions in solution. The Cu^{2+} ion charge balances two Al sites on the zeolite surface.

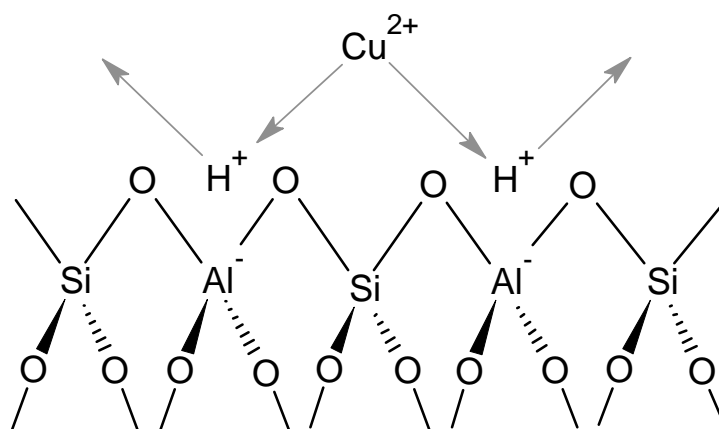


Figure 3.1 Diagram illustrating cation exchange of metal ion Cu^{2+} in solution onto a zeolite surface with the exchange cation H^+ .

Zeolites with low silica to alumina ratio have a greater concentration of exchangeable cation sites and a larger cation exchange capacity when compared to higher ratios. Copper ions exchanged on the zeolites can have different properties depending on the form and location found within the zeolite. In under-exchanged zeolites, square pyramidal coordinated copper ions are observed in the vicinity of two framework aluminium ions and are preferentially occupied first, followed by the square planer ions adjacent to one aluminium framework ion. In zeolites with high $\text{SiO}_2:\text{Al}_2\text{O}_3$ ratios or high copper loadings however the square planer copper ions can become dominant. The square pyramidal copper ions have lower catalytic activity than the equivalent square planer copper ions. Catalysts with similar copper exchange ratios yet different $\text{SiO}_2:\text{Al}_2\text{O}_3$ ratios and overall copper loadings have been observed to have similar catalytic activity (Neyestanaki et al. 1994; Torre-Abreu et al. 1997b; Pârvulescu et al. 1999).

It is possible to increase the copper loading onto zeolites by increasing the pH of the copper salt solution using ammonia. The effect is for the copper to be exchanged at the Brønsted acid sites in the form of $[\text{Cu}^{2+}(\text{OH})]^{+}$ or $[\text{Cu}(\text{NH}_4)_4]^{2+}$. The monovalent copper species become more dominant with higher pHs relative to the divalent copper ions present in lower pHs. (Chen et al. 2004). When

dehydrated the hydrolysed cations are known to form Cu-O-Cu bridges which can increase the activity of the catalyst (Neyestanaki et al. 1994).

Platinum can also exist in a number of different forms on the zeolite surface, often depending on its precursor and the method of deposition. It can form di- and tetravalent species as well as the often less active PtO_x species. Aside from cation exchange it has also been known to coordinate with silanol ($\equiv\text{Si-OH}$) sites on the zeolite surface (Ho et al. 1998). Transition metal cations are also known to interact with platinum on zeolite surfaces (Raddi de Araugo and Schmal 2002).

3.1.2 Characterisation Techniques

The techniques used to characterise the zeolite samples were atomic absorption spectroscopy, temperature programmed reduction and X-Ray diffraction.

3.1.2.1 Atomic Absorption Spectroscopy

Atomic Absorption spectroscopy (AAS) is a characterisation technique used to quantify the content of metals in aqueous solution by measuring the absorbance of a sample at a characteristic wavelength. It can be used to analyse 70 different elements. Liquid samples are analyzed by passing them through a flame of between 2000-3000K. The intensity of the absorption is dependent on the number of atoms in the flame and can be described by the Beer-Lambert law (Harris 1995).

$$A = \epsilon c d \quad \text{Equation 3.1}$$

Where:

A = absorbance

ϵ = molar absorptivity coefficient ($\text{mol}^{-1} \text{dm}^3 \text{cm}^{-1}$)

d = path length (cm)

c = concentration (mol dm^{-3})

This equation can be used to determine the amount of metal present in aqueous solution.

3.1.2.2 Temperature Programmed Reduction

Temperature Programmed Reduction (TPR) is a versatile technique used primarily for the qualitative analysis of reducible catalysts by performing a continuous analysis of the gas phase (Delannay 1984). With the introduction of a reducing agent, the reducibility of any component present on the surface of the solid is represented by a gas consumption maximum at a characteristic temperature. Low temperatures represent more easily reduced surface species where as high temperatures indicate the opposite. With this relationship TPR is used to qualitatively characterize samples. The magnitude of the peaks can be quantitatively representative of the amount of reducible metal species present (Coq et al. 1995).

TPR does not produce different data sets for different reactions; rather it produces the sum of all hydrogen consumption for all reactions. Two peaks may represent two separate reducible species or two reduction steps of the same initial species. Solids can be reduced in several steps, until the reducible species cannot be reduced further. These steps will occur at different temperatures in the TPR profile. It is also possible for two or more reduction steps of different solids to occur concurrently, resulting in a larger peak at that temperature. To differentiate between parallel and consecutive reduction it is usually necessary to have an understanding of the reaction mechanisms taking place (Heidebrecht et al. 2008).

3.1.2.3 X-Ray diffraction

X-Ray Diffraction (XRD) is a non destructive technique for the characterization of crystalline structures on a solid surface (Delannay 1984). The technique involves passing a broad band X-ray beam through a crystal and recording the diffraction pattern of the various planes within the crystal (Atkins 2000). Compounds and elements have their own unique diffraction pattern, which can

be used to differentiate them from each other. For a maximum to occur at a particular angle of incidence, Bragg's law must be satisfied (Cullity 1978).

$$n\lambda = 2d_{hkl} \sin \theta_{hkl} \quad \text{Equation 3.2}$$

Where:

n = order of diffraction

λ = wavelength of incident x-ray

d_{hkl} = interplanar distance between planes h, k and l

θ_{hkl} = diffraction angle from planes h, k and l

The diffraction angle θ represents the angle at which the X-rays are reflected from a particular lattice plane of a crystal. By deriving the diffraction angle experimentally, the distance between the layers d can be derived through Bragg's law.

X-ray powder diffraction is a method conventionally used where the sample crystal is not necessarily orientated to act as a diffraction grating at any one wavelength. This method uses a broad-band X-ray beam on powdered samples and records the diffraction pattern. The output is usually a profile with the half angle of diffraction on the x-axis and diffraction intensity on the y-axis. Different crystallites in the sample will be orientated on different planes and give rise to cones of intensity at different half angles.

XRD profiles can be used for identifying substances when compared with known profiles, they can also be used to determine phase diagrams when the proportion of each phase of a sample is unknown (Atkins 2000). Another common application is the derivation of crystal size through the Scherrer Equation.

$$B(2\theta) = \frac{K\lambda}{L\cos\theta} \quad \text{Equation 3.3}$$

B = Peak width

θ = Diffraction angle

K = Scherrer constant

L = Crystal size

λ = X-Ray Wavelength

From Equation 3.3 the peak width B is inversely proportional to the crystal size L. (Scherrer 1918; Langford and Wilson 1978).

3.2 Experimental

3.2.1 Catalyst Preparation

Copper and platinum zeolites were prepared using a conventional ion exchange technique. For the exchange step a known quantity of metal salt was dissolved in distilled water and to this the beta zeolite (Zeolyst International) was added. The zeolite to water ratio was kept at 1g of zeolite to 50 ml of water. The suspension was stirred for 24 hours before removing the zeolite by vacuum filtration. The filter cake was washed with distilled water to remove any non-exchanged species and then dried over night in air at room temperature to remove the bulk of the adsorbed water. The dried zeolite was then calcined in a Lenton Thermal Designs muffle furnace at 450°C (ramp rate 1°C min⁻¹) for 5 hours. The calcination step removes any traces of adsorbed water and decomposable salts left over from the exchange process. The salts used were Cu(NO₃)₂.3H₂O (Fluka) and Pt(NH₃)₄Cl₂.xH₂O (Aldrich) for copper and platinum exchanged zeolites,

respectively. Both are easily dissolved in water. The exchange process was also pH controlled for specific samples using NH_4OH (ACS 30% NH_3) to bring the pH up to 7. The pH was monitored using a Thermo Orion model 420A+ pH meter. All the zeolites used were supplied by Zeolyst International.

For the bi-metallic zeolites the standard process used in this work was to create a calcined, pH modified copper zeolite using the ion exchange procedure and then exchange platinum without altering the pH onto the calcined copper zeolite. A number of other exchange orders were also examined, including platinum followed by copper and the simultaneous exchange of platinum and copper.

3.2.2 Catalyst Characterisation

3.2.2.1 Atomic absorption spectroscopy

The copper and platinum content of the modified beta zeolite was analysed using atomic absorption spectrophotometry (AAS). To prepare the sample 3 ml of concentrated hydrofluoric acid (8% HCl merck) was added to 10 ml of distilled water in a 50 ml PTFE beaker, followed by 100 mg of modified zeolite. The zeolite was allowed to dissolve for 10 minutes before being transferred to a 100 ml PTFE volumetric flask and diluted to the mark with distilled water. This prepared solution was examined with a Varian/Spectra AA 220 atomic absorption spectrophotometer and compared with known copper standards prepared from a 1000 mg dm^{-3} stock solution (Reagecon) in the range of 1 to 20 mg dm^{-3} and a blank solution of distilled water. Figure 3.2 shows a typical copper solution AAS calibration graph.

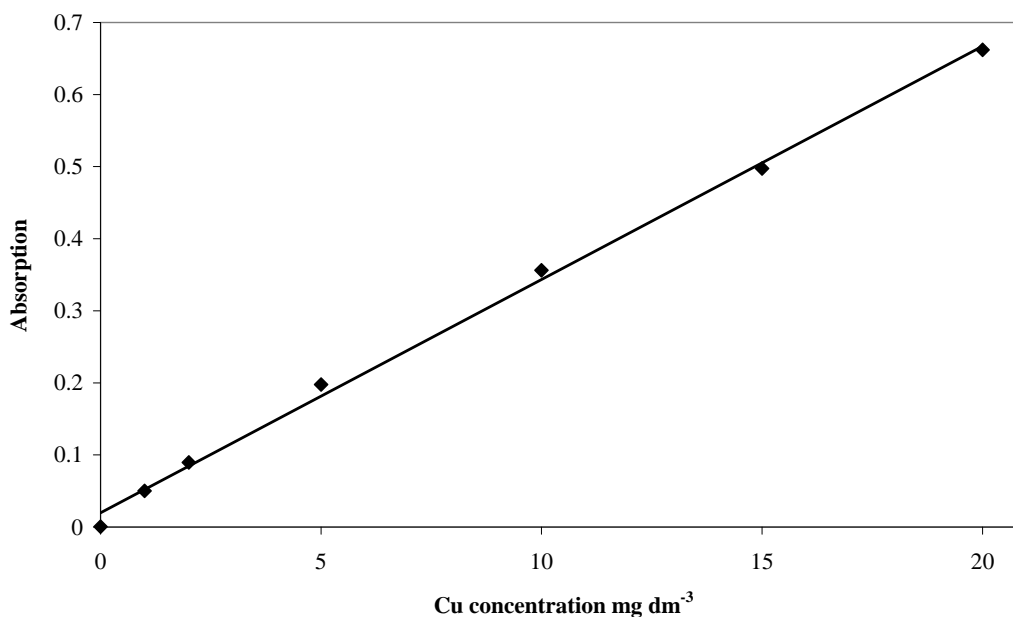


Figure 3.2 AAS trend line for copper standard solutions at 324.7 nm. R^2 value 0.9976.

A platinum standard curve was also performed for each analysis, resulting in a straight line relationship. Table 3.1 highlights the experimental conditions used for each metal.

Table 3.1 Experimental conditions necessary for AA analysis of Cu and Pt.

<i>Metal</i>	<i>Lamp Wavelength (nm)</i>	<i>Standard Range (mg dm⁻³)</i>	<i>Flame</i>
Cu	324.7	1 – 20	Air-acetylene
Pt	265.9	1 – 10	Air-acetylene

3.2.2.2 Temperature Programmed Reduction

The experimental set up for the Temperature Programmed Reduction (TPR) studies were derived from the proposed classical procedure (Lemaitre and Gerard 1981). The TPR rig used consisted of a gas delivery system, a reactor and a Thermal Conductivity Detector (TCD) as shown in Figure 3.3. The gas delivery system consists of a 5% H₂/N₂ and helium tank (BOC), the flow from which was monitored using a set of Tylan General mass flow controllers. The gas flow was directed through the reference section of the TCD and via a four way valve,

flowed through the reactor and then into the sample section of the TCD. The reactor consisted of a 560 mm quartz tube with a 6 mm internal diameter (H. Baumbach) inserted into a cylindrical muffler furnace controlled by a Lenton Thermal Designs Eurotherm temperature controller. For TPR experiments 35 mg of catalyst was inserted inside the reactor and suspended with quartz wool. The pre-treatment step involved passing helium through the reactor at a rate of 20 ml/min while heating up to 450°C at 10°C/min. The temperature inside the furnace was monitored by a thermocouple attached to a Eire Lec digital thermometer. The reactor was then cooled to 40°C. In the reduction step, 20 ml/min of 5% H₂ in N₂ was passed through the reactor while heating up to 650°C at a rate of 10°C/min. The consumption of hydrogen was monitored by a Gow-Mac TCD, model 40-201 operating at 80°C and 90mA. The exhaust gases exited through a vent into a fume hood. The conductivity of the exhaust gases was graphed using JCL6000 Chromatography software with a plot of conductivity versus temperature.

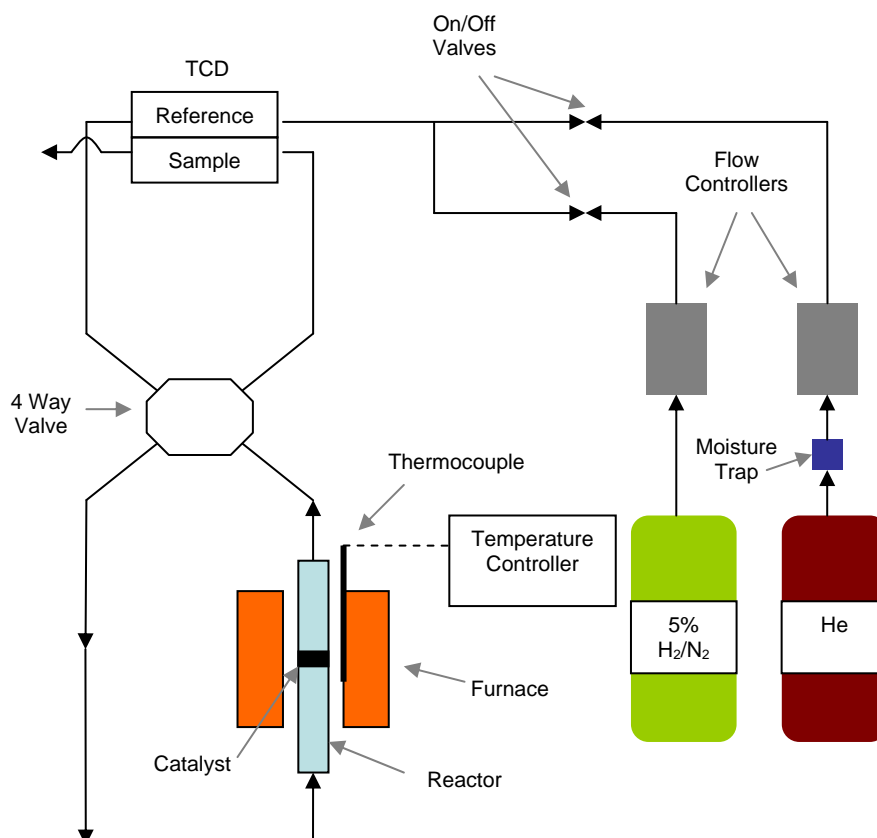


Figure 3.3 Schematic of the experimental setup for temperature programmed reduction experiments

3.2.2.3 X-Ray Diffraction

A Philips X'pert PRO MPD (multi purpose diffractometer) X-Ray Diffractometer PW3050/60 was used to characterise the zeolite samples. Samples were prepared using the standard cation exchange procedure shown in section 3.2.1 and ground with a pestle and mortar before analysis. A Cu K α diffractometer anode operating at 40 kV with a current of 35 mA was used with a scan range of 0-70° (2 θ) and a step size of 0.017° (2 θ) and 0.2° /s.

3.3 Results and Discussion

3.3.1 Catalyst Preparation

All zeolite catalysts were prepared using the cation exchange procedure outlined in section 3.2.1. Different catalysts were synthesised to cover a broad range of metal loadings and a number of exchange techniques. The nomenclature used throughout this chapter reflects the metal loading in wt% for each metal in order of exchange, the silica to alumina ratio and any modifiers for varying technique. For example '1.6Cu-0.08Pt/ β -25' represents a beta zeolite that was first modified with copper by ion exchange, followed by platinum. It also shows that the final zeolite had an actual loading of 1.6 wt% Cu and 0.08 wt% Pt. The silica to alumina ratio will also be included, for example '0.7Cu/ β -150' has a silica to alumina ratio of 150:1. The (p) suffix indicates that the exchange solution was treated with aqueous ammonia in order to bring the pH up to 7.0, whereas the (s) indicates that both metals were exchanged simultaneously. In the case of the bimetallic zeolites, every copper step was pH modified; because of this the (p) was omitted.

Table 3.2 lists the copper modified beta zeolites prepared in this work. Included in the table are the theoretical and actual copper loading of each sample. The theoretical loadings represent the wt% loading of copper onto the zeolite if the total amount of metal in the exchange solution was deposited onto the zeolite surface. The actual loading was defined experimentally by the AAS procedure

outlined in section 3.2.2. The % exchange represents the percentage of exchange sites occupied if all the metal loaded is assumed to be cation exchanged. For this, copper and platinum were assumed to be exchanged in their divalent cationic form. In the case of copper this effectively means that one mole of copper is required for every two moles of framework aluminium, as every copper ion would charge balance two aluminium framework sites (see Equation 3.4). 100% exchange would mean that every aluminium site on the zeolite would be charge balanced. The amount of framework aluminium was estimated from the silica to alumina ratio specified by the manufacturer.

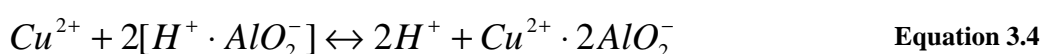


Table 3.2 Summary of prepared copper zeolite catalysts

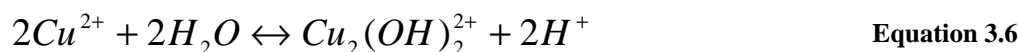
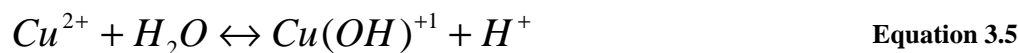
<i>Sample Name</i>	<i>SiO₂:Al₂O₃ ratio</i>	<i>Theoretical Loading (wt%)</i>	<i>Actual Loading (wt%)</i>	<i>pH of Exchange Solution</i>	<i>% Exchange</i>
0.9Cu/β-25	25:1	1	0.88	5.3	22.4
1.3Cu/β-25	25:1	2	1.33	5.4	33.8
2.1Cu/β-25(p)	25:1	2	2.13	7.0	54.3
2.3Cu/β-25(p)	25:1	3	2.33	7.0	59.3
4.6Cu/β-25(p)	25:1	5	4.55	7.0	115.7
0.7Cu/β-150	150:1	2	0.73	4.2	105
2Cu/β-150(p)	150:1	2	2.04	7.0	294.8
2.2Cu/β-300(p)	300:1	2	2.16	7.0	615.4

The pH of the exchanging solution was monitored during the zeolite modification process. When the zeolite was added to the exchanging solution the pH dropped to between 4 and 5.5. This can be explained by the displacement of extra framework protons into solution. Actual copper loadings were found to be around 60-80% of the theoretical loading on the 25:1 silica to alumina ratio beta zeolites. However, in samples where the solution pH was adjusted to 7, close to 100% of the theoretical exchange was achieved and copper loading as high as 4.6 wt% were obtained. The addition of ammonium hydroxide to raise pH in copper

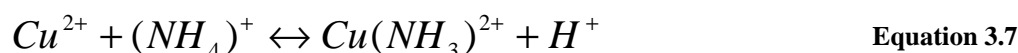
ion exchange was first introduced by Iwamoto et al., resulting in a more active catalyst for NO decomposition, compared to using the standard ion exchange procedure or indeed a repeated ion exchange method (Iwamoto et al. 1990).

From Table 3.2 the 0.7Cu/ β -150 solid, which was prepared without pH modification resulted in a zeolite with close to 100% Cu exchange. When the exchange solution was pH treated (2Cu/ β -150(p)), the actual copper loading was close to 2 wt% and represented all the copper in solution, which corresponded to almost 300% of predicted exchange. Similarly, the pH treated 300:1 copper zeolite (2.2Cu/ β -300(p)) presented a copper loading that considerably exceeded the amount of available exchange sites.

As previously outlined in section 3.1.1, the increase of exchange solution pH with the addition of ammonium hydroxide can result in the hydrolysis of aqueous copper cations. Two examples of copper hydrolysis are shown in Equation 3.5 and Equation 3.6 (Schreier et al. 2005).



Possible hydrolyzed copper ions can include $[CuOH]^+$, $[Cu_2(OH)_2]^{2+}$, $[Cu_2OH]^{3+}$ and $[Cu_3(OH)_2]^{4+}$. In these ions the valence of copper remains at 2, but the charge per copper ion is less than 2 (Schreier et al. 2005). Upon thermal treatment such as the calcination step used in these experiments, these ions can form Cu^+ cations and $[Cu-O-Cu]^{2+}$ dimer species. When treated with ammonium hydroxide, the formation of copper ammine complexes are also possible such as $[Cu(NH_4)_4]^{2+}$ and $Cu(NH_3)^{2+}$ (see Equation 3.7).



These complexes tend not to be thermally stable, and the amine groups are removed at higher temperatures, leaving copper (Neyestanaki et al. 1994; Centi and Perathoner 1995).

A number of the copper catalysts synthesised exhibited percentage exchange values beyond 100%. Since this was calculated based on the assumption that Cu^{2+} ions were exchanging in a ratio of 1:2 with aluminium sites, the excess in these over exchanged catalysts can be assumed to be an increase in the relative proportion of the previously discussed copper complexes which would only occupy one site. Another copper species group that is reported to exist is monovalent copper. Monovalent copper ion exchange generally become more prevalent in cases where there is a shortage of exchange sites, such as in zeolites with high silica to alumina ratios or where there is excess copper and favourable pH conditions. Monovalent ions often have weaker electrostatic bonding with exchange sites than their multivalent counterparts, they can also act as site blockers for divalent ions (Öhman et al. 2002). The catalysts 2Cu/ β -150(p) and 2.2Cu/ β -300(p) exhibited a percentage exchange of 294 and 615, respectively. Assuming monovalent cations could only theoretically account for up to 200% exchange, the excess could be caused by the precipitation of non-exchanged copper species or clusters such as $\text{Cu}(\text{OH})_2$ and CuO , formed as a result of increased pH conditions and deposited on the zeolite surface or pore structure (Neyestanaki et al. 1994; Centi and Perathoner 1995; Torre-Abreu et al. 1997a). Schreier et al. proposed that the over exchange occurring at high pHs was more a function of strong electrostatic adsorption occurring between silanol surface groups and copper ammine ions as opposed to the Brønsted sites (Schreier et al. 2005). Due to the likelihood of non cation exchanged and monovalent copper species resulting in the formation of an 'over-exchanged' zeolite, the theoretical value for percentage exchange should be used with caution.

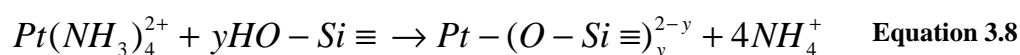
A series of Pt exchanged Beta zeolite were prepared and Table 3.3 summarizes the characteristics of these catalysts, including % exchange and the theoretical and actual loading,

Table 3.3 Summary of prepared platinum zeolite catalysts

<i>Sample Name</i>	<i>SiO₂:Al₂O₃ ratio</i>	<i>Theoretical</i>	<i>Actual</i>	<i>% Exchange</i>
		<i>Loading (wt%)</i>	<i>Loading (wt%)</i>	
0.04Pt/β-25	25:1	0.1	0.037	0.28
0.05Pt/β-25	25:1	0.2	0.049	0.40
0.07Pt/β-25	25:1	0.4	0.065	0.54
0.19Pt/β-25	25:1	0.6	0.17	1.54
0.2Pt/β-25	25:1	1	0.20	1.62

Due to its cost and its activity, platinum is generally used in significantly lower wt% loadings than copper. The level of platinum taken up by the zeolite from the exchanging solution varied between 5-37%. As platinum concentration increased in solution, the platinum loading also increased although the exchange efficiency (the proportion of the platinum in solution exchanged) decreases.

Two different types of exchanged platinum ions are reported to exist: these are cations associated with aluminium exchange sites and Pt associated with silanol groups. Silanol groups are common in some siliceous zeolites where dealumination and stacking faults result in these defects (Schreier et al. 2005). Particularly the two closely related polymorphs in zeolite beta are suggested to contribute to the presence of silanol defects (Ho et al. 1998). The coordination of platinum with silanol is shown in Equation 3.8.



The presence of platinum amines are likely to increase if the pH were raised and are somewhat more stable than their copper equivalents. The relationship with silanol is also likely to become one of strong electrostatic attraction to deprotonated silanol groups (Schreier et al. 2005).

The estimated actual % exchange in the samples listed in Table 3.3 are low relative to the amount of platinum in solution. This may suggest that there is an

excess of available aluminium sites, however not all of these sites may be available for platinum exchange. Pt ions are primarily multivalent (Pt^{2+} and Pt^{4+} ions are commonly identified) which means more than one aluminium site needs to be present in proximity to each other. Platinum particles and complexes are also known to be relatively larger than other metals such as copper, which may limit their diffusion into the zeolite structure (Schreier et al. 2005). The relative size can also affect which exchange sites are available. Smirnov et al. suggested that Pt has a tendency to exchange in channel intersections where the channel diameter is larger and where many of the aluminium sites were located in the medium pore MFI zeolites examined (Smirnov et al. 2000).

Platinum has also been reported to deposit in the form of PtO either on the surface or occluding the channels (Ho et al. 1998)

Table 3.4 Summary of prepared zeolite catalysts containing both platinum and copper

<i>Sample Name</i>	<i>Theoretical Loading (wt%) Cu/Pt</i>	<i>Actual Loading (wt%) Cu/Pt</i>	<i>% Exchange Cu/Pt</i>
1.4Cu-0.04Pt/ β -25	2 / 0.2	1.35 / 0.035	34.4 / 0.28
1.6Cu-0.08Pt/ β -25	2 / 0.4	1.57 / 0.079	39.9 / 0.66
0.04Pt-1.2Cu/ β -25	2 / 0.4	1.23 / 0.039	31.4 / 0.32
1.2Cu-0.1Pt/ β -25(S)	2 / 0.4	1.16 / 0.098	29.5 / 1.18
1.3Cu-0.09Pt/ β -25	2 / 0.6	1.29 / 0.088	32.9 / 0.74
2.4Cu-0.08Pt/ β -25	5 / 1	2.38 / 0.078	60.7 / 0.64
0.1Pt-2.4Cu/ β -25	5 / 1	2.42 / 0.14	61.6 / 1.14

Table 3.4 shows the prepared bimetallic catalysts. The percentage exchange of platinum is relatively low so as to be unlikely to inhibit the exchange of copper or vice versa purely by competition for active sites. This assumption may be false however if only a smaller quantity of aluminium sites are available for platinum exchange. The results show a comparable amount of platinum in the bimetallic catalysts relative to the monometallic equivalents, until the theoretical loading increases beyond 0.4 wt% where the platinum loading stops increasing relative to increasing platinum in solution and does not exceed 0.1 wt%.

The copper loading appeared to be relatively lower than in the case of the monometallic catalysts with the same theoretical loading.

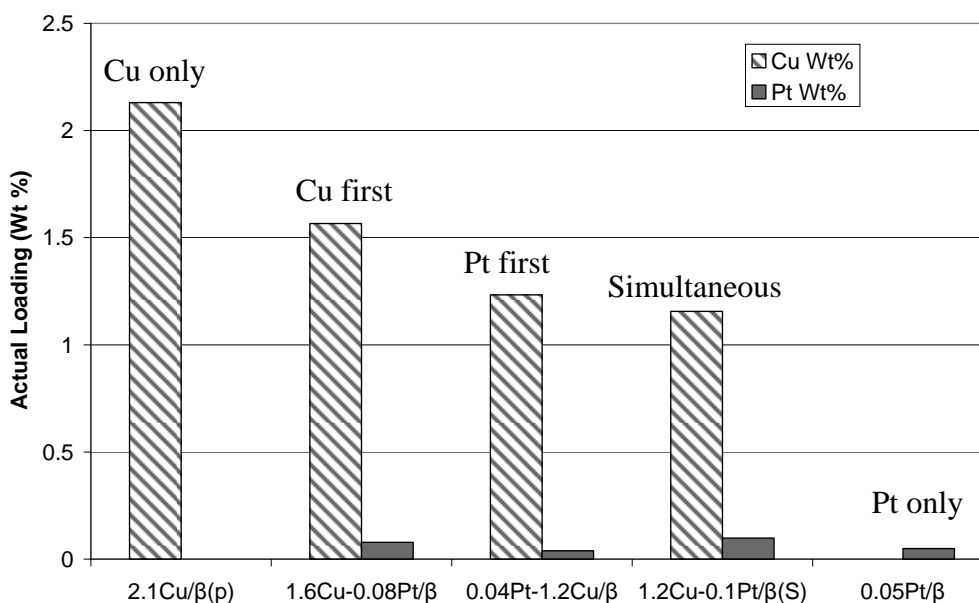


Figure 3.4 Comparison of various cation exchange procedures for BEA zeolites ($\text{SiO}_2:\text{Al}_2\text{O}_3 = 25:1$) with a theoretical loading of 2% Cu and 0.4% Pt.

Figure 3.4 shows the relative copper and platinum loadings for a range of catalysts created by different exchange procedures. In each case enough copper and platinum was provided in solution to give a loading of 2% and 0.4 % respectively. Each copper exchange step included pH adjustment to 7.0. It is clear from the results that copper loading decreases noticeably with the inclusion of exchanged platinum, regardless of procedure. The sample where copper is exchanged in the first step also seems to exhibit a higher copper loading than in the cases where platinum was exchanged first or simultaneously. The lowest copper loading was observed by a relatively small margin in the sample where copper and platinum were exchanged in a mixed solution simultaneously. This sample also exhibits that highest platinum loading, possibly due to higher pH conditions. The mixed metal solution was pH treated meaning the platinum would have exchanged under higher pH conditions than in the other examples.

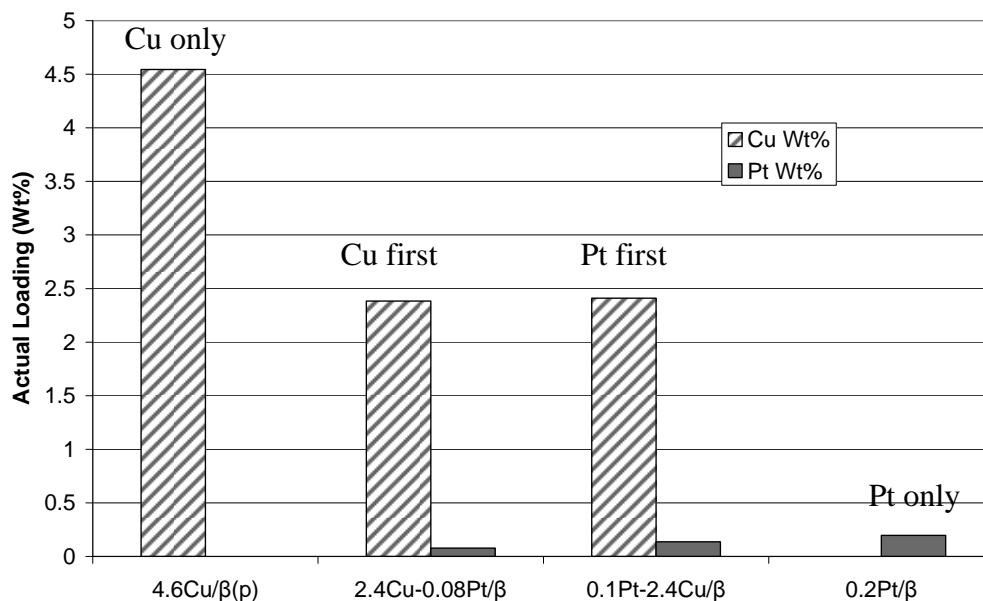


Figure 3.5 Comparison of various cation exchange procedures for BEA zeolites ($\text{SiO}_2:\text{Al}_2\text{O}_3 = 25:1$) with a theoretical loading of 5% Cu and 1% Pt.

Figure 3.5 makes a similar comparison, but with much larger theoretical loadings of copper and platinum (5% and 1% respectively). In these samples platinum loading follows a different trend with the highest loading observed where platinum is exchanged on its own followed by the bimetallic catalyst where platinum was exchanged in the first step. Whereas copper loading is considerably higher when exchanged on its own, there is little difference between the two bimetallic catalysts regardless of the order of exchange.

Comparing the results from Figure 3.4 and Figure 3.5 a noticeable decrease in exchanged copper between the mono and bimetallic zeolites is visible, however there is no distinct correlation as to the behaviour of platinum between the two. It is possible that the relationship between the two metals changes with their proportionate ratio. Tzou et al. (1991) suggests that in Y zeolites the Cu/Pt ratio can alter the nature of CuPt bimetallic particles forming in the zeolite structure, with an increased occurrence of CuPt alloys at ratios above 3:1 (Tzou and Kusunoki 1991). The increased copper loading in Figure 3.5 could also be obstructing access into the zeolite structure; this could be the cause of the reduced platinum content where copper is exchanged first.

3.3.2 Temperature Programmed Reduction

Temperature Programmed Reduction (TPR) was performed on all of the prepared catalysts. The TPR profiles for three different copper loadings are shown in Figure 3.6. Copper loadings of less than 2.1 wt% were observed to have no distinct TPR profile.

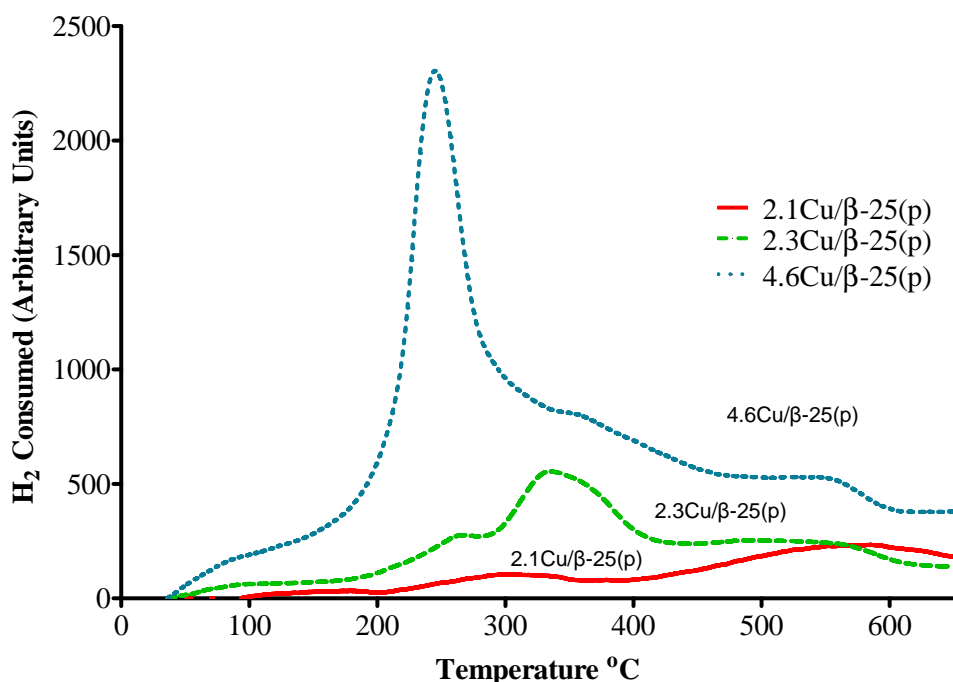


Figure 3.6 Temperature programmed reduction profile of three prepared catalysts with varying copper loading. (5% H₂/N₂, flow rate = 20ml/min, ramp rate = 10°C/min, 35 mg catalyst)

The temperature of reduction is clearly reduced as the copper loading is increased. There is also a relative change in the shape of the profile, with a smaller low temperature peak occurring in 2.3Cu/β-25(p) at 265°C and a high temperature peak at 330°C. In the 4.6Cu/β-25(p) sample the low temperature peak appears to become dominant and the high temperature peak reduced to a shoulder. The profile for 2.1Cu/β-25(p) is less distinct, with a H₂ consumption maximum at 300 and 570°C, the latter is present in the profiles of the other catalysts albeit as a shoulder.

Figure 3.7 shows the TPR profiles for three catalysts with different silica to alumina ratios. In this case the TPR profiles also show some changing relationship between reducible components with three distinct peaks. The 150:1

and 300:1 zeolites both share the two initial peaks at c.200-250°C and at c. 300°C. The 25:1 zeolite has a single peak at c. 300°C and a larger peak with a maximum at 580°C. The later peak is also present in the 150:1 zeolite and virtually absent from the 300:1. The relevant peak maxima temperature for all the copper catalyst TPR profiles are shown in Table 3.5.

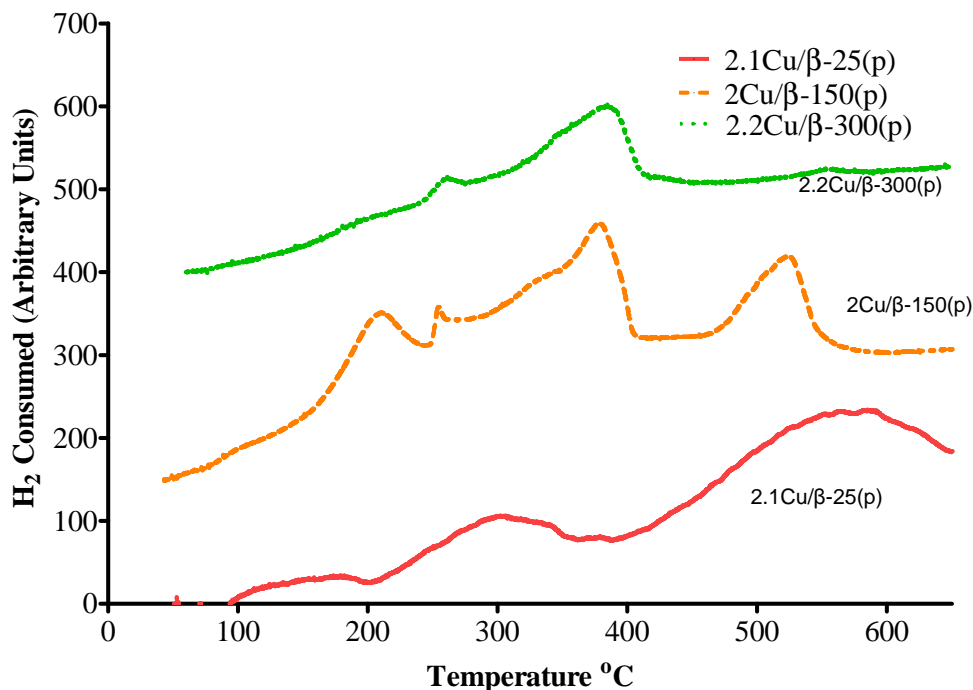


Figure 3.7 Temperature programmed reduction profiles of three prepared catalysts with varying SiO₂/Al₂O₃ ratio and the same theoretical copper loading (2wt%). (5% H₂/N₂, flow rate = 20ml/min, ramp rate = 10°C/min, 35 mg catalyst).

Table 3.5 Relevant peak maxima temperatures observed in the TPR profiles in Figure 3.6 and Figure 3.7.

<i>Catalyst</i>	<i>Temperature of peak maxima (°C)</i>		
2.1Cu/β-25(p)		300	580
2.3Cu/β-25(p)	262*	330	563*
4.6Cu/β-25(p)	244	350*	551*
2Cu/β-150(p)	210	377	525
2.2Cu/β-300(p)	260	386	

* Shoulder

Three principal reduction reactions have been proposed for copper exchanged zeolites in the literature:



The reactions in Equation 3.9 and Equation 3.10 are known to occur at a similar low reduction temperatures, while Equation 3.11 is more likely to occur at higher temperatures. The three groups of reduction maxima observed in Table 3.5 are similar to those reported in the literature (Torre-Abreu et al. 1999). From this work the low temperature peak in the range of 210-262 °C may correspond to the reduction of CuO to Cu⁰, the 300-386 °C peak to the reduction of Cu²⁺ to Cu⁺, and the 525-580 °C peak to the reduction of Cu⁺ to Cu⁰ (Torre-Abreu et al. 1999). From these assumptions it is possible to use the TPR profiles to highlight specific copper species by their reducibility. The reduction of Cu⁺ to Cu⁰ can be dependent on the products of the earlier reduction of Cu²⁺ to Cu⁺, so only a dominant high temperature peak would indicate that Cu⁺ species exist on the original sample.

The catalyst 2.1Cu/β-25(p) exhibits two maxima which correspond to the reduction of Cu²⁺ and Cu⁺. The relatively larger high temperature peak at 580°C suggests that both Cu²⁺ and Cu⁺ species exist on the zeolite. The 2.3Cu/β-25(p) shows a relatively larger peak for Cu²⁺ reduction with a smaller shoulder before it indicative of CuO reduction. The Cu⁺ peak is masked partially in this profile but appears similar in intensity to that seen in 2.1Cu/β-25(p). The relationship shifts for the 4.6Cu/β-25(p) where the probable reduction peak for CuO greatly exceeds that for Cu²⁺. The Cu²⁺ and CuO reduction peaks commonly overlap, however it is reasonable to say that when these combined low temperature peaks exceed the high temperature Cu⁺ reduction peak that an excess of CuO is present on the catalyst surface due to its single step reduction not impacting on the higher temperature peak (Torre-Abreu et al. 1997a).

The general trend appears to be that as the initial copper concentration in the exchange solution is increased, there is an increased proportion of CuO species on the zeolite. Rather than being cation exchanged these species are most likely simply deposited in the zeolite pore structure or surface. All three catalysts shown in Figure 3.6 were pH adjusted during exchange, the result is likely to be an increased presence of Cu^+ species. This is only immediately apparent on the 2.1Cu/ β -25(p) catalyst as in the other samples it is difficult to tell due to the enlarged low temperature peak.

The profiles in Figure 3.7 show three catalysts with different silica to alumina ratios. The 150:1 zeolite shows two similarly sized peaks, with the lower temperature one being somewhat larger. This could indicate that most of the copper species are Cu^{2+} with a smaller quantity of CuO species. The small earlier maxima could be the CuO reduction peak but it is unusually separated and examples have not occurred in the literature. The percentage exchanged calculated for this catalyst (295%) suggests a very high level of over exchange and large amount of copper species being deposited on areas other than the aluminium sites. This may indicate that a large proportion of the low temperature peak at 377°C is actually CuO reduction and not Cu^{2+} and that the higher temperature peak is representative of the one step reduction of Cu^+ species. This assumption seems to fit the profile of the 300:1 zeolite also, where the aluminium sites are even fewer, the maxima at 386°C is only slightly smaller than that for the 150:1 zeolite and the high temperature peak is virtually absent, this would suggest that almost all of the copper is in the form of CuO species.

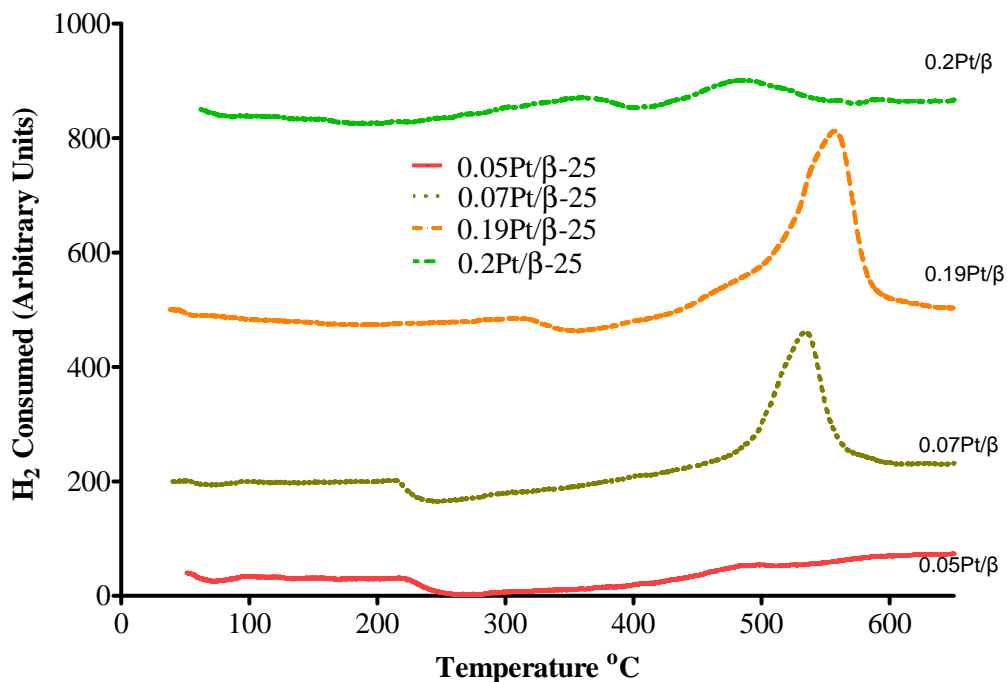


Figure 3.8 Temperature programmed reduction profile of four prepared catalysts with varying platinum loading. (5% H₂/N₂, flow rate = 20ml/min, ramp rate =10°C/min, 35 mg catalyst).

Table 3.6 Relevant peak maxima temperatures observed in the TPR profiles in Figure 3.8.

<i>Catalyst</i>	<i>Temperature of peak maxima (°C)</i>	
0.05Pt/β-25	226	
0.07Pt/β-25	214	534
0.19Pt/β-25	315	556
0.2Pt/β-25	360	488

Figure 3.8 shows the TPR profiles for four catalysts with varying platinum loading. The principal peak maxima are shown in Table 3.6. Two distinct maxima are visible in the profiles, a small peak or shoulder at approximately 220-340°C and another at around 520°C. Ho et al. identified similar profiles on platinum exchanged beta zeolites, and suggested amongst others that a peak at around 250°C corresponds to Pt⁴⁺ platinum species and one between 430 and 530°C corresponds to Pt²⁺ species which have coordinated with the silanol imperfections on the zeolite surface as outlined in Equation 3.8. Other reducible platinum species were observed at 80°C (PtO) and 150°C (Pt²⁺) but these do not occur in the profiles in Figure 3.8 (Ho and McKay 1999).

The low temperature maxima corresponding to Pt^{4+} species, appears to occur in each profile in similar levels. As the platinum weight increases, this maximum is also observed at increasingly higher temperatures. The high temperature peak is virtually absent from the catalyst with lowest platinum loading, but as exchanged platinum is increased, this peak becomes more prominent. This seems to indicate that as more platinum is loaded it will primarily be coordinated with silanol as $\text{Pt}-(\text{O}-\text{Si}\equiv)_y^{2-y}$. The $0.2\text{Pt}/\beta-25$ catalyst appears to be the exception, and shows a greater balance between Pt^{4+} exchanged on aluminium sites and $\text{Pt}-(\text{O}-\text{Si}\equiv)_y^{2-y}$. This could be as a result of it having by far the highest platinum concentration in solution during exchange, giving greater opportunity for the sites to be occupied.

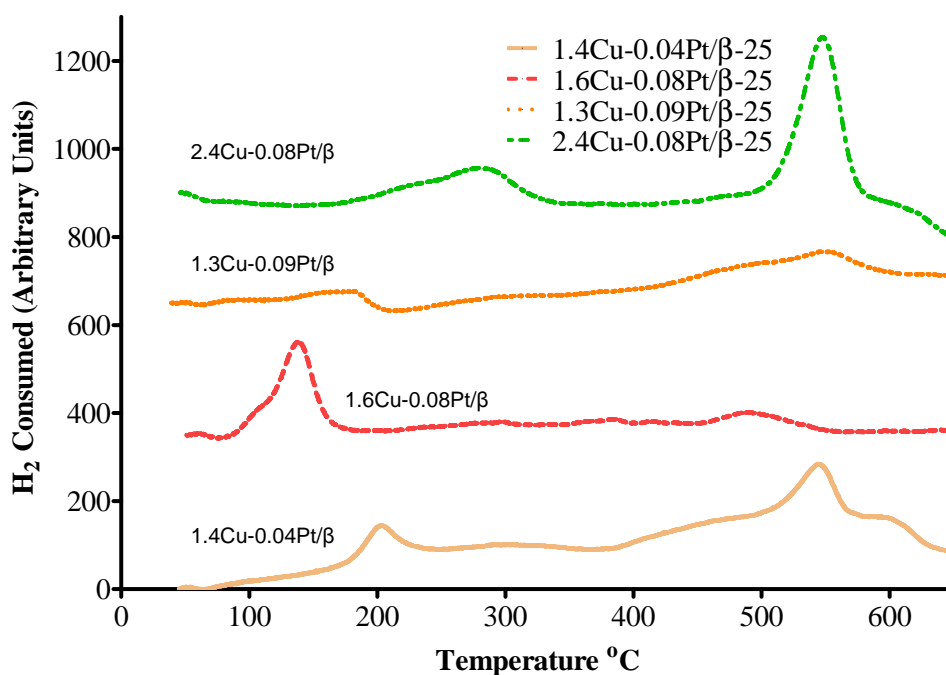


Figure 3.9 Temperature programmed reduction profile of four prepared bimetallic catalysts with varying platinum and copper loading. (5% H_2/N_2 , flow rate = 20ml/min, ramp rate = $10^\circ\text{C}/\text{min}$, 35 mg catalyst).

The TPR profiles for four bimetallic catalysts are shown in Figure 3.9. In most of the profiles copper loading is likely to be too low to be detected, with the possible exception of the catalyst $2.4\text{Cu}-0.08\text{Pt}/\beta-25$, which has the highest copper loading and has the characteristic copper peak observed in previous profiles at 290°C . This may represent Cu^{2+} or CuO species, the corresponding high temperature peak may be masked by the distinct $\text{Pt}-(\text{O}-\text{Si}\equiv)_y^{2-y}$ peak at

550°C. The Pt-(O-Si≡)_y^{2-y} peak also occurs on the low platinum catalyst 1.4Cu-0.04Pt/β-25 and possibly on 1.6Cu-0.08Pt/β-25 and 1.3Cu-0.09Pt/β-25 to a lesser degree. Since the peak for the reduction of Cu⁺ also occurs close to this temperature, there is a chance that only one or the other is present or that they occur in tandem. The low temperature peak at 135°C for 1.6Cu-0.08Pt/β-25 has been attributed to Pt²⁺ or PtO for platinum beta zeolites, this may also be the case for the peak at 200°C for 1.4Cu-0.04Pt/β (Ho et al. 1998; Dalla Costa and Querini 2010).

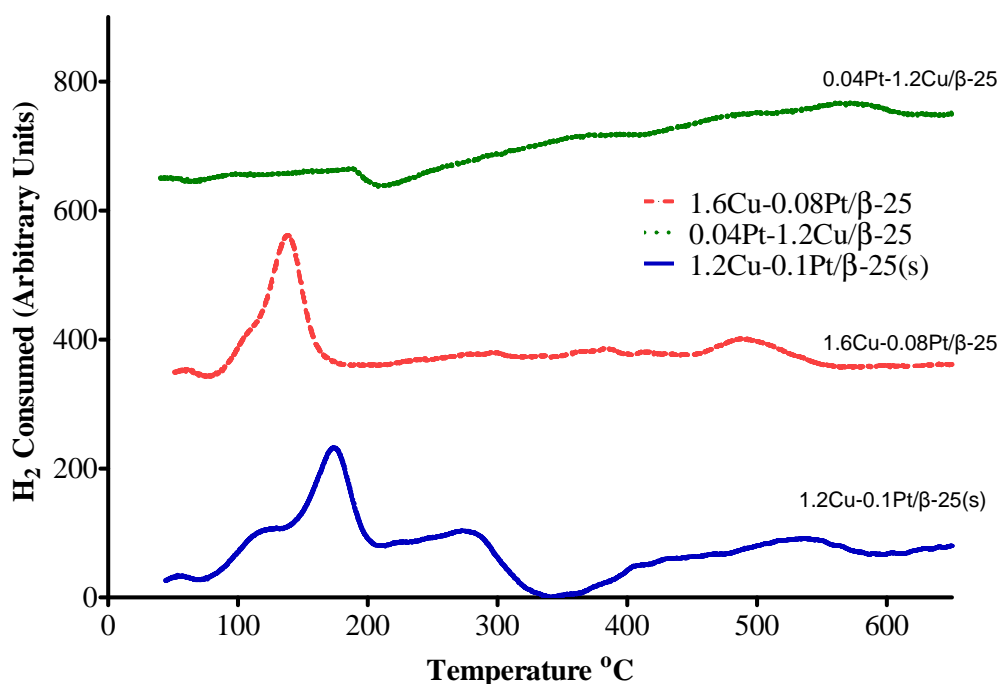


Figure 3.10 Temperature programmed reduction profile of three prepared bimetallic catalysts with different exchange orders and constant theoretical loading of 2%Cu and 0.4%Pt. (s) denotes simultaneous exchange (5% H₂/N₂, flow rate = 20ml/min, ramp rate =10°C/min, 35 mg catalyst).

Figure 3.10 shows the TPR profiles of three different exchange orders, two-step copper followed by platinum exchange, two-step platinum followed by copper exchange and one-step simultaneous exchange. The same low temperature peak representing Pt²⁺ or PtO reduction is present in 1.6Cu-0.08Pt/β-25 and 1.2Cu-0.1Pt/β-25. The catalyst, on which platinum was exchanged first (0.04Pt-1.2Cu/β-25), experienced the lowest platinum loading and consequently no visible low temperature peak. This may indicate platinum leaching during the second exchange step. The simultaneously exchanged catalyst had a peak at 280°C which is reminiscent of the Cu²⁺ or CuO reduction peak typically

observed on copper catalysts. A proportionate peak at 540°C suggests that the two step reduction of Cu^{2+} species is occurring. The two step catalysts both show only a mild increase in H_2 consumption at higher temperatures. This may be associated with either Cu^+ or silanol coordinated Pt reduction or a combination of both.

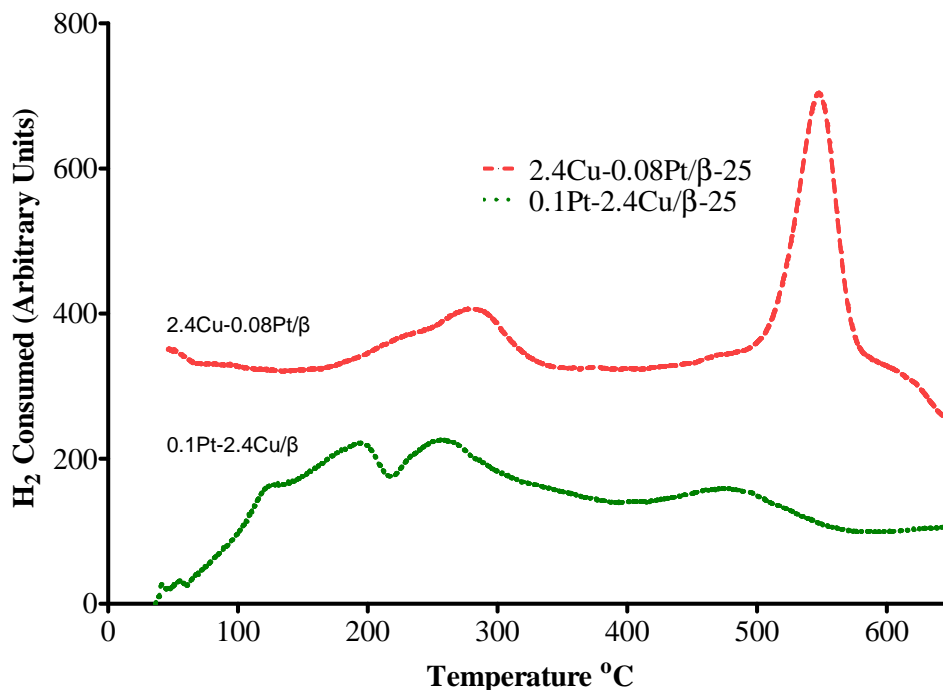


Figure 3.11 Temperature programmed reduction profile of three prepared bimetallic catalysts with different exchange orders and constant theoretical loading of 5%Cu and 1%Pt. (5% H_2/N_2 , flow rate = 20ml/min, ramp rate = 10°C/min, 35 mg catalyst).

Figure 3.11 shows the TPR profiles for two bimetallic catalysts with different exchange orders, this time with much higher theoretical platinum and copper loading. For the catalyst where copper was exchanged first (2.4Cu-0.08Pt/β-25), the characteristic $\text{CuO}/\text{Cu}^{2+}$ and silanol coordinated platinum reduction peaks were found at 280 and 545 °C respectively. It is difficult to tell which copper species are present due to the high temperature platinum maxima masking the equivalent copper peak. The copper peak is similar in intensity and shape to that observed on the profile of 2.3Cu/β-25(p) in Figure 3.6 (which has a similar copper loading) except that it occurs at a lower temperature. The peak in 2.4Cu-0.08Pt/β-25 occurs at the same approximate temperature (280°C) as its counterpart on 1.2Cu-0.1Pt/β-25(s) in Figure 3.10. Therefore the lower reduction temperature may be due to the presence of platinum.

There is no apparent low temperature platinum peak in 2.4Cu-0.08Pt/ β -25, this could indicate that most of the platinum on the catalyst is coordinated with silanol surface groups. For the catalyst in which platinum was exchanged first (0.1Pt-2.4Cu/ β -25), the copper peak is also present at the same temperature as in 2.4Cu-0.08Pt/ β -25, however it overlaps partially with a low temperature platinum peak. The peak maxima at 480°C may indicate the presence of the high temperature copper peak. If this is so, then it would appear that copper is present in both Cu²⁺ and Cu⁺ species, whereas most the platinum is present as Pt²⁺ and/or PtO. If this is the case, while copper seems to be changed very little relative to exchange order, platinum coordination changes significantly with high silanol coordination when exchanged in the second step and high exchange on aluminium sites as Pt²⁺ or deposition as Pt oxides when exchanged first. This may be caused by leaching of silanol coordinated platinum during the copper exchange, or possibly due to the increased copper loading occupying more available aluminium sites when exchanged first and thus forcing the platinum to exchange at the silanol sites. The other bimetallic zeolites with lower copper loadings in Figure 3.10 (1.6Cu-0.08Pt/ β -25 and 0.04Pt-1.2Cu/ β -25) and Figure 3.9 (1.3Cu-0.09Pt/ β -25 and 1.4Cu-0.04Pt/ β -25) show little to no evidence of high temperature platinum peaks, where as the mono metallic platinum zeolites in Figure 3.8 (0.07Pt/ β -25 and 0.19Pt/ β -25) show a prevalence of high temperature platinum reduction with little to no occurrence of the low temperature peak. This suggests that whereas platinum will preferentially coordinate with silanol when deposited on its own, it is more commonly found as Pt²⁺ or PtO species in bimetallic zeolites, except where copper is over exchanged in the first step preventing it from either occluding in the pores or coordinating with aluminium sites. It is also possible when copper is exchanged last it covers the platinum or otherwise prevents access to the surface. This would have the effect of masking platinum.

To summarize, copper was found to over-exchange when pH treated and as either the amount of copper in solution was increased or the number of

exchanged sites decreased. The result was to increase the proportion of monovalent and oxide copper species on the zeolite.

Platinum was found to exchange independently of the aluminium exchange sites when exchanged on its own, instead attaching to the silanol groups. However the presence of copper appears to affect the location to which platinum exchanges, which may be a shift towards aluminium sites such as Pt^{2+} or as PtO .

3.3.3 X-Ray Diffraction

X-Ray Diffraction (XRD) was performed on six different catalysts in order to possibly identify any metal particles on the catalyst surface.

No significant difference was noted between the diffractograms of each of the six catalysts examined, except for one minor peak on the Cu/Pt catalyst at $2\theta = 40.5^\circ$ (highlighted in Figure 3.12) which could possibly represent the platinum phase (Rioux and Vannice 2005; Villegas et al. 2006). This peak is not present on the Pt catalyst diffractogram which could indicate a difference in platinum dispersion between the monometallic and bimetallic zeolite. The overall similarity of the diffractograms suggests that the metals are well dispersed and the zeolite structure largely unchanged.

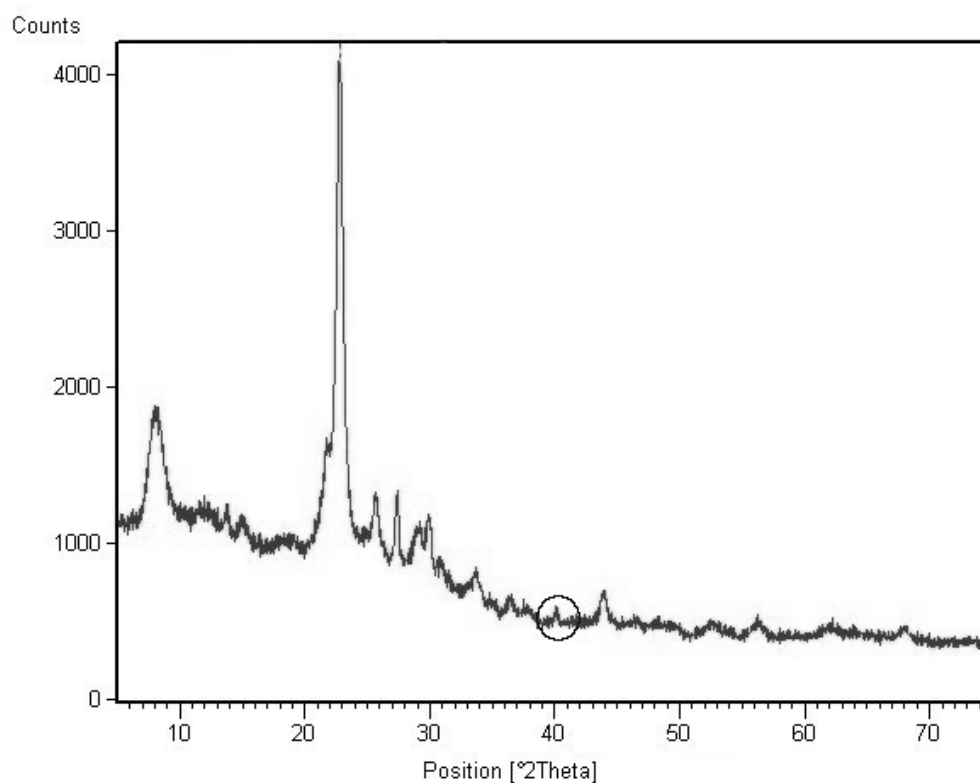


Figure 3.12 XRD diffraction pattern for the catalyst 1.6Cu-0.08Pt/β.

3.4 Conclusions

The aim of the work in this chapter was to develop a procedure for the preparation of a range of metal exchanged zeolites and to define the characteristics of the exchanged metal using a number of techniques. Copper, platinum and bimetallic copper-platinum zeolites were prepared with repeatable metal loading. The exchange of copper under normal pH conditions was found to be inhibited with increasing silica to alumina ratio. This corresponds predictably to the decrease in aluminium exchange sites which are characteristic of high silica zeolites. When the pH of the exchange solution was raised to pH 7 however, copper loading was found to increase significantly even in cases where the amount of copper exceeded the expected quantity of exchange sites. This over exchange was confirmed by the TPR profiles. The profiles of pH treated zeolites appear to have both Cu^{2+} and Cu^+ species exchanged on the surface, as the copper loading increases and the amount of available exchange sites decreases, a larger proportion of exchanged copper becomes deposited in the form of CuO . This trend is also apparent with increasing silica to alumina ratio. pH treated zeolites under the same experimental conditions will appear to exchange similar amounts of copper, regardless of silica to alumina ratio. However, the TPR profiles appear to suggest that a greater amount of this exchanged copper is deposited as unexchanged CuO , accounting for almost all copper at $\text{SiO}_2:\text{Al}_2\text{O}_3=300:1$.

Platinum was found to exchange only in small amounts (relative to the salt concentration in solution) under normal conditions, and is suspected of coordinating primarily with silanol groups. However on zeolites where both copper and platinum was exchanged it was found that nature of platinum on the zeolites changes to cation exchanged Pt^{2+} or PtO species except in catalysts where excess platinum is present. This shift in the nature of platinum species also appears to be represented in the XRD results, where the diffractogram for the bimetallic zeolite shows a possible platinum phase peak which is not present in the diffractogram for the platinum zeolite.

Both copper and platinum occur in different states on the catalyst depending on the exchange technique. It is conceivable that these may affect the adsorption and oxidation of phenol. Copper has been noted to be more active in $[\text{Cu-O-Cu}]^{2+}$ and Cu^{2+} species than as the CuO and Cu^+ observed in over exchanged zeolites. Similarly platinum is known to be more active in its metallic state than as oxidized PtO_x particles (Neyestanaki et al. 1994; Torre-Abreu et al. 1997a). Also as the amount of exchanged metal is increased its electrostatic interaction with the frame work aluminium is weakened, and its distribution on the zeolite surface changes (Torre-Abreu et al. 1997a). For these reasons, the catalyst with the highest metal loading may not be the optimal catalyst, furthermore the bimetallic copper and platinum catalyst may illicit different qualities than those exhibited in their monometallic equivalents.

3.5 References

- Atkins, P. W. (2000). *Physical chemistry*. Oxford, Oxford University Press.
- Centi, G. and S. Perathoner (1995). *Nature of active species in copper-based catalysis and their chemistry of transformation of nitrogen oxides*. Applied Catalysis A: General **132**(2): 179-259.
- Chen, H., M. Matsuoka, J. Zhang and M. Anpo (2004). *The reduction behavior of the Cu ion species exchanged into Y zeolite during the thermovacuum treatment*. Journal of Catalysis **228**: 75-79.
- Coq, B., B. Tachon, F. Figueras, G. Mabilon and M. Prigent (1995). *Selective catalytic reduction of nitrogen monoxide by decane on copper-exchanged mordenites*. Applied Catalysis B: Environmental **6**: 271-289.
- Cullity, B. D. (1978). *Elements of X-ray diffraction*. Addison, Wesley publishing company.
- Dalla Costa, B. O. and C. A. Querini (2010). *Isobutane alkylation with solid catalysts based on beta zeolite*. Applied Catalysis A: General **385**: 144-152.
- Delannay, F. (1984). *Characterization of heterogeneous catalysis*. New York, Marcel Dekker.
- Harris, D. C. (1995). *Quantitative chemical analysis*. New York, W.H. Freeman.
- Heidebrecht, P., V. Galvita and K. Sundmacher (2008). *An alternative method for parameter identification from temperature programmed reduction (TPR) data*. Chemical Engineering Science **63**(19): 4776-4788.
- Ho, L., C. Hwang, J. Lee, I. Wang and C. Yeh (1998). *Reduction of platinum dispersed on dealuminated beta zeolite*. Journal of Molecular Catalysis A: Chemical **136**: 293-299.
- Ho, Y. S. and G. McKay (1999). *Pseudo-second order model for sorption processes*. Process Biochemistry **34**: 451-465.
- Huuhtanen, M., K. Rahkamaa-Tolonen, T. Maunula and R. L. Keiski (2005). *Pt-loaded zeolites for reducing exhaust gas emissions at low temperatures and in lean conditions*. Catalysis Today **100**: 321-325.

- Iwamoto, M., H. Yahiro, Y. Torikai, T. Yoshioka and N. Mizuno (1990). *Novel preparation method of highly copper ion-exchanged ZSM-5 zeolites and their catalytic activities for no decomposition*. Chem. Lett.: 1967-170.
- Langford, J. I. and A. J. C. Wilson (1978). *Scherrer after sixty years: A survey and some new results in the determination of crystallite size*. Journal of Applied Crystallography **11**: 102-113.
- Lemaitre, J. and P. Gerard (1981). *Characterization of hydrous nickel containing silicates by temperature programmed reduction*. Bulletin de Mineralogie **104**(5): 655-660.
- Maduna Valkaj, K., A. Katovic and S. Zrncevic (2007). *Investigation of the catalytic wet peroxide oxidation of phenol over different types of Cu/ZSM-5 catalyst*. Journal of Hazardous Materials **144**: 663-667.
- Mohd Saaid, I., A. Rahman Mohamed and S. Bhatia (2002). *Activity and characterization of bimetallic ZSM-5 for the selective catalytic reduction of NO_x* . Journal of Molecular Catalysis A: Chemical **198**: 241-250.
- Mravec, D., J. Hudec and I. Janotka (2005). *Some possibilities of catalytic and noncatalytic utilization of zeolites*. Chemical Papers **59**(1): 62-69.
- Neyestanaki, A. K., N. Kumar and L. Lindfors (1994). *Catalytic combustion of propane over Pt and Cu modified ZSM-5 zeolite catalysts*. Fuel **74**(5): 690-696.
- Öhman, L. O., B. Ganemi, E. Björnbom, K. Rahkamaa, R. L. Keiski and J. Paul (2002). *Catalyst preparation through ion-exchange of zeolite Cu-, Ni-, Pd-, CuNi- and CuPd-ZSM-5* Materials Chemistry and Physics **73**: 263-267.
- Pârvulescu, V. I., P. Grange and B. Delmon (1999). *Catalytic removal of NO*. Catalysis Today **46**(4): 233-316.
- Pirkanniemi, K. and M. Sillanpää (2002). *Heterogeneous water phase catalysis as an environmental application: A review*. Chemosphere **48**: 1047-1060.
- Raddi de Araugo, L. R. and M. Schmal (2002). *Pt-Cr/ZSM-5 catalysts for propane and cyclohexane conversion*. Applied Catalysis A: General **235**(1-2): 139-147.
- Rioux, R. M. and M. A. Vannice (2005). *Dehydrogenation of isopropyl alcohol on carbon-supported Pt and Cu-Pt catalysts*. Journal of Catalysis **233**: 147-165.

- Scherrer, P. (1918). *Bestimmung der grösse und der inneren struktur von kolloidteilchen mittels röntgenstrahlen*. Nachrichten von der Königlichen Gesellschaft der Wissenschaften zu Göttingen **26**: 98-100.
- Schreier, M., S. Teren, L. Belcher, J. R. Regalbuto and J. T. Miller (2005). *The nature of 'overexchanged' copper and platinum zeolites*. Nanotechnology **16**: 582-591.
- Scirè, S., S. Minicò and C. Crisafulli (2003). *Pt catalysts supported on h-type zeolites for the catalytic combustion of chlorobenzene*. Applied Catalysis B: Environmental **45**: 117-125.
- Smirnov, A. V., E. V. Mazin, V. V. K. Yuschenko, E. E. S. N. Nesterenko, I. I. Ivanova, L. Galperin, R. Jensen and S. Bradley (2000). *Benzene alkylation with propane over Pt-modified MFI zeolites*. Journal of Catalysis **194**: 266-277.
- Torre-Abreu, C., C. Henriques, F. R. Ribeiro, G. Delahay and M. F. Ribeiro (1999). *Selective catalytic reduction of NO on copper-exchanged zeolites: The role of the structure of the zeolite in the nature of copper-active sites*. Catalysis Today **54**: 407-418.
- Torre-Abreu, C., M. F. Ribeiro, C. Henriques and G. Delahay (1997a). *Characterisation of CuMFI catalysts by temperature programmed desorption of no and temperature programmed reduction. Effect of the zeolite Si/Al ratio and copper loading*. Applied Catalysis B: Environmental **12**(2-3): 249-262.
- Torre-Abreu, C., M. F. Ribeiro, C. Henriques and F. R. Ribeiro (1997b). *Selective catalytic reduction of NO with propene over CuMFI zeolites: Dependence on Si/Al ratio and copper loading*. Applied Catalysis B: Environmental **11**: 383-401.
- Traa, Y., B. Burger and J. Weitkamp (1999). *Zeolite-based materials for the selective catalytic reduction of NO_x with hydrocarbons*. Microporous and Mesoporous Materials **30**(1): 3-41.
- Tzou, M. and M. Kusunoki (1991). *Bimetallic CuPt particles supported in Y zeolite: Structural characterization by EXFAS*. Journal of Physical Chemistry **95**: 5210-5215.
- Villegas, J. I., N. Kumar, T. Heikkilä, V. P. Lehto, T. Salmi and D. Y. Murzin (2006). *Isomerization of n-butane to isobutane over Pt-modified beta and ZSM-5 zeolite catalysis: Catalyst deactivation and regeneration*. Chemical Engineering Journal **120**(1-2).
- Viswanadham, N., R. Kamble, S. K. Saxena and M. O. Garg (2008). *Studies on octane boosting of industrial feedstocks on Pt/H-BEA zeolite*. Fuel **87**: 2394-2400.

- Weitkamp, J. (2000). *Zeolites and catalysis*. *Solid State Ionics* **131**: 175-188.
- Wichtelová, B., Z. Sobalík and J. Dědeček (2003). *Redox catalysis over metallo-zeolites: Contribution to environmental catalysis*. *Applied Catalysis B: Environmental* **41**(1-2): 97-114.

Chapter 4

Adsorption of Phenol onto Modified Beta Zeolite

4 Adsorption of Phenol onto Modified Beta Zeolite

4.1 Introduction

Copper exchanged zeolite beta has been shown to be applicable to a range of different industrial applications. These include hydrocarbon and ammonia selective catalytic reduction for the treatment of nitrogen oxides (Corma et al. 1997; Wilken et al. 2010), the desulphurisation of gasoline (Gong et al. 2009), the synthesis of diethyl carbonate (Zhang et al. 2010) and the gas phase oxidation of ammonia (Lenihan and Curtin 2009). Functionally, Cu beta (BEA) zeolites possess similar redox properties to the widely used ZSM-5 support, including similar copper species, and an analogous response to temperature change and oxygen content in SCR (Corma et al. 1997).

As highlighted in previous chapters, zeolite beta has a large 12 membered ring channel structure, forming two perpendicular straight channels and a third mutually perpendicular torturous or sinusoidal channel formed when the straight channels intersect. The large pore diameter not only facilitates the accommodation of larger molecules such as phenol but provides full access to cation exchange sites throughout the structure (Wang et al. 2010). Considering the zeolite framework consists of tetrahedral coordinated (T) atoms which are usually either silicon or aluminium, the exchange sites occur where there is an excess negative charge resulting from an aluminium T atom balanced by an easily displaced cation. After heat treatment, these exchanged cations become localized, and in some cases migrate from the surface into the pore structure (Curtin et al. 1997; Delabie et al. 2002).

As highlighted in Chapter 3, ion exchanged copper occurs in Cu^+ or Cu^{2+} species. Cu^{2+} occupies two proximate alumina exchange sites; this is therefore largely dependent on the quantity and distribution of alumina T sites, in the zeolite. Divalent copper species tend to cause local distortions in the zeolite framework as they coordinate with lattice oxygen atoms (Curtin et al. 1997; Delabie et al. 2002). Cu^+ species only occupy one exchange site and as a result become more

prevalent in high silica zeolites. Figure 4.1 shows two possible instances of Cu exchanged onto a single aluminium site. Cu^+ species can also be increased by raising the pH conditions during exchange. This has the effect of creating hydrates and ammine copper species which upon heat treatment form monovalent copper species or as dimeric oxygen bridged $[\text{Cu-O-Cu}]^{2+}$ (Curtin et al. 1997; Kazansky and Pidko 2005). This more efficient use of exchange sites is referred to as ‘over exchange’ and leads to higher copper loadings.

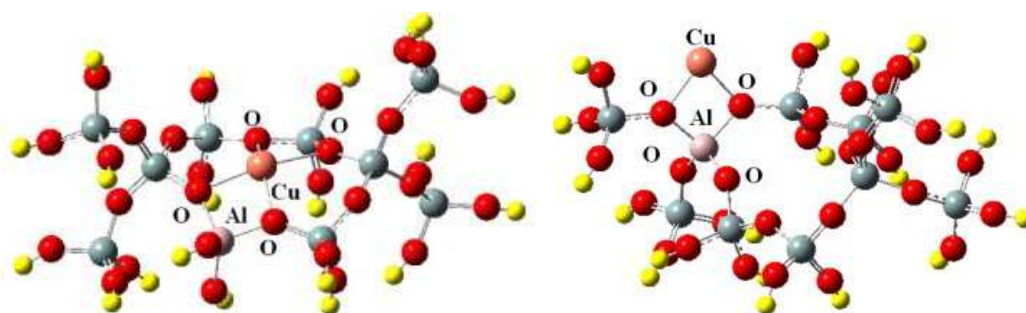


Figure 4.1 Molecular diagram showing the optimized geometries of two possible monovalent copper positions on beta zeolites (sites T1 and T9) (Wang et al. 2010) .

Copper oxides are also known to exist on the zeolite surface, they tend to form in larger quantities at high copper loadings where few accessible exchange sites remain and often have negligible catalytic activity (Dědeček et al. 2001).

The zeolite pore structure also provides a suitable environment for the formation of nano-sized copper clusters within exchanged zeolites. These can also be catalytically active (Petranovskii et al. 2005). As a large pore zeolite, the distance between exchanged copper cations can be relatively large at 4-6 Å, this increases with the silica to alumina ratio and in turn reduces the chance of copper cluster formation (Dědeček et al. 2001).

In Chapter 2 the adsorption of phenol onto beta zeolite was successfully conducted. The hydrophobicity of the zeolite was deemed to be the prime limiting factor in this process, and the large pore size was shown to be at least theoretically able to accommodate the phenol molecule. The latter conclusion was also arrived at by Atoguchi et al. (Atoguchi et al. 2004) In Chapter 3 the beta zeolite was modified with copper through cation exchange to facilitate the

oxidation of adsorbed phenol. However, it was observed that in most instances copper occupied the majority of available cation exchange sites and also possibly deposited as oxides in the pore structure or surface of the zeolite. As a result it is possible that the adsorption characteristics of Cu-BEA have changed relative to the unmodified zeolite. The copper ions and other species have larger ionic radii than the hydrogen cations they replace, when they occupy sites in the pore structure or occlude in the pores the result is a measurable decrease in pore volume and thus total surface area (Ene et al. 2010). Curtin et al. observed a sharp decrease in surface area and pore volume at high zeolite copper loadings, an additional result being that many of the copper species will not participate in catalytic reactions. If it is assumed that phenol may adsorb onto any part of this surface area, then a reduction could cause a decrease in adsorption capacity. Additionally, the occupation of a significant amount of Brønsted sites may alter the zeolite surface chemistry and in turn its affinity for the adsorbate. Also of importance is the ability for the exchanged copper to survive the aqueous adsorption process.

The objective of the work in this chapter is to establish whether the adsorption capacity of Cu-BEA is comparable to its unmodified equivalent and also if it can retain the exchanged copper throughout the adsorption process. Without significant loss to adsorption capacity or catalyst metal, it is envisaged that Cu-BEA would be a viable material for concentrating the pollutant (phenol) and facilitating its destruction in the oxidation step.

4.1.1 Characterization Techniques

The techniques used to characterize the modified zeolite include BET surface analysis and atomic absorption spectroscopy. For a background explanation of atomic absorption spectroscopy, refer to Chapter 3 section 3.2.2.1, for background on the BET surface area analysis, refer to Chapter 2 section 2.1.6.

4.2 Experimental

4.2.1 Adsorbent Preparation

The copper exchanged zeolites were prepared following the procedure in Chapter 3 section 3.2.1. Batches were prepared by mixing zeolite Beta (Zeolyst International) with an appropriate amount of aqueous $\text{Cu}(\text{NO}_3)_2 \cdot 3\text{H}_2\text{O}$ (Fluka) solution at a ratio of 1 g of zeolite to 50 ml of solution. The suspension was stirred for 24 hours before removing the zeolite by vacuum filtration. The filter cake was washed with distilled water to remove any non-exchanged species and then dried overnight in air to remove the bulk of the adsorbed water. The dried zeolite was then calcined in a Lenton thermal designs muffle furnace at 450°C for 5 hours in air. Some solutions were brought up to pH 7 at the start of exchange using aqueous ammonia to increase copper loading. Two silica to alumina ratios were examined: 25:1 and 150:1.

4.2.2 Adsorption Studies

Adsorption isotherms were prepared for phenol adsorption onto Cu-BEA using a batch technique. 200 mg of dried modified zeolite powder was added to 50 ml centrifuge flasks followed by 20 ml of phenol solution (concentration range 10 – 3000 mg dm^{-3}). The centrifuge flasks were attached to an Analogue Orbital shaker for 1 hour. Afterwards the flasks were centrifuged in a Hettich Rotofix 32 centrifuge at 6000 rpm for 20 min to separate the zeolite from solution. 10 ml of the supernatant was removed, the phenol concentration in this solution was determined using a Shimadzu UV-160IPC UV-Visible spectrophotometer at 270 nm against a standard range of solutions with known phenol concentrations. The thermodynamic parameters were determined by performing the adsorption isotherm at different temperatures. The temperature was kept constant throughout the residence time using an ice slush bath.

The ISOFIT Isotherm Fitting software was used to fit experimental data to a range of isotherm models. ISOFIT supplies corresponding predicted data as well as two standard methods of ‘goodness of fit’: the coefficient of determination and

the Weighted Sum of Square Error (WSSE) from which the Root Mean Square Error (RMSE) can be derived through Equation 4.1. (m) is the number of observations and (p) is the number of parameters in the isotherm model.

$$RMSE = \sqrt{\frac{WSSE}{(m - p)}} \quad \text{Equation 4.1}$$

4.2.3 Surface Characteristics

The samples were characterized by nitrogen gas adsorption/desorption isotherms using a Quantachrome Autosorb AS-1 gas sorption system in order to determine surface area and pore volume. Samples were pretreated under vacuum at 300°C for 18 hours before analysis. The apparent surface areas of the zeolites were measured using the Brunauer-Emmett-Teller (BET) (Brunauer et al. 1940) method, the mesopore volume by the Barret-Joyner-Halenda (BJH) (Barrett et al. 1951) method, and the micropore volume by the Dubinin-Radushkevich (DR) (Dubinin et al. 1947) method.

4.2.4 Aqueous Stability Studies

Initial aqueous stability tests were carried out under normal adsorption conditions. After ion exchange and before calcination the 5 g filter cake was once again placed in a beaker with 500 ml of distilled water and stirred for 1 hour. The solution was filtered again and the process was repeated 3 times. On each instance as well as the initial filtration after ion exchange the supernatant was removed and examined for copper using a Varian/Spectra AA 220 atomic adsorption spectrophotometer.

The calcined modified zeolite was also examined for metal leaching in aqueous solution under a pH range between 1 and 11. 10 ml of distilled water was pH adjusted using hydrochloric acid or aqueous ammonia solutions followed by the addition of 0.1 g of modified zeolite. The solution was shaken for the typical adsorption contact time of 1 hour. The solution was then centrifuged, filtered and

diluted to within the copper standard concentration range, followed by copper analysis using AAS to detect the concentration of copper in solution.

4.3 Results and Discussion

To examine the effect of modification of the zeolite on phenol adsorption, a number of modified zeolites were tested under the same adsorption conditions as the unmodified counterparts. The zeolites examined and their characteristics are summarized in Table 4.1. The surface area and pore volume were derived using nitrogen adsorption desorption and the copper loading was via AAS.

Table 4.1 Summary of the characteristics for the beta zeolites examined in this section

Sample	SiO ₂ :Al ₂ O ₃ ratio	Cu Loading wt%	Exchange pH	Surface Area (m ² g ⁻¹)	Total Pore Volume (cc g ⁻¹)
H-β-25:1	25:1	0	-	529	0.772
1.3Cu/β-25	25:1	1.3	5.4	559	0.683
2.1Cu/β-25(p)	25:1	2.1	7.0	565	0.548
H-β-150	150:1	0	-	541	0.964
0.7Cu/β-150	150:1	0.7	4.2	513	0.821
2.0Cu/β-150(p)	150:1	2.1	7	480	0.760

The surface area for the 25:1 SiO₂:Al₂O₃ zeolite slightly increased as a result of the exchange process. In the case of the 150:1 zeolite however, the addition of exchanged copper causes a noticeable drop in surface area. A drop in total pore volume is common in both SiO₂: Al₂O₃ ratios with increasing copper.

A number of factors can contribute to a change in an adsorbents physical surface characteristics as a result of cation exchange. These include:

- Surface screening
- Pore Blocking
- Pore opening

Surface screening occurs when larger ions conceal some of the 'roughness' on the adsorbent surface. This can result in a loss of surface area. Pore blocking occurs where cations are exchanged or deposited within or at the entrance of the pore structure and are large enough to obstruct the passage of the adsorbate into the internal structure. This results in a decrease in pore volume and surface area. Pore opening usually occurs where the exchanged cation has a larger hydration sphere, this may result in structural expansion in the pore openings (Huang et al. 2004). Larger cations in some cases are known to increase the adsorption affinity to non-polar molecules such as N₂, this is due to their tendency to be less shielded by the first adsorbate layer than smaller cations (Pillai et al. 2010).

The copper cation is larger than the H⁺ cation on the native zeolite. Additionally in solution Cu will have a larger hydration sphere. These two factors would suggest that surface screening and/or pore blocking are the source of the decrease in pore volume observed. The decrease in pore volume is similar in both silica to alumina ratios; this would suggest that the trend is largely independent of the type of copper species present.

The nitrogen adsorption and desorption isotherms for each zeolite retained the same overall shape and hysteresis loop despite the presence of copper. The shape of the isotherm corresponds largely to a mixed Type I-IV isotherm which reflects a mixed micro and mesoporous adsorption system. The hysteresis loop is representative of mesoporous adsorption/desorption. The loop appears closest to a Type C hysteresis according to the de Boer classification (de Boer 1958). This type is usually produced by wedge shaped mesopores with open ends.

4.3.1 Adsorption Studies

Figure 4.2 shows the adsorption isotherms for the unmodified 25:1 beta zeolite (H- β -25) with two variants with different copper loadings (1.3Cu/ β -25 and 2.1Cu/ β -25(p)).

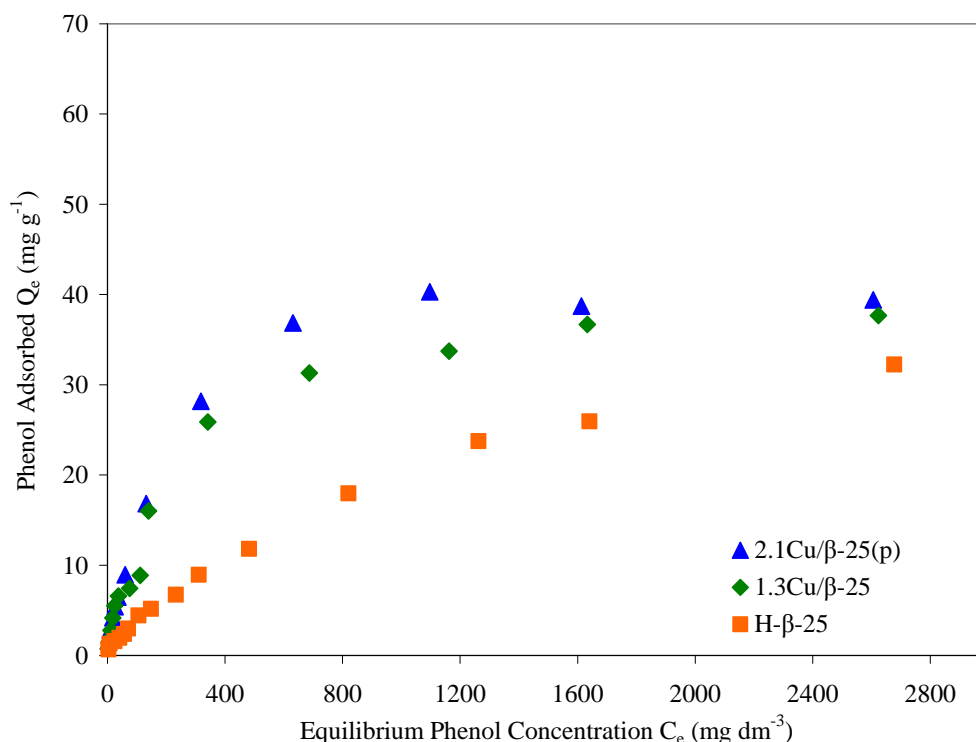


Figure 4.2 Phenol adsorption isotherms for three different zeolites with varying copper content @ 294K. Silica to alumina ratio 25:1. Initial phenol concentration range 10-3000 mg dm⁻³. ▲ 2.1Cu/ β -25(p), ◆ 1.3Cu/ β -25 and ■ H- β -25 .

The isotherms show a significant increase in phenol adsorption capacity on the modified zeolites, from the maximum of 32.3 mg g⁻¹ on the unmodified H- β -25 zeolite to a maximum of 37.7 and 40.3 mg g⁻¹ for the 1.3Cu/ β -25 and 2.1Cu/ β -25(p) zeolites respectively. The Cu-Beta zeolites also show a more defined conformity to the Type I Brunauer isotherm model with a distinct plateau representing saturation. The unmodified zeolites isotherm however, shows a continuing increase of phenol adsorption with increasing equilibrium concentration throughout the concentration range. This would suggest that not only do the modified Cu-Beta zeolites have a higher observed adsorption capacity compared to the unmodified zeolite, but that they also adsorb phenol more efficiently at lower concentrations.

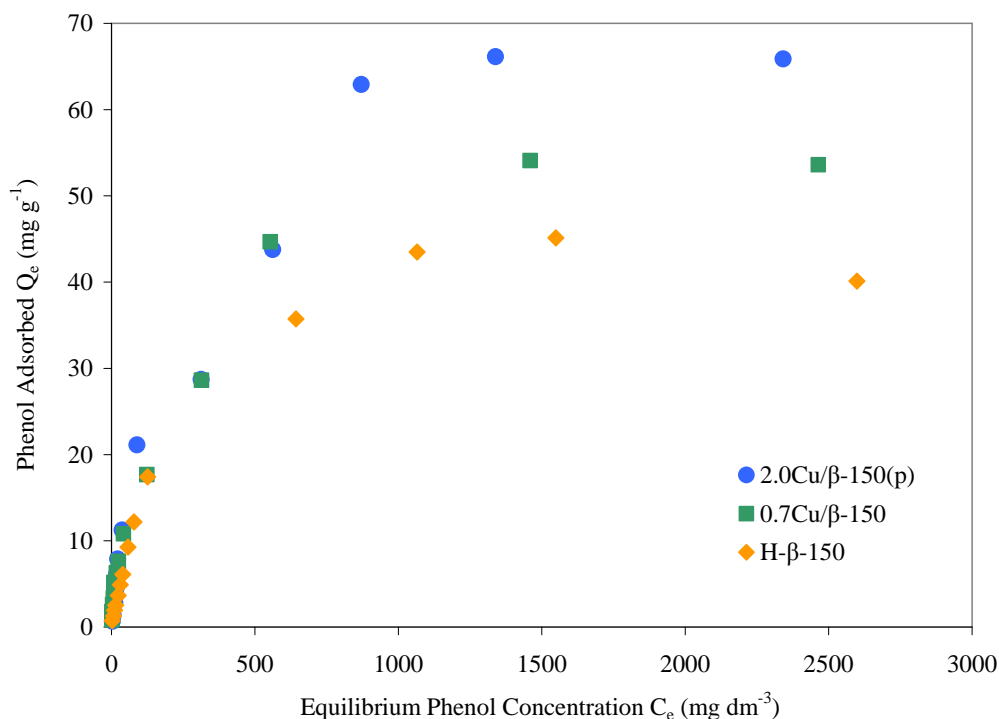


Figure 4.3 Phenol adsorption isotherms for three different zeolites with varying copper content @ 294K. Silica to alumina ratio 150:1. Initial phenol concentration range 10-3000 mg dm⁻³. ●2.0Cu/β-150(p), ■0.7Cu/β-150 and ◆H-β-150.

Figure 4.3 shows the phenol adsorption isotherms for the unmodified and copper exchanged beta zeolites with a SiO₂:Al₂O₃ ratio of 150:1. These exhibit a similar trend in that the Cu modified zeolites show an increase in phenol adsorption over the unmodified counterpart. Notably in this case, there is less convergence at higher equilibrium concentrations and the differences between the three zeolites remain distinct up to 3000 mg dm⁻³ initial phenol concentration. H-β-150 showed an adsorption maximum of 45.1 mg g⁻¹, where as a maximum of 54.1 and 66.1 mg g⁻¹ was observed for 0.7Cu/β-150 and 2.0Cu/β-150(p), respectively. Similar to the 25:1 zeolites, the modified 150:1 zeolites resemble closely a Type I isotherm with adsorption equilibrium at around 1000 mg dm⁻³ equilibrium concentration.

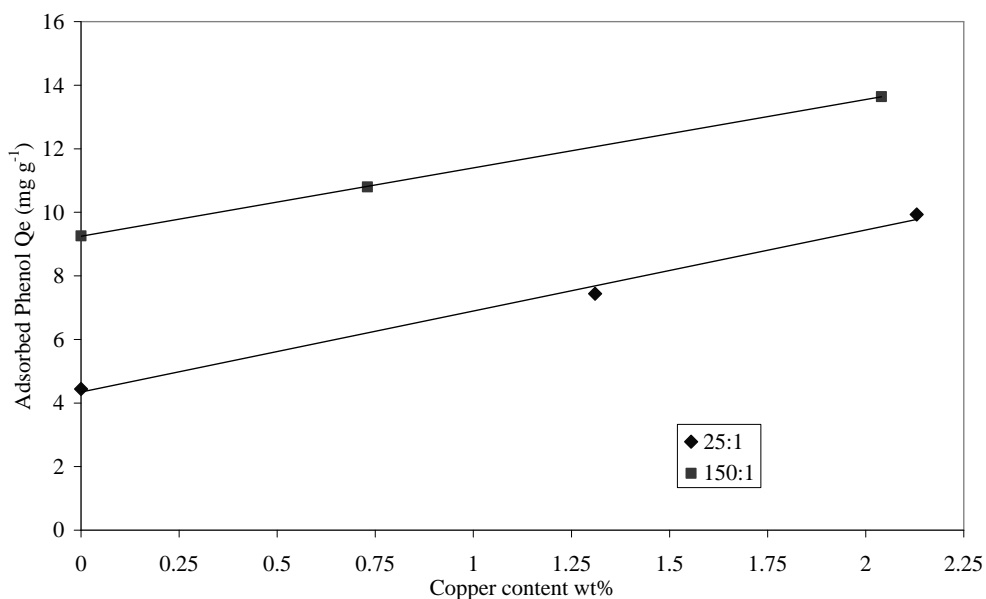


Figure 4.4 Plot showing the relationship of phenol adsorption to copper loading on beta zeolites of two different silica to alumina ratios: \blacklozenge 25:1 and \blacksquare 150:1. Initial phenol concentration 150 mg dm^{-3} .

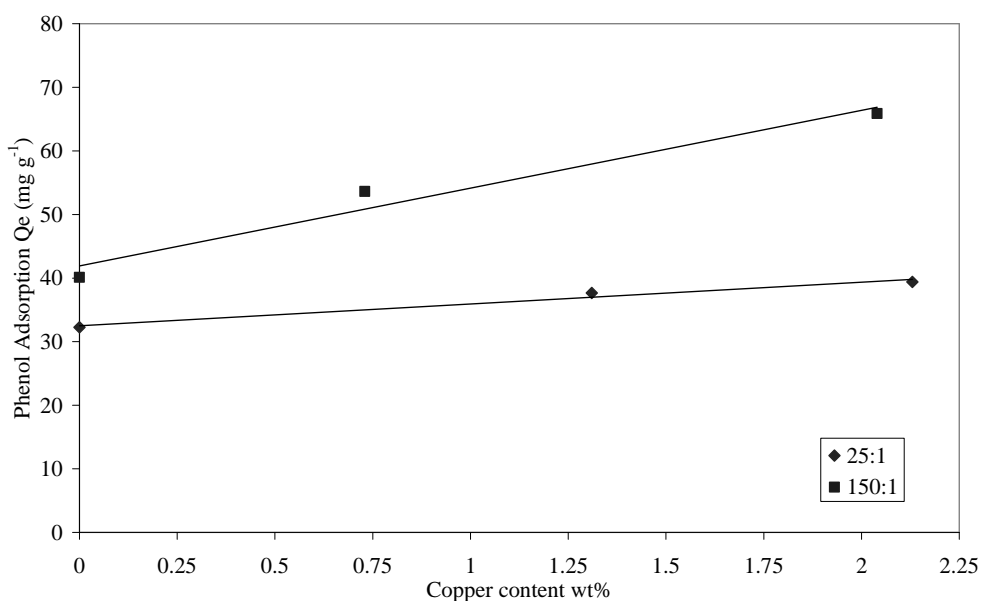


Figure 4.5 Plot showing the relationship of phenol adsorption to copper loading on beta zeolites of two different silica to alumina ratios: \blacklozenge 25:1 and \bullet 150:1. Initial phenol concentration 3000 mg dm^{-3} .

Figure 4.4 illustrates the proportionate increase of phenol adsorption as the copper loading is increased. At lower concentrations the increase for both zeolites (of different silica to alumina ratios) is similar. It appears that copper has a significant positive effect on the zeolites adsorption capacity. Figure 4.5 shows the relative increase at 3000 mg dm^{-3} which is assumed to be at saturation. The

effect of increasing copper on the 25:1 zeolites is low relative to the 150:1 which still shows a significant positive relationship between phenol adsorption and copper content. It appears that although the modified copper zeolite with a silica to alumina ratio of 25:1 has a similar maximum adsorption regardless of copper content, the increasing copper improves adsorption at lower concentrations.

As in chapter 2, the ISOFIT software was applied to the phenol adsorption isotherms for the four Cu modified zeolites featured in this chapter. The goodness of fit measures: Root Mean Square Error (RMSE) and the coefficient of determination R^2 , are displayed in Table 4.2 for the four best fitting isotherm models.

Table 4.2 Table summarising goodness-of-fit measures for four representative isotherm models for the adsorption of phenol onto zeolites of varying copper loading @ 294K . Phenol concentration range 10 – 3000 mg dm⁻³.

<i>Isotherm Model</i>	<i>Sample</i>	<i>RMSE</i>	<i>R²</i>
Langmuir	1.3Cu/β-25	1.556	0.901
	2.1Cu/β-25(p)	1.444	0.959
	0.7Cu/β-150	2.510	0.821
	2.0Cu/β-150(p)	4.106	0.943
Langmuir-Freundlich	1.3Cu/β-25	1.619	0.905
	2.1Cu/β-25(p)	1.508	0.959
	0.7Cu/β-150	2.389	0.916
	2.0Cu/β-150(p)	3.965	0.969
Freundlich	1.3Cu/β-25	3.593	0.864
	2.1Cu/β-25(p)	4.883	0.959
	0.7Cu/β-150	4.373	0.772
	2.0Cu/β-150(p)	5.875	0.878
Toth	1.3Cu/β-25	1.619	0.902
	2.1Cu/β-25(p)	3.692	0.876
	0.7Cu/β-150	2.566	0.907
	2.0Cu/β-150(p)	4.052	0.959

The two 25:1 SiO₂:Al₂O₃ copper zeolites show lower RMSE values for the Langmuir model while the two 150:1 copper zeolites show a slightly better fit in the generalized Langmuir-Freundlich model. The Toth and Freundlich isotherm exhibit a poorer fit. Figures 4.6 and 4.7 help to illustrate this relationship.

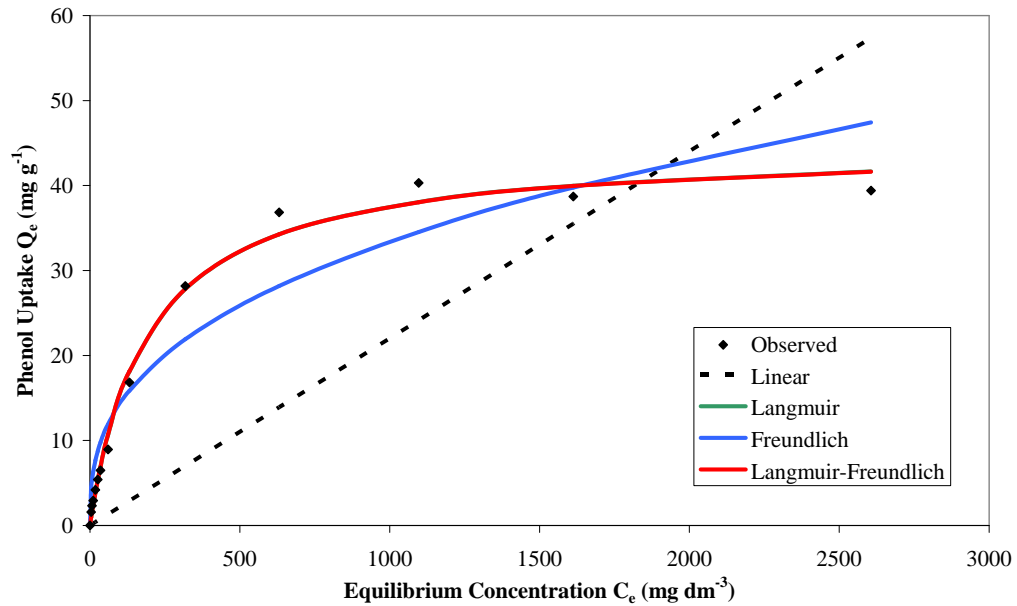


Figure 4.6 Plots of adsorption isotherms comparing observed data to simulated data from a range of isotherm models. 2.1Cu/β-25(p) @ 294K . Phenol concentration range 10 – 3000 mg dm⁻³ . Langmuir and Langmuir-Freundlich simulated data overlaps.

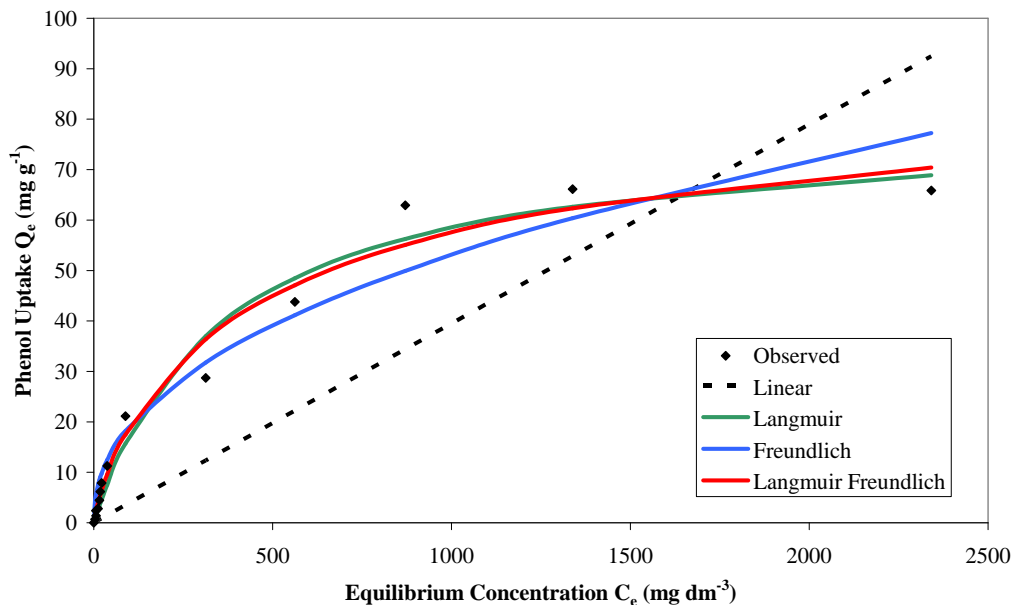


Figure 4.7 Plots of adsorption isotherms comparing observed data to simulated data from a range of isotherm models. 2.0Cu/β-150(p) @ 294K . Phenol concentration range 10 – 3000 mg dm⁻³ .

The 2.1Cu/β(p) zeolite shown in Figure 4.6 shows a more distinct Type I Brunauer relationship with a steep climb at low concentrations as the surface of the zeolite is covered and a clear plateau as saturation is reached. This is characteristic of the Langmuir model. For the 2.0Cu/β-150(p) zeolite shown in Figure 4.7 the transition to the maximum is less distinct with an interstitial zone

approximately between 100 and 1000 mg dm⁻³ equilibrium concentration before the adsorption plateau. In this section the relationship between increasing phenol uptake and equilibrium concentration is still increasing but reduced relative to the previous section between 0 and 100 mg dm⁻³. It is important to note that the lengthening of this interstitial phase appears to coincide with the higher adsorption maximum present in 2.0Cu/β-150(p), whereas at lower concentrations the isotherm follows a similar trend to 2.1Cu/β-25(p). For this type of curve, the distinction between Langmuir and Freundlich type models is not as discernable, so it is appropriate that the Generalized Langmuir Freundlich model fits slightly better. The isotherm constants for the three representative models as derived by ISOFIT are shown in tables 4.3, 4.4 and 4.5.

Table 4.3 Langmuir constants for the adsorption of phenol onto zeolite beta catalysts with a range of copper loading and SiO₂/Al₂O₃ ratios.

<i>Sample</i>	$K_L (dm^3 g^{-1})$	$A_L (dm^3 mg^{-1})$	$Q_0 (mg g^{-1})$
H-β-25	0.0356	0.000731	48.646
1.3Cu/β-25	0.158	0.00373	42.312
2.1Cu/β-25(p)	0.231	0.00516	44.773
H-β-150	0.202	0.00412	50.267
0.7Cu/β-150	0.234	0.00381	61.270
2.0Cu/β-150(p)	0.221	0.00278	79.476

The Langmuir parameters for the modified and unmodified zeolites are shown in Table 4.3. The Langmuir constants K_L and A_L correspond to adsorption capacity and the affinity or energy of adsorption respectively. Dividing K_L by A_L gives Q_0 the maximum adsorption (Yousef and El-Esweed 2009). The modified 25:1 zeolites were shown in Table 4.2 to have a comparatively good fit to the Langmuir model. The unmodified 25:1 beta zeolite was examined in chapter 2, where it was found to have a better correlation with the Freundlich model. Despite this the Langmuir constants show a clear and proportionate increase in adsorption capacity and the energy of adsorption as the copper content is increased. This relationship is characteristic of improved adsorption. The predicted maximum adsorption (Q_0) however shows no clear correlation.

Conversely the 150:1 ratio modified zeolites show no correlation with regards to K_L and an inverse relationship between A_L and increasing copper. It should be

noted that the modified 150:1 zeolites showed a poorer fit to Langmuir relative to other models. The adsorption maximum however shows an increase relative to increasing copper, with values that are quite close to the maximum adsorptions in the observed data.

Table 4.4 Freundlich constants for the adsorption of phenol onto zeolite beta catalysts with a range of copper loading and SiO₂/Al₂O₃ ratios.

<i>Sample</i>	$K_F (dm^3 g^{-1})$	$1/n_f$
H-β-25	0.148	0.712
1.3Cu/β-25	1.771	0.407
2.1Cu/β-25(p)	2.638	0.367
H-β-150	2.162	0.641
0.7Cu/β-150	2.892	0.391
2.0Cu/β-150(p)	2.513	0.442

The Freundlich isotherm model parameters are shown in Table 4.4. Overall the Freundlich isotherm performed worse in terms of goodness of fit compared to the Langmuir and Langmuir-Freundlich models. The Freundlich constants are K_F which is representative of adsorption capacity, and the heterogeneity factor $1/n_f$. In this case there is little correlation between the change in copper loading and the Freundlich parameters, although the 25:1 silica to alumina ratio zeolites do show a proportionate increase in K_F .

Table 4.5 Generalised Langmuir-Freundlich constants for the adsorption of phenol onto zeolite beta catalysts with different copper loading and SiO₂/Al₂O₃ ratios.

<i>Sample</i>	$Q_0 (mg g^{-1})$	$b (dm^3 mg^{-1})$	$1/n$
H-β-25	124.986	0.000126	0.790
1.3Cu/β-25	42.374	0.00371	0.999
2.1Cu/β-25(p)	44.715	0.00519	0.999
H-β-150	48.957	0.00413	0.999
0.7Cu/β-150	68.705	0.00275	0.799
2.0Cu/β-150(p)	90.701	0.00196	0.818

The Generalized Langmuir-Freundlich model showed a good overall correlation with all the examined zeolites. The parameters are shown in Table 4.5. As the

heterogeneity factor $1/n$ approaches unity, the isotherm approaches that of the Langmuir. The zeolites 1.3Cu/ β -25, 2.1Cu/ β -25(p) and H- β -150 all showed good correlation with the Langmuir isotherm as determined by the RMSE, in each of these cases the heterogeneity factor has been close to 1. The other three zeolites exhibited hybrid isotherms and as a result lower heterogeneity factor. When the isotherm approaches Langmuir it implies that the adsorption sites are largely homogeneous and a single type of adsorption interaction is taking place. The 0.7Cu/ β -150 and 2.0Cu/ β -150(p) zeolites had a $1/n$ value somewhat lower than unity, indicating that more than one form of interaction is present, that different adsorption sites are active or that some multilayer adsorption is taking place. This is a possible cause associated with the intermediate phase observed in the adsorption isotherms for the 150:1 zeolites.

The adsorption maximum Q_0 , shows a proportionate increase for both silica to alumina ratio samples with increasing copper loading. The Q_0 value for H- β -25 appears to be unaccountably high; this is likely due to the fact that it did not reach an adsorption maximum in the concentration range examined. In all cases the adsorption maxima as predicted by the Langmuir-Freundlich model are higher than those in the observed data within the concentration range.

The adsorption energy/affinity b , seems to increase for the 25:1 zeolites with increasing copper, and decrease for the 150:1. The trend and values are similar to those observed in the related Langmuir parameter (A_L) in Table 4.3.

Overall both the Langmuir and Langmuir-Freundlich models show a good quality of fit for the observed data with some variation. The 1.3Cu/ β -25, 2.1Cu/ β -25(p) and H- β -25 zeolites showed a greater tendency towards the Langmuir model, where as the other adsorbents showed evidence of a more heterogeneous system. The shift away from Langmuir correlation when copper was added to the 150:1 SiO₂:Al₂O₃ zeolite, may suggest an additional adsorption mechanism. This could be due to the exchanged copper operating as sorption sites for phenol. Cu⁺ ions exchanged on zeolites are known to form π bonds with

organic molecules. In the case of benzene these bonds were found to be present in low benzene concentrations and of moderate strength (Kukulska-Zajac et al. 2006). If this type of interaction is present it may explain the change in the isotherm profiles observed in the copper modified zeolites and the increase in adsorption capacity.

An alternative cause of the increased adsorption capacity of the modified zeolites is the change in acid-base properties resulting from cation exchange. Larger metal cations and those with higher valencies can increase the basicity of the zeolite and thus increase its affinity to acidic molecules such as phenol. The effect is caused by an increased electronegativity with increasing cation size which in turn influences the amount of negative charge on the framework oxygen. This effect should increase with metal loading and also with lower framework alumina content (Correa and Mota 2003; Walton et al. 2006).

The TPR profiles in section 3.3.2 suggest that there are Cu^+ species present in the 2.1Cu/ β -25(p) and 2.0Cu/ β -150(p) which were both pH adjusted during the exchange process. There is likely to be less Cu^+ relative to Cu^{2+} species at lower copper loadings and without pH treatment, but this could not be confirmed however as the TPR profiles for these zeolites were not sensitive.

The greater difference in adsorption capacity between 2.0Cu/ β -150(p) and 0.7Cu/ β -150 when compared to the 25:1 zeolites could be due simply to the larger difference in copper loading in the former case.

4.3.2 Thermodynamic Parameters

The thermodynamic parameters, enthalpy (ΔH), Gibbs free energy (ΔG) and entropy (ΔS) changes for a sample copper zeolite (2.1Cu/ β -25(p)) and its parent zeolite (H- β -25) for phenol adsorption are summarized in Table 4.6.

Table 4.6 Thermodynamic parameters for phenol adsorption onto a copper zeolite, in comparison to its parent zeolite.

<i>Sample</i>	ΔH (kJ mol^{-1})	ΔG (kJ mol^{-1})		ΔS ($\text{J K}^{-1} \text{mol}^{-1}$)	
		283 K	294 K	283 K	294 K
H- β -25	-7.51	-1.42	-1.74	-21.53	-19.63
2.1Cu/ β -25(p)	-30.37	-0.99	-0.57	-103.81	-101.38

Like the parent zeolite the enthalpy change for 2.1Cu/ β -25(p) is negative, indicating an exothermic adsorption process. However it has become significantly more negative. While still in the range of physisorption, there is likely to be a larger proportion of stronger interactions taking place as well. This may be related to the larger adsorption capacity occurring in the modified zeolite.

The Gibbs free energy remains negative, albeit slightly less negative after the cation exchange process. The reduced spontaneity this represents may be due to the larger energy involved in bonding.

Entropy change is significantly more negative in the modified zeolites. The cause of this could be due to a reduction in the pore diameter caused by the increased ionic radius of the exchanged copper species. As was discussed in Chapter 2, as a molecule approached the size of the pore diameter there is a corresponding reduction in entropy as it becomes more confined. As in Table 4.1, the pore volume for the copper modified zeolites was shown to decrease, this could be related to a reduction of pore diameter as explained above and in turn correspond with the increase in entropy.

4.3.3 Aqueous Stability

An important consideration when modifying the zeolite to improve catalytic performance is to make sure that the metal catalyst can survive the aqueous adsorption step. Catalytic deactivation can occur from significant metal leaching. This can lead to a secondary issue due to the toxic nature of copper ions in

aqueous environments. It is important that the amount leached is within environmental limits.

Figure 4.8 shows the percentage of initial copper loading on the 1.3Cu/ β zeolite lost as the pH of solution is changed. At neutral pH and above, the exchanged copper appears to be relatively stable with a maximum loss of 1.87% at pH 7. At low pH the copper loss steadily increases with a maximum at pH 1 of 98% representing almost all of the copper exchanged. This is most likely a result of dealumination where the framework Al^{3+} is removed from the zeolite structure and the associated charge balancing cation, Cu^{2+} or Cu^+ , is released into solution (Rokosz et al. 1997; Oumi et al. 2001).

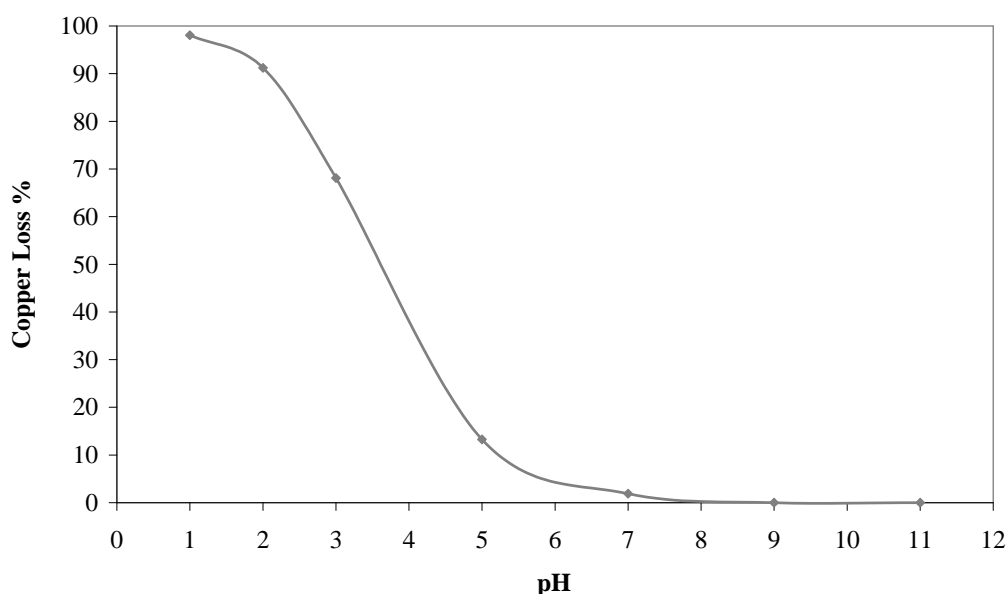
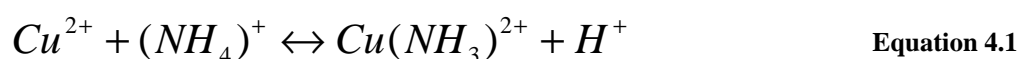


Figure 4.8 The loss of exchanged copper from 1.3Cu/ β expressed as a percentage of initial Cu loading, relative to the change in the pH of solution. Contact time 1 hour, temperature 294K, pH range 1-11.

From pH 9 onwards the colour of the copper zeolite changed to a bright blue and no recorded copper was found in solution. The colour change is likely to be synonymous with the conversion of copper ions into copper ammine species in the presence of aqueous ammonia at high pH. An example of this is shown in Equation 4.1.



Schreier et al. (2005) noted that at pHs above 9 where copper amine species are formed, they exhibited a dual mechanism of interaction with the zeolite surface. Aside from the pH independent cation exchange, these species would also form strong electrostatic interaction with silanol groups on the zeolite surface (Schreier et al. 2005). It is possible that this second avenue of interaction which occurs at high pHs helps to stabilize some of the copper species that would otherwise have leached under lower pH conditions.

The Environmental Protection Agency sets a typical limit for copper in waste water at 0.5 mg dm^3 (EPA 1997). At pH 7 the maximum copper loss observed was 1.87% which corresponds to approximately 2.7 mg dm^3 in solution. This would suggest that the copper does not reach an acceptable level of leaching until above pH 7.

In an attempt to reduce the amount of copper loss to environmentally acceptable levels, a rinsing step was added to the preparation procedure. Figure 4.9 shows the relationship between copper concentration in solution and the number of rinses. It shows a considerable decrease in the amount of copper leached with each step, it also falls below acceptable levels by the second rinsing step. This could indicate that there is a finite amount of copper on the zeolite that will be leached under pH conditions close to neutral, possibly representing unbound or weakly bonded copper species on the zeolite surface. If this is the case it could mean that dealumination is not significant at this pH, this is important due to the potential negative environmental impact from the presence of Aluminium in wastewater streams.

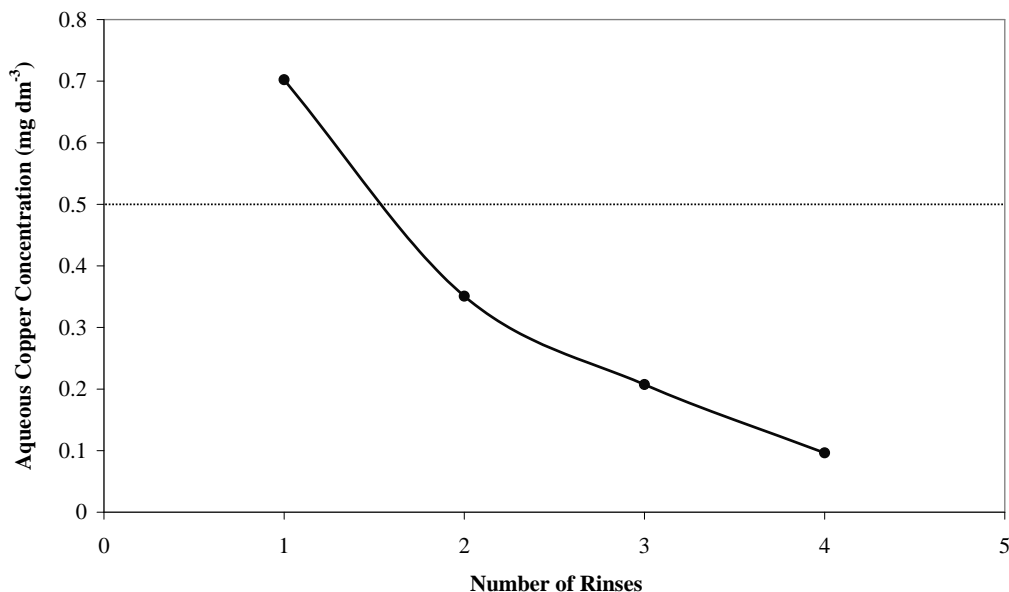


Figure 4.9 Graph summarizing the effect of repeated washing on the concentration of leached copper adjusted for standard adsorption conditions. 5 g of 1.8Cu/ β (p), pH 6, 400ml, 294K, contact time 1hr. Line at 0.5 mg dm⁻³ represents EPA limit for copper in wastewater.

4.4 Conclusion

In this chapter the copper modified beta zeolites were shown to have improved phenol adsorption characteristics relative to the native zeolite. There was also a smaller increase in adsorption relative to increasing copper loading. The highest observed levels of phenol adsorption were 39.4 mg g⁻¹ for 2.1Cu/ β (p) and 65.8 mg g⁻¹ for 2.0Cu/ β -150(p). These represent a 23 and 46% increase respectively, from the unmodified zeolite. The difference between the two samples is most likely due to the added hydrophobic character of the higher silica to alumina ratio, giving it a larger base adsorption capacity for phenol.

The Generalized Langmuir-Freundlich proved to be the isotherm model with the best overall fit for these results. The modified 25:1 zeolites were found to have an affinity somewhat closer to Langmuir, where as the 150:1 showed a better relationship to the Langmuir Freundlich model, possibly due to a more heterogeneous adsorption mechanism.

The Langmuir-Freundlich isotherms gave extrapolated adsorption maxima (Q_0) which were for the most part representative of the observed results. The exception being the 2.0Cu/ β -150(p) zeolite, which predicated an increase in phenol uptake up to 91 mg g⁻¹.

The thermodynamic parameters: enthalpy change and entropy change became significantly more negative for the modified zeolite, reflecting the significant increase in adsorption capacity in the copper modified zeolite. Overall the parameters suggested a spontaneous, exothermic adsorption process.

An examination of the surface characteristics showed a different relationship for the two silica to alumina ratios with increasing copper. In the case of the 25:1 zeolite, the total pore volume decreased, while the BET surface area increased with increasing copper. Conversely both surface characteristics decreased when the 150:1 zeolite was modified with copper. This was possibly due to the differing state of exchanged copper that occurs on the two silica to alumina ratios and with pH treatment during exchange. Another cause of this disparity could be the less even distribution of copper on the 150:1 zeolites due to their decreased number of aluminium sites.

The differing states of exchanged copper could also explain the slightly different adsorption mechanism that appears to be present in the case of the modified 150:1 zeolites, as observed in the adsorption isotherms and the isotherm model constants. This could be as a result of the varying surface characteristics and/or different interactions between the phenol and different forms of exchanged copper.

Overall the increased adsorption would appear to be not entirely dependent on the change in surface area and pore volume, at least not consistently between the two silica to alumina ratios. The nitrogen may also be adsorbing in locations that the larger phenol molecule would not be able to access. However the different surface characteristics of the two zeolites may go some way to explaining the differences in the adsorption isotherms.

A change in surface chemistry may also be a contributing factor. With more of the Brønsted sites occupied with copper the polarity and acidity of the surface may change and the exchanged copper in its different states may provide new adsorption sites for phenol. Increased electrostatic interaction with copper species may contribute to the increased affinity with phenol.

The copper modified zeolite experiences copper loss after the initial exchange process when the pH is lower than 7. Without artificially raising the pH the zeolite is usually slightly acidic and will lose some of the exchanged copper. This is likely to be weakly exchanged or agglomerated copper species, and after several washing steps the copper leaching reduces to environmentally acceptable levels. Lowering the pH further results in further copper loss due to dealumination, culminating in 98% loss at pH 1.

Copper modified zeolite beta shows good adsorption characteristics and acceptable stability under normal conditions. This should make it a viable adsorbent as well as a catalyst and should maintain its catalytic character for use in the oxidation step.

4.5 References

- Atoguchi, T., T. Kanougi, T. Yamamoto and S. Yao (2004). *Phenol oxidation into catechol and hydroquinone over H-MFI, H-MOR, H-USY and H-BEA in the presence of ketone*. Journal of Molecular Catalysis A: Chemical **220**(183-187).
- Baiker (1985). *Experimental methods for the characterisation of catalysts. I. Gas adsorption methods, pycnometry and porosimetry*. International Chemical Engineering **25**: 12-28.
- Barrett, E. P., L. G. Joyner and P. P. Halenda (1951). *The determination of pore volume and area distributions in porous substances. I. Computations from nitrogen isotherms*. Journal of the American Chemical Society **73**: 373-380.
- Brunauer, S., L. S. Deming, W. E. Deming and E. Teller (1940). *On a theory of the van der waals adsorption of gases*. Journal of the American Chemical Society **62**: 1723-1732.
- Brunauer, S., P.H. Emmet and E. Teller (1938). *Adsorption of gases in multilayered layers*. J. Am. Chem. Soc. **60**: 309-319.
- Corma, A., V. Fornes and E. Palomares (1997). *Selective catalytic reduction of NO_x on Cu-beta zeolites*. Applied Catalysis B: Environmental **11**(2): 233-242.
- Correa, R. J. and C. J. A. Mota (2003). *Effect of the compensating cation on the adsorption of t-butylchloride on zeolite γ* . Applied Catalysis A: General **255**(2): 255-264.
- Curtin, T., P. Grange and B. Delmon (1997). *The direct decomposition of nitrogen monoxide*. Catalysis Today **35**: 121-127.
- de Boer, J. H. (1958). *The structure and properties of porous materials*. London, Butterworths.
- Dědeček, J., O. Bortnovsky, A. Vondrová and B. Wichtelová (2001). *Catalytic activity of Cu-Beta zeolite in NO decomposition: Effect of copper and aluminium distribution*. Journal of Catalysis **200**: 160-170.
- Delabie, A., K. Pierloot, M. H. Groothaert, R. A. Schoonheydt and L. G. Vanquickenborne (2002). *The coordination of Cu^{II} in zeolites - structure and spectroscopic properties*. European Journal of Inorganic Chemistry **2002**(3): 515-530.
- Dubinin, M. M., E. D. Zaverina and L. Radushkevich (1947). *Adsorption cycle modelling*. Doklady Akademii Nauk SSSR **21**: 1351.

- Ene, A. B., T. Archipov and E. Roduner (2010). *Spectroscopic study of the adsorption of benzene on Cu/HZSM5 zeolites*. Journal of Physical Chemistry **114**: 14571-14578.
- EPA (1997). *IPC licencing BATNEEC guidance notes*. Dublin, EPA Publications.
- Gong, Y., T. Dou, S. Kang, Q. Li and Y. Hu (2009). *Deep desulfurization of gasoline using ion-exchange zeolites: Cu(i)- and ag(i)-beta*. Fuel Processing Technology **90**(1): 122-129.
- Huang, F., J. Lee, C. Lee and H. Chao (2004). *Effects of cation exchange on the pore and surface structure and adsorption characteristics of montmorillonite*. Colloids and Surfaces A: Physiochemical and Engineering Aspects **239**: 41-47.
- Kazansky, V. B. and E. A. Pidko (2005). *A new insight in the unusual adsorption properties of Cu⁺ cations in Cu-ZSM-5 zeolite*. Catalysis Today **110**: 281-293.
- Kukulska-Zajac, E., P. Kozyra and J. Datka (2006). *The interaction of benzene with Cu⁺ sites in zeolites: IR studies and DFT quantum chemical calculations*. Applied Catalysis A: General **307**(1): 46-50.
- Lenihan, S. and T. Curtin (2009). *The selective oxidation of ammonia using copper-based catalysts: The effects of water*. Catalysis Today **145**(1-2): 85-89.
- Oumi, Y., R. Mizuno, K. Azuma, S. Nawata, T. Fukushima, T. Uozumi and T. Sano (2001). *Reversibility of dealumination - realumination process of BEA zeolite*. Microporous and Mesoporous Materials **49**(1-3): 103-109.
- Petranovskii, V., V. Gurin and R. Machorro (2005). *Spectroscopic observation and ab initio simulation of copper clusters in zeolites*. Catalysis Today **107-108**: 892-900.
- Pillai, R. S., G. Sethia and R. V. Jasra (2010). *Sorption of CO, CH₄, and N₂ in alkali metal ion exchanged zeolite-X: Grand canonical monte carlo simulation and voumetric measurement*. Industrial Engineering and Chemistry Research **49**: 5816-5825.
- Rokosz, M. J., A. V. Kucherov, H. W. Jen and M. Shelef (1997). *Spectroscopic studies of the stability of zeolitic deNO_x catalysts*. Catalysis Today **35**: 65-73.

- Schreier, M., S. Teren, L. Belcher, J. R. Regalbuto and J. T. Miller (2005). *The nature of 'overexchanged' copper and platinum zeolites*. *Nanotechnology* **16**: 582-591.
- Walton, K. S., M. B. Abney and M. D. LeVan (2006). *CO₂ adsorption in Y and X zeolites modified by alkali metal cation exchange*. *Microporous and Mesoporous Materials* **91**(1-3): 78-84.
- Wang, Y., Z. Lei, R. Zhang and B. Chen (2010). *Adsorption of NO and N₂O on Cu-bea zeolite*. *Journal of Molecular Structure: THEOCHEM* **957**(1-3): 41-46.
- Wilken, N., K. Kamasamudram, N. W. Currier, J. Li, A. Yezerets and L. Olsson (2010). *Heat of adsorption for NH₃, NO₂ and NO on Cu-Beta zeolite using microcalorimeter for NH₃ SCR applications*. *Catalysis Today* **151**(3-4): 237-243.
- Yousef, R. I. and B. El-Esweed (2009). *The effect of pH on the adsorption of phenol and chlorophenols onto natural zeolite*. *Colloids and Surfaces A: Physicochemical and Engineering Aspects* **334**: 92-99.
- Zhang, P., S. Huang, Y. Yang, Q. Meng, S. Wang and X. Ma (2010). *Effect of SSIE structure of Cu-exchanged β and Y on the selectivity of diethyl carbonate by oxidative carbonylation of ethanol: A comparative investigation*. *Catalysis Today* **149**(1-2): 202-206.

Chapter 5

Catalytic Oxidation of Adsorbed Phenol

5 Catalytic Oxidation of Adsorbed Phenol

5.1 Introduction

The aqueous phase oxidation of phenol has been examined extensively. A wide range of methods exist, suitable to a broad variety of operating conditions and costs, efficiency and reliability requirements. Some of the most prominent methods include: electrochemical oxidation (Carvalho et al. 2006), ozonation (Wu et al. 2000), catalytic wet air oxidation (CWAO) (Alejandre et al. 1998), chemical oxidation (e.g. Fenton process), photo catalytic oxidation (Sýkora et al. 1997), wet peroxide oxidation (Quintanilla et al. 2007) and supercritical oxidation (Pérez et al. 2004). These methods are often combined, for example the photo-Fenton process (a combined Fenton and photocatalytic process), and in many situations they can be augmented by the use of supported heterogeneous catalysts. Support or catalytic materials can include oxides of titanium and aluminium, silicates, clays, activated carbons and zeolites. These are often modified with transition metals. However, many forms of catalytic oxidation for the treatment of aqueous phase pollutants have several common disadvantages. The reaction is usually achieved only under high temperature (125-320°C) and pressures (0.5-2 MPa) and requires the treatment of large volumes of raw wastewater. In addition to this many techniques require feed chemicals (e.g. oxidizing agents), oxygen enrichment, homogeneous catalysts and pH buffering. Consequently there is a high associated cost with techniques such as WAO (Zhao et al. 2004). Due to the oxidation taking place at high temperatures and pressures in the aqueous phase, catalyst leaching and or instability is also a disadvantage. Total decomposition of the pollutant is also not always possible and long reaction times are common (Alejandre et al. 1998).

Dry air oxidation combined with aqueous adsorption, eliminates a number of these issues. The adsorption can occur under mild conditions, minimizing the damage to the adsorbent/catalyst. It also pre-concentrates the pollutant which means a larger volume of water does not have to be sustained at high temperatures and pressures. The only feed that is required is air and organic

pollutants can be oxidised completely into the terminal products of H₂O and CO₂. The oxidation simultaneously regenerates the catalyst, unlike CWAO systems which often require separate regeneration units. The milder conditions involved result in an improved catalyst lifespan and reduced running costs.

To date most work on dry air catalysis systems for phenol treatment have focused on activated carbon (Matatov-Meytal and Sheintuch 1997; Zhao et al. 2004) and mixed oxide supports often with impregnated transition metal oxide catalysts (Marc-Loudon 1995; Centi et al. 2000). There is however little research on the use of cation exchanged zeolites, which have a number of advantages as outlined in Chapter 3 section 3.1.1.

In this chapter the second stage of the two step treatment will be explored (illustrated in Figure 5.1). This step consists of the simultaneous oxidation of adsorbed phenol and regeneration of the catalyst in air. The aim of this step is to convert the adsorbed phenol into its terminal products CO₂ and H₂O while minimizing products of incomplete oxidation, using copper and platinum modified H-Beta zeolites. Principal goals include determining the ideal catalyst for minimizing oxidation conditions. Criteria include: a fast reaction rate, a low oxidation temperature and confirmation of complete phenol removal.

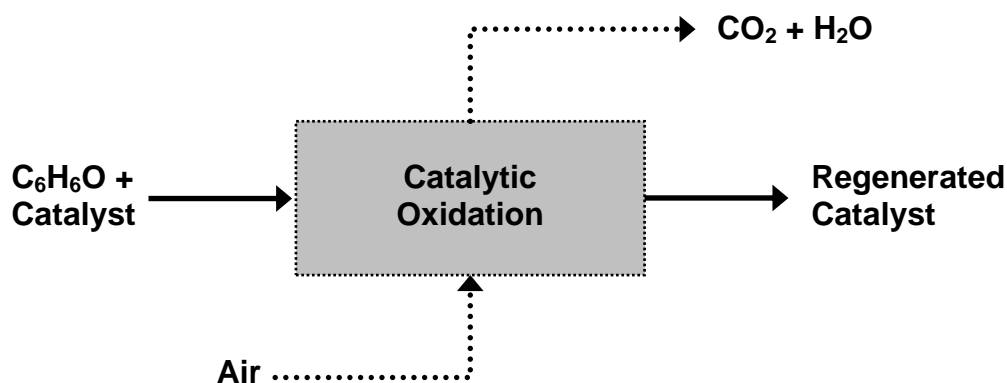


Figure 5.1 Overview of the proposed catalytic oxidation process

Two primary analytical methods will be used to evaluate the oxidation of phenol on zeolite beta. The first is Temperature Programmed Oxidation which will be outlined in section 5.2.2 and the second is Thermo Gravimetric Analysis.

5.1.1 Thermo Gravimetric Analysis

Thermo Gravimetric Analysis (TGA) is an experimental technique which measures the mass of a sample as a function of temperature in a controlled atmosphere. Samples are heated at a constant rate or held at a constant temperature (dynamic and isothermal measurement, respectively) while the mass changes are monitored. Alternatively, non-linear temperature programs can be used for certain experiments. The change in mass occurs as the sample loses material. This loss can occur in a number of ways including reaction with the atmosphere (e.g. oxidation), thermal decomposition and evaporation. The mass measurements are usually represented as a TGA curve with temperature or time plotted on the x axis and mass or percentage mass on the y axis. The plot produces steps which represent specific species or incidences of mass change.

The thermobalance can take a number of different configurations. Generally however, they accommodate two crucibles for comparison, one of which contains the sample. The deviation from the null position or the restoring force is then used to calculate the change in mass. Buoyancy correction is used to compensate for the change in density of the gas as temperature increases. Without this correction the sample would appear to increase in mass with increasing temperature (Dodd and Tonge 1987; Gabbot 2008)

5.2 Experimental

5.2.1 Catalyst Preparation

Copper and platinum zeolites were prepared using a conventional ion exchange technique. For the exchange step a known quantity of metal salt was dissolved in distilled water and to this the zeolite was added. The zeolite to solution ratio was kept at 1g of zeolite to 50 ml of water. The suspension was stirred for 24 hours before removing the zeolite by vacuum filtration. The filter cake was washed with distilled water to remove any non-exchanged species and then dried overnight in air to remove the bulk of the adsorbed water. The dried zeolite was then calcined in a Lenton thermal designs muffle furnace at 450°C for 5 hours.

The calcination step removes any traces of adsorbed water and decomposable salts left over from the exchange process. The salts used were $\text{Cu}(\text{NO}_3)_2 \cdot 3\text{H}_2\text{O}$ (Fluka) and $\text{Pt}(\text{NH}_3)_4\text{Cl}_2 \cdot x\text{H}_2\text{O}$ (Aldrich) for copper and platinum exchange, respectively. Both are easily dissolved in water. The exchange process was also pH controlled for specific samples using NH_4OH (ACS 30% NH_3) at the start of exchange to bring the pH up to 7. The pH was monitored using a Thermo Orion model 420A+ pH meter. All the zeolites used were supplied by Zeolyst International.

For the bi-metallic zeolites the standard process used in this work was to perform all the exchange steps for copper and repeat them for platinum on the calcined copper zeolite. The two metals were also exchanged in two other procedures, with the platinum and copper steps reversed and with both of the metals exchanging in the same solution.

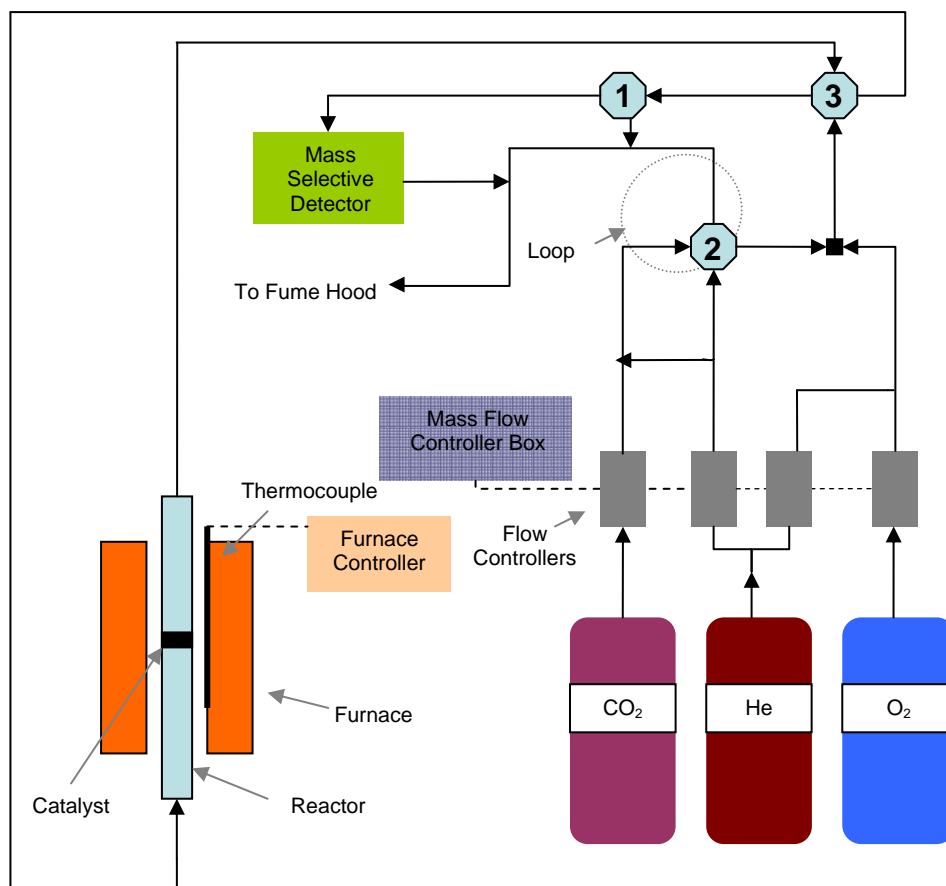
Accurately weighed amounts of each adsorbent were added to phenol solutions of 2000 mg dm^{-3} to saturate the zeolite. They were then stirred for one hour to reach equilibrium. Each sample was filtered using a Buchner funnel and dried in air overnight at room temperature. The phenol loaded modified zeolite was then subjected to temperature programmed oxidation.

5.2.2 Temperature Programmed Oxidation Studies

The Temperature Programmed Oxidation (TPO) rig is shown in Figure 5.2. The principal components were a gas delivery system, a reactor and a detector. There were three feed gasses (all gases were supplied by BOC). Helium was used as a carrier gas, it was mixed with 15% O_2/He . 15% CO_2/He was used as an internal standard. A set of Tylan Model FC280/280A Mass flow controllers regulated the flow of each feed gas. These flow controllers were operated by a Vacuum General Dyna Mass DM2600. The gas delivery system used a system of valves to control the flow of the feed gases to the various components of the TPO rig.

The feed gases were fed into the reactor which consisted of a 560 mm quartz tube with an 8 mm outer diameter and a 6 mm internal diameter. Suspended by quartz wool within the reactor was the sample catalyst bed. A thermocouple was inserted into the 'hot zone' within the reactor. The reactor tube was surrounded by a muffle furnace which brought the catalyst bed up to the specified temperature. The furnace was controlled by a Carbolite 2416 furnace controller. The exhaust gases from the reactor were continuously analysed using an Agilent Technologies 5975C inert Mass Selective Detector (MSD).

In a typical TPO procedure, 100 mg of phenol adsorbed catalyst was inserted into the reactor. Before testing the catalyst bed was pre-treated in a 3% O₂/He mixture at 50 ml min⁻¹ for 60 minutes at room temperature. After pre-treatment the sample was subjected to an increase in temperature at 10°C min⁻¹ up to 750°C. The temperature was held at this temperature for 10 minutes before bringing it back down to room temperature at the same rate. The products leaving the reactor were continuously monitored by the MSD and subsequently analysed using a HP Compaq dc7700 PC with the MSD Chemstation 5975C software.



1. 3 way valve. Sends gases to fume hood or to MSD.
2. 6 way valve. Controls emptying and filling of CO₂ loop.
3. 4 way valve. Sends gases through reactor or bypass straight to MSD

Figure 5.2 Schematic of the temperature programmed oxidation setup.

In the MSD the products of oxidation are ionised. These molecular ions can then be separated in high vacuum by their mass to charge (m/e) ratio. The ionisation causes the molecules to fragment into small groups of charged particles as opposed to a single ion. This mass fragmentation pattern is unique to each ion, thus a characteristic pattern can be identified. In gaseous samples some ion intensities may overlap when they occur at the same atomic mass, an example is CO and N₂ which both occur at $m/e = 28$. The mass fragment of phenol is presented in Figure 5.3. Phenolic mass fragments are characterised by large intensities in the molecular ion and minimal dehydration provided there is no adjacent functional group. The loss of CO from the molecular ion can create a significant intensity at $m/e = 66$, additionally the loss of CHO can create a peak

at $m/e = 65$. The latter case only becomes more prevalent in higher homologues of phenol (Fahmey et al. 2001). Table 5.1 lists the relevant ions to be monitored.

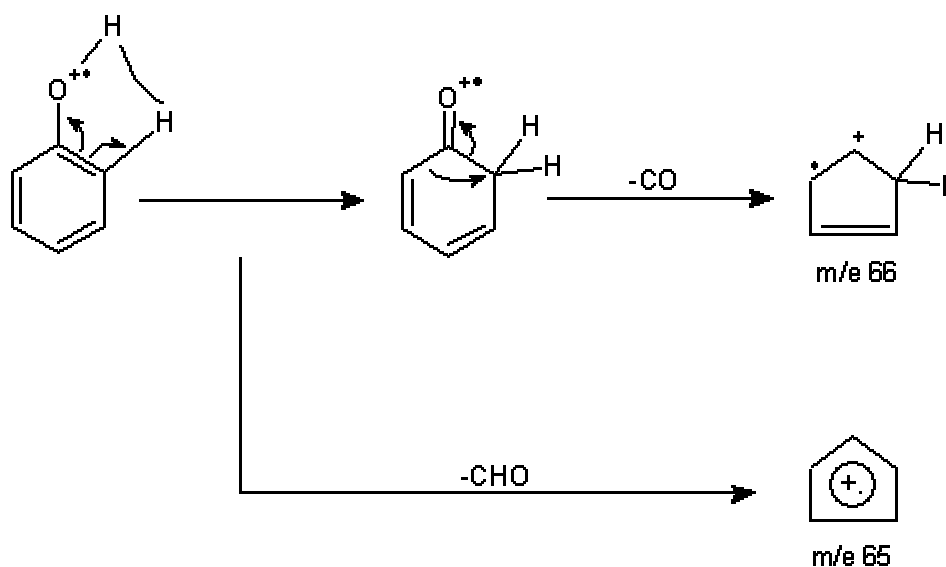


Figure 5.3 Principal mass spectral fragmentation of phenol (Fahmey et al. 2001)

Table 5.1 Ions Monitored

Ion	H_2O^+	CO^+	O_2^+	CO_2^+	$C_5H_6^+$	$C_5H_7^+$	$C_6H_5O^+$	$C_6H_6O^+$
a.m.u.	18	28	32	44	65	66	93	94

5.2.3 Thermo Gravimetric Analysis

TGA was performed on a Labsys Setram TG-DTA/DSC in air. Approximately 10 mg of zeolite was placed in 100 μ l Al_2O_3 crucible. The analysis consists of three steps. The sample was first stabilized for 30 minutes at 30°C, then the temperature was raised at 10°C per minute up to 700°C, and finally brought back down to 30°C at 50°C per minute. The TGA profile was generated from the weight loss observed during the second step (the temperature ramp) as a function of increasing temperature.

5.3 Results and Discussion

5.3.1 Temperature Programmed Oxidation

This section will report on the TPO studies performed on Beta zeolite. Figure 5.4 represents the TPO profile for the unmodified H-Beta zeolite after saturation with phenol. The most abundant ions have been represented. Given the controlled nature of the adsorbate and feed gas the principal ions are easily differentiated by their mass fragment.

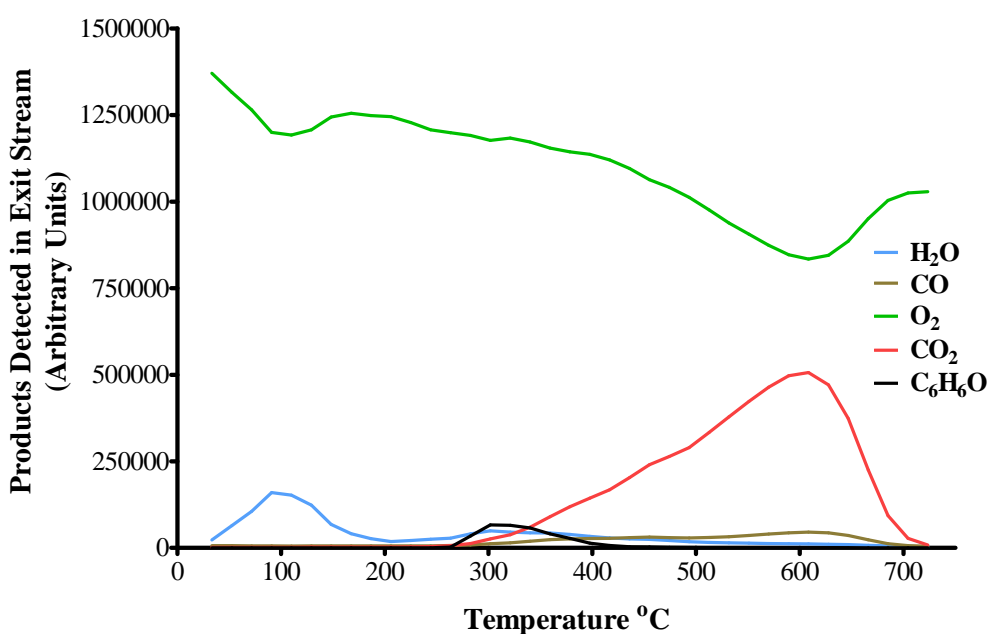


Figure 5.4 Formation of species as a function of temperature from phenol saturated H- β -25. (100 mg sample, 50 ml min⁻¹, 3% O₂ in He, 10°C min⁻¹).

The products detected were water, oxygen, carbon monoxide, carbon dioxide and phenol. A number of trace components were also detected. The O₂ profile occurs at a mass fragment of 32 and represents the constant O₂ present in the feed gas. The abundance of O₂ decreases when consumed in oxidation. Immediately after the temperature starts to increase, water is detected reaching a maximum at 100°C. This represents the adsorbed water that remained after the drying step. Phenol was observed between 263 and 416°C with a maximum at approximately 300°C. This temperature is at a significantly higher temperature than its boiling

point of 182°C. At 257°C the oxidation of the organic component begins, this is represented by an increase in CO₂ as the terminal component of the oxidation reaction and a corresponding decrease in the level of O₂ as it is consumed by the oxidation reaction. A significantly smaller amount of CO is formed representing an amount of incomplete oxidation of the organic component or a fragment of CO₂. The CO profile shadows that of the CO₂. The oxidation in this case is not completed until 720°C and achieves a maximum at 610°C judging by the CO₂ profile. Since there is no catalyst metal on this zeolite this oxidation is most likely a result of the acid sites on the zeolite surface. These acid sites consist of the Brønsted acid sites located at the tetrahedrally coordinated and charged balanced aluminium atoms on the external surface and pore structure, and the Lewis acid sites which are located at the unsaturated aluminium atoms created from local defects in the tertiary building units that compose the zeolite. The Lewis sites occur predominantly in the microporous structure (Jansen et al. 1997). The respective donation or removal of a proton by these acid sites serves to catalyse organic reactions by creating carbocationic intermediates (Correa and Mota 2003).

At the same time as the phenol peak occurs, the expected fragmentation products of phenol produced smaller correlating profiles. The profiles for these mass fragments are shown in Figure 5.5.

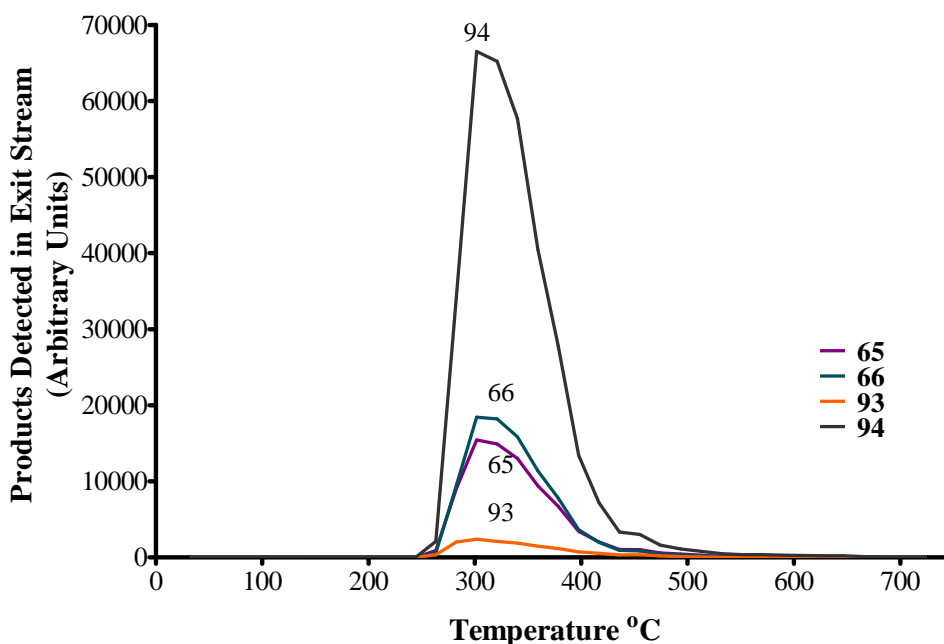


Figure 5.5 Formation of the fragmentation products of phenol as a function of temperature from phenol saturated H- β -25 zeolite. (100 mg sample, 50 ml min⁻¹, 3% O₂ in He, 10°C min⁻¹).

The mass fragments at 65 (C₅H₆⁺) and 66 (C₅H₇⁺) represent the two most common intermediates outlined in section 5.2.2. The abundance of 66 is slightly larger than 65. This is a tendency expected for molecular phenol, where the ion resulting from the loss of neutral CO is believed to be more prevalent in the mass fragment (Fahmey et al. 2001). A trace amount of what is most probably the phenolate ion is formed at a mass fragment of 93 (C₆H₅O⁺).

5.3.1.1 Copper Zeolites

Table 5.2 lists the copper exchanged zeolites with a $\text{SiO}_2:\text{Al}_2\text{O}_3$ ratio of 25:1, examined by temperature programmed oxidation. The object of adding copper to the zeolite is to reduce the temperature at which oxidation takes place, to eliminate the desorption of phenol and other large fragments and to increase the proportion of the adsorbed species that is oxidized.

Table 5.2 Summary of copper zeolites examined in this section

Sample	$\text{SiO}_2:\text{Al}_2\text{O}_3$ ratio	Cu Loading wt%	Exchange pH
H- β -25	25:1	0	-
0.9Cu/ β -25	25:1	0.88	5.3
1.3Cu/ β -25	25:1	1.3	5.4
2.1Cu/ β -25(p)	25:1	2.1	7.0
3.0Cu/ β -25(p)	25:1	3.0	7.0
4.6Cu/ β -25(p)	25:1	4.6	7.0

Figure 5.6 shows a typical profile for the decomposition of phenol on a copper zeolite (in this case 2.1Cu/ β -25(p)).

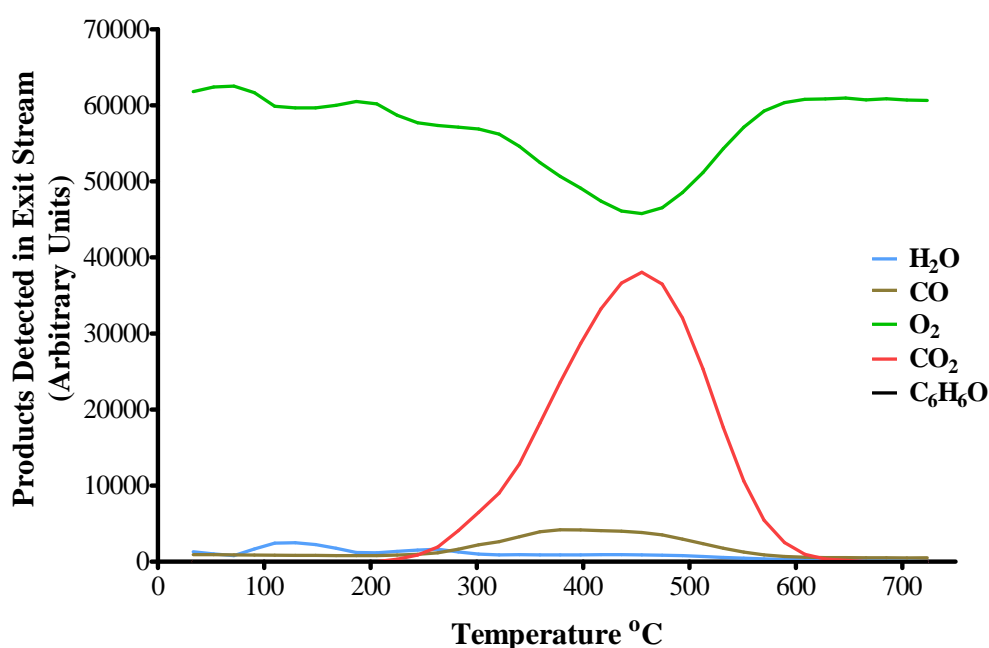


Figure 5.6 Formation of species as a function of temperature from phenol saturated 2.1Cu/ β -25(p) zeolite. (100 mg sample, 50 ml min⁻¹, 3% O₂ in He, 10°C min⁻¹).

In contrast to Figure 5.4, no mass fragment for phenol or its fragmentation products were detected. This could be because total oxidation to CO₂ occurs at a lower temperature compared to the unmodified zeolite. Another possibility is that the phenol adsorbs much more strongly to the exchanged copper zeolite, this possibility was highlighted in Chapter 4 section 4.3.1. The oxidation appears to begin at 215°C and concludes at 627°C. A clear maximum occurs at 455°C. The water profile is relatively smaller than the unmodified zeolite; this could be due to the larger proportion of adsorbed phenol on the modified zeolite.

For comparison purposes a blank sample was prepared. This involved the use of an adsorption solution containing only distilled water. The resulting profile is shown in Figure 5.7

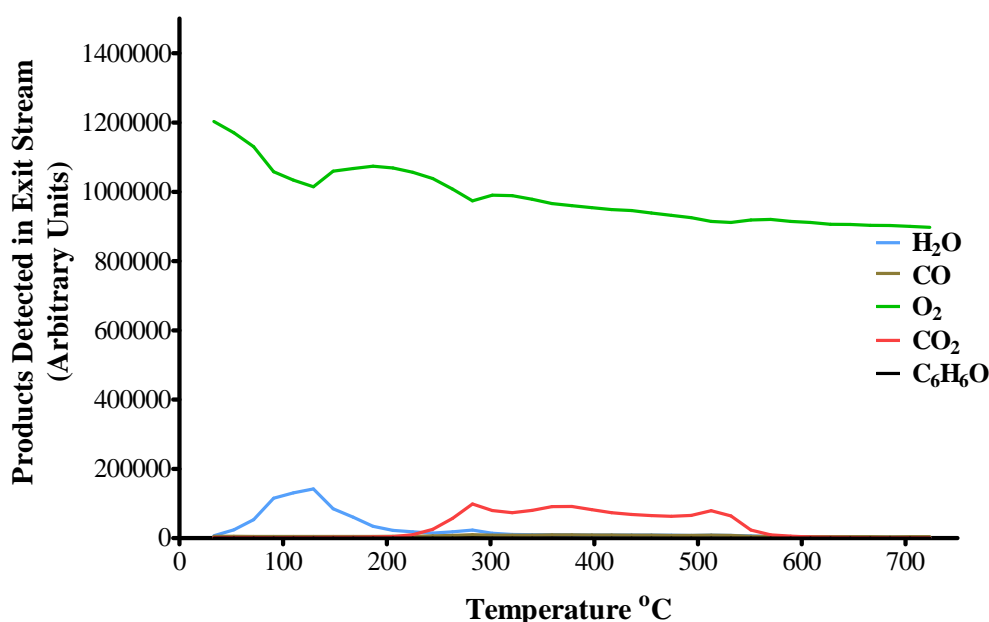


Figure 5.7 Formation of species as a function of temperature from water saturated 2.1Cu/β-25(p) zeolite. (100 mg sample, 50 ml min⁻¹, 3% O₂ in He, 10°C min⁻¹).

In this case CO₂ was detected and occurred at roughly the same temperature range, except that it was no longer detected above 575°C. This much smaller CO₂ profile most likely represented the product of a small quantity of organic material adsorbed on the surface of the zeolite. The CO and phenol mass fragments were absent, but the water peak was noticeably larger in the absence of phenol.

The MSD is subject to sensitivity drift giving differences in relative abundance over time. As a result a CO₂ pulse of a known volume was used as an internal standard. This served as a benchmark for comparing peaks from various samples. When comparing the catalytic activity of different solids, as the most pronounced product of oxidation, CO₂ was used as a representative indicator. A range of CO₂ volumes were also injected into the gas assembly in order to establish a calibration graph as in Figure 5.8. This was then used to determine the amount of CO₂ produced from the peak area in the TPO profiles.

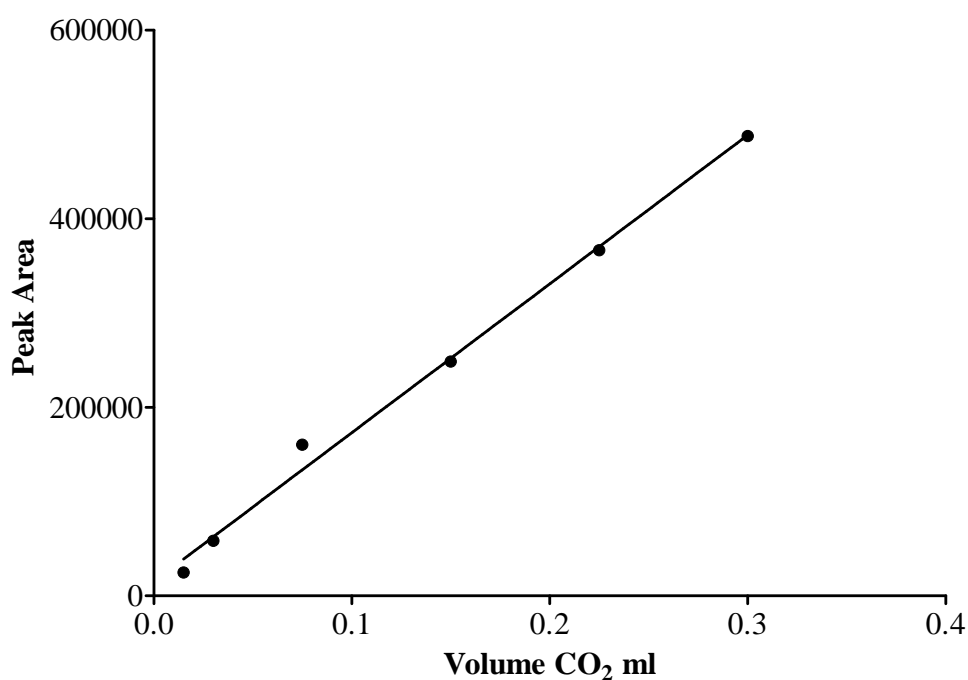


Figure 5.8 CO₂ calibration graph

Figure 5.9 shows the profile of CO₂ production during phenol TPO on a range of different zeolite samples with different copper loadings. The origin of each profile is close to zero but has been staggered for clarity.

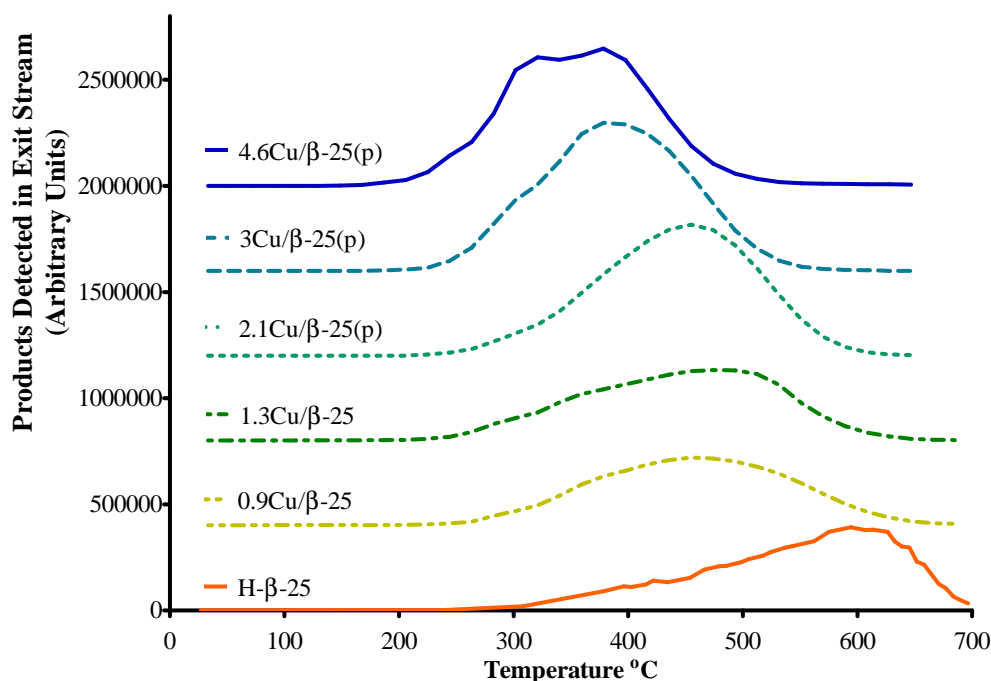


Figure 5.9 Formation of CO₂ as a function of temperature from phenol saturated H-β-25 zeolite with varying copper loading. (100 mg sample, 50 ml min⁻¹, 3% O₂, 10°C min⁻¹).

Each of the CO₂ profiles reaches a distinct maximum point, the exception being 4.6Cu/β-25(p) which exhibits what appears to be a split peak at 320 and 378°C. This split could be a result of the increasing proportion of CuO in the surface copper as highlighted in Chapter 3 section 3.2.2.2. As the copper loading is increased, there appears to be a clear shift to lower temperatures in terms of the start, maximum and end of CO₂ production. In order to illustrate this Figure 5.10 compares the temperature at maximum CO₂ detection to the copper loading. The result is a clear trend of temperature reduction relative to increasing copper.

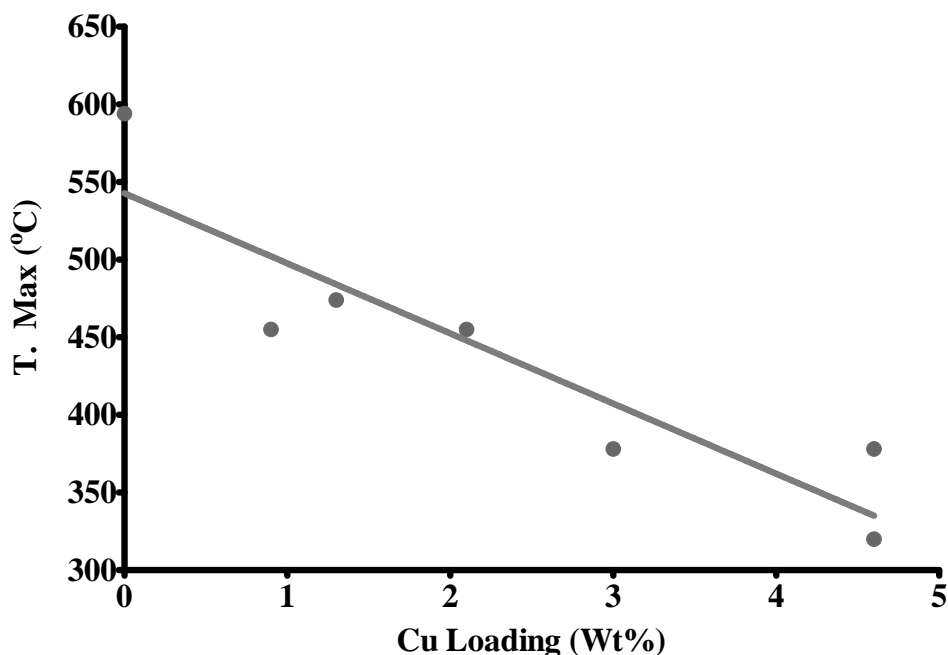


Figure 5.10 Comparison of the temperature of maximum CO₂ detection during TPO versus copper loading.

The CO₂ peaks have a tendency to occur over a shorter temperature range as copper loading is increased despite an increase in the amount of CO₂ produced. This appears to indicate improved catalytic activity and a faster oxidation rate, with the length of time CO₂ was produced reducing from 44 to 32 minutes. Overall there is a continuous reduction in the temperature marking the start of oxidation, with increasing copper. In each case, other than the unmodified zeolite, the CO₂ profile envelops the temperature range where the phenol mass fragment was observed in the unmodified zeolite and no phenol mass fragment was observed. Table 5.3 shows the relative amount of CO₂ produced, as derived from the CO₂ calibration shown in Figure 5.8. The amount of phenol oxidized was then predicted from this and adjusted relative to a blank sample.

Table 5.3 Summary of CO₂ production as a function of zeolite mass and the corresponding amount of adsorbed phenol needed to produce it. Phenol loading was adjusted with a blank TPO profile.

Sample	CO ₂ produced (mg g ⁻¹)	Oxidized Phenol (mg g ⁻¹)
H-β-25	91	25
0.9Cu/β-25	83	23
1.3Cu/β-25	87	24
2.1Cu/β-25(p)	126	38
3Cu/β-25(p)	136	41
4.6Cu/β-25(p)	127	37

The results show a significant increase in the amount of phenol oxidized on the pH modified zeolites. Outside of this relationship there is no distinct trend of increasing CO₂ production or phenol oxidation relative to increasing copper loading.

Figure 5.11 shows the profiles for the CO mass fragment. In each case the profiles broadly match the start and end points of the CO₂ mass fragment.

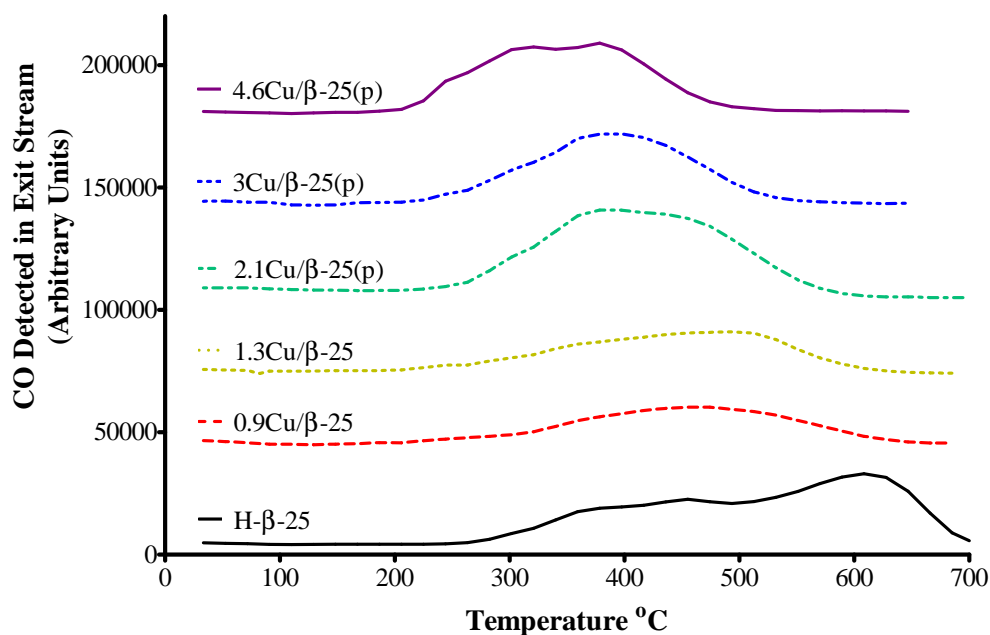


Figure 5.11 Formation of CO as a function of temperature from phenol saturated H-β-25 zeolite with varying copper loading. (100 mg sample, 50 ml min⁻¹, 3% O₂ in He, 10°C min⁻¹).

As shown in Table 5.4 the CO peak area is in general close to 5% of the peak area of the corresponding CO₂ profile. The exception is the unmodified beta zeolite which produces somewhat more CO relative to CO₂. This may be a result of a less complete oxidation in the absence of copper. CO₂ commonly forms the fragments CO and O₂ in the same proportions each time upon electron impact ionisation. The comparable CO proportion in each of the copper zeolites would suggest that the CO observed is a consequence of CO₂ fragmentation as opposed to incomplete combustion.

Table 5.4 Comparison of the relative peak areas of the CO peaks as a percentage of the CO₂ peak area.

<i>Sample</i>	<i>Relative size of CO to CO₂ peak (%)</i>
H-β-25	9.0
0.9Cu/β-25	5.3
1.3Cu/β-25	5.0
2.1Cu/β-25(p)	4.4
3Cu/β-25(p)	4.7
4.6Cu/β-25(p)	5.1

To summarize the modification of the zeolite with cation exchanged copper has the following effects:

- The temperature of oxidation is significantly reduced, both in the case of the start temperature and the temperature at which the maximum oxidation was observed.
- The time it took for all the adsorbed phenol to be oxidised during the TPO experiments was reduced.
- The relative amount of CO produced as a result of oxidation was reduced.
- No phenol fragments common to phenol or any intermediates were detected.

The first two effects also become more pronounced as the copper loading is increased. However, the TPO profiles do not change proportionately with increasing copper throughout the range of samples. This is illustrated by Figure 5.12

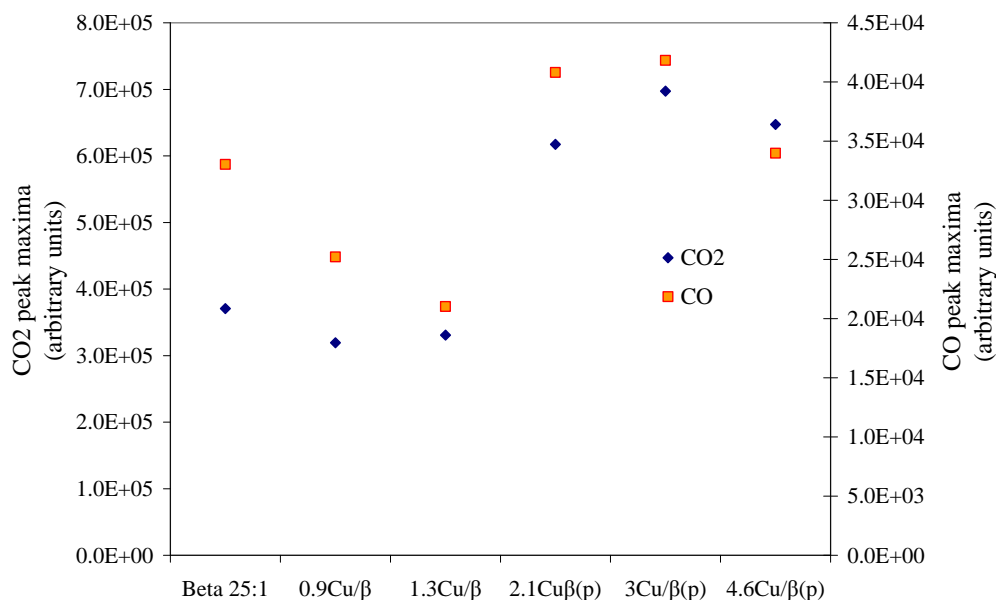


Figure 5.12 TPO performance summary for Cu modified beta zeolites. Showing CO and CO₂ peak maxima. (100 mg sample, 50 ml min⁻¹, 3% O₂, 10°C min⁻¹).

The graph summarizes the abundance at the peak maximum on each of the TPO profiles. There is a clear difference between the first set of samples and the pH treated copper zeolites (denoted by (p)), with noticeably higher peak maxima on the latter. We can see also from Figure 5.9 that the shape of the TPO profile changes significantly on the pH modified zeolites. The reduction in oxidation temperature appears to be more proportionate to copper content, as observed in Figure 5.10. The increase in the abundance of oxidation products at the peak maxima could be a result of an increased proportion of adsorbed phenol. In Chapter 3 it was noted that the copper exists in different species on the pH treated zeolites, there is also evidence that these species exhibit unique interactions with phenol or change the overall surface chemistry of the zeolite as noted in Chapter 4. For example exchanged Cu⁺ ions present in over exchanged zeolites can form π bonds with aromatic molecules (Kukulka-Zajac et al. 2006). The over-exchanged zeolites are likely to cover more of the aluminium exchange sites with copper species which would in turn decrease surface acidity and

increase the affinity for phenol. In addition to this the pH modification could also result in increased copper exchange on the silanol acid sites, which would further enhance this effect (Schreier et al. 2005).

5.3.1.2 Platinum Zeolites

Platinum was also examined for its capacity to catalytically oxidize the adsorbed phenol. As a catalyst, platinum is known to be a good oxidizing catalyst on zeolites at relatively low temperatures (Traa et al. 1999). The platinum zeolites examined are summarised in Table 5.5.

Table 5.5 Summary of platinum zeolites examined in this section

Sample	SiO ₂ :Al ₂ O ₃ ratio	Theoretical Loading wt%	Pt Loading wt%
0.05Pt/β-25	25:1	0.2	0.05
0.07Pt/β-25	25:1	0.4	0.07
0.2Pt/β-25	25:1	1	0.2

The TPO profile for the beta zeolite loaded with 0.07 wt% Pt is shown in Figure 5.13. Unlike the Cu zeolites the CO₂ profile appears to suggest that the oxidation takes place in two steps. The first starts at the relatively low temperature of approximately 170°C followed by a sharp increase in CO₂ production up to 265°C where the level of CO₂ produced begins to fall. A second broader CO₂ peak emerges in the temperature range of 280-575°C. In this example there are two maxima at 244 and 398°C.

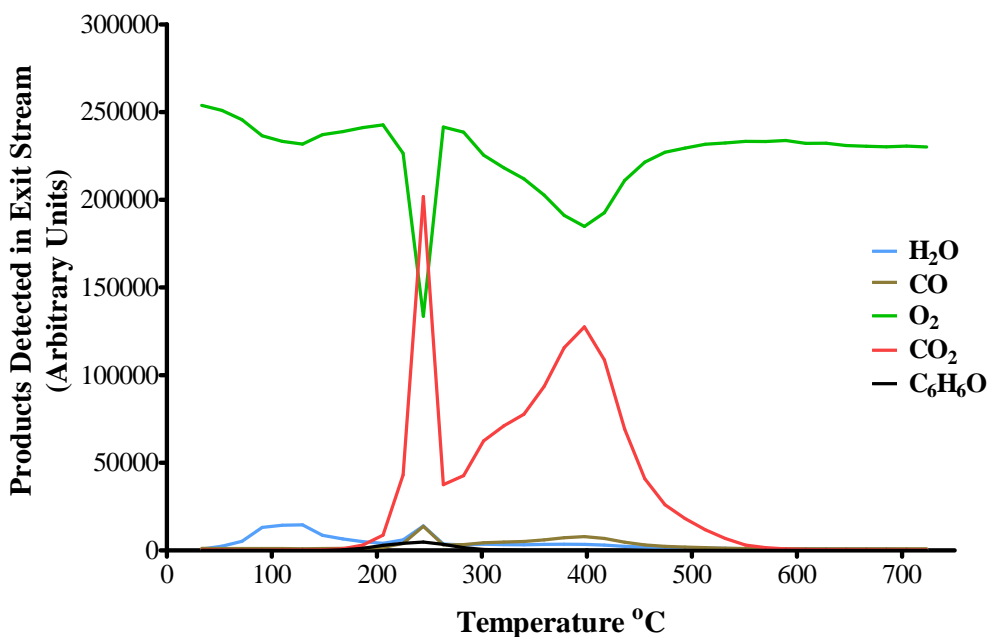


Figure 5.13 Formation of species as a function of temperature from phenol saturated 0.07Pt/ β zeolite. (100 mg sample, 50 ml min⁻¹, 3% O₂, 10°C min⁻¹).

This apparent two step oxidation is ubiquitous in all of the Pt zeolites studied. Mass fragments at 54, 65, 51 and 94 were observed at the same time as the low temperature oxidation peak. The first three represent fragments of phenol and the last is phenol itself. 54 and 51 m/e are possibly important as they were not present in the desorbed phenol fragments from the unmodified H- β -25. They are also both likely to be aliphatic fragments e.g. C₄H₆⁺ for 54 m/e and C₄H₃⁺ for 51 m/e. While these may be the result of normal fragmentation of the adsorbed phenol, considering that they occur at the same temperature as a significant CO₂ peak they may also be a product of some incomplete oxidation due to the presence of platinum. In addition, these fragments occur earlier than the temperature at which phenol desorption was observed in Figure 5.4 for H- β -25. The low temperature CO₂ peak appears to represent the partial oxidation of phenol, while the bulk of the oxidation takes place at the higher temperature peak.

Figure 5.14 shows the relative amount of CO₂ detected from the TPO of phenol over zeolites with several different platinum loadings.

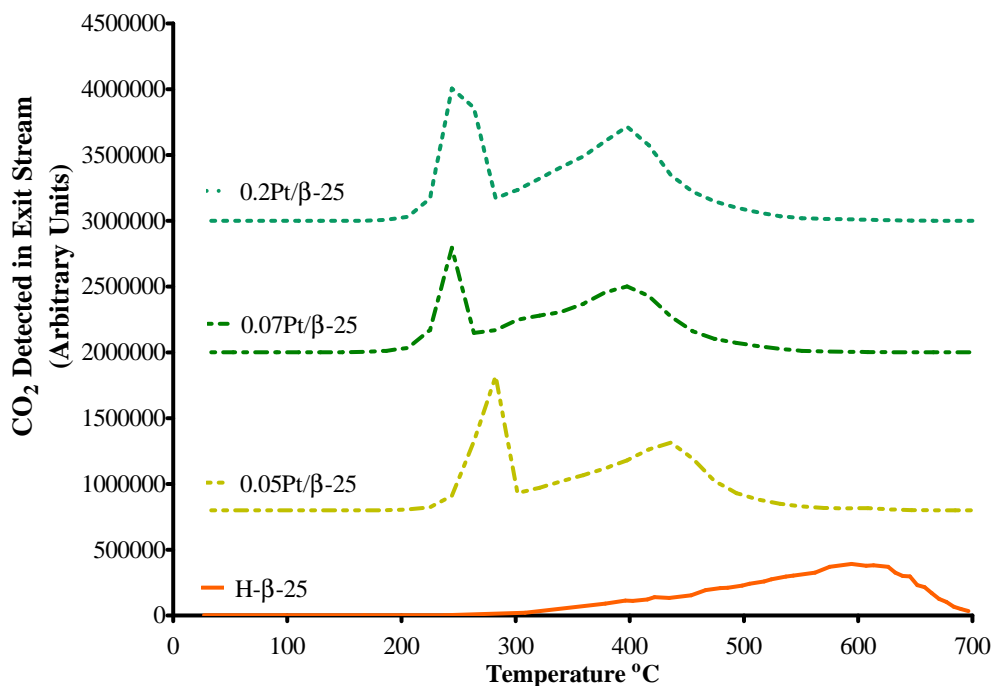


Figure 5.14 Formation of CO₂ as a function of temperature from phenol saturated H-β-25 zeolite with varying platinum loading. (100 mg sample, 50 ml min⁻¹, 3% O₂ in He, 10°C min⁻¹).

It is immediately apparent that the platinum loaded zeolites exhibit oxidation at significantly lower temperatures and over shorter periods than in the case of the unmodified zeolite. 0.05Pt/β-25 and 0.07Pt/β-25 both showed the desorbing phenol fragments listed previously in this section, however they were absent from 0.2Pt/β-25. This catalyst had 65% more exchanged platinum than the next highest, this probably helped to reduce the amount of desorbing phenol by increasing oxidation at this point. This is also suggested by the noticeably broader low temperature peak for 0.2Pt/β-25. A summary of the parameters of the CO₂ profiles shown in Figure 5.14 are presented in Table 5.6.

Table 5.6 Summary of CO₂ mass fragment production on a variety of platinum zeolites.

<i>Sample</i>	<i>Start Temp (°C)</i>	<i>Max 1(°C)</i>	<i>Max 2(°C)</i>	<i>End Temp (°C)</i>	<i>Temperature Change(°C)</i>
H-β-25	257	-	594	697	440
0.05Pt/β-25	225	286	486	550	325
0.07Pt/β-25	205	244	397	531	326
0.2Pt/β-25	205	244	397	531	326

Increasing platinum loading from 0.05 to 0.07 wt% resulted in a slight decrease in the temp associated with the first oxidation peak, increasing the loading above 0.07 wt% did not improve the performance of the oxidation in terms of lowering temperature.

A summary of the CO₂ produced and the predicted quantity of adsorbed phenol is shown in Table 5.7.

Table 5.7 Summary of CO₂ production as a function of zeolite mass and the corresponding amount of adsorbed phenol needed to produce it. Phenol loading was adjusted with a blank TPO profile.

<i>Sample</i>	<i>CO₂ produced (mg g⁻¹)</i>	<i>Oxidized Phenol (mg g⁻¹)</i>
H-β-25	91	25
0.05Pt/β-25	114	34
0.07Pt/β-25	104	30
0.2Pt/β-25	117	35

Although the amount of phenol oxidized is notably higher in the platinum zeolites when compared to the unmodified H-β-25, there is no significant overall trend relative to increasing platinum loading. 0.07Pt/β-25 and 0.2Pt/β-25 had almost identical temperature characteristics.

Figure 5.15 shows the respective profiles for the CO mass fragment. The peak area comparison is shown in Table 5.8.

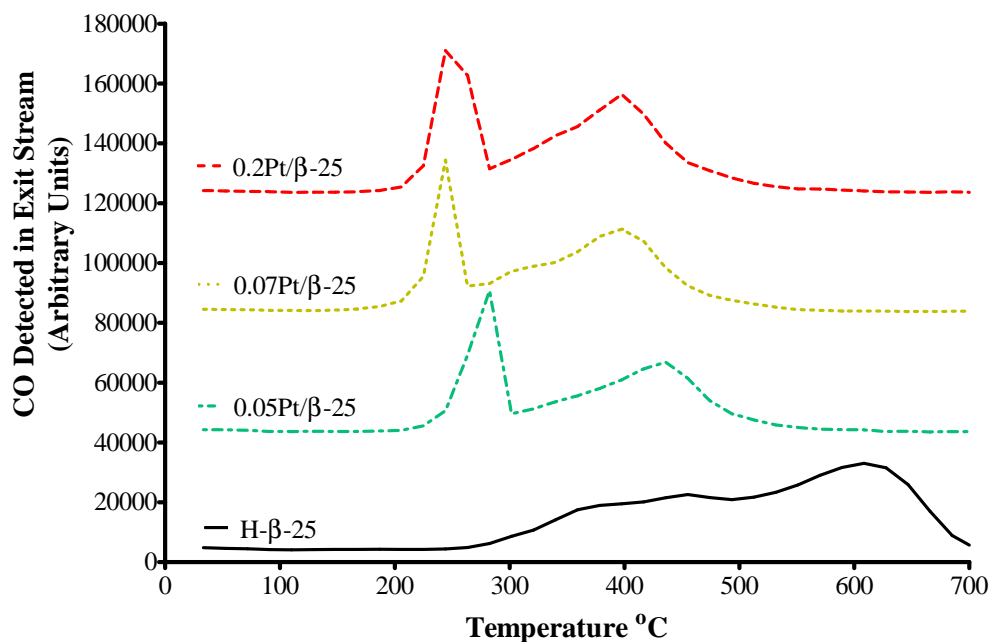


Figure 5.15 Formation of CO as a function of temperature from phenol saturated H- β -25 zeolite with varying platinum loading. (100 mg sample, 50 ml min⁻¹, 3% O₂ in He, 10°C min⁻¹).

Table 5.8 Comparison of the peak area of the CO peaks as a percentage of the CO₂ peak area.

<i>Sample</i>	<i>Relative size of CO to CO₂ peak (%)</i>
H- β -25	9.0
0.05Pt/ β -25	4.7
0.07Pt/ β -25	5.7
0.2Pt/ β -25	4.6

As in the case of the copper zeolites, the platinum zeolites exhibit a similar ratio of the CO mass fragment at around 5% of CO₂. The slightly higher amount of CO produced in the 0.07Pt/ β zeolite accounts somewhat for the lower mass of CO₂ detected (shown in Table 5.6).

To summarize, the platinum modified zeolites exhibited favourably low phenol oxidation temperatures relative to the unmodified zeolite. This low temperature oxidation was achieved using a considerably lower metal loading than with copper. The Pt catalysts exhibit what appears to be a different oxidation pathway, which possibly involves a partial oxidation at lower temperatures or oxidation of a particular fraction of the surface phenol. The low temperature peak could also be due to the oxidation of desorbing phenol and its fragments, which occur at a similar temperature. Alternatively the low temperature peak could represent the oxidation of the phenol that is in close proximity to the platinum. Similar profiles are present in the literature. For example the gas phase oxidation of methyl-isobutyl-ketone over platinum zeolite, where the adsorbed organic was observed to first oxidize into coke at lower temperatures and at higher temperatures the less reactive coke was oxidized (Tsou et al. 2005). In all the platinum zeolites a quantity of phenol and its fragments were detected in tandem with the initial CO₂ peak, however these were smaller than those observed in the unmodified zeolite.

Copper zeolites of a loading of 3 wt% or higher, oxidized phenol at lower temperatures than any of the platinum zeolites examined. In addition to this the over exchanged copper zeolites also appear to convert more phenol into CO₂ either through increased adsorption or oxidation potential. In light of this and the detection of desorbed phenol in the TPO profile for the platinum zeolites, it would appear that the over-exchanged copper zeolite is the better catalyst for the oxidation of adsorbed phenol.

5.3.1.3 Bimetallic Zeolites

In this section the zeolites with both copper and platinum are examined. The materials used are shown in Table 5.9. The monometallic platinum catalysts exhibited oxidation at comparatively low temperatures, however when compared to the pH modified copper catalysts the amount of CO₂ produced was smaller and a number of samples produced evidence of incompletely oxidized organic chemicals in the exit streams. By introducing copper and platinum to one zeolite, it may be possible to produce a catalyst with the advantages of both metals.

Table 5.9 Summary of the bimetallic zeolites containing both copper and platinum examined in this section

<i>Sample</i>	<i>SiO₂:Al₂O₃ ratio</i>	<i>Theoretical Loading wt% (Cu/Pt)</i>	<i>Loading wt% (Cu/Pt)</i>
1.4Cu-0.04Pt/β-25	25:1	2/0.2	1.4/0.04
1.6Cu-0.08Pt/β-25	25:1	2/0.4	1.6/0.08
1.3Cu-0.09Pt/β-25	25:1	2/0.6	1.3/0.09
2.4Cu-0.08Pt/β-25	25:1	5/1	2.4/0.08

Figure 5.16 shows the CO₂ profiles for three bimetallic zeolites with varying platinum loading. Each was prepared from a stock of copper zeolite with 2.1 wt% of exchanged copper (2.1Cu/β-25(p)) with the exception of 2.4Cu-0.08Pt/β-25 which was prepared using 4.6Cu/β-25(p). For comparison the CO₂ profile of the zeolite with only platinum exchanged (0.07Pt/β-25:1) and the base copper zeolite (2.1Cu/β-25(p)) were included. As noted in Chapter 3 section 3.3.1, the copper content decreases, most likely due to the lower pH during platinum exchange.

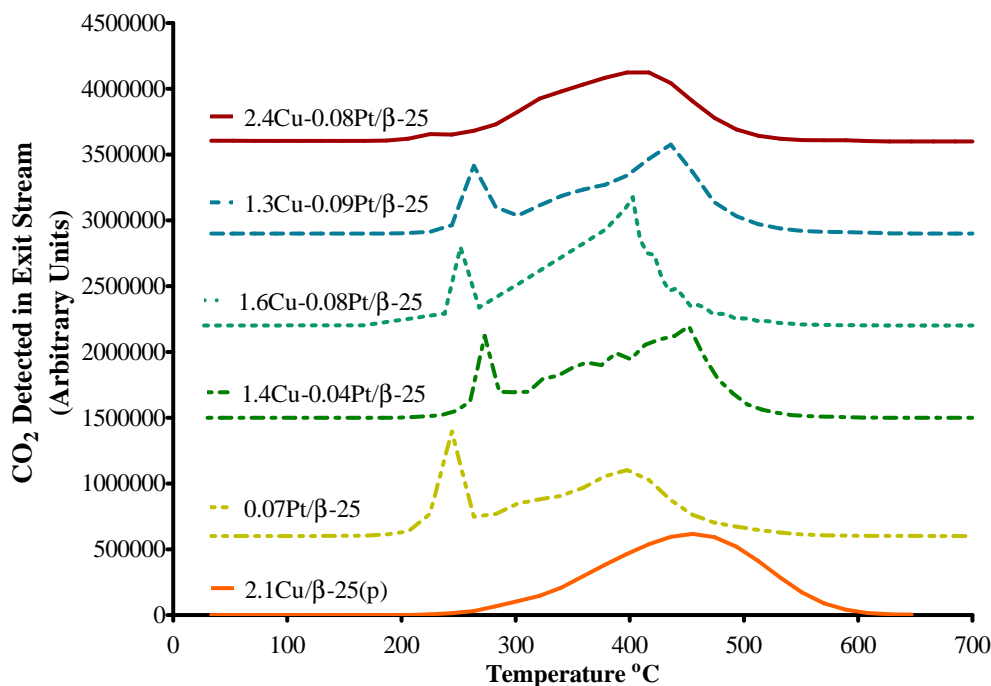


Figure 5.16 Formation of CO₂ as a function of temperature from phenol saturated H-β-25 zeolite with varying platinum and copper loading. (100 mg sample, 50 ml min⁻¹, 3% O₂, 10°C min⁻¹).

Each of the bimetallic zeolites exhibits a low temperature peak characteristic of the monometallic platinum zeolites, although these peaks appear less intense. The broader high temperature peak is also present. However in the bimetallic zeolites it is consistently larger, therefore it is possible to conclude that these profiles contain characteristics of both metals in their monometallic equivalents. The exception is 2.4Cu-0.08Pt/β-25, where no low temperature peak is present and the profile is almost indistinguishable from that of a monometallic copper zeolite. This is probably due to the excess copper masking the platinum or impeding access to certain sites. No phenol fragments were detected in any of the samples.

Table 5.10 summarises the temperature and CO₂ data from the profiles in Figure 5.16. Despite using the same initial copper zeolite for three of the samples, the final copper loading (as examined in Chapter 3) varies between 1.3 and 1.6 wt%.

Table 5.10 Summary of CO₂ mass fragment production on a variety of bimetallic zeolites.

<i>Sample</i>	<i>Start Temp (°C)</i>	<i>Max 1 (°C)</i>	<i>Max 2 (°C)</i>	<i>End Temp (°C)</i>	<i>Temperature Range (°C)</i>
2.1Cu/β-25(p)	244	-	455	601	357
0.07Pt/β-25	205	244	397	531	326
1.4Cu-0.04Pt/β-25	235	273	452	541	306
1.6Cu-0.08Pt/β-25	183	252	403	511	328
1.3Cu-0.09Pt/β-25	225	263	436	550	325
2.4Cu-0.08Pt/β-25	220	-	402	531	311

The phenol oxidation temperatures appear to be somewhat higher in general for the bimetallic zeolite when compared to the zeolites that only contain platinum. However they are notably lower than both the original copper zeolite (2.1Cu/β-25(p)). In terms of temperature reduction the best performing zeolite in this set appears to be 1.6Cu-0.08Pt/β-25. It would appear that the extra copper as opposed to the small increase in platinum contributes more to a reduced oxidation temperature when compared to 1.3Cu-0.09Pt/β-25. 2.4Cu-0.08Pt/β-25 has as similar oxidation range to the other bimetallic zeolites, however the excess copper does not appear to contribute further to temperature reduction. This could be because the platinum appears to be no longer a contributing factor at this copper loading.

Table 5.11 Summary of CO₂ production as a function of the mass of the indicated bimetallic zeolites and the corresponding amount of adsorbed phenol needed to produce it. Phenol loading was adjusted with a blank TPO profile.

<i>Sample</i>	<i>CO₂ produced (mg g⁻¹)</i>	<i>Oxidized Phenol (mg g⁻¹)</i>
1.4Cu-0.04Pt/β-25	117	35
1.6Cu-0.08Pt/β-25	129	39
1.3Cu-0.09Pt/β-25	109	31
2.4Cu-0.08Pt/β-25	97	27

Table 5.11 shows the CO₂ detected and the estimated amount of oxidized phenol for the bimetallic zeolites. There is a perceivable trend of increasing CO₂ detection with increasing copper loading. However, this increase appears to be independent of platinum loading. The sample 1.6Cu-0.08Pt/β-25 was the best performing bimetallic zeolite overall. It exhibited lower oxidation temperatures and greater phenol oxidation than any of the monometallic platinum samples. This sample also has a comparable amount of phenol oxidation to that of the original copper zeolite (2.1Cu/β-25(p) see Table 5.3). The increased phenol oxidation is likely to be due to an increased amount of adsorbed phenol brought on by the improved adsorption affinity of copper zeolites (see Chapter 4 section 4.2.2). The 2.4Cu-0.08Pt/β-25 sample seems to show a point of diminished returns as the increased copper masks any beneficial effect from the Pt and gives it the poorest performance of the bimetallic zeolites and less phenol oxidation than copper zeolites of similar loading.

In Chapter 3 a number of bimetallic zeolites were synthesised with different exchange orders. TPO experiments were conducted in order to ascertain any change in catalytic activity corresponding to the change in synthesis procedure. The first study is shown in Figure 5.17. The same theoretical loading of 2wt% Cu and 0.4wt% Pt was used in each sample.

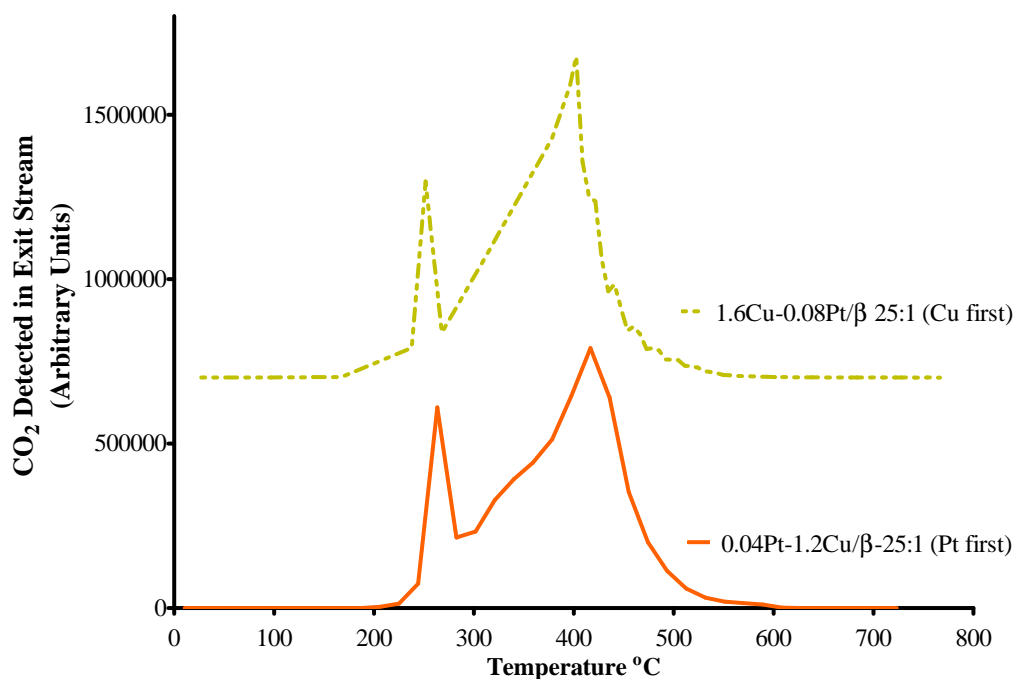


Figure 5.17 Formation of CO₂ as a function of temperature from phenol saturated bimetallic H- β -25 zeolite prepared using different methods. Theoretical loading 2wt% Cu, 0.4 wt% Pt. (100 mg sample, 50 ml min⁻¹, 3% O₂, 10°C min⁻¹).

In Figure 5.17 each zeolite exhibits the same two step profile characteristic of the Pt and bimetallic catalyst. The lowest temperatures were observed in the zeolite where copper was exchanged first with a start temperature at 183°C however the difference between the two profiles is slight; the peak areas of both profiles are almost identical. The 1.6Cu-0.08Pt/ β -25 sample had the highest average loading of the two metals; exchanging platinum first appears to result in an overall lower yield. Despite this, the exchange order appears to have a very minimal effect on phenol oxidation.

To summarize the combination of copper and platinum exchange onto zeolite beta produces a CO₂ profile somewhere in between that of the platinum and copper monometallic zeolites. With the presence of copper the low temperature peak associated with platinum becomes less prominent while the high temperature peak becomes larger. The bimetallic zeolites exhibited lower oxidation temperatures than monometallic copper of a similar loading (2.1Cu/ β -25(p)) and in certain cases (for example 1.6Cu-0.08Pt/ β -25) comparable to platinum zeolites. This would suggest that platinum has a favourable effect on

temperature reduction when added in even small quantities to the copper zeolite, where as increasing the copper loading can lower the temperature further. This effect appears to have a point of diminishing returns as was observed in 2.4Cu-0.08Pt/ β -25 where the platinum was masked by the high level of copper and in TPO was virtually indistinguishable from a monometallic copper profile.

The bimetallic zeolites also show a larger mass of CO₂ production relative to platinum zeolites, this could be due to the enhanced adsorption effect of copper zeolites meaning more available phenol.

For the exchange order, the procedure seemed to have very little influence on the oxidation of phenol, with almost identical profile, temperature and peak area.

5.3.1.4 Effect of Silica to Alumina Ratio

Beta zeolites with varying silica to alumina ratios were also modified with copper to examine their effects on the TPO of phenol. The results of this study are shown in Figure 5.18.

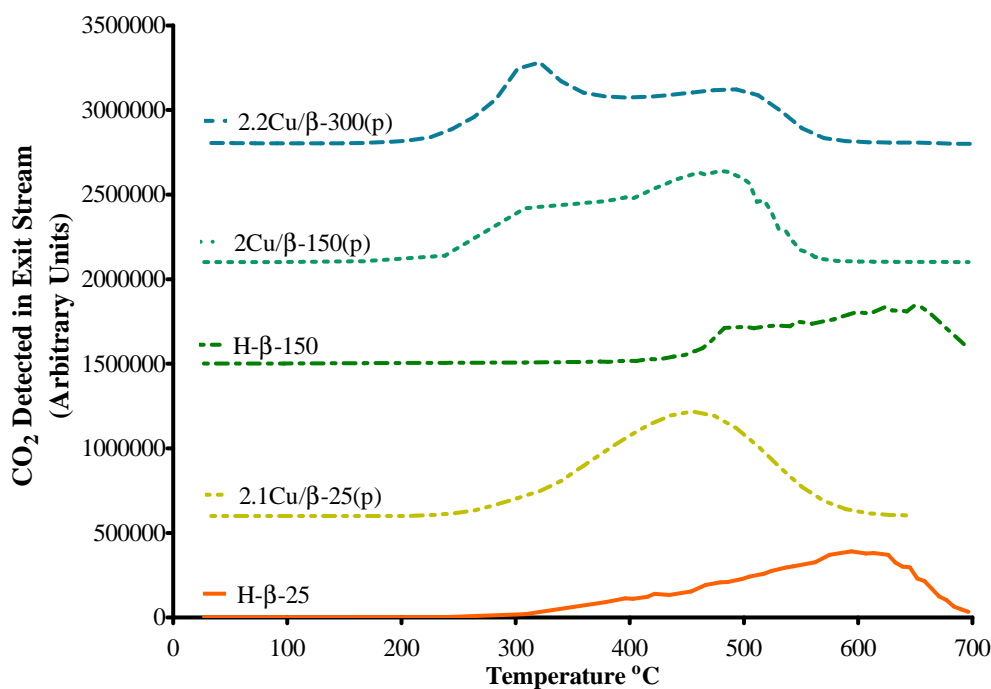


Figure 5.18 Formation of CO₂ as a function of temperature from phenol saturated H- β -25 zeolite with varying silica to alumina ratio and copper loading. (100 mg sample, 50 ml min⁻¹, 3% O₂, 10°C min⁻¹).

All the copper zeolites were synthesised using the same theoretical copper loading (2wt%) and exhibited a similar ability to incorporate copper with pH treatment, however as was examined in Chapter 3 the state of the exchanged copper changes greatly due to the reduction in available aluminium exchange sites. A summary of the CO₂ profiles resulting from the TPO experiments are shown in Table 5.12 and Table 5.13. Phenol fragments were not detected in any of the samples except for 2.2Cu/β-300(p) which showed mass fragments at 65 and 94. Unlike previous examples these occurred across the whole temperature range of CO₂ production.

Table 5.12 Summary of CO₂ mass fragment production on a variety of zeolites with varying silica to alumina ratio, with and without copper.

<i>Sample</i>	<i>Start Temp (°C)</i>	<i>Maximum Temp (°C)</i>	<i>End Temp (°C)</i>	<i>Temperature Range (°C)</i>
H-β-25	257	594	697	440
2.1Cu/β-25(p)	244	455	601	357
H-β-150	438	649	700	619
2.0Cu/β-150(p)	238	479	568	330
2.2Cu/β-300(p)	225	320	570	345

Table 5.13 Summary of CO₂ production as a function of zeolite mass and the corresponding amount of adsorbed phenol needed to produce it. Phenol loading was adjusted with a blank TPO profile.

<i>Sample</i>	<i>CO₂ produced (mg g⁻¹)</i>	<i>Oxidized Phenol (mg g⁻¹)</i>
H-β-25	91	25
2.1Cu/β-25(p)	127	38
H-β-150	72	18
2.0Cu/β-150(p)	128	38
2.2Cu/β-300(p)	109	31

The unmodified H-β-150 beta zeolite shows considerably poorer oxidation performance than the zeolite H-β-25, the minimum temperature required for

oxidation was 483°C and the overall production of CO₂ was low (123 mg g⁻¹). The likely cause of this is the large reduction in the catalytically active Brønsted acid sites that would result from the lower alumina content of H-β-150.

The addition of copper to the zeolites resulted in a reduction in the temperature required for phenol oxidation and a considerably higher level of CO₂ production. However, from Figure 5.18 there is a difference between the copper exchanged zeolites with different SiO₂:Al₂O₃. In the sample 2.0Cu/β-150(p), there is an abrupt increase in CO₂ production at 238°C followed by a plateau from 308°C. This leads into a peak which is reminiscent of that found in 2.1Cu/β-25(p). A similar effect occurs in 2.2Cu/β-300(p), except that there is a larger low temperature CO₂ peak. Comparison with the TPR results in Chapter 3 would appear to go some way to explaining this. 2.1Cu/β-25(p) was shown to have the majority of its exchanged copper in the form of Cu⁺ species (indicated by a large high temperature peak of H₂ consumption) with some Cu²⁺, whereas 2.0Cu/β-150(p) showed a probable mixture of Cu²⁺ (due to a two step oxidation) and CuO. In the case of 2.2Cu/β-300(p) the late Cu⁺ peak was absent altogether and most of the copper was believed to be in the form of CuO. This could mean that the lower temperature shoulder in the CO₂ profile present in the copper zeolites with a higher SiO₂:Al₂O₃ ratio is as a result of increasing CuO and the later peak is representative of oxidation occurring at the cation exchanged Cu⁺ or Cu²⁺ species.

5.3.2 Thermo Gravimetric Analysis

In this section, the phenol saturated zeolites were examined under TGA. The purpose of this was to confirm proportionately the loss of adsorbed components on the zeolite surface due to oxidation and also to examine the temperatures at which oxidation takes place. A comparison of the TGA and TPO results for 2.1 Cu Beta 25:1 (p) is shown in Figure 5.19.

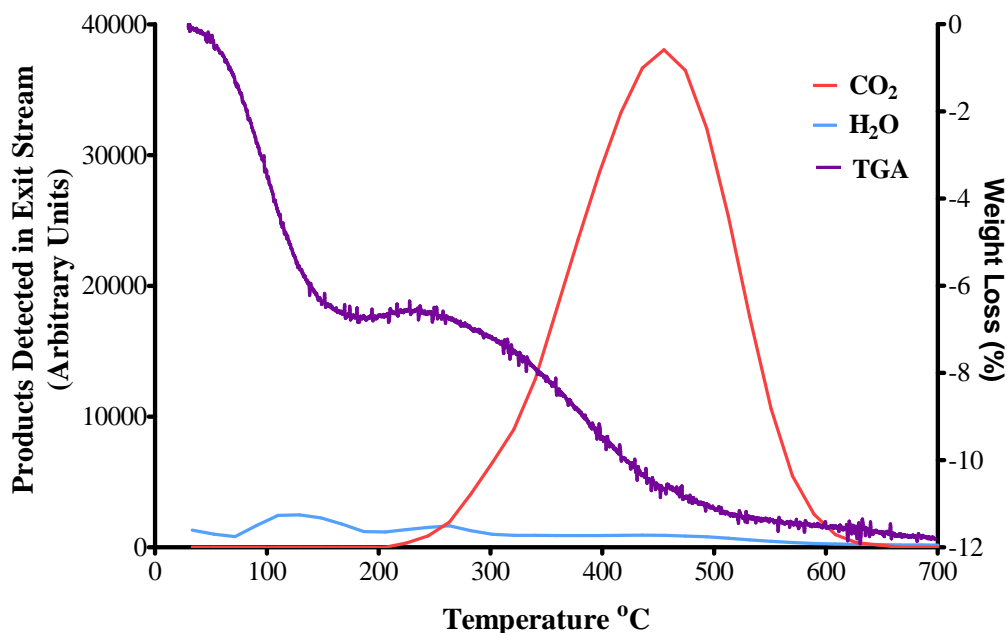


Figure 5.19 Comparison of TGA and TPO profiles for phenol saturated 2.1Cu/ β -25(p). TGA performed under air, $10^{\circ}\text{C min}^{-1}$ 10mg sample.

The initial weight loss from approximately 50 to 180°C observed in the TGA represents the loss of physically adsorbed water and is mirrored by the desorption of water in the TPO profile. At approximately 210°C in the TGA profile, the weight begins to drop again, this occurs concurrently with the CO₂ profile from the TPO. This weight loss is likely to represent the oxidation of surface phenol. The TGA curve is quite steep until approximately 460°C where it begins to level out, this point also matches the maximum CO₂ detection observed in the TPO. It is clear that the TGA and TPO results closely match each other. The total weight loss from the oxidation and desorption of the adsorbed components represents 11.5% of the total mass.

Figure 5.20 compares a copper zeolite under different conditions: in air, in nitrogen and in air without phenol.

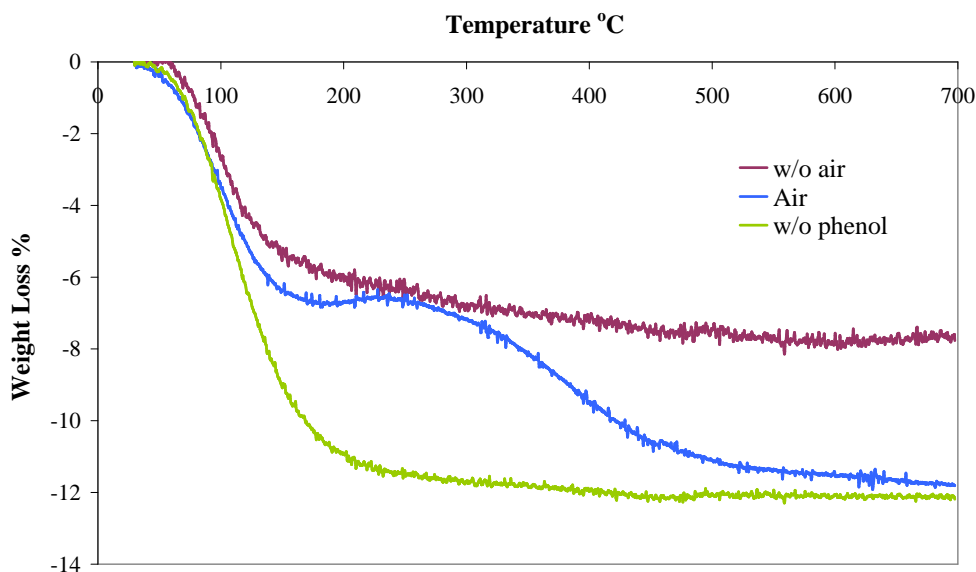


Figure 5.20 TGA profiles for 2.1Cu/β-25(p) with phenol in air, with phenol without air and without phenol in air. 10°C per min⁻¹ in air.

The TGA profile in the presence of oxygen shows the typical two step weight loss. The first loss is associated with the desorption of water and the second at approximately 250°C with the oxidation of the adsorbed organic component. When phenol is absent the second weight loss step is not present. However, the weight loss associated with water increases to 12% of total weight. Since the total weight loss is the same as the sample with phenol, it can be concluded that phenol and water occupy the same adsorption capacity and that the two components are in competition. The TGA profile for the phenol saturated sample without air, shows the water desorption weight loss but no second step as there is no oxygen to oxidize the adsorbed phenol.

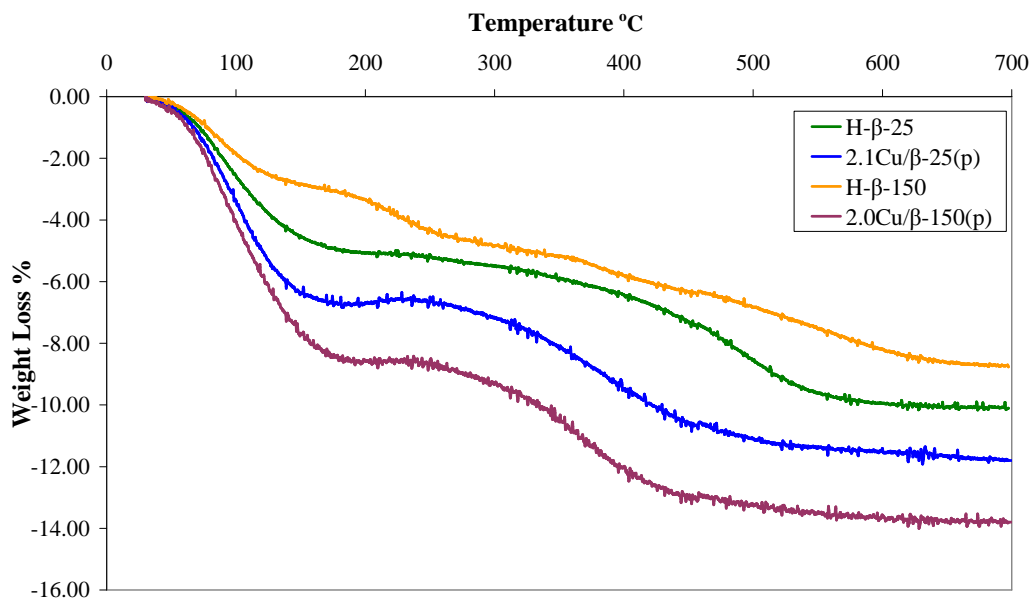


Figure 5.21 TGA profiles for four different phenol saturated zeolites with varying copper and silica to alumina ratios. $10^{\circ}\text{C per min}^{-1}$ in air.

TGA results for a range of zeolites are examined in Figure 5.21. The 150:1 zeolite shows a continuous fall in mass from 200-650°C following the desorption of water amounting to only 5% of total mass. This matches the TPO profile in Figure 5.18 which shows a relatively weak CO_2 peak occurring at a high temperature with no distinct peak in oxidation. The two copper zeolites show similar profiles to each other. However the 2.0Cu/β-150(p) zeolite shows a greater weight loss which is consistent with its greater phenol adsorption capacity. Unlike the profiles in Figure 5.18, there is no apparent difference in the shape of the profiles of the two catalysts.

As the most hydrophobic zeolite, the unmodified 150:1 shows the least water uptake, the copper zeolites are both notably higher, possibly due to an increased surface polarity resulting from the larger cation, increasing the zeolites affinity with water (Walton et al. 2006).

The TGA profiles shown in Figure 5.21 correspond well with their respective TPO profiles regarding the temperature of maximum CO_2 detection and regarding the estimated proportion of oxidized phenol. Overall the TGA data confirms the improved oxidation ability of the copper modified catalysts.

5.3.3 Mass Balance

Where available the phenol uptake during adsorption was compared to the quantity of phenol oxidized, as derived from the CO₂ mass fragment peak area from the TPO studies, and the organic weight loss in the TGA studies. This information is summarized in Table 5.14.

Table 5.14 Comparison of oxidized and adsorbed phenol onto a range of copper zeolites. Phenol oxidized as determined by TPO and TGA. Adsorbed phenol as determined by batch adsorption studies. Phenol concentration 2000 mg dm⁻³

<i>Sample</i>	<i>Phenol Oxidized/Adsorbed(mg g⁻¹)</i>			<i>% Oxidized in TPO</i>
	<i>TPO</i>	<i>TGA</i>	<i>Adsorption</i>	
H-β-25	25	30	32	78
2.1Cu/β-25(p)	38	38	40	95
H-β-150	18	21	45	40
2.0Cu/β-150(p)	38	39	66	58

For each of the methods studied there is a clear increase in phenol oxidation/adsorption for the copper modified zeolites, and there is only a small disparity between the estimated phenol oxidation in the TPO and TGA studies. This difference is probably due to TGA not differentiating between different desorbing components such as CO. Of the two unmodified zeolites, H-β-25 performed the best when compared to H-β-150 due to its greater number of acid sites, oxidizing 28% more adsorbed phenol. However, when approximately the same amount of copper is exchanged onto each zeolite, the amount of oxidized phenol is almost identical at 38 mg g⁻¹. This would seem to suggest that the acid sites play less of a part in catalytic oxidation over copper zeolites. On 2.1Cu/β-25(p) this amount of oxidized phenol represents 95% of the total adsorbed phenol, where as due to the much greater adsorption capacity of 2.0Cu/β-150(p), only 58% of surface phenol is oxidized. This could possibly suggest that 38 mg g⁻¹ of oxidized adsorbed phenol represents an upper limit for this copper loading. However, since the phenol is almost completely removed in the case of 2.1Cu/β-25(p) at saturation, it cannot be confirmed that if there were more surface phenol that there would be no further oxidation. In addition to this the TPO profile for 2.0Cu/β-150(p) was noticeably different when compared to 2.1Cu/β-25(p) (see

Figure 5.18), and the TPR profiles discussed in Chapter 3 revealed a greater proportion of CuO in 2.0Cu/ β -150(p). It is possible that this species has poorer access to the adsorbed phenol due to a propensity to form crystallites (Bartholomew 2001).

5.4 Conclusion

The temperature programmed oxidation studies examined in this chapter showed that the oxidation of adsorbed phenol to the relatively benign products of carbon dioxide and water was possible over copper and platinum modified Beta zeolites. It was also shown that a high proportion of the adsorbed phenol was oxidized on the over exchanged copper zeolites, up to 95% in the case of 2.1Cu/ β -25(p).

The introduction of copper to the parent Beta zeolite was shown to cause a considerable reduction in oxidizing temperature (decrease of over 200°C), a factor which increased as the copper loading increased. Combined with improved adsorption characteristics and the absence of desorbing molecular phenol and its usual fragments, the pH treated copper zeolite appeared to be a viable and adaptable catalyst for the oxidation of adsorbed phenol.

The platinum zeolites caused a further temperature reduction over the copper equivalents; however this was coupled with a change in the relationship between carbon dioxide production and temperature. The platinum zeolites appear to oxidize in two phases, with part of the organic component oxidizing at approximately 250°C and the remaining part oxidized at a higher temperature of 400°C. The low temperature peak may represent a less strongly adsorbed organic component and/or the proportion of the adsorbate in close proximity to the exchanged platinum. The high temperature peak could be an intermediate organic component such as coke which may be more difficult to oxidize. The disadvantages of the platinum zeolite are the limited effect of changing the metal loading and the presence of desorbing phenol and other organic mass fragments. The platinum zeolites also had smaller peak areas than the copper zeolites,

indicating either a poorer adsorption affinity or that not all the phenol was oxidized.

Bimetallic zeolites offered temperature characteristics similar to the platinum monometallic zeolites; in that a two step oxidation was observed. However, the greater the copper loading of the bimetallic catalyst the lower the oxidation temperature. It was also observed that the relative size of the high temperature peak grew compared with the lower temperature peak and the peak areas of carbon dioxide production became comparable to monometallic copper zeolites of a similar loading. By approximately 2.4 wt% Cu the platinum becomes masked by copper and the profile is almost indistinguishable from that of a copper zeolite. Another positive effect of the addition of copper is that unlike the monometallic platinum zeolites, no desorbed phenol fragments were detected.

For the bimetallic zeolites it was revealed that whether platinum or copper is exchanged first, it makes little difference to the oxidation of phenol.

Silica to alumina ratio was also found to have an effect on oxidation. This appears to be as a result of an increase in deposited CuO or its location. This is likely due to the lack of exchange sites and results in some of the oxidation taking place at lower temperatures. The overall peak areas of the 150:1 and 25:1 copper zeolites were similar despite the increased adsorption noted in Chapter 4, so this could be an indicator of less complete oxidation taking place on the higher silica to alumina ratio.

This study has shown that dual purpose adsorbent/catalysts can be used for the extraction and oxidation of adsorbed phenol and that a simple ion exchange procedure on a commercial zeolite can vastly reduce the temperature of oxidation and the increase the amount of surface phenol oxidized.

5.5 References

- Atoguchi, T., T. Kanougi, T. Yamamoto and S. Yao (2004). *Phenol oxidation into catechol and hydroquinone over H-MFI, H-MOR, H-USY and H-BEA in the presence of ketone*. Journal of Molecular Catalysis A: Chemical **220**(183-187).
- Baiker (1985). *Experimental methods for the characterisation of catalysts. I. Gas adsorption methods, pycnometry and porosimetry*. International Chemical Engineering **25**: 12-28.
- Barrett, E. P., L. G. Joyner and P. P. Halenda (1951). *The determination of pore volume and area distributions in porous substances. I. Computations from nitrogen isotherms*. Journal of the American Chemical Society **73**: 373-380.
- Bartholomew, C. H. (2001). *Mechanisms of catalyst deactivation*. Applied Catalysis A: General **212**(1-2): 17-60.
- Brunauer, S., L. S. Deming, W. E. Deming and E. Teller (1940). *On a theory of the van der Waals adsorption of gases*. Journal of the American Chemical Society **62**: 1723-1732.
- Brunauer, S., P.H. Emmet and E. Teller (1938). *Adsorption of gases in multilayered layers*. J. Am. Chem. Soc. **60**: 309-319.
- Corma, A., V. Fornes and E. Palomares (1997). *Selective catalytic reduction of NO_x on Cu-Beta zeolites*. Applied Catalysis B: Environmental **11**(2): 233-242.
- Correa, R. J. and C. J. A. Mota (2003). *Effect of the compensating cation on the adsorption of t-butylchloride on zeolite Y*. Applied Catalysis A: General **255**(2): 255-264.
- Curtin, T., P. Grange and B. Delmon (1997). *The direct decomposition of nitrogen monoxide*. Catalysis Today **35**: 121-127.
- de Boer, J. H. (1958). *The structure and properties of porous materials*. London, Butterworths.
- Dědeček, J., O. Bortnovsky, A. Vondrová and B. Wichtelová (2001). *Catalytic activity of Cu-beta zeolite in NO decomposition: Effect of copper and aluminium distribution*. Journal of Catalysis **200**: 160-170.
- Delabie, A., K. Pierloot, M. H. Groothaert, R. A. Schoonheydt and L. G. Vanquickenborne (2002). *The coordination of Cuⁱⁱ in zeolites - structure and spectroscopic properties*. European Journal of Inorganic Chemistry **2002**(3): 515-530.

- Dubinin, M. M., E. D. Zaverina and L. Radushkevich (1947). *Adsorption cycle modelling*. Doklady Akademii Nauk SSSR **21**: 1351.
- Ene, A. B., T. Archipov and E. Roduner (2010). *Spectroscopic study of the adsorption of benzene on Cu/HZSM5 zeolites*. Journal of Physical Chemistry **114**: 14571-14578.
- EPA (1997). *IPC licencing BATNEEC guidance notes*. Dublin, EPA Publications.
- Fahmey, M. A., M. A. Zayed and Y.H. Keshk (2001). *Comparative study on the fragmentation of some simple phenolic compounds using mass spectrometry and thermal analysis*. Thermochemica Acta **366**: 183-188.
- Gong, Y., T. Dou, S. Kang, Q. Li and Y. Hu (2009). *Deep desulferization of gasoline using ion-exchange zeolites: Cu(i)- and Ag(i)-Beta*. Fuel Processing Technology **90**(1): 122-129.
- Huang, F., J. Lee, C. Lee and H. Chao (2004). *Effects of cation exchange on the pore and surface structure and adsorption characteristics of montmorillonite*. Colloids and Surfaces A: Physiochemical and Engineering Aspects **239**: 41-47.
- Kazansky, V. B. and E. A. Pidko (2005). *A new insight in the unusual adsorption properties of Cu⁺ cations in Cu-ZSM-5 zeolite*. Catalysis Today **110**: 281-293.
- Kukulska-Zajac, E., P. Kozyra and J. Datka (2006). *The interaction of benzene with Cu⁺ sites in zeolites: IR studies and DFT quantum chemical calculations*. Applied Catalysis A: General **307**(1): 46-50.
- Lenihan, S. and T. Curtin (2009). *The selective oxidation of ammonia using copper-based catalysts: The effects of water*. Catalysis Today **145**(1-2): 85-89.
- Oumi, Y., R. Mizuno, K. Azuma, S. Nawata, T. Fukushima, T. Uozumi and T. Sano (2001). *Reversibility of dealumination - realumination process of BEA zeolite*. Microporous and Mesoporous Materials **49**(1-3): 103-109.
- Petranovskii, V., V. Gurin and R. Machorro (2005). *Spectroscopic observation and ab initio simulation of copper clusters in zeolites*. Catalysis Today **107-108**: 892-900.
- Pillai, R. S., G. Sethia and R. V. Jasra (2010). *Sorption of CO, CH₄, and N₂ in alkali metal ion exchanged zeolite-X: Grand canonical monte carlo simulation and volumetric measurement*. Industrial Engineering and Chemistry Research **49**: 5816-5825.

- Rokosz, M. J., A. V. Kucherov, H. W. Jen and M. Shelef (1997). *Spectroscopic studies of the stability of zeolitic deNO_x catalysts*. Catalysis Today **35**: 65-73.
- Schreier, M., S. Teren, L. Belcher, J. R. Regalbuto and J. T. Miller (2005). *The nature of 'overexchanged' copper and platinum zeolites*. Nanotechnology **16**: 582-591.
- Walton, K. S., M. B. Abney and M. D. LeVan (2006). *CO₂ adsorption in y and x zeolites modified by alkali metal cation exchange*. Microporous and Mesoporous Materials **91**(1-3): 78-84.
- Wang, Y., Z. Lei, R. Zhang and B. Chen (2010). *Adsorption of NO and N₂O on Cu-BEA zeolite*. Journal of Molecular Structure: THEOCHEM **957**(1-3): 41-46.
- Wilken, N., K. Kamasamudram, N. W. Currier, J. Li, A. Yezerets and L. Olsson (2010). *Heat of adsorption for NH₃, NO₂ and NO on Cu-beta zeolite using microcalorimeter for NH₃ scr applications*. Catalysis Today **151**(3-4): 237-243.
- Yousef, R. I. and B. El-Esweed (2009). *The effect of pH on the adsorption of phenol and chlorophenols onto natural zeolite*. Colloids and Surfaces A: Physicochemical and Engineering Aspects **334**: 92-99.
- Zhang, P., S. Huang, Y. Yang, Q. Meng, S. Wang and X. Ma (2010). *Effect of SSIE structure of Cu-exchanged β and Y on the selectivity of diethyl carbonate by oxidative carbonylation of ethanol: A comparative investigation*. Catalysis Today **149**(1-2): 202-206.

Chapter 6

Regeneration and Reuse of the Catalytic Adsorbent

6 Regeneration and Reuse of the Catalytic Adsorbent

6.1 Introduction

In Chapters 4 and 5 the adsorption and catalytic oxidation of aqueous phenol over copper modified beta zeolites was established as a credible technique for treating phenol contaminated wastewaters. This two step method successfully transferred the pollutant to the solid phase and then completely eliminated it from the surface of the solid. However, in order to fully assess the viability of this technique the issue of regenerability must be addressed. Ideally the catalytic oxidation step should be sufficient to regenerate the adsorbent/catalyst, but it should also retain its characteristics so that it may be reused.

6.1.1 Catalyst Deactivation

All heterogeneous catalysts are subject to deactivation over time and as a result of continuous use. The primary mechanisms of deactivation can be broken down into several categories including: Thermal degradation, fouling, poisoning, attrition/crushing and leaching. (Bartholomew 2001; Moulijn et al. 2001; Shim and Kim 2010).

The physical processes associated with thermally induced degradation are usually referred to as *sintering*. The two principal forms of deactivation resulting from sintering are 1) the loss of catalytic surface area due to crystallite growth and 2) the loss of support area due to support collapse and of catalytic surface area due to pore collapse on active crystallites. Sintering is more likely to occur in reaction temperatures in excess of 500°C and in the presence of water vapour. The process is usually irreversible, but kinetically slow. The mechanisms for sintering centre on the growth or redispersion of metal crystallites. Crystallite growth occurs through crystallite migration, atomic migration and vapour transport. These mechanisms cause the smaller metal species and existing crystallites to coalesce on the surface and form larger crystallites. These three

dimensional particles have a lower available surface area than the smaller particles and thus can lower activity. Redispersion typically occurs in the presence of Cl or O₂, the metal forms chloride or oxide species which causes them to break into smaller crystallites upon reduction. Sintering depends on a number of factors, including temperature, the strength of the metal interactions with the support, the thermal stability of the support and the pore size (non-porous supports tend to exhibit more sintering (Bartholomew 2001)). The migration of particles also becomes more likely with metals with lower melting points. The Tamman and Hüttig temperatures are linked to melting points and represent the temperatures at which atoms become mobile. Well reported examples for some Cu catalysts show that sintering can be problematic at temperatures above 230°C, however this was found to be related to small amounts of chlorine present in the feed forming a mobile copper phase (Moulijin et al. 2001). In the case of zeolites, at temperatures in excess of 500°C and in the presence of water vapour, dealumination can occur (Janssens 2009). Thermal degradation can occur in all stages of a catalysts life span, including calcination during synthesis, reaction and thermal regeneration (Moulijin et al. 2001).

Fouling is the physical deposition of species onto the surface of the catalyst. This has the effect of blocking the active sites and pores. Two of the more common deposits include carbon which is usually produced from the disproportionation of CO (see Equation 6.1) and coke which is produced from the decomposition or condensation of hydrocarbons onto the catalyst surface (Forzatti and Lietti 1999).



Coking leaves a layer of hydrogen deficient carbon which covers the active sites of the catalyst and blocks the micropores of the support, while carbon deposits can encapsulate supported metal catalysts or create carbonaceous deposits under the metal crystallites which form filaments. These filaments can lift the catalyst metal from the surface (Moulijin et al. 2001). Not all forms of carbonaceous material build up cause deactivation, for example carbon filaments do not necessarily cause deactivation unless a sufficient mass of carbon has

accumulated in the free surface area between the filaments or to cause pore blocking. Typically, the base metals Fe, Co and Ni are more prone to coke production than noble metals and other transition metals such as Cu. The addition of noble metals to base metals can greatly reduce coke formation (Bartholomew 2001). Fouling also covers other deposits on the catalyst surface including ash, soot, dust and various chemical by-products such as the formation of ammonium(bi)sulphate in SCR (Moulijin et al. 2001).

Poisoning is the strong adsorption of feed impurities onto the catalyst surface. This strong adsorption hinders the adsorption of less strongly adsorbing components. If the latter components are reactants then this could reduce catalytic activity. Poisons can also obstruct the active site or react directly with it e.g. basic compounds on an acid site (Forzatti and Lietti 1999). Since many oxidation procedures take place in air, the ambient air itself can be a source of impurities that gradually build up and reduce the catalytic activity. Aside from strongly chemisorbing impurities such as H₂S, poisoning can also be caused by metals or compounds reducible to metals. These can alloy with the catalyst metals on the surface creating species with less activity (Moulijin et al. 2001). Poisons are sometimes defined as reversible and irreversible by the strength of their adsorption in the reaction conditions. Reversible poisoning can usually be regenerated by removing the impurities from the feed gas. Irreversible poisoning is a result of bulk changes to the catalyst which are not easily reversed and often involve permanent damage (Forzatti and Lietti 1999).

Mechanical deactivation arises most commonly from *crushing* and thermal shock. Crushing is the physical damage which may occur during loading and transport of the catalyst, while thermal shock is the physical stress from thermal expansion and contraction as the catalyst is heated and cooled. Mechanical strength is to an extent based on the shape of the catalyst support. Catalysts with macropores are generally weaker than a non-porous spherical catalyst (Moulijin et al. 2001).

Leaching is another form of deactivation which is a key factor in process design for catalysts that operate some part of their lifespan in the aqueous phase.

Supports such as alumina are prone to dissolving in extremely high (>pH 12) or low (<pH 3) pH conditions, whereas activated carbon tends to be more stable under these conditions (Moulijn et al. 2001).

As mentioned above, the most common forms of deactivation for supported copper catalysts are sintering (in excess of 300°C) and H₂S poisoning, both of which can be accentuated by the presence of chlorine. However, copper catalysts are generally more resistant to carbon formation and coking (Twiggs and Spencer 2001).

6.1.2 Catalyst Regeneration

Typically if a catalyst becomes deactivated it must either be disposed of or regenerated, the first option leads to additional environmental impact from waste disposal and the added cost of replacement (Kim et al. 2007a). Regeneration can take many forms, some of which are outlined in Figure 6.1.

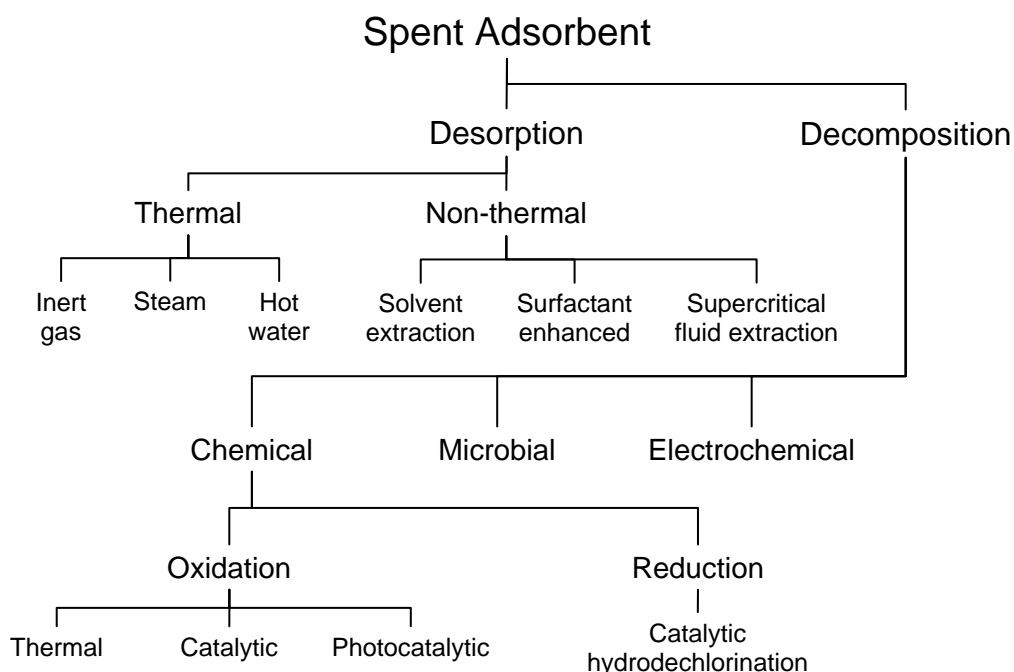


Figure 6.1 Summary of available techniques for regeneration of spent adsorbents (Sheintuch and Matatov-Meytal 1999)

Adsorbent regeneration techniques can be divided into two principal categories: Desorption and Decomposition. Desorption techniques involve the removal of the adsorbate from the adsorbent through thermal or non-thermal (extractive) techniques. Desorption techniques have the added advantage of preserving the adsorbate, this allows for the possibility of recovery and reuse where applicable. However the strongly acidic and steam conditions that are often used can physically damage the catalyst and cause metal loss. In addition to this, any feed chemicals used must either be recovered or treated after use. Milder desorption conditions may also not be sufficient to remove strongly adsorbed species (Sheintuch and Matatov-Meytal 1999). Decomposition methods involve the complete mineralisation or transformation of the adsorbate. These include using microorganisms, electrochemical cells or catalytic oxidation to break down even strongly adsorbed organic pollutants and regenerate the catalyst. Catalytic oxidation in the presence of air can completely eliminate the adsorbed organic with only relatively benign gaseous waste products. In order to minimize thermal degradation however, it is important to minimize the operating temperature.

Activated carbons are a common adsorbent for treating phenols and other organics due to their high adsorption capacity, however regeneration can be difficult. Conventional methods include offsite thermal treatment in rotary kilns or furnaces, reducing the adsorption capacity by 5-15% each time through thermal degradation and oxygen attack (Sheintuch and Matatov-Meytal 1999). Solvent or surfactant regeneration can still leave the adsorbent with over 50% of the original adsorption capacity but the pollutant is merely transferred rather than destroyed (Bhummasobhana et al. 1996).

Zhao et al. used a two step adsorption/catalytic dry oxidation system using a copper modified activated carbon for the treatment of phenol. The oxidation temperature was 190°C, but this resulted in a decrease in adsorption capacity of 50% (from 140 to 70 mg g⁻¹) after nine cycles (Zhao et al. 2004). In this Chapter the durability of the copper modified beta zeolite under oxidation conditions will be determined, with a focus on maintaining adsorption capacity and catalytic activity over a number of cycles.

6.2 Experimental

6.2.1 Catalyst Preparation

An over-exchanged copper zeolite (1.8Cu/ β -25(p)) with a theoretical loading of 2% was selected as a representative adsorbent/catalyst. It was prepared using a conventional ion exchange technique. For the exchange step 0.776 g of $\text{Cu}(\text{NO}_3)_2 \cdot 3\text{H}_2\text{O}$ (Fluka) was dissolved in 500 ml distilled water, to this the 5 g of H- β -25 (Zeolyst) was added. The pH of the suspension was adjusted to 7 by the addition of an 8% solution of ammonium hydroxide (ACS). The pH was monitored using a Thermo Orion model 420A+ pH meter. The suspension was stirred for 24 hours before removing the zeolite by vacuum filtration. The filter cake was washed with distilled water to remove any non-exchanged species and then dried for 24 hours in air to remove the bulk of the adsorbed water. The dried zeolite was then calcined in a Lenton thermal designs muffle furnace at 450°C for 5 hours. The calcination step removed any traces of adsorbed water and decomposable salts left over from the exchange process.

Phenol saturated samples were prepared by placing 5 g of 1.8Cu/ β -25(p) to a 500 ml aqueous solution of phenol (2000 mg dm⁻³). It was then stirred for one hour to reach equilibrium. This was followed by filtration using a Buchner funnel and it was then dried in air overnight at room temperature. The phenol loaded modified zeolite was then subjected to temperature programmed oxidation.

6.2.2 Atomic Absorption Spectroscopy

The copper zeolite was analysed by AAS to determine its copper metal loading. The procedure is the same as that outlined in Chapter 3 section 3.2.2.1.

6.2.3 Temperature Programmed Oxidation Studies

The TPO set up and procedure was described in detail in Chapter 5 section 5.2.2. 100 mg of phenol adsorbed 1.8Cu/ β -25(p) was inserted into the reactor. Before testing the catalyst bed was pre-treated in a 3% O₂/He mixture for 60 minutes at room temperature. After pre-treatment the sample was subjected to an increase in temperature at 10°C min⁻¹ up to 350, 500 or 700 °C. The temperature was held at this temperature for 10 minutes before bringing it back down to room temperature. The maximum temperature was varied for some experiments but the general procedure remained the same. The products leaving the reactor were analysed by the MSD using a HP Compaq dc7700 PC with the MSD Chemstation 5975C software.

In the repeat adsorption/oxidation studies the phenol saturated zeolite was calcined in 10 g batches in air using the same temperature program as the TPO in order to approximate the effect of repeated oxidation steps. 1.8Cu/ β -25(p) was subjected to six adsorption and oxidation cycles, each involved a 1 hour adsorption step in 2000 mg dm⁻³ phenol solution at 294 K, followed by calcination in air up to 700°C at a rate of 10°C per minute. Samples were removed for AAS and TPO analysis after each adsorption and oxidation step respectively.

6.2.4 Thermo Gravimetric Analysis

The TGA procedure was similar to that discussed in Chapter 5 section 5.2.3. In this case 10 mg of phenol saturated catalyst was heated at a rate of 10°C min⁻¹ in air up to three different maximum temperatures: 350, 500 and 700°C.

6.3 Results and Discussion

Table 6.1 presents the copper contents of the 1.8Cu/ β -25(p) zeolite after repeated adsorption/oxidation cycles. The copper content of the unused calcined sample was 1.8wt% (cycle 0). This sample was subjected to an adsorption step followed by an oxidation step up to 700°C. Following this oxidation step the copper content of the sample fell to 1.7wt % which corresponded to an overall copper loss of 6%. A significant further loss of copper was observed in subsequent cycles and this loss continued until the fifth cycle where the copper remains steady at about 0.5 wt%, approximately 26% of its original weight.

Table 6.1 Summary of the effect of multiple adsorption/oxidation cycles on the copper content of 1.8Cu/ β -25(p).

<i>Number of Adsorption/Oxidation Cycles</i>	<i>Copper Loading wt%</i>	<i>Copper Leaching % (incremental)</i>	<i>Copper Leaching % (cumulative)</i>
0	1.84	0	0
1	1.73	6	6
2	1.26	27	31
3	0.9	29	51
4	0.68	25	63
5	0.48	24	74
6	0.49	0	74

This level of copper leaching was not found in the washing study performed in Chapter 3, and since it only occurs after the first cycle, it is likely that the leaching occurs as a result of aqueous adsorption following exposure to high temperatures as opposed to the oxidation step on its own.

6.3.1 Temperature Programmed Oxidation

Figure 6.2 shows the TPO profiles for CO₂ evolution from a number of the repeat adsorption and oxidation cycles. It is clear that after a small decrease in the peak height following Cycle 1, the oxidation of phenol remains relatively constant up to 6 adsorption/oxidation cycles. In addition, no phenol or phenol fragments were detected in the exit stream even after six cycles. The quantity of adsorbed phenol derived from the CO₂ peak areas are shown in Table 6.2.

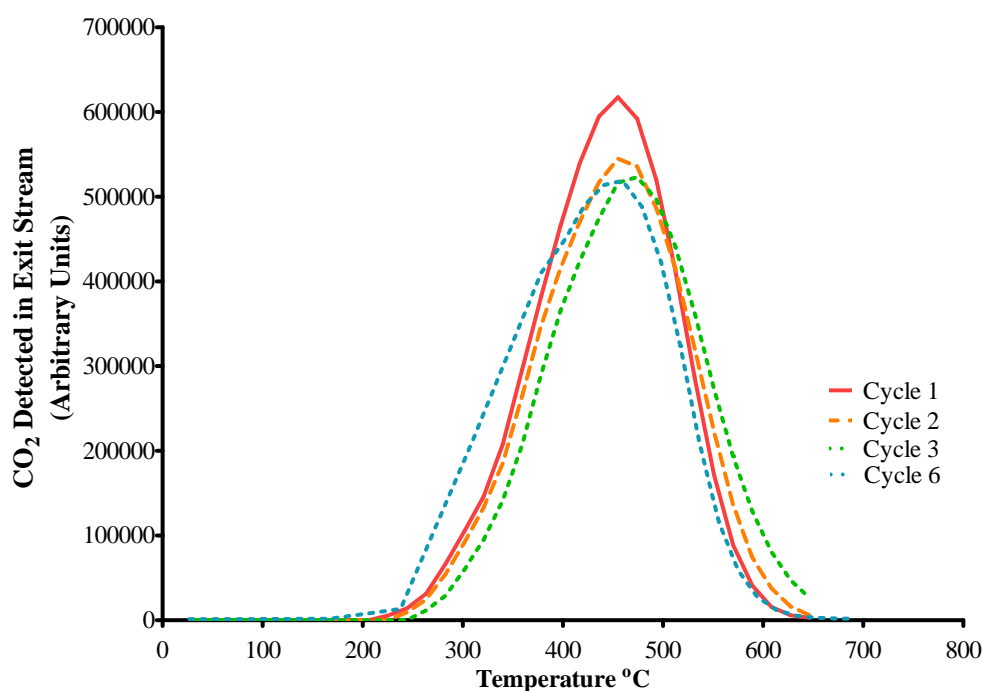


Figure 6.2 Comparison of CO₂ mass fragment detected from the TPO of copper 1.8Cu/ β -25(p). after the indicated number of adsorption/oxidation steps. 2000 mg dm⁻³ phenol, 3% O₂, ramped to 700°C at 10°C/min.

Table 6.2 Adsorbed phenol determined from the peak area of the CO₂ mass fragment detected in the exit stream, over a number of adsorption/oxidation cycles

<i>Number of Adsorption/Oxidation Cycles</i>	<i>Adsorbed Phenol (mg g⁻¹)</i>
1	64.38
2	60.30
3	58.55
6	62.47

From table 6.2 it is clear that there was only a slight reduction in the amount of phenol oxidised with increasing adsorption/oxidation cycles. This is in stark

contrast to the significant reduction in exchanged copper as a result of leaching shown in Table 6.1. The limited effect of copper leaching on the catalytic oxidation step would suggest that a relatively small amount of the exchanged copper is responsible for the catalytic activity. This active copper would also appear to be more resistant to leaching compared to the bulk of the copper present.

Supported copper catalysts are known to exhibit substantial change under higher temperature. In alumina supported copper, prolonged calcination at temperatures above 600°C can drastically increase the proportion of tetrahedrally coordinated copper ions to octahedral copper. Another possible process resulting in a change in copper species could be sintering. On silica supports the Cu²⁺ ions have been observed to crystallize into bulk CuO at temperatures above 700°C and as low as 500°C in over exchanged zeolites. This formation of CuO crystallites has also been observed in the gas phase under increasing temperature and in the presence of water for zeolites such as ZSM-5 and Y. When these large CuO crystallites form it can damage the zeolite crystallinity and has been known to cause deactivation in the case of HC-SCR. This CuO or any copper aggregates that may have formed on the surface are likely to be less stable than the isolated copper ions or polynuclear species. In SCR these components have also been observed to be less catalytically active due to decreased access to surface copper in the aggregates (Centi and Perathoner 1995).

A number of studies into the deactivation of copper zeolite catalysts have been performed. Kharas et al. and Tabata et al. examined CuZSM-5 catalysts for deactivation in hydrocarbon SCR. In both cases deactivation was observed at high temperatures 600-800°C and 500°C, respectively. In both cases the formation of CuO crystallites from sintering was attributed as the main cause of deactivation, and no significant carbon growth, dealumination or poisoning was observed. Kharas et. al also observed damage to the zeolite crystallinity and micropore volume. However no micropore deterioration was observed in Tabata et al. (Kharas et al. 1993; Tabata et al. 1994). Sintering is often affected by porosity (micropores and mesopores) as they impede surface migration. Since the micropore diameter is larger in Beta zeolite than in ZSM-5, it is possible that the

extent of sintering is reduced. Márquez et al. highlighted the formation of CuO aggregates on copper modified zeolite Beta, and tied their formation to the larger proportion of reduced copper in SCR at high temperatures (500°C) (Márquez and Palomares 2001).

The maintenance of most of the catalytic activity in the current work may be due to a species which is less easily mobilised (higher melting point), has stronger interactions with the zeolite or resides within pores or part of the structure where sintering does not take place. As observed from the TPR studies in Chapter 3 section 3.3.2, the zeolite 2.1Cu/ β -25(p) was found to both contain Cu²⁺ and Cu⁺ species and relatively little CuO. Considering that the majority of oxidation takes place by approximately 430°C, it is possible that the Cu²⁺, species which reduces at lower temperatures is responsible for the bulk of the catalytic activity. If this is the case then it may be part of the over-exchanged Cu⁺ species (possibly those that don't form stronger polynuclear species or reside within the pores) that migrates and forms CuO aggregates, without significantly effecting oxidation. After oxidation, the CuO aggregates formed remain on the zeolite until the next adsorption step where they are leached into solution.

6.3.2 Effect of oxidation temperature

In the case of 1.8Cu/ β -25(p), the oxidation begins at approximately 200°C and reaches a maximum at around 450°C. The bulk of the oxidation takes place well below the 700°C upper limit used in the TPO experiments. It is apparent that complete phenol oxidation can be obtained at lower oxidation temperatures. Sintering has been observed to be temperature dependent, causing greater crystallite growth and activity loss with higher temperatures (Kharas et al. 1993). If the higher oxidation temperature causes a loss in catalyst stability, then reducing it could alleviate the copper leaching observed in Table 6.1.

To examine the effect of oxidation temperature on the stability of copper, the zeolite 1.8Cu/ β -25(p) was applied to a full adsorption/oxidation cycle, followed by another aqueous adsorption step with phenol. This last step should remove copper that has become unstable after the first oxidation cycle. This experiment was performed at a number of different temperatures with the same adsorbent/catalyst, a residence time of 10 minutes followed after the target temperature was reached. The copper content of the 1.8Cu/ β -25(p) after the various treatments are shown in Table 6.3.

Table 6.3 Copper leaching exhibited after one adsorption/oxidation step and followed by a further adsorption step.

<i>Oxidation Temperature (°C)</i>	<i>Copper Loading wt%</i>	<i>Copper Loss %</i>
Original sample	1.78	-
350	1.76	1.1
500	1.75	1.7
700	1.61	9.6

The results show minimal copper leaching after oxidation at 350°C and 500°C, however at 700°C the leaching approaches 10% of total copper. This suggests that the copper species become considerably more unstable when treated at temperatures between 500 and 700°C.

Thermogravimetric analysis was also performed on 1.8Cu/ β -25(p) after oxidation at each of the three temperatures in order to determine if the phenol was completely oxidized, by comparing the weight loss in each case to a zeolite without adsorbed phenol. The results are shown in Figure 6.3.

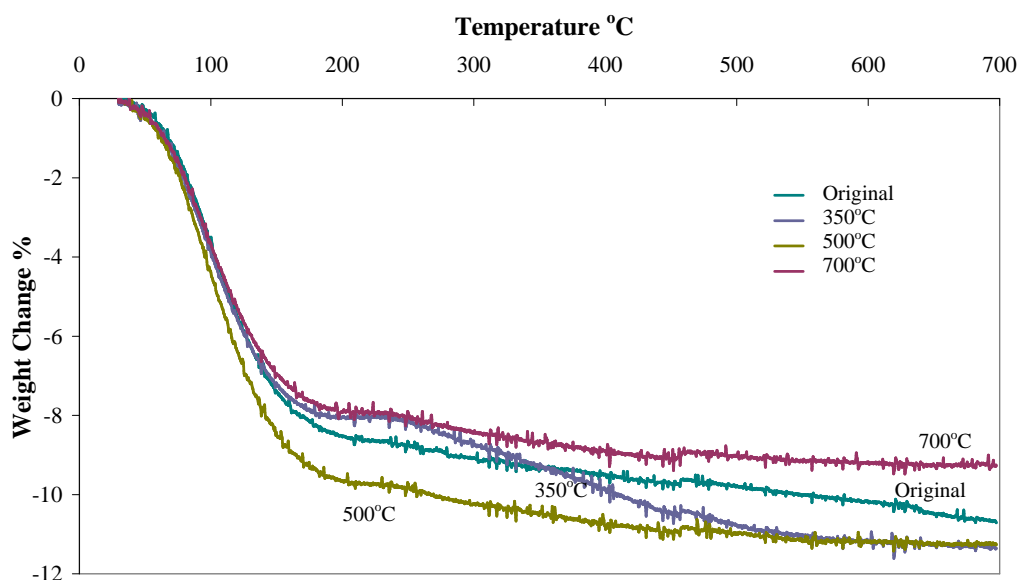


Figure 6.3 TGA of 1.8Cu- β -25(p) after 1 adsorption and oxidation cycle at three different oxidation temperatures. Adsorption conditions: Phenol concentration 2000 mg dm⁻³ for 1 hour. Oxidation conditions: 3% O₂/He, ramp rate 10°C/min, 10 minute residence time.

The sample labelled *original* is the TGA of 1.8Cu/ β -25(p) zeolite without adsorbed phenol. As the temperature increases, there is a sharp drop in weight between 30 and 200°C, this is associated with the evaporation of adsorbed water. After this point the profile levels out with a slight decrease in mass observed up to 700°C. This is most likely associated with the removal of trace organics or dehydroxylation of the zeolite. The other three samples were saturated with phenol and calcined at three different temperatures. The TGA of the sample oxidized at 350°C presents a clear weight loss between approximately 250 and 600°C. This can be associated with the oxidation of a significant amount of organic material that remained following the oxidation step at 350°C. The samples that were treated at 500 and 700°C show almost identical weight loss profiles, the only significant difference being the larger weight loss observed between 80 and 200°C associated with the desorption of water in the case of the catalyst oxidized at 500°C. This would suggest that the organic component is equally oxidized in both examples, but that the 500°C sample retained more water. Overall it would

appear that complete oxidation can be obtained at temperatures as low as 500°C but lower temperatures would not completely regenerate the zeolite or would require longer oxidation times to do so.

Since complete oxidation appears to occur at the significantly lower temperature of 500°C, the copper zeolite was subjected to a number of adsorption/oxidation cycles at both 500°C and 700°C to determine whether the reduced temperature had an effect on copper leaching. The results of this are shown in Figure 6.4.

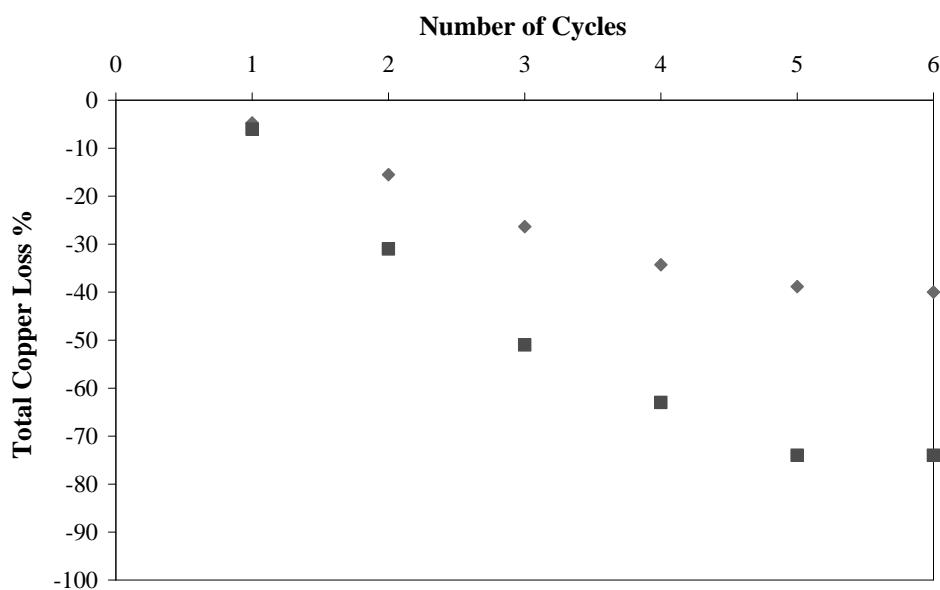


Figure 6.4 Comparison of copper leaching after 6 adsorption/catalysis cycles at two different oxidation temperatures on 1.8Cu/ β -25(p). ♦ 500°C and ■ 700°C.

The results of the leaching study show that at 500°C the amount of copper leaching is reduced significantly from 74% to 40% after 6 cycles. Although much reduced however, the copper loss is still significant as illustrated in Table 6.4. It is also important to note that the amount of copper in solution still greatly exceeds the EPA emission limit value of 0.5 mg dm⁻³ (as mentioned in Chapter 4) until the 6th cycle (EPA 1997).

Table 6.4 Copper concentration in adsorption solution exhibited after multiple adsorption/oxidation cycles with varying oxidation temperature

<i>Number of Adsorption/Oxidation Cycles</i>	<i>Cu concentration in solution (mg dm⁻³)</i>	
	<i>500°C</i>	<i>700°C</i>
1	0.8	1.2
2	1.9	4.8
3	1.9	3.6
4	1.4	2.3
5	0.8	2.0
6	0.2	0.0

6.3.3 Effect of adsorption pH

In Chapter 4 section 4.3.3 the exchanged copper was found to be stable under solution pH of 5-11. The phenol solution containing the zeolite has an average pH of 5. In Chapter 3 it was noted that the copper uptake increased significantly during the ion exchange procedure when the pH was increased to 7. The adjustment of pH during the aqueous adsorption phase may also have the effect of decreasing copper leaching and maintaining or rejuvenating the character of the copper species. To this end, a study was performed over 4 adsorption/oxidation cycles at 700°C with each adsorption step pH adjusted with aqueous ammonia. The results are shown in Table 6.5.

Table 6.5 Copper leaching exhibited after multiple adsorption/catalysis cycles with varying adsorption solution pH, on 1.8Cu/β-25(p).

<i>Number of Adsorption/Catalysis Cycles</i>	<i>Copper Loading</i>	<i>Copper Loading</i>
	<i>wt% pH 5</i>	<i>wt% pH 7</i>
0	1.8	1.8
1	1.7	1.8
2	1.3	1.8
3	0.9	1.8
4	0.7	1.8

The zeolite exposed to adsorption at pH 7 exhibited no apparent copper leaching after four cycles. Higher pH during cation exchange can cause over exchange yielding larger proportions of CuO particles on the external surface if there is a lack of exchange sites, however it also results in the formation of copper hydroxide molecules which can be cation exchanged and are contiguous to the formation of stable and often catalytically active polynuclear copper species in the zeolite channels (Centi and Perathoner 1995). This transformation may be responsible for the increased stability of the exchanged copper after multiple cycles. If this is the case the copper that is sintered during oxidation can be restored through pH treatment in this manner.

6.4 Conclusion

Regeneration and reuse of the copper zeolite as an adsorbent/catalyst was shown to be viable under certain conditions. The principal issues that can arise from successive catalyst reuse include: loss of adsorption capacity, incomplete oxidation of the absorbed component, and loss of integrity due to successive leaching of the catalytic component.

The TPO studies showed that after six adsorption catalysis cycles, there was little change in the amount of CO₂ produced as a result of adsorbed phenol oxidation. This would suggest that neither adsorption nor oxidation is greatly affected. However analysis of the reused copper zeolite by AAS showed severe leaching of the exchanged component, which appeared to form an upper limit at 74% of total copper after five cycles.

It was discovered that both the temperature of oxidation and the pH of adsorption had a substantial effect on the degree of copper leaching. A possible cause of this was crystallite formation through sintering in the oxidation phase, followed by leaching of this component during the adsorption phase.

It was found that when the maximum oxidation temperature was reduced to 500°C complete oxidation of the adsorbed phenol was still achieved. This was confirmed by TGA on copper zeolites which underwent oxidation at several different temperatures. The only noted side effect being an increase in the remaining proportion of adsorbed water.

Repeat cycles at 500°C showed much lower copper leaching than at 700°C, at approximately half the level on each cycle. However, the amount of copper lost is still significant until the 6th cycle.

Aside from oxidation temperature, the pH of the adsorption solution also appears to affect the amount of copper leaching. Adjusting the pH to 7 resulted in no detectable copper leaching after 4 successive cycles, even at 700°C.

In summary, the 1.8Cu/β-25:1(p) beta zeolite proved a stable and viable adsorbent and catalyst for sustained reuse, provided that the pH of the adsorption solution is maintained. It also appears that even without pH control; the oxidation and adsorption capacity is largely maintained, suggesting that a smaller more stable proportion of exchanged copper is active in adsorption and catalysis.

6.5 References

- Bartholomew, C. H. (2001). *Mechanisms of catalyst deactivation*. Applied Catalysis A: General **212**(1-2): 17-60.
- Bhummasobhana, A., J. F. Scamehorn, S. Osuwan, J. H. Harwell and S. Baramée (1996). *Surfactant-enhanced carbon regeneration in liquid-phase application*. Separation Science and Technology **31**(5): 629-641.
- Centi, G. and S. Perathoner (1995). *Nature of active species in copper-based catalysis and their chemistry of transformation of nitrogen oxides*. Applied Catalysis A: General **132**(2): 179-259.
- EPA (1997). *IPC licencing BATNEEC guidance notes*. Dublin, EPA Publications.
- Forzatti, P. and L. Lietti (1999). *Catalyst deactivation*. Catalysis Today **52**(2-3): 165-181.
- Janssens, T. V. W. (2009). *A new approach to the modeling of deactivation in the conversion of methanol on zeolite catalysts*. Journal of Catalysis **264**(2): 130-137.
- Kharas, K. C. C., H. J. Robota and D. J. Liu (1993). *Deactivation in Cu-ZSM-5 lean-burn catalysts*. Applied Catalysis B: Environmental **2**(2-3): 225-237.
- Kim, S. C., S. W. Nahm, W. G. Shim, J. W. Lee and H. Moon (2007). *Influence of physicochemical treatments on spent palladium based catalyst for catalytic oxidation of VOCs*. Journal of Hazardous Materials **141**(1): 305-314.
- Márquez, F. and A. Palomares (2001). *EXFAS electron spectroscopy as a new tool of local characterisation of copper in Cu-beta zeolite*. Solid State Sciences **3**(6): 637-640.
- Moulijn, J. A., A. E. van Diepen and F. Kapteijin (2001). *Catalyst deactivation: Is it predictable?: What to do?* Applied Catalysis A: General **212**(1-2): 3-16.
- Sheintuch, M. and Y. I. Matatov-Meytal (1999). *Comparison of catalytic processes with other regeneration methods of activated carbon*. Catalysis Today **53**(1): 73-80.

- Shim, W. G. and S. C. Kim (2010). *Heterogeneous adsorption and catalytic oxidation of benzene, toluene and xylene over spent and chemically regenerated platinum catalyst supported on activated carbon*. Applied Surface Science **256**(17): 5566-5571.
- Tabata, T., M. Kokitsu, O. Okada, T. Nakayama, T. Yasumatsu and H. Sakane (1994). *Deterioration mechanism of Cu-ZSM-5 as a catalyst of selective reduction of NO_x by hydrocarbons from the exhaust of stationary natural gas-fuelled engine*. Studies in Surface Science and Catalysis **88**: 409-416.
- Twigg, M. V. and M. S. Spencer (2001). *Deactivation of supported copper metal catalysts for hydrogenation reactions*. Applied Catalysis A: General **212**(1-2): 161-174.
- Zhao, J., Z. Liu and D. Sun (2004). *TPO-TPD study of an activated carbon-supported copper catalyst-sorbent used for catalytic dry oxidation of phenol*. Journal of Catalysis **227**: 297-303.

Conclusion

7 Conclusion

The purpose of this research was to develop a material and method for the two step adsorption and catalytic oxidation for the treatment of organic pollutants in wastewater streams. Importantly, the oxidation step must be capable of simultaneously regenerating the catalyst. The model pollutant selected was phenol and the adsorbent/catalyst was to be transition metal supported zeolite Beta. Zeolite Beta was selected based on its large surface area, pore size, three dimensional structure, hydrothermal stability and cation exchange capacity. The final material is required to: adsorb phenol, oxidize it under moderate conditions and remain stable in an aqueous environment and at the temperature of oxidation.

The aqueous adsorption of phenol onto zeolite Beta was found to be fast, mostly occurring in the first 10 minutes and an adsorption maximum was reached within an hour. The adsorption rate was found to conform strongly to the pseudo second order kinetics. The adsorption of phenol was found to be functionally independent of pH.

When the temperature was varied between 283 and 333 K the adsorption of phenol was found to increase with decreasing temperature with an observed maximum of 26.8 mg g^{-1} at 10°C ($\text{SiO}_2:\text{Al}_2\text{O}_3 = 25:1$). The enthalpy change was found to be negative; indicating an exothermic reaction which suggests the presence of energetically heterogeneous adsorption sites on the zeolite surface. The values for entropy change suggested a predominance of physisorption. The Gibbs free energy was shown to be negative, which suggests a feasible and spontaneous adsorption process. The entropy change was significantly negative suggesting a significant reduction in surface disorder and the possibility of adsorbate confinement within the zeolite structure.

The adsorption of phenol was examined on four Beta zeolites with differing silica to alumina ratios ($\text{SiO}_2:\text{Al}_2\text{O}_3 = 25:1, 75:1, 150:1$ and $300:1$) with adsorption maxima between 17 mg g^{-1} ($25:1$) and 36 mg g^{-1} ($150:1$). The

adsorption of phenol was found to increase with increasing silica, suggesting that hydrophobic interaction was an important factor in the uptake of phenol. The zeolite with the highest silica to alumina ratio; 300:1, exhibited lower phenol adsorption (22 mg g^{-1}) than the 75:1 and 150:1. It was noted that this zeolite appeared to have different surface characteristics than the other three zeolites, most notably a considerably lower mesopore volume. The Toth and Generalised Langmuir-Freundlich models were found to be the best fitting isotherm models overall, although the Langmuir isotherm became more prominent amongst the poorer adsorbing zeolites (25:1 and 300:1).

The 25:1, 150:1 and 300:1 beta zeolites were modified for the catalytic oxidation phase using an adapted cation exchange procedure with copper and platinum. A range of catalysts were created with varying levels of copper and platinum loading and combinations of each metal. The copper loading was found to increase when the pH was raised to 7. Using this technique the copper could become significantly 'over exchanged' with higher copper concentrations during exchange. Copper loadings ranged between 0.9 to 4.6 wt%. Through Temperature Programmed Reduction (TPR) studies the presence of Cu^{2+} and Cu^+ species were identified on under exchanged zeolites, however as the number of aluminium exchange sites were reduced (higher SiO_2 : Al_2O_3 ratio) and the amount of copper ions in solution were increased; copper oxide species became more prevalent. This could represent a proportion of un-exchanged copper deposited on the surface.

In the case of platinum, it was found to primarily coordinate with silanol groups on the zeolite surface as opposed to cation exchange. The exception was where platinum and copper were exchanged onto the same material. In this case the TPR results suggested that cation exchanged Pt^{2+} or PtO species were present. The copper content in the bimetallic zeolites was found to be less compared to the monometallic copper zeolites.

The copper zeolite was stable between the pH ranges of 7 and 11. However with a three part washing step added into the exchange procedure, the leaching was reduced to environmentally safe levels at pH 5 as well.

The 150:1 and 25:1 silica to alumina ratio copper zeolites were also examined for their phenol adsorption capacity. It was found that the cation exchange significantly increased phenol adsorption by up to 46% at the adsorption maximum. Specifically to 39.4 mg g^{-1} for the sample 2.1Cu/ β (p) and 65.8 mg g^{-1} for 2Cu/ β -150(p). This increase may be a result of change in surface acidity or interaction between phenol and the copper species. Again the Langmuir-Freundlich isotherm model proved to have the best overall fit with the 25:1 zeolites showing slightly greater Langmuir affinity.

The catalytic oxidation of the adsorbed organic component on the surface of the copper zeolite was performed up to 700°C and the products were examined using a mass selective detector. The findings showed that up to 95% of the adsorbed phenol could be oxidized by copper modified zeolites resulting in the relatively benign products of water, carbon dioxide. The carbon monoxide produced was low enough to be a fragment of CO_2 . The complete destruction was confirmed by examining CO_2 peak area and by thermogravimetric analysis. When compared to the unmodified zeolite, the presence of copper considerably reduced the temperature of maximum oxidation from 594°C to as little as 378°C for the catalyst 4.6Cu/ β (p). It was found that the temperature reduction was proportionate to increasing phenol. The TPO profile for the oxidation of phenol on the unmodified zeolite also revealed the desorption of a proportion of the adsorbed phenol and its fragments at approximately 300°C , in the case of the copper zeolites however no phenol desorption was detected.

The platinum zeolites were noted for a distinct two part oxidation represented by two peaks in the TPO profiles, one at approximately 250°C , the other at close to 400°C . The first peak possibly represents a more volatile or less strongly bonded component being oxidized first. No significant change in oxidation temperature was found upon changing the metal loading. Although a relatively small loading

of platinum is required to reduce the temperature of oxidation significantly (as little as 0.05wt%). The peak area was noticeably lower than the copper zeolites, possibly indicating poorer adsorption or incomplete oxidation. In addition to this, some phenol and organic fragments were detected in the oxidation products.

Bimetallic zeolites containing both ion exchanged copper and platinum were also examined for the oxidation of adsorbed phenol. They were found to behave similarly to the monometallic platinum zeolite, however it was noted that as the proportion of copper was increased; the high temperature peak became proportionately larger and the profile began to resemble that of the monometallic copper zeolites.

The oxidation of phenol on the copper modified 150:1 and 300:1 showed very similar temperature characteristics to the 25:1, with a slightly lower start and end temperature but a peak maximum at higher temperature. The CO₂ profile for the higher silica zeolites differ from the 25:1 most likely due to the increasing proportion of CuO due to the lower quantity of available alumina exchange sites. This trend causes what appears to be a slightly lower temperature peak or shoulder overlapping with a higher temperature peak which becomes more prominent with increasing silica. The 2.0Cu/β-150(p) sample exhibited an almost identical CO₂ peak area to the equivalent copper loading on 25:1. However, due to greatly increased phenol adsorption, this amounted to only 58% of the total adsorbed phenol.

After repeated adsorption and catalysis step it was found that the copper zeolites exhibit severe copper metal loss, up to 74% of the original loading after 6 cycles. However TPO studies showed very little reduction in oxidation as a result of this leaching. When the temperature was reduced from 700 to 500°C it was found that the copper leaching was reduced by approximately one half. Total oxidation of phenol was confirmed at the lower temperature using TGA. In light of this, the cause of the leaching is possibly the sintering of surface copper at high temperatures into CuO crystallites which may be more easily

leached in the adsorption stage. It was also found that increasing the pH of the adsorption solution up to pH 7 could eliminate copper leaching almost entirely.

The findings in this study suggest that copper modified zeolite beta is a suitable material for the adsorption of phenol between pHs 5-11 and that this copper zeolite can facilitate the subsequent complete oxidation of phenol in gas phase catalytic oxidation. The best performing catalyst is the pH modified over exchanged beta zeolite with a silica to alumina ratio of 25:1. This combination gives a good balance of adsorption capacity, low oxidation temperatures, consistency of surface characteristics after exchange and a high capacity for the exchange of copper ions due to its increased alumina sites. One encountered problem was the leaching of copper after high temperature oxidation, however this can be alleviated by reducing the oxidation temperature and/or altering the pH of the adsorption solution.

Publications and Oral Presentations Based on the Work of this Thesis

Refereed Journal Publications Under Review

Smart D., Enright D., Curtin T and O'Dwyer T.F., 2011, *The Influence of Silica to Alumina Ratio on the Adsorption of Phenol from Aqueous Solution using Beta Zeolites*, submitted to Adsorption Science and Technology.

Oral Presentations

Smart D., Enright D., Curtin T., O'Dwyer T.F., 2010, *Development of a Novel Two Step Process for the treatment of Phenolic Wastewater*, Environ 10, 17-19 Feb, LIT , Limerick, Ireland.

Smart D., Enright D., Curtin T. and O'Dwyer T.F., 2008, *Development of a Novel Process for the Removal of Selected Organic Compounds from Waste Streams* 9th European Meeting on Environmental Chemistry, 3-6 Dec, University of Girona, Girona, Spain.

Smart D., Enright D., Curtin T. and O'Dwyer T.F., 2008, *Development of a Novel Process for the Removal of Selected Organic Compounds from Waste Streams* Strive EPA Conference, 3-6 Nov, Dublin.

Smart D., Enright D., Curtin T., O'Dwyer T.F., 2008, *Development of a Novel Process for the Removal of Selected Organic Compounds from Waste Streams*, Environ 08, 1-3 Feb, Dundalk IT, Dundalk, Ireland.

Poster Presentations

Enright D., Smart D., Curtin T., O'Dwyer T.F., 2008, *Development of a Novel Process for the Removal of Selected Organic Compounds from Waste Streams*, Chemistry Researcher's Colloquium, June, University College Cork, Ireland.

Smart D., Enright D., Curtin T., O'Dwyer T.F., 2007, *Development of a Novel Process for the Removal of Selected Organic Compounds from Waste Streams*, Strive Workshop EPA, 1-3 Nov, Dublin Ireland.